Use of Commercial Block Copolymers as Soot Dispersants in Engine Oil

David J. Growney

The University of Sheffield

Department of Chemistry

PhD Supervisor: Prof S. P. Armes FRS

Submitted to the University of Sheffield
In fulfilment of the requirements for the award of
Doctor of Philosophy

May 2015

Declaration

The work described in this thesis was undertaken at the University of Sheffield between October 2011 and May 2015, under the supervision of Professor S. P. Armes. Unless otherwise stated, it is the work of the author and has not been submitted in whole or any other part for any other degree at this or any other institute.

Signature: _____

David J. Growney May 2015

Acknowledgements

The last 3 ½ years have been some of the best years of my life, and an amazing experience for me. Firstly, I would like to thank my supervisor Prof. Steve Armes. From inspiring me as a young 4th year undergraduate student to finding the perfect (car based!!) PhD project, you have been invaluable in my continuing motivation and high aspirations. I thank you for the many hours sat in E37 going through endless text and Figures for publications, and presentations for conferences and teleconferences. I also thank you for your seemingly endless stream of ideas and knowledge, I have learnt a great deal from you and I hope my thesis conveys this. I would also like to thank my sponsors (BP Castrol) for their generous funding, without which this project could not have taken place. In particular, Gordon Lamb and Najib Aragrag are thanked for their continuous support and ideas throughout the course of the project. I want to say a massive thanks to Oleksandr Mykhaylyk (Sasha/SAXS god…), for many hours of discussions and support with SAXS, and of course for the collaborative work in Chapters 2, 3 and 5 of this thesis. Lee Fielding is thanked for continued support on most things Chemistry, ongoing banter, plus many TEM and SEM images (and SAXS)! Matt Derry is also thanked for support with various Chemistry problems plus banter on tap. Prof. Patrick Fowler is thanked for the in-depth maths discussions and help with effective density calculations. Thibault Derouineau and Laurie Middlemiss are thanked for their invaluable work during two 12 week summer projects (2013 and 2014).

I want to say a big thank you to everyone in E37 (both past and present) for helping create by far the best Armes group office... Matt Derry, Lee Fielding, Yin Ning, Mark Williams, Amy Cockram (plus Charlotte Mable, Kate Kirkham, Joe Lovett, Junjie Yuan and Albert). Andrew Morse needs a special mention for help getting me through 4th year undergrad and also giving plenty of assistance at the start of my PhD. Obviously the rest of the group also need a mention for making my time in Sheffield so memorable: Liam R, Lizzy Jones, Vicki Cunningham, Nick Warren, Nick Penfold, Pengcheng Yang, Andreas Hanisch, Irene Canton, Jeppe Madsen, Beulah McKenzie, Kay Doncom, Matt Rymaruk, Marzena Kocik, and a number of great MChem and placement students. Also to past Armes group members who helped me out in the early days! Babsy is thanked for all the SAXS help and general banter, and Amy Walsh for our many conversations on adsorption and dispersions! Claire Hurley is thanked for XPS analyses and ToF SIMS. Thanks also to Denise, Rachel, Brittany and Louise in the accounts department, Pete Farran and Nick Smith down in stores for putting up with receiving many many car parts and Richard Wilkinson for continuous technical support. Also to Pauline and Sharon for all the coffee to fuel me through my PhD, and John the porter for delivering endless parcels! Also, to friends who have helped me through and supplied banter at regular intervals, especially Jamie Smith and Alex Duke, and band mates Mark Sweet and Dave Hewitt. I also want to mention Kate Tranter. I have only known you for just over ten months but you have been my rock in the hardest year of my PhD and for this I am eternally grateful. Thanks for putting up with my ongoing Chemistry-based chatter and feeding me pies and ale when times were hard!

Last but in no way least, I would like to thank my family. Without your support I wouldn't be where I am today. Firstly to the best Mum, Dad and Sister I could ever wish for, without you I couldn't function, and I love you all dearly. I dedicate this thesis to the three of you; know that I will always strive to be the best that I can be for your continuing love, support and respect.

Publications

Primary publications resulting from work in this thesis

1. "Micellization and adsorption behavior of a near-monodisperse polystyrene-based diblock copolymer in nonpolar media" D. J. Growney, O. O. Mykhaylyk, S. P. Armes, *Langmuir,* **2014**, *30* (21), 6047-6056.

2. "Star Diblock Copolymer Concentration Dictates the Degree of Dispersion of Carbon Black Particles in Nonpolar Media: Bridging Flocculation versus Steric Stabilization" D. J. Growney, O. O. Mykhaylyk, T. Derouineau, L. A. Fielding, A. J. Smith, N. Aragrag, G. D. Lamb and S. P. Armes, *Macromolecules,* **2015**, *48*, 3691-3704.

3. "Determination of effective particle density for sterically-stabilized carbon black particles: Effect of diblock copolymer stabilizer composition" D. J. Growney, P. W. Fowler, O. O. Mykhaylyk, L. A. Fielding, M. J. Derry, N. Aragrag, G. D. Lamb and S. P. Armes. *Langmuir*, **2015**, *31*, 8764-8773.

4. "Is carbon black a suitable model colloidal substrate for diesel engine soot?" D. J. Growney, O. O. Mykhaylyk, L. A. Middlemiss, L. A. Fielding, M. J. Derry, N. Aragrag, G. D. Lamb and S. P. Armes. *Langmuir*, **2015**, *31*, 10358-10369.

Secondary publications resulting from work conducted on other projects

1. "Sulfate-based anionic diblock copolymer nanoparticles for efficient occlusion within zinc oxide" Y. Ning, L. A. Fielding, T. S. Andrews, D. J. Growney and S. P. Armes, *Nanoscale,* **2015**, **7**, 6691-6702.

Oral Presentations at Conferences

1. "Micellar structure and adsorption behavior of a polystyrene-based block copolymer" D. J. Growney, S. P. Armes, 245th ACS National Meeting, 7th-11th April 2013, New Orleans, USA.

2. "Assessment of the degree of dispersion of sterically-stabilised carbon black dispersions in *n*-alkanes using a LUMiSizer" D. J. Growney, S. P. Armes, International Workshop Dispersion Analysis and Materials Testing 2014, 23rd - 24th January 2014, Berlin, Germany.

3. "Star diblock copolymer concentration dictates colloidal stability of carbon black particles in non-polar media: bridging flocculation versus steric stabilization" D. J. Growney, S. P. Armes, 248th ACS National Meeting, 10th - 14th August 2014, San Francisco, USA.

4. “Effect of block composition on micelle size and steric stabilizer layer thickness: polystyrene-based diblock copolymers are effective dispersants for carbon black particles in *n*-dodecane” D. J. Growney, S. P. Armes, International Colloid and Interface Science Symposium, 6th - 9th July 2014, London, UK.

5. “Star diblock copolymer concentration dictates the degree of dispersion of carbon black particles in non-polar media: bridging flocculation versus steric stabilization” D. J. Growney, S. P. Armes, Nomination for Young Scientist Award 2015 at International Workshop Dispersion Analysis and Materials Testing 2015, 22nd - 23rd January 2015, Berlin, Germany.

Poster Presentations at Conferences

1. “Effect of temperature on the micellisation of polystyrene-based block copolymers in *n*-alkanes” D. J. Growney, S. P. Armes, Macro Group 2012 Polymer Conference, 9th - 12th July 2012, Warwick University, UK.

2. “Effect of temperature on the micellisation of polystyrene-based block copolymers in *n*-alkanes” D. J. Growney, S. P. Armes, 245th ACS National Meeting, 7th - 11th April 2013, New Orleans, USA.

3. “Effect of temperature on the micellisation of polystyrene-based block copolymers in *n*-alkanes” D. J. Growney, S. P. Armes, Macrogroup YRM 2013, June 24th - 25th 2013, Nottingham University, UK.

4. “Effect of block composition on micelle size and steric stabiliser layer thickness: polystyrene-based diblock copolymers are effective dispersants for carbon black particles in *n*-dodecane” D. J. Growney, S. P. Armes, International Colloid and Interface Science Symposium, 6th - 9th July 2014, London, UK.

5. “Effect of block composition on micelle size and steric stabiliser layer thickness: polystyrene-based diblock copolymers are effective dispersants for carbon black particles in *n*-dodecane” D. J. Growney, S. P. Armes, Macrogroup YRM 2014, 24th - 25th July 2014, Durham University, UK.

6. “Effect of block composition on micelle size and steric stabiliser layer thickness: polystyrene-based diblock copolymers are effective dispersants for carbon black particles in *n*-dodecane” D. J. Growney, S. P. Armes, 248th ACS National Meeting, 10th - 14th August 2014, San Francisco, USA.

Abstract

The micellar self-assembly behaviour of a near-monodisperse *linear* poly(styrene-*b*-hydrogenated isoprene) (PS-PEP) diblock copolymer is examined in *n*-alkanes. Direct dissolution leads to formation of polydisperse colloidal aggregates that are kinetically frozen artefacts of the solid-state morphology. Dynamic light scattering (DLS) and transmission electron microscopy (TEM) studies indicate that heating such copolymer dispersions up to 90 - 110^{o}C gives well-defined spherical micelles that persist on cooling to 20^{o}C. These observations are also consistent with small-angle X-ray scattering (SAXS) studies, which indicate the formation of star-like micelles in *n*-heptane and *n*-dodecane following a thermal cycle. Variable temperature ^{1}H NMR studies in deuterated *n*-alkanes confirm partial solvation of the polystyrene micelle cores occurs on heating. Increased mobility of the core-forming polystyrene chains is consistent with the evolution in morphology via exchange of individual copolymer chains, as observed by DLS. Adsorption of this diblock copolymer onto a model colloidal substrate (carbon black) has been investigated using X-ray photoelectron spectroscopy (XPS). A Langmuir-type adsorption isotherm has been constructed using a supernatant depletion assay based on the aromatic chromophore in the polystyrene block. Comparable results were obtained using thermogravimetric analysis (TGA) to directly determine adsorbed amounts. Based on maximum adsorbed amounts at 20^{o}C, these studies strongly suggest that *individual* copolymer chains adsorb onto carbon black from chloroform (a non-selective solvent), whereas *micellar* adsorption occurs from *n*-alkanes. This is important, because such copolymers are used as soot dispersants for engine oils.

A near-monodisperse PS-PEP *star* diblock copolymer is examined in *n*-alkanes. Variable temperature ^{1}H NMR studies using deuterated *n*-dodecane confirm that the outer polystyrene blocks are only partially solvated at 25^{o}C, and solvation remains essentially constant on heating to 100^{o}C. Physical adsorption of this copolymer onto carbon black is examined, with particular attention being paid to the effect of copolymer concentration on colloidal stability. Isotherms are constructed for copolymer adsorption onto carbon black at 20^{o}C using a supernatant depletion assay based on UV spectroscopy analysis of the polystyrene aromatic chromophore. In addition, TGA is used to directly determine the amount of adsorbed copolymer on carbon black. Analytical centrifugation, optical microscopy (OM) and TEM studies indicate that the star copolymer acts as a flocculant for the carbon black particles at low concentration, with steric stabilisation observed above a certain solvent-dependent critical copolymer concentration. This is attributed to the spatial location of the polystyrene block, which enables copolymer adsorption onto *multiple* carbon black particles at low coverage, whereas all polystyrene 'stickers' adsorb onto *single* carbon black particles at high coverage, leading to steric stabilisation. SAXS is used to characterise copolymer-coated carbon black particles, providing complementary insights regarding changes in the fractal morphology that occur with increasing copolymer concentration. Moreover, SAXS also provided direct evidence for the presence of the copolymer chains at the particle surface.

The effect of copolymer composition on both micelle diameter and dispersant performance (for carbon black particles) has been assessed for PS-PEP and poly(styrene-*b*-hydrogenated butadiene) diblock copolymers in *n*-dodecane. Direct dissolution at 20^{o}C produces kinetically-frozen polydisperse aggregates, and higher polystyrene contents accentuate such an effect. Heating to 110^{o}C produces relatively small, well-defined spherical micelles that persist on cooling to 20^{o}C. Physical adsorption of these diblock copolymer micelles onto carbon black has been investigated by constructing Langmuir-type adsorption isotherms based on UV spectroscopy, which were also supported by TGA. Stokes' law is used to calculate particle velocities in two very similar solvents (*n*-dodecane and d_{26}-dodecane). Although each copolymer forms micelles with similar DLS and SAXS diameters, subtly different effective densities (0.92-1.02 g cm^{-3}) are observed for the micelle-stabilised carbon black particles, which are substantially lower than the solid-state density of carbon black (1.89 g cm^{-3}). Since the rate of sedimentation of sterically-stabilised carbon black particles depends on the density *difference* between the particles and the solvent, significant errors can be incurred in analytical centrifugation studies unless care is taken to determine accurate effective particle densities.

Finally, the carbon black used in this project is assessed for its suitability as a mimic for diesel soot. Particle size, morphology, density and surface composition are assessed using BET surface area analysis, TEM, helium pycnometry and XPS. The extent of adsorption of a poly(ethylene-co-propylene) (dOCP) statistical copolymer or a PS-PEP diblock copolymer onto these two substrates is compared indirectly using a supernatant depletion assay based on UV spectroscopy. TGA is also used to directly determine the extent of copolymer adsorption. Degrees of dispersion are examined using OM, TEM and analytical centrifugation. SAXS reveals some structural organisation differences between carbon black and diesel soot particles: for example, the mean radius of gyration for soot is significantly smaller. Soot particle suspensions in *n*-dodecane comprise relatively loose mass fractals compared to the corresponding carbon black suspensions. SAXS also provides evidence for copolymer adsorption and indicates that addition of either copolymer transforms the initially compact agglomerates into relatively loose aggregates, while the primary particles remain unchanged. It is believed that this is also the case for diesel soot. In favourable cases, similar experimental data is obtained for carbon black and diesel soot with both copolymer dispersants. However, it is not difficult to identify certain copolymer-particle-solvent combinations for which substantial differences can be observed. Such observations are most likely the result of dissimilar surface chemistries, which can have a profound effect on the colloidal stability.

Contents

List of Tables

List of Figures

Figure 1.14. Transmission electron microscopy images of (a) Regal 250R and (b) Elftex 8 carbon blacks……….……….……………………….……….........……......………..21

Figure 1.15. Analytical centrifugation set-up for the LUMiSizer® instrument……....23

Figure 1.16. Typical raw profile sedimentation plot obtained by analytical centrifugation (LUMiSizer®) for 500 nm silica in water at 1 wt% (density 1.99 g cm^{-3})…………………………………………………………………………...……...24

Figure 1.17. LUMiSizer® volume-average particle size distribution obtained for a 1.0 % w/v aqueous dispersion of 500 nm silica particles by analysis of the raw profile sedimentation plot shown in Figure 1.16. Inset shows an SEM image for these silica particles……………………………………….………………….…………..……..….26

Figure 1.18. Schematic representation showing the typical scattering of an incident beam and illustrating the various terms defined in equation 12……………..……...27

Figure 1.19. Typical length scales probed by various scattering methods, where SANS is small angle neutron scattering and USAXS is ultra-small angle X-ray scattering…………………………………….………………….……………….…...…28

Figure 1.20. (A) Synthesis of PLMA macro-CTA via RAFT solution polymerisation of LMA in toluene at 70°C, followed by RAFT dispersion polymerisation of BzMA in *n*-dodecane at 70°C. (B) Thermo-responsive behaviour exhibited by 20% w/w $PLMA_{16}$−$PBzMA_{37}$ diblock copolymer nanoparticles in *n*-dodecane, plus schematic representation of the corresponding change in copolymer morphology. A soft free-standing gel is formed at 20°C, which becomes a free-flowing solution on heating to 70°C. This thermal transition is reversible: a worm gel is reformed on cooling to 20°C..…......…...…...........………….............…..…………….............…..………......29

Figure 1.21. SAXS patterns recorded for a 1.0 % w/w dispersion of $PLMA_{16}$−$PBzMA_{37}$ nanoparticles in *n*-dodecane on heating from 20°C to 160°C. Patterns are offset by a factor of 0.1 (90°C) and 0.01 (160°C) for clarity; fits to the data (solid lines) are shown as black lines. Inset shows all three scattering patterns plotted on the same scale……..…….………...…...…...……...….....………....…………...………..…..30

Figure 1.22. TEM images recorded for a 20% w/w $PLMA_{16}$−$PBzMA_{37}$ worm gel. Initially, highly anisotropic worms are observed at 20°C on dilution to 0.01% w/w solids [see image (A)]. On heating this 20% w/w gel to 90°C, degelation occurs. Allowing the hot 20% w/w worm gel to cool from 90 to 20°C (followed by dilution to 0.01% w/w solids prior to preparing a TEM grid) revealed mainly a worm phase [see image (B)], with a minor population of isolated spheres (see red arrows)…….……....31

Figure 1.23. Schematic cartoon representing the hierarchical structure of a typical carbon black mass fractal. SAXS patterns obtained from this material are described in Chapter 3…….…………….……….....…......…..…………...……....…………..…..32

Abbreviations

BET	Brunauer Emmett and Teller
DLS	Dynamic light scattering
dOCP	Dispersant olefin copolymer
DSC	Differential scanning calorimetry
GPC	Gel permeation chromatography
^{1}H NMR	Proton nuclear magnetic resonance
IEP	Isoelectric point
M_n	Number-average molecular weight
M_w	Weight-average molecular weight
OM	Optical microscopy
PDI	Polydispersity index
PS	Polystyrene
PB	Poly(hydrogenated butadiene)
PEP	Poly(hydrogenated isoprene)
PSD	Particle size distribution
PS-PEP	Poly(styrene-*b*-hydrogenated isoprene)
PS-PB	Poly(styrene-*b*-hydrogenated butadiene)
R_g	Radius of gyration
SAXS	Small angle X-ray scattering
SEM	Scanning electron microscopy
TEM	Transmission electron microscopy
T_g	Glass transition temperature
TGA	Thermogravimetric analysis
UV	Ultra-violet
XPS	X-ray photoelectron spectroscopy

Chapter 1

Introduction

1.1 Polymers

A polymer or macromolecule comprises long chains made up of individual repeat units covalently bonded together. Such chains are constructed via polymerisation, which is the process by which small molecule monomer units are linked together. This is the basis of a diverse sector of materials science, with polymers being used for polyethylene plastic bags,[1] flexible plastic bottles,[2] hydrogel contact lenses,[3] stimulus responsive or 'smart' polymers for use in biotechnology and medicine,[4] poly(vinyl chloride) pipes,[5] insulation for electric cables,[6] photovoltaic elements in solar cells,[7] dental filling materials,[8] polyester fibres for clothing applications[9] and poly(ethylene-*co*-propylene) dispersant additives in engine oils.[10, 11, 12]

1.1.1 Polymer architectures

Polymers can be either linear or non-linear. There are four types of linear polymers, namely homopolymers, alternating copolymers, block copolymers and statistical copolymers. Non-linear polymers can be divided into four main categories; branched polymers, graft copolymers, star polymers and cross-linked gels (not covered here), see Figure 1.1.

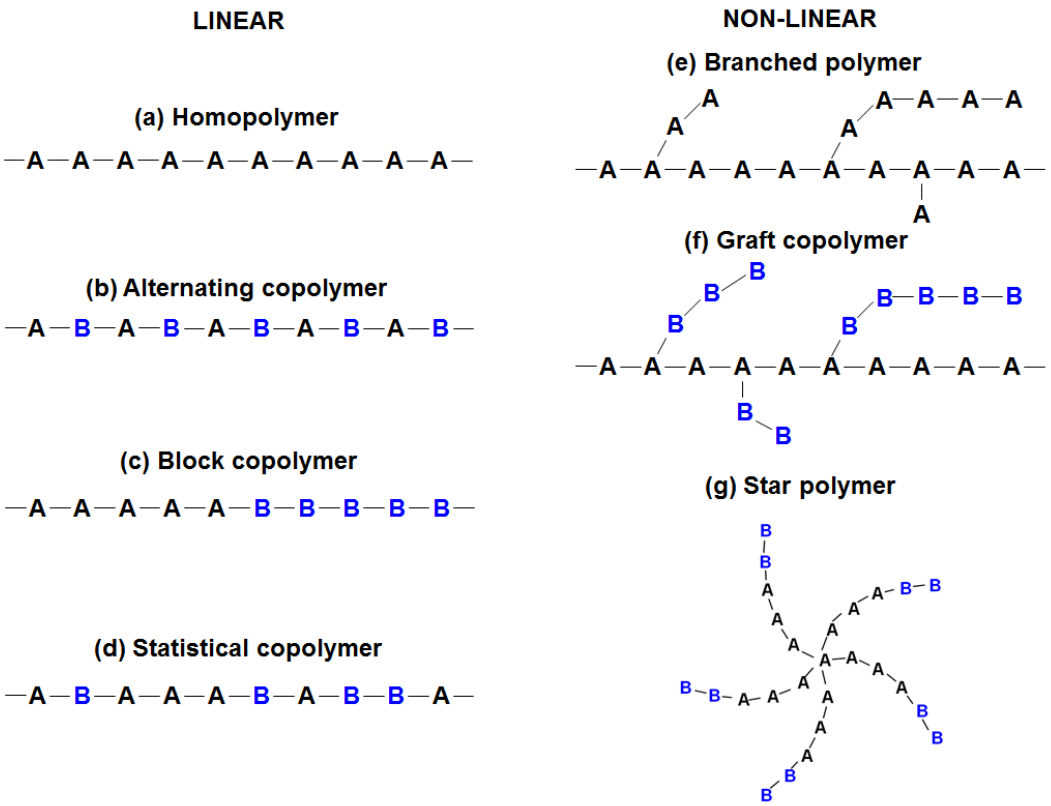

Figure 1.1. Schematic representation of the main types of linear and non-linear soluble polymer architectures, where A and B denote different monomer units.

1.1.2 Nomenclature

Homopolymers are known as polyA or poly(A), alternating copolymers as poly(A-*alt*-B), block copolymers as poly(A-*b*-B) and statistical copolymers as poly(A-*stat*-B). Finally, graft copolymers are denoted as poly(A-*g*-B). Diblock copolymers and star copolymers (made from cross-linked block copolymers) are of particular relevance to this thesis.

Stereochemistry must also be taken into account, as this can lead to different physical and chemical properties. Three main categories exist for vinyl polymers, namely isotactic ('R' groups point in one direction), syndiotactic (alternating 'R' groups) and atactic (random distribution of 'R' groups), see Figure 1.2.

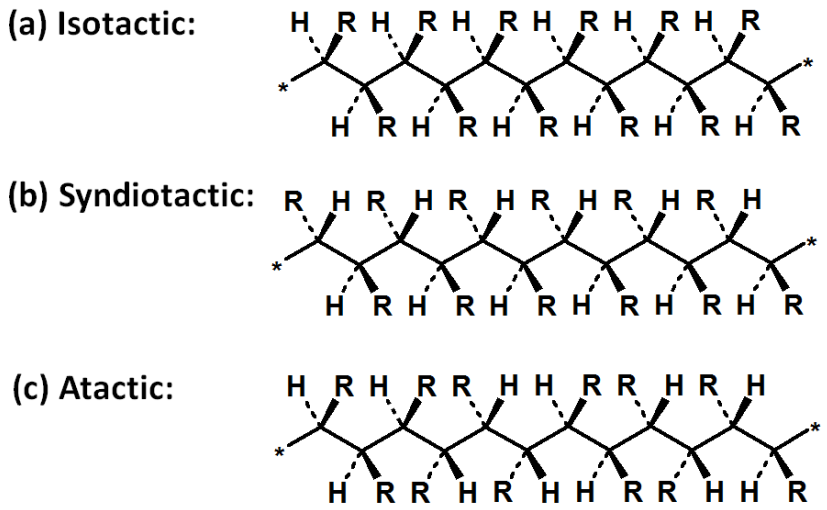

Figure 1.2. The three types of stereochemistry that are typical of linear vinyl polymers.

1.1.3 Polymer characterisation

Synthetic polymers are generally polydisperse, i.e. they exhibit no unique molecular weight. An ideal polymer would comprise identical chains and so have a single molecular weight, but in practice a molecular weight distribution (MWD) is always observed. There are three important moments on the MWD curve, corresponding to number-average (M_n), weight-average (M_w) and z-average (M_z) molecular weight. These are illustrated graphically in Figure 1.3.

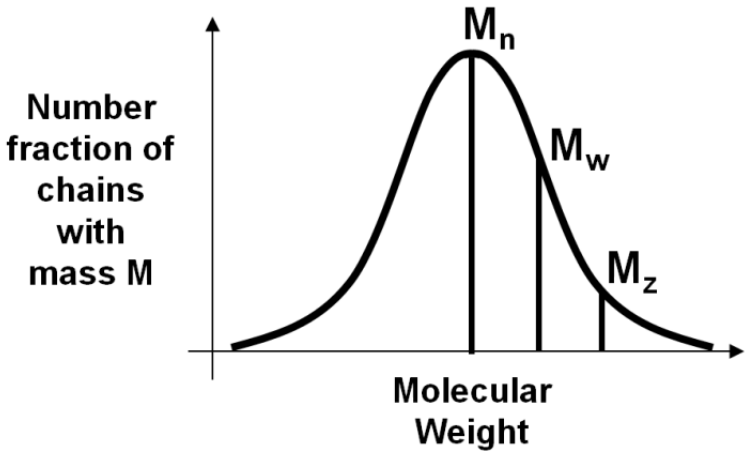

Figure 1.3. Schematic representation of the three most important moments of molecular weight: number-average (M_n), weight-average (M_w) and z-average (M_z).
The equations for calculating each of these molecular weights are detailed below.

$$\langle M_n \rangle = \frac{\sum n_i M_i}{\sum n_i} \quad (1)$$

$$\langle M_w \rangle = \frac{\sum w_i M_i}{\sum w_i} = \frac{\sum n_i M_i^2}{\sum n_i M_i} \quad (2)$$

$$\langle M_z \rangle = \frac{\sum n_i M_i^3}{\sum n_i M_i^2} \quad (3)$$

Here *n* is number of chains of molecular weight *M*. M_n is biased towards low molecular weight species, whilst M_w is biased towards high molecular weight species. In practice, M_z is rarely used. It is important to note that by definition $M_n < M_w < M_z$ for all polymers. From the first two values, a polydispersity index (PDI) can be calculated for a specific molecular weight distribution, where PDI is defined as M_w/M_n. Furthermore, the degree of polymerisation (D_p) can also be defined, see equation 4.

$$D_p = \frac{M_n}{\text{Molecular weight of monomer}} \quad (4)$$

If the D_p is less than ten, then the chains are known as oligomers, rather than polymers.

Various experimental techniques can be used to determine polymer molecular weights. Chemical methods generally rely on end-group analysis, and include UV spectroscopy, Fourier transform infrared spectroscopy (FT-IR) and nuclear magnetic resonance (NMR) spectroscopy. Equation 5 shows how such methods can yield M_n.

$$M_n = \frac{\text{Polymer concentration}}{\text{End-group concentration}} \quad (5)$$

Furthermore, scattering can be used to interrogate dilute polymer solutions, where polymer chains are assumed to behave as random coils. Here the scattering intensity is

proportional to the square of the particle mass; hence giving M_w. Static light scattering, neutron scattering and X-ray scattering can all be used to determine this parameter.

The most convenient method for polymer molecular weight characterisation is gel permeation chromatography (GPC). A dilute polymer solution is pumped through a column packed with microporous gel beads, and fractionation occurs as low molecular weight polymer chains get trapped within the pores for a characteristic residence time. This method gives the *whole* molecular weight distribution curve. The main disadvantage is that calibration is required using near-monodisperse standards. These standards are expensive and often not available for the polymer of interest. Hence in many cases GPC only reports *relative* M_n values.

1.1.4 Methods of polymerisation

In 1929, Carothers distinguished between polymers on the basis of their chemical composition.[13] Two main categories were identified, namely condensation and addition polymers. Today, polymers are distinguished on the basis of their polymerisation mechanism, where, broadly speaking, ‘step’ polymerisation = condensation and ‘chain’ polymerisation = addition. In general, step polymerisations produce heteroatom polymer backbones, while chain polymerisations produce homoatom backbones. Figure 1.4 shows three examples for each of these polymerisation mechanisms.

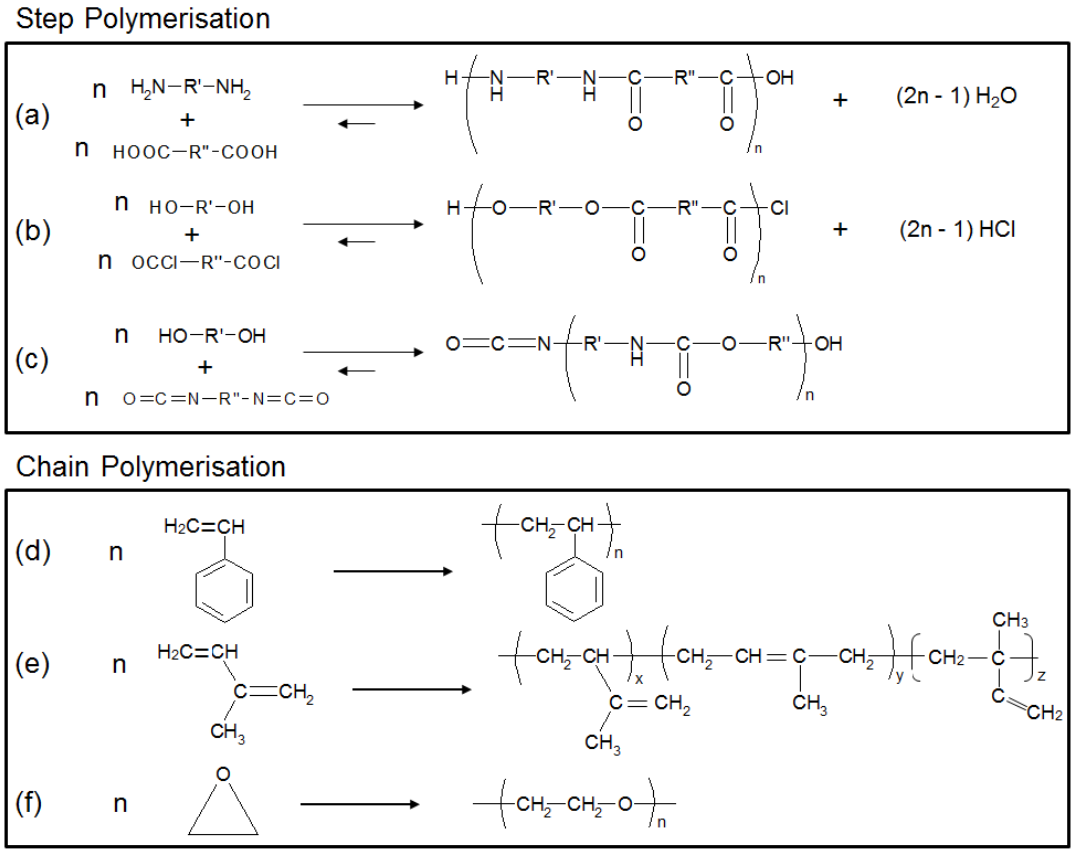

Figure 1.4. Reaction schemes depicting three examples of chain and step polymerisation. No condensate is formed in reaction (c).

Reaction scheme (f) shows a typical ring-opening polymerisation. It is important to note that, although this is a chain reaction, such polymerisations form a heteroatom backbone.

Step polymerisation

Step polymerisations fall into two categories, depending on the type of monomers used. The first category involves two different bifunctional (or polyfunctional) monomers in which each monomer possesses only one type of functional group. The second category involves a single monomer containing two different functional groups, see Figure 1.5.[14]

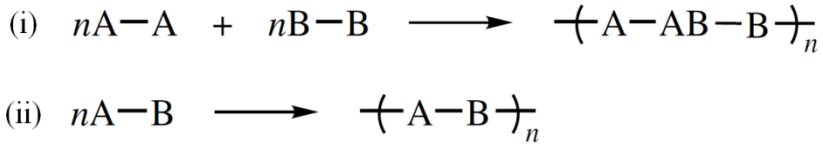

Figure 1.5. The two categories of step polymerisation (i) and (ii), where A and B represent two different functional groups.[14]

The synthesis of polyamides may involve either type of step polymerisation. Polyamides can be obtained from the reaction of di amines with di acids or from the reaction of amino acids with themselves. The synthesis of polymers with sufficiently high molecular weight using step polymerisation is generally rather more difficult than the corresponding small molecule reaction, since very high conversions (>98–99%) are required. Thus, a favourable equilibrium and the absence of cyclisation or other side reactions are desirable for such polymerisations. Finally, for case (i) in Figure 1.5, the A and B functional groups must be used in precisely stoichiometric amounts to achieve high molecular weight polymers.[14]

Free radical polymerisation

Free radical polymerisation of unsaturated vinyl monomers is the most widely used form of chain polymerisation.[15] Four distinct steps define such a polymerisation, as highlighted in Figure 1.6. Firstly, primary free radicals are generated (R•), usually via heat or the application of ultra-violet radiation to an initiator (I). Homolytic dissociation gives two radicals (where k_d is the first-order rate constant for dissociation), then initiation occurs when a free radical reacts with a monomer unit (Figure 1.6 (b)), thus forming a chain-initiating radical (R-M_1•), where k_i is the rate constant for initiation. Propagation then proceeds via rapid sequential addition of monomer units at a rate constant k_p. Several thousand monomers can be added within a few seconds here.[15] Termination is the final step, where radicals are eliminated via combination (rate constant k_{tc}) or disproportionation (rate constant k_{td}), see Figure 1.6.

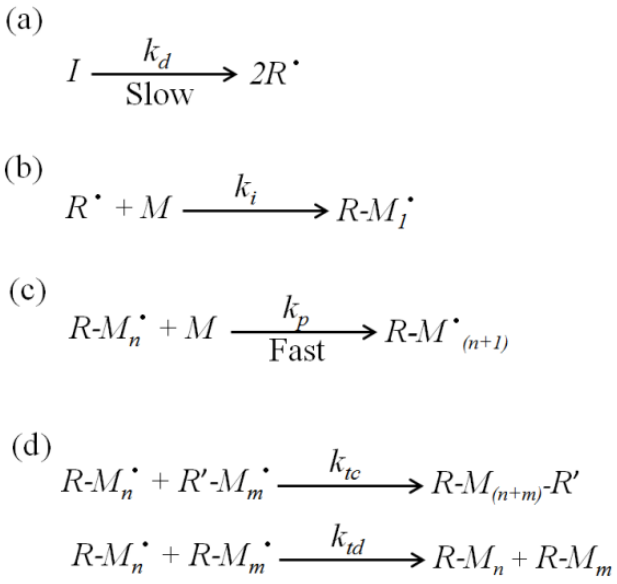

Figure 1.6. The four steps involved in free radical polymerisation: (a) is the relatively slow decomposition of initiator to form free radicals; (b) is the initiation step; (c) is propagation of the growing chain; (d) is termination (by either combination or disproportionation).

Anionic polymerisation

Many different copolymer architectures are now accessible via anionic polymerisation chemistry, including homopolymers,[16, 17] macromonomers,[18, 19] statistical copolymers,[20, 21, 22] block copolymers,[23, 24, 25] graft copolymers[26] and star copolymers.[27, 28, 29] Anionic polymerisation is a type of chain polymerisation that enables excellent control over the molecular weight distribution compared to free radical polymerisation.[30] Anionic polymerisation has so-called 'living' character: the evolution of molecular weight is proportional to monomer conversion and there is no intrinsic termination because polymeric anions are mutually repulsive and hence cannot react with each other. Thus sequential addition of a second monomer B after complete polymerisation of monomer A leads to the formation of well-defined AB diblock copolymers with low polydispersities (M_w/M_n < 1.10-1.20). Anionic polymerisation can be initiated using alkali metals, with an early literature example being the polymerisation of isoprene using sodium or potassium.[31] However, organolithium initiators are more commonly used today.[32, 33] For example, sec-butyllithium reacts with styrene to afford an anionic

monomer-initiator adduct, see Figure 1.7. This species immediately reacts with further styrene to produce a propagating anionic polymer chain via exclusively head-to-tail addition. The polymerisation continues until all monomer in solution has been used up, producing linear polymer chains with similar degrees of polymerisation. At the end of the reaction, a protic solvent such as methanol can be introduced to terminate the polymerisation, if desired. The synthesis of linear poly(styrene-*b*-hydrogenated isoprene) by anionic polymerisation, including catalytic hydrogenation of the polyisoprene block, is shown in Figure 1.8. Such commercially available diblock copolymers are examined in this thesis.

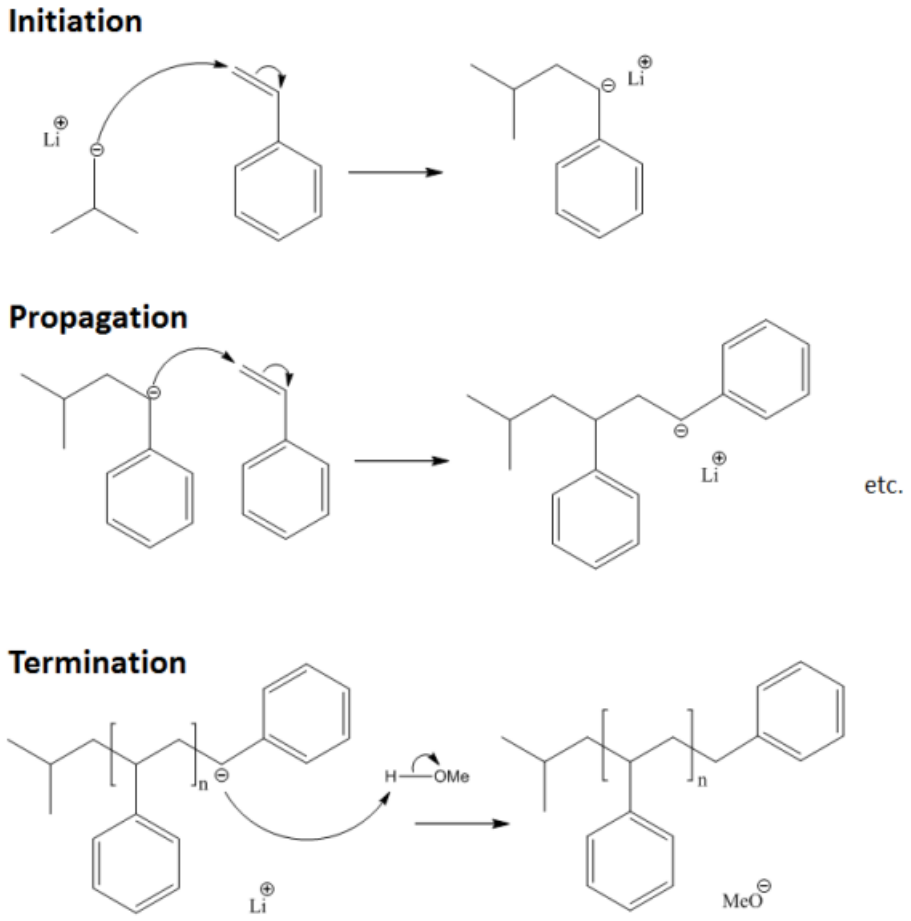

Figure 1.7. Anionic polymerisation of styrene using *sec*-butyllithium initiator followed by termination of the living polystyryl anion via methanol addition.

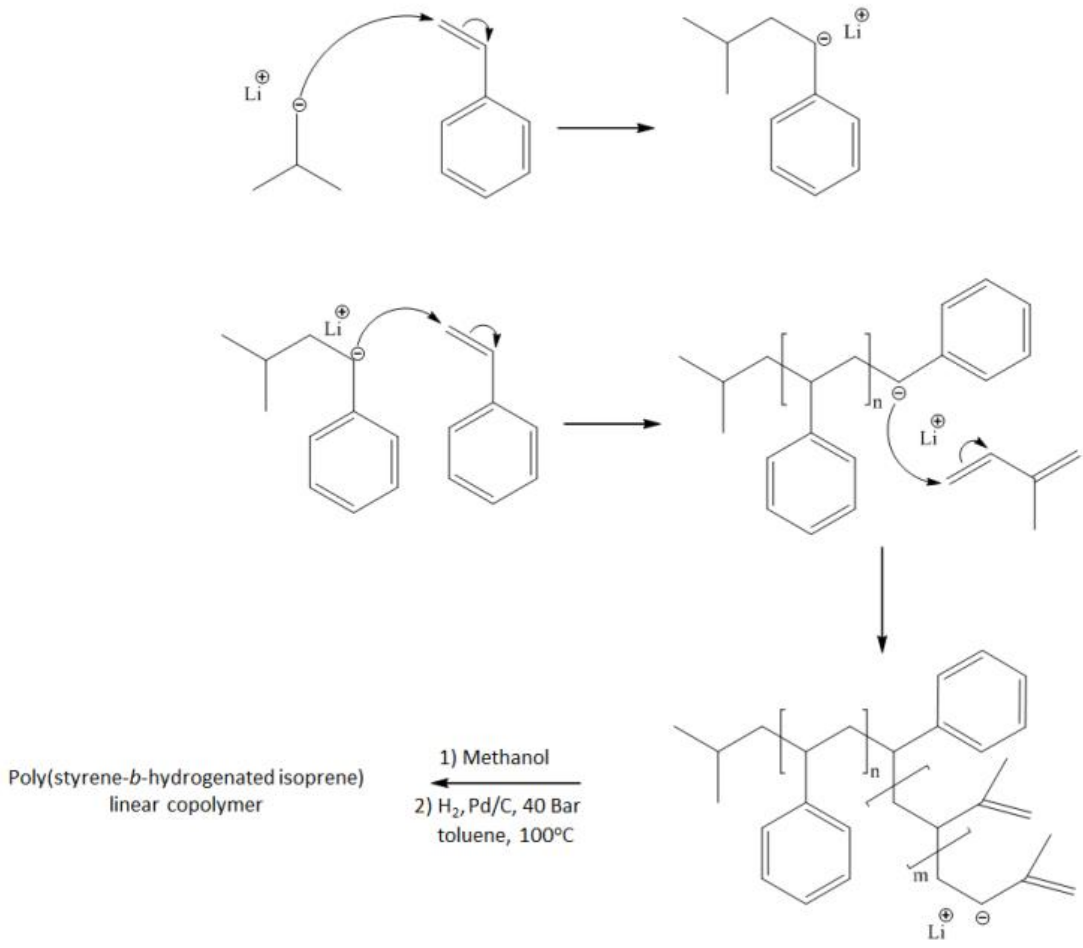

Figure 1.8. Synthesis of poly(styrene-*b*-hydrogenated isoprene) linear diblock copolymer via living anionic polymerisation, followed by catalytic hydrogenation of the pendent vinyl groups in the polyisoprene block.[34]

In addition to linear diblock copolymers, non-linear star polymers can also be prepared by anionic polymerisation. For example, poly(styrene-*b*-hydrogenated isoprene) star copolymers can be synthesised via the 'arm first' approach: linear polystyrene chains are prepared first, followed by chain extension with isoprene, then DVB cross-linking to form the unsaturated star diblock precursor and finally catalytic hydrogenation to produce the final saturated star diblock copolymer (see Figure 1.9).[35]

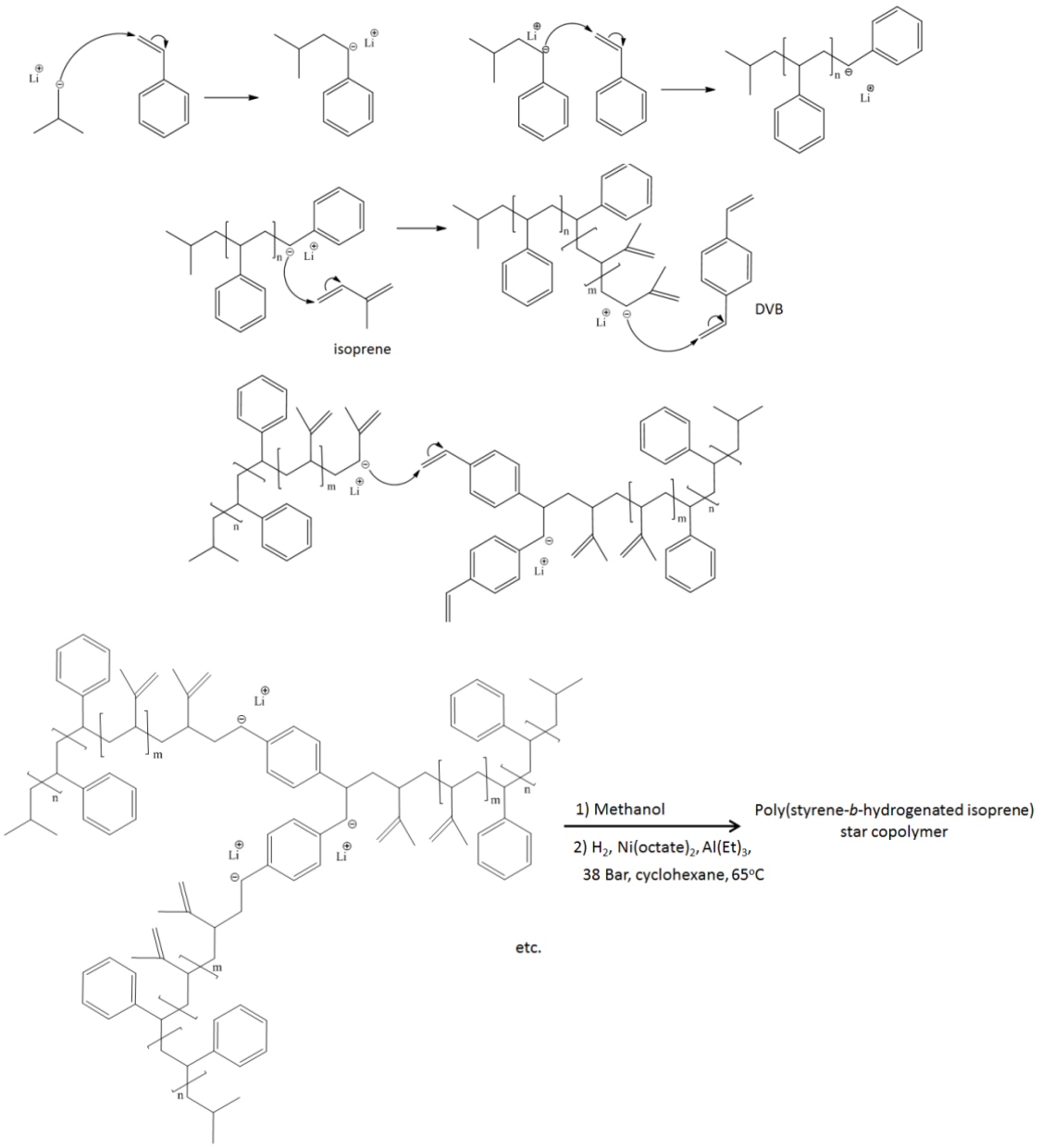

Figure 1.9. Mechanism for the synthesis of poly(styrene-*b*-hydrogenated isoprene) star diblock copolymer via the 'arm first' approach: styrene is polymerised first, followed by isoprene, then cross-linking with divinylbenzene and finally catalytic hydrogenation.[35]

Engine oil additive polymerisation

Focusing on polymeric engine oil additives, diblock copolymers are synthesised using anionic polymerisation. Poly(styrene-maleic anhydride) viscosity index improvers and pour point depressant additives use free radical alternating copolymerisation,[36, 37] while poly(isobutylsuccinic anhydride) (PIBSA) detergent additives use cationic polymerisation.[38] Poly(styrene-*b*-hydrogenated isoprene) linear and star copolymers are synthesised using living anionic polymerisation, as are dispersant olefin copolymers (OCPs).[35, 39, 40]

1.2 Colloidal Dispersions

A colloidal dispersion comprises a suspension of insoluble particles in a continuous phase, with at least one dimension in the 1 nm to 1 μm range.[41] It is well-documented that polymers that are soluble in the continuous phase can influence the stability of colloidal dispersions *via* four different mechanisms: steric stabilisation, bridging flocculation, depletion stabilisation and depletion flocculation.[42 43, 44, 45, 46, 47, 48, 49, 50, 51, 52, 53] The dominant mechanism depends both on the system and on the polymer concentration. For example, steric stabilisation and depletion effects are usually observed at higher polymer concentrations,[20, 52, 54] whilst bridging flocculation is normally associated with a relatively low polymer concentration. Bridging flocculation and steric stabilisation are particularly pertinent to the work presented in this thesis.

1.2.1 Polymer Adsorption

There are two main types of polymer adsorption. Physisorption is the interaction of the adsorbate with the interface via interactions such as van der Waals forces and hydrogen bonding. Chemisorption is when the polymer becomes chemically bonded to the substrate surface. For homopolymers in solution, or indeed an AB diblock copolymer in a non-selective solvent, adsorption of individual copolymer chains will occur. Four main features characterise such adsorption; loops, trains, tails and bridges.[55] Tails are non-adsorbed polymer chain-ends, trains are sections of the polymer chain that are in direct contact with the surface, loops connect trains and have no physical contact with the surface, and bridges exist between particles (and lead to bridging flocculation). The mode and strength of adsorption can be assessed via the bound fraction (p). A low

bound fraction indicates weak adsorption with loops, bridges and tails, while a high bound fraction indicates adsorption of train segments.[56] The bound fraction can be determined via NMR spectroscopy based on the chain mobility in solution.[56] Infrared spectroscopy can also be used, with a shift in frequency indicating whether polymer segments are in a bound or un-bound state.[57]

1.2.2 Adsorption Isotherms

An adsorption isotherm is a useful way of quantifying the adsorbed amount of a polymer on a surface. Such an isotherm is generally a plot of the adsorbed amount of polymer (Γ) versus the equilibrium concentration of polymer remaining in solution after adsorption (C_{eq}). The point at which a typical adsorption isotherm reaches a plateau depends on a number of parameters. The available substrate surface area, molecular weight of polymeric adsorbate, polymer solvency and polymer composition must all be considered.[58, 59] For Langmuir adsorption (as found in this thesis), the adsorbed amount is calculated using equation 6:

$$\Gamma = \frac{q_m K_a C_{eq}}{1 + K_a C_{eq}} \tag{6}$$

Here Γ is the adsorbed amount (mg m^{-2}), q_m is the monolayer capacity, K_a is the equilibrium constant and C_{eq} is the equilibrium adsorbate concentration.[60, 61] The surface area of the substrate for adsorption must be known (in order to calculate the monolayer capacity, q_m), and the amount of adsorbate both initially added and remaining in solution following adsorption must also be known. Two Langmuir-like high affinity isotherms are shown in Figure 1.10 for PEO physically adsorbed onto silica and onto polystyrene latex in water, with the plateau region indicating monolayer coverage.[62]

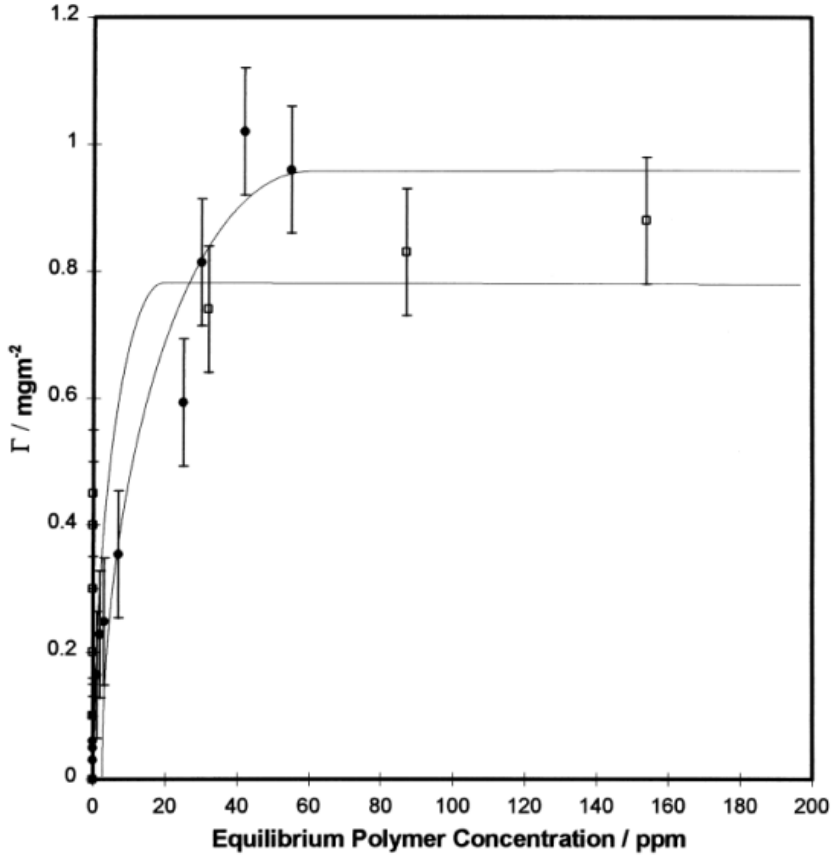

Figure 1.10. Adsorption isotherms for PEO physically adsorbed onto silica (circles) and onto polystyrene latex (squares) in water.[62]

It is often difficult to precisely determine the adsorbed amount of polymer at monolayer coverage using such a non-linear form of the isotherm. Plotting the Langmuir equation 6 in its linear form, see equation 7, enables an accurate monolayer capacity (q_m) to be determined from the gradient of the slope. A plot of C_{eq}/Γ versus C_{eq} gives a straight line.[61]

$$\frac{C_{eq}}{\Gamma} = \frac{1}{q_m} C_{eq} + \frac{1}{K_a q_m} \tag{7}$$

It is common to determine the adsorbed amount using an indirect approach. This involves determining polymer concentration in the continuous phase before and after adsorption. The adsorbed amount can then be calculated by difference. Centrifugation can be used to separate the colloidal substrate from the excess polymer. The polymer concentration in the supernatant can then be determined provided there is a convenient

spectroscopic handle to assess the polymer remaining in the continuous phase after adsorption. IR spectroscopy can be used,[63] but UV spectroscopy can be more convenient and more sensitive.[64] For example, a polystyrene-based copolymer can be quantified by using the UV aromatic chromophore at 262 nm. Such a method is suitable for monitoring the adsorption of such a polymer onto the surface of carbon black in *n*-alkanes.[65] The general protocol used for the adsorption isotherm studies conducted in this thesis is detailed in Figure 1.11.

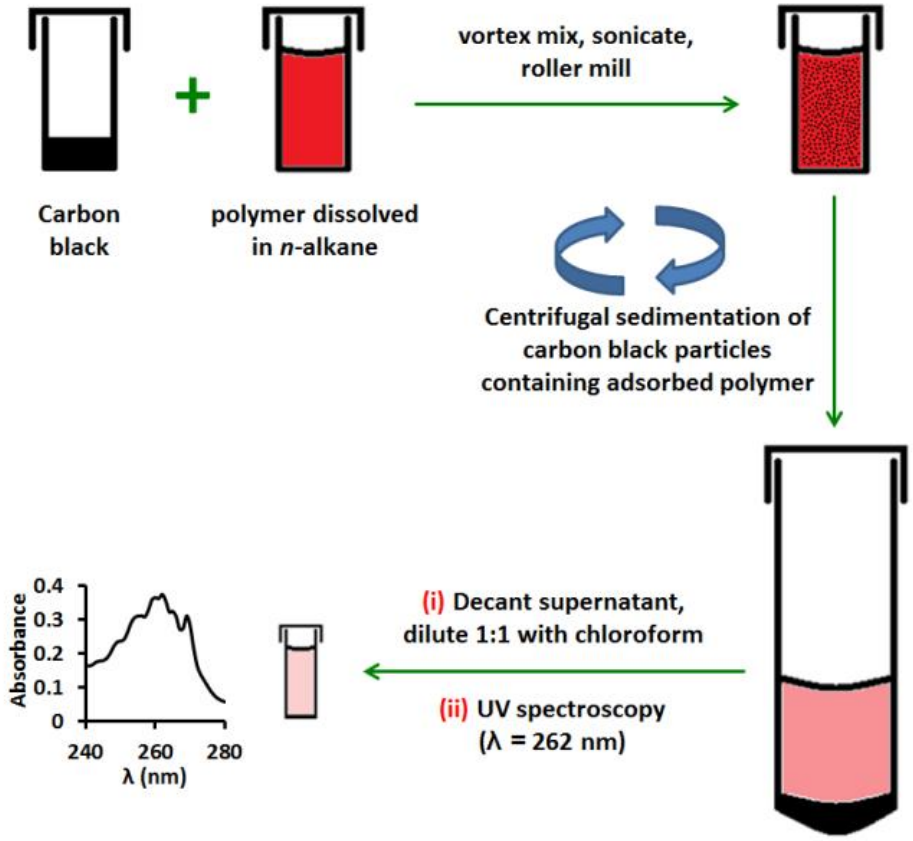

Figure 1.11. Protocol used to determine the adsorbed amount of copolymer on carbon black particles via a UV supernatant depletion assay, as used in this thesis.

It is essential to dilute the *n*-alkane supernatant with chloroform when studying the adsorption of polystyrene-core diblock copolymer micelles. Unlike *n*-alkanes, chloroform is a good solvent for polystyrene, which leads to dissociation of the micelles to produce molecularly-dissolved copolymer chains. This is important, because otherwise the micelles scatter the UV radiation, causing systematic errors in the supernatant assay.

1.3 Effect of polymers on colloidal stability of particles

Steric stabilisation is an important, generic and highly versatile colloidal stabilisation mechanism that is applicable for both aqueous and non-aqueous dispersions.[52] It has been widely used for many applications, including the preparation of inks,[66] latex paints[67] and coatings,[68] the efficient dispersion of diesel soot in engine oils,[34] and for the preparation of electrically conducting polypyrrole particles.[69] The appropriate design of effective steric stabilisers requires an understanding of the interaction of the polymeric stabiliser with the particle surface, the continuous phase, and also the conformation that the adsorbed polymer chain adopts at the solid/liquid interface.[50, 54] In particular, the polymeric stabiliser should be strongly adsorbed, provide high coverage of the particles and form a thick, well-solvated steric barrier in order to offset the ever-present attractive van der Waals forces operating between colloidal particles.

Ruehrwein and Ward first proposed the principle of bridging flocculation in 1952.[42] This phenomenon is now widely used for papermaking,[70] water treatment,[71] industrial effluent treatment,[72] and in the mining industry[73] to obtain efficient solid–liquid separations.[74] High molecular weight polymers are known to be particularly efficient bridging flocculants.[75] If the dimensions of the polymer chains are sufficiently large, then adsorption of such chains onto two or more particles can occur simultaneously, such bridging leads to particle aggregation, with strong kinetic effects being well-documented.[48, 76, 77] Specific interactions such as hydrogen bonding have been demonstrated to enhance the extent of bridging flocculation.[78, 79] It is also well-documented that initial bridging flocculation can be replaced by steric stabilisation at higher polymer concentrations.[80, 81]

There are numerous reports of bridging flocculation in the literature that are based on high molecular weight water-soluble polymers, for example the addition of poly(ethylene oxide) or polyacrylamide or poly(*N*-vinylpyrrolidone) to either silica sols or polystyrene latex in aqueous solution.[45, 79, 82, 83] However, there appear to be rather few studies of bridging flocculation in *non-aqueous* media.[84, 85] This subject is discussed in Chapter 3 of this thesis.

Depletion stabilisation arises from the exclusion depletion of free polymer between the surfaces of colloidal particles in solution when in close proximity. Closer approach of the particles can only be achieved by further depletion of the segment concentration between the particles, and in a good solvent for the polymer, this is energetically unfavourable.[51, 86, 87] Hence, the colloidal particles remain stable in solution without any direct interaction with the polymer in solution.

Depletion flocculation was first reported by Asakura and Oosawa in 1958.[88] The existence of a 'depletion zone' next to a surface in contact with a solution of non-adsorbing polymer was proposed, within which the polymer segment concentration is lower than that of the bulk solution. Such a depletion zone exists as a result of the restricted conformational entropy of the polymer chains in this region, which is not compensated by sufficient adsorption energy. The lower polymer segment concentration thus causes flocculation.[53]

1.4 Polymers as Steric Stabilisers

Block copolymers are of particular importance for steric stabilisation in colloidal systems. It is well-documented that AB diblock copolymers form colloidal aggregates when dissolved in a solvent that is selective for one of the two blocks.[89, 90] If the volume fraction of the soluble block is sufficiently large to confer steric stabilisation, well-defined spherical micelles are generally obtained.[91, 92, 93, 94] So-called *star-like* micelles are formed if the soluble block is relatively long compared to the core-forming solvophobic block.[95] On the other hand, if the solvophilic block is significantly shorter than the core-forming block, then so-called *crew-cut* micelles are produced.[96] Over the last two decades there have been numerous literature examples of amphiphilic AB diblock copolymers forming spherical micelles in aqueous solution.[24, 97, 98, 99, 100, 101] There is also a considerable volume of older literature describing the micellisation behaviour of wholly hydrophobic AB diblock copolymers in organic solvents.[91, 102] In particular, polystyrene-based AB diblock copolymers that form polystyrene-core micelles in non-polar solvents such as *n*-alkanes have been extensively studied.[103, 104, 105, 106, 107, 108] Such diblock copolymers are readily prepared using anionic

polymerisation,[109, 110] the soluble block usually based on either polybutadiene, polyisoprene or their hydrogenated derivatives.[104, 105, 106, 111, 112, 113, 114, 115]

There have been a number of reports describing the interfacial adsorption of block copolymer micelles.[34, 116, 117, 118, 119, 120] For example, Winnik *et al*. reported the adsorption of poly(ethylene oxide)-polystyrene diblock copolymer micelles onto polystyrene latex particles from aqueous solution,[121] while Alexandridis *et al*. found that even rather weakly hydrophobic anchor blocks based on poly(propylene oxide) are sufficient to enable relatively high affinity adsorption of Pluronic block copolymer micelles onto either carbon black at pH 7[122] (see Figure 1.12) or silica at low pH.[123] Thomas and co-workers used neutron reflectivity to confirm the presence of cationic diblock copolymer micelles adsorbed at the air-water interface.[124] Also, Webber and co-workers showed that similar copolymers also adsorb at the planar mica/water interface to produce ordered micelle monolayers, as visualised directly by atomic force microscopy.[125, 126] Such adsorbed micelle layers can confer effective steric stabilisation,[49] which may offer technological advantages for aqueous ink dispersions based on carbon black particles,[127] or act as soot dispersants in non-aqueous engine oil formulations.[34]

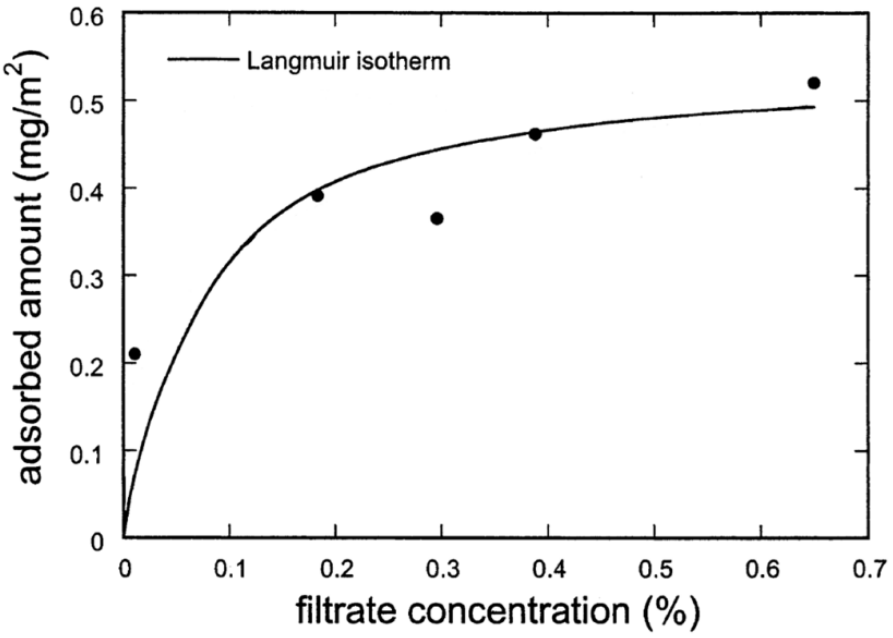

Figure 1.12. Langmuir adsorption isotherm for the adsorption of Pluronic poly(ethylene oxide)-poly(propylene oxide)-poly(ethylene oxide) block copolymer micelles onto carbon black at 24°C, pH 7.[122]

1.5 Polymers as Bridging Flocculants

The star diblock copolymer architecture is particularly relevant to the study of polymer-induced bridging flocculation. Star diblock copolymers have been examined for various potential applications, including drug carriers[128] and thermo-responsive gelators.[129,130, 131, 132] The synthesis of such star diblock copolymers can be achieved using anionic polymerisation,[28] atom transfer radical polymerisation[133] or reversible addition-fragmentation chain transfer (RAFT) polymerisation.[134] Alonzo and co-workers[76] recently reported the kinetics of adsorption of polystyrene poly(2-vinylpyridine) (PS-P2VP) star diblocks onto a planar silicon surface from toluene. Figure 1.13 shows a schematic cartoon representing the likely adsorption in this case, where the P2VP corona block interacts preferentially with the silicon surface. A dome-like structure is formed by the adsorbed copolymer, with concentration-dependent adsorption kinetics being observed in situ using a phase-modulated ellipsometer. Initially, adsorption was rapid, followed by a progressively slower rate of adsorption as the equilibrium adsorbed amount was attained. The overall timescale for adsorption was ~ 2.8 hours.[76]

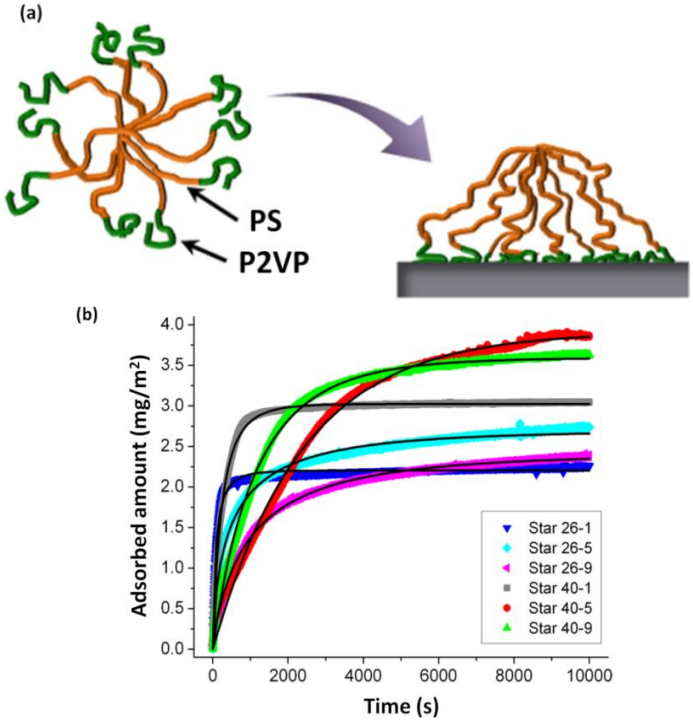

Figure 1.13. (a) Schematic illustration of the adsorption of a polystyrene-core polystyrene-poly(2-vinylpyridine) (PS-P2VP) star diblock copolymer onto a planar silicon surface from toluene at 25°C. (b) Kinetics of adsorption for a selection of these star copolymers (first number in sample code is number of arms, second number is styrene to vinylpyridine ratio).[76]

Star diblock copolymers are also used as viscosity modifiers in engine oil formulations.[35, 135, 136] The appropriate choice of polymer allows a lubricant to meet high-temperature viscosity specifications whilst maintaining acceptable low-temperature fluidity.[137] Star diblocks allow good thickening performance to be achieved, although their effect on other engine oil properties must also be considered. For example, bridging flocculation of soot particles may cause adverse engine component wear. The influence of a commercial star diblock copolymer on the colloidal stability of carbon black particles in non-polar *n*-alkanes is discussed in Chapter 3.

1.6 Carbon black – A model colloidal substrate

The generic term 'carbon black' is used to describe a range of industrial products; thermal, furnace, channel and acetylene blacks.[138] Each of these comprise elemental carbon, usually in the form of fractal structures of aggregates, which are in turn made up of 5-10 nm primary particles (see Figure 1.23). Small angle X-ray scattering (SAXS) analysis of a commercial carbon black is described in Chapter 3. Carbon black can be obtained by the partial combustion of hydrocarbons. Thermal decomposition can also be used, whereby carbon black is formed in the absence of oxygen. Carbon black manufacture on an industrial scale is conducted under precisely controlled conditions by this method.[138] Transmission electron microscopy images of two typical commercial carbon blacks (Regal 250R and Elftex 8, Cabot Corporation, Billerica, USA) are shown in Figure 1.14. Regal 250R is used throughout this thesis.

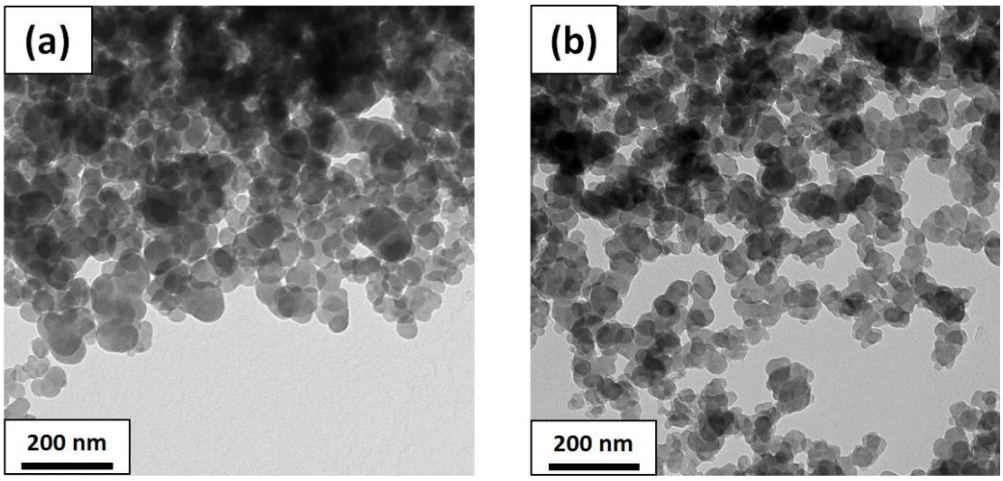

Figure 1.14. Transmission electron microscopy images of (a) Regal 250R and (b) Elftex 8 carbon blacks.

Carbon black is a cheap and readily available material. A number of papers have been published detailing both the surface chemistry and structural morphology of carbon blacks in various systems.[139, 140, 141, 142] It has many uses, including black ink for inkjet printing,[143] as a filler for vehicle tyre formulations,[144] as a semiconductor for plastic materials[138] and, of particular relevance to the current work, as a soot mimic for engine oil optimisation studies (see Section 1.9.5 of this Chapter).[145] Such a mimic is required because of the costly and labour-intensive route required to obtain genuine engine soot.[145] In Chapter 5, a particular carbon black (Regal 250R) is compared directly to genuine diesel soot in order to validate the use of such a model colloidal substrate.

1.7 Analytical Centrifugation

Characterisation of the stability of dispersions is crucial for gaining a greater understanding of these systems, which are important for various fields such as coatings,[146] paper making,[70] ceramics[147] and cosmetics.[148] Detailed knowledge of the particle size distribution (PSD) is highly desirable. In this respect, determination of the PSD by analytical centrifugation has great potential, although it is a relatively new technique in this area. The general method dates back to 1925, and was developed by Svedberg to assist for his studies of colloids and proteins. He was awarded the 1926 Nobel Prize for his invention.[149]

A LUMiSizer® instrument has been used to assess the dispersion stability of carbon black particles in this thesis. To extend the measurement range to include higher particle concentrations, two effects must be taken into account. Firstly, hindered settling, which is a manifestation of particle–particle interactions and secondly, multiple scattering affecting the optical detection system.[150, 151] PSDs of dispersions are measured by particle sedimentation in a centrifugal field. Analysis of the variation of extinction at a particular position during the measurement is performed by using either the line start or homogeneous start technique.[150] Such a method (also known as Constant Position analysis) leads to an integral which is solved approximately. It is essential that all particles have passed the near IR light detector prior to analysis. Figure 1.15 displays the instrument set-up. Typical measurement times as conducted in this thesis are 60-90 minutes. Up to 12 samples can be measured simultaneously, the centrifugal speed can

be varied between 200 and 4000 rpm and the instrument temperature can range from 4°C to 60°C.

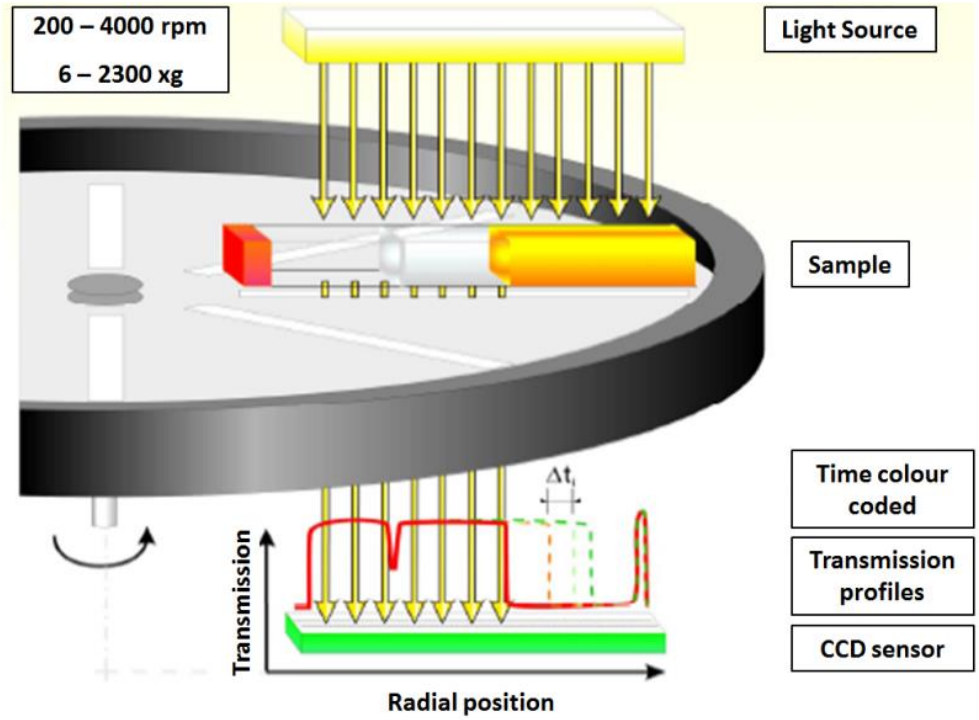

Figure 1.15. Analytical centrifugation set-up for the LUMiSizer® instrument.[151]

The basic principles of the LUMiSizer® are the same as those for disc centrifuge photosedimentometry (DCP).[152, 153, 154, 155] This instrument was chosen in preference to DCP for the work conducted out in this thesis due to the relative ease of sample preparation and lack of cleaning between sampling (LUMiSizer® cells are disposable, where the DCP disc requires careful cleaning between samples). Moreover, the variable temperature feature is useful for temperature-dependent studies and the ability to analyse twelve samples simultaneously enables high throughput.

The dispersion of interest is added to a 2 mm path length polyamide centrifuge cell, then near IR light (λ = 870 nm) is transmitted through the transparent cell stroboscopically as the centrifuge rotates. As the dispersion sediments to the bottom of the cell under the centrifugal field, an increase in light transmission is observed, giving raw profile plots of transmission versus cell position (see Figure 1.16).

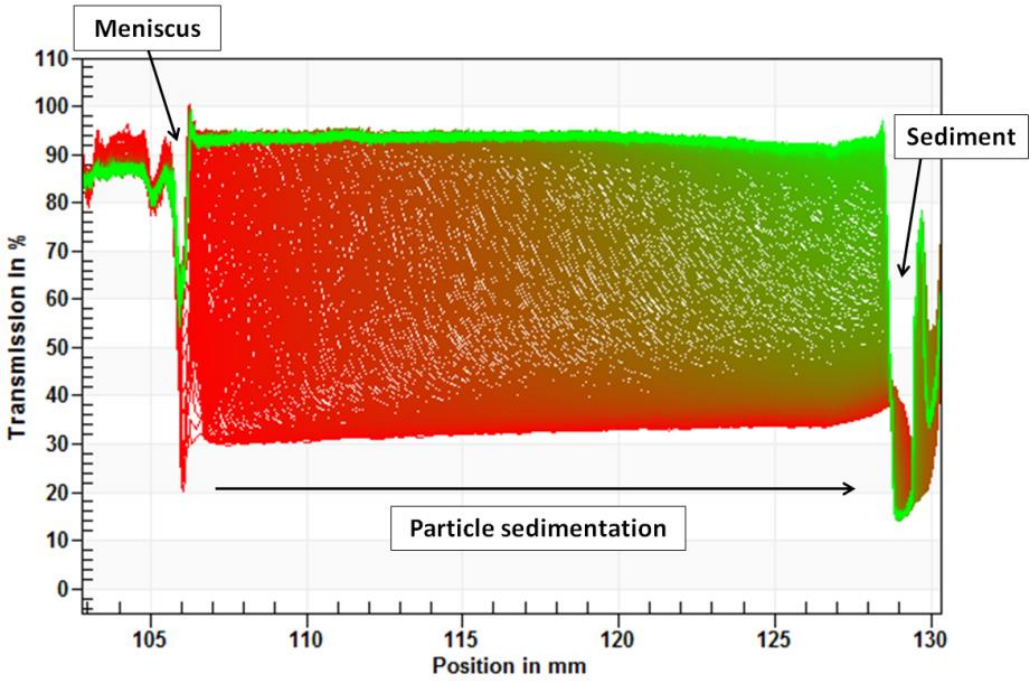

Figure 1.16. Typical raw profile sedimentation plot obtained by analytical centrifugation (LUMiSizer®) for 500 nm silica in water at 1 wt% (density 1.99 g cm^{-3}).

The solution meniscus is located from the characteristic reduction in transmission, as shown in Figure 1.16. The variation of colour indicates when each transmission profile was recorded, red being the first and green the last. These raw profile plots can be used as qualitative analyses of dispersion stability. If two dispersions are subjected to the same centrifugal field, their relative colloidal stabilities can be assessed.

Transmission profiles can also be converted into particle size distributions using Stokes' Law. For this analysis, the density and viscosity of the continuous phase are required, plus the density of the dispersed particles, see equation 8.

$$X = \sqrt{\frac{18.\eta_F}{(\rho_P - \rho_F).\omega^2.t_m}}.\ln\left(\frac{r_m}{r_0}\right) \quad (8)$$

Here, X is the mean volume-average particle diameter, η_F is the viscosity of the continuous phase, ρ_P is the density of the particles, ρ_F is the density of the continuous phase, ω is the angular velocity (rad s^{-1}), t_m is the time taken for the particles to reach

the measurement position, r_m is the measurement position recorded at t_m and r_0 is the original position of the meniscus.

1.7.1 Determining the Effective Particle Density

As indicated by equation 8, it is essential to know the density of the dispersed particles in order to determine an accurate volume-average particle diameter. For example, if sterically-stabilised particles are being sized, the density of both the core and the shell must be known, and a resulting *effective* composite density must be calculated. When a diblock copolymer adsorbs onto the surface of carbon black, the overall particle density is significantly reduced. This is because the resulting solvated copolymer shell is much less dense than the carbon black core. To a good approximation, the shell density is equal to that of the continuous phase. Analytical centrifugation can be used to determine this reduced effective particle density. Thus, Stokes' law is used in combination with particle velocities, which are deduced via analytical centrifugation measurements.[150] In principle, centrifugation of sterically-stabilised carbon black dispersions prepared in two comparable solvents with differing densities and viscosities (for example, *n*-dodecane and d_{26}-dodecane) should produce two different particle velocities (V_1 and V_2), see equations 9 and 10.

$$V_1 = \frac{(\rho_p - \rho_{F,1}) \cdot X^2 \cdot \omega^2}{18 \cdot \eta_1} \cdot r \qquad (9)$$

$$V_2 = \frac{(\rho_p - \rho_{F,2}) \cdot X^2 \cdot \omega^2}{18 \cdot \eta_2} \cdot r \qquad (10)$$

Here ρ_P is the particle density, $\rho_{F,1}$ (or $\rho_{F,2}$) is the solvent density, η_1 (or η_2) is the dynamic viscosity of the solvent, ω is the angular velocity, X is the diameter of the particles and r is the position of the measurement taken. Combining equations 9 and 10 to eliminate the experimental constants X, ω, r and rearranging terms leads to an expression for the effective density, ρ_P, see equation 11.

$$\rho_p = \frac{(V_1 . \eta_1 . \rho_{F,2}) - (V_2 . \eta_2 . \rho_{F,1})}{(V_1 . \eta_1) - (V_2 . \eta_2)} \quad (11)$$

Thus an effective particle density can be deduced, which then enables physically realistic volume-average particle diameters to be determined. A typical volume-average particle size distribution obtained for a 1.0 % w/v aqueous dispersion of 500 nm silica particles by analysis of the raw profile sedimentation plot (see Figure 1.16) is shown in Figure 1.17.

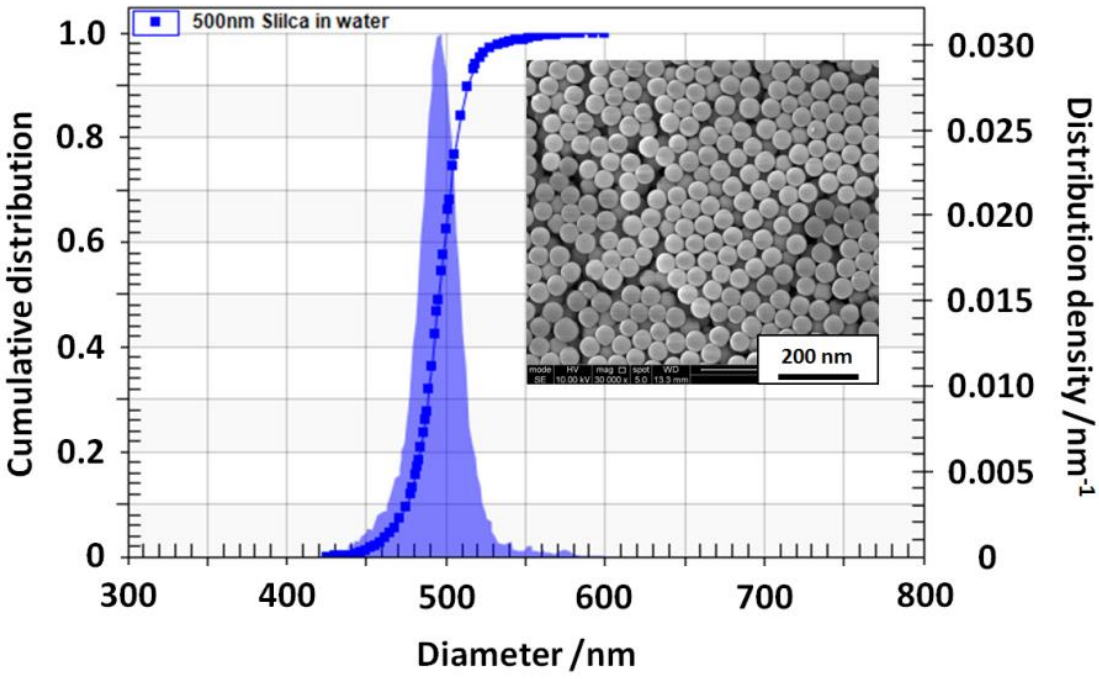

Figure 1.17. LUMiSizer® volume-average particle size distribution obtained for a 1.0 % w/v aqueous dispersion of 500 nm silica particles by analysis of the raw profile sedimentation plot shown in Figure 1.16. Inset shows an SEM image for these silica particles.

1.8 Small Angle X-ray Scattering

Small angle X-ray scattering (SAXS) is a robust technique that can be applied to characterise many colloidal systems.[156] In scattering experiments, the particle length scale is inversely proportional to the scattering vector (q), which is defined by equation 12.

$$q = k_i - k_s \tag{12}$$

Here k_i is the incident wave vector, k_s is the scattered wave vector, θ is half of the angle between the incident beam and the scattered wave vector (see Figure 1.18) and λ is the wavelength of the incident X-ray beam.

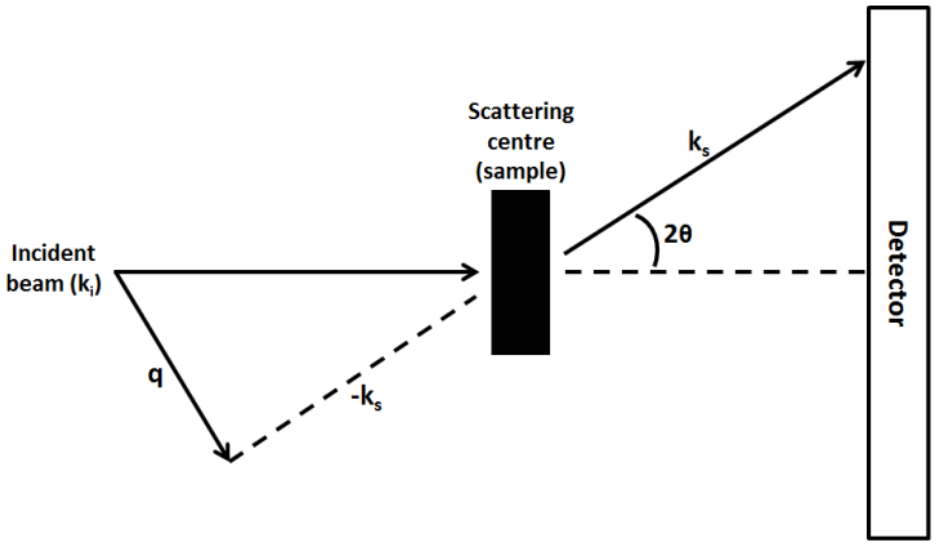

Figure 1.18. Schematic representation showing the typical scattering of an incident beam and illustrating the various terms defined in equation 12.

In Figure 1.18, the isosceles triangle has two sides of equal length $2\pi/\lambda$, which give equation 13 via trigonometry.

$$q = \frac{4\,\pi\,sin\theta}{\lambda} \tag{13}$$

Substitution of the Bragg law of diffraction (equation 13) into equation 14 gives an expression that relates the scattering length scale (d) to the scattering vector (q), see equation 15.

$$\lambda = 2\,d\,sin\theta \tag{14}$$

$$d = \frac{2\,\pi}{q} \tag{15}$$

X-ray scattering is useful over length scales of ≈ 1-1000 nm. Figure 1.19 puts this into perspective relative to other available scattering techniques.

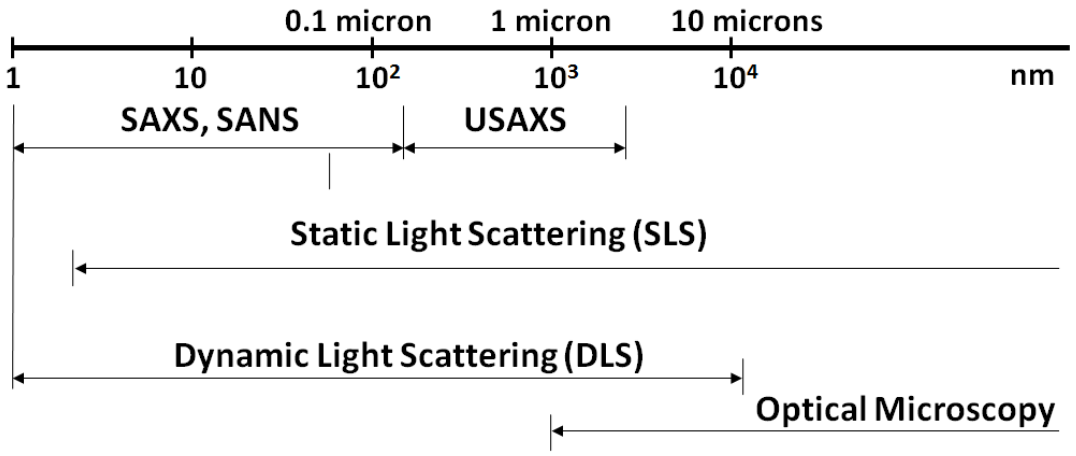

Figure 1.19. Typical length scales probed by various scattering methods, where SANS is small angle neutron scattering and USAXS is ultra-small angle X-ray scattering.

A typical X-ray scattering pattern contains a huge amount of information about both the shape and the size of the scattering object (form factors) and also the inter-particle interactions (structure factors). In order to extract such data, a suitable model is used to fit the scattering pattern based on background knowledge of the sample from other techniques such as DLS and transmission electron microscopy (TEM).

SAXS is particularly well suited for the study of polymer adsorption onto colloidal substrates, such as carbon blacks, because of the high electron density contrast between the particle and the polymer. Measurements are generally conducted at 1-10 % w/w solids and provide size, shape and structural information. Moreover, SAXS is usually non-destructive, and is statistically robust, since millions of particles are analysed.

The use of SAXS to characterise diblock copolymers in solution is well known.[65, 115, 157] For example Di Cola *et al.* examined the micellar structures of poly(styrene-*b*-isoprene) diblock copolymers in selective solvents over various temperatures.[158] Spherical micelles, cylindrical micelles and vesicles were identified by SAXS by varying the solvents for each block. Complete micellar dissociation was observed above 80°C, which was fully reversible on cooling. The effect of temperature on diblock copolymer morphology has also been studied by Fielding *et al.* for poly(lauryl methacrylate)-*b*-poly(benzyl methacrylate) (PLMA−PBzMA) in *n*-dodecane.[159] Transmission electron microscopy was also used in combination with SAXS to investigate the structural changes that occurred during a worm-to-sphere-to-worm thermal cycle. Figure 1.20 shows (a) the synthesis of $PLMA_{16}$−$PBzMA_{37}$ and (b) the thermo-responsive behaviour exhibited by 20% w/w $PLMA_{16}$−$PBzMA_{37}$ diblock copolymer nanoparticles in *n*-dodecane, Figure 1.21 shows the X-ray scattering patterns obtained between 20°C and 160°C.

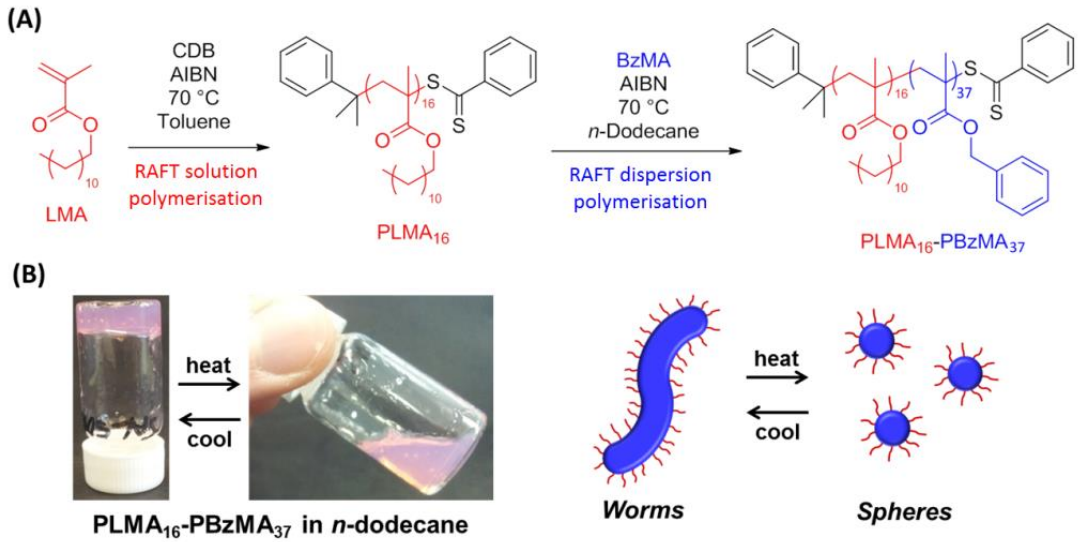

Figure 1.20. (A) Synthesis of PLMA macro-CTA via RAFT solution polymerisation of LMA in toluene at 70°C, followed by RAFT dispersion polymerisation of BzMA in *n*-dodecane at 70°C. (B) Thermo-responsive behaviour exhibited by 20% w/w $PLMA_{16}$−$PBzMA_{37}$ diblock copolymer nanoparticles in *n*-dodecane, plus schematic representation of the corresponding change in copolymer morphology. A soft free-standing gel is formed at 20°C, which becomes a free-flowing solution on heating to 70°C. This thermal transition is reversible: a worm gel is reformed on cooling to 20°C.[159]

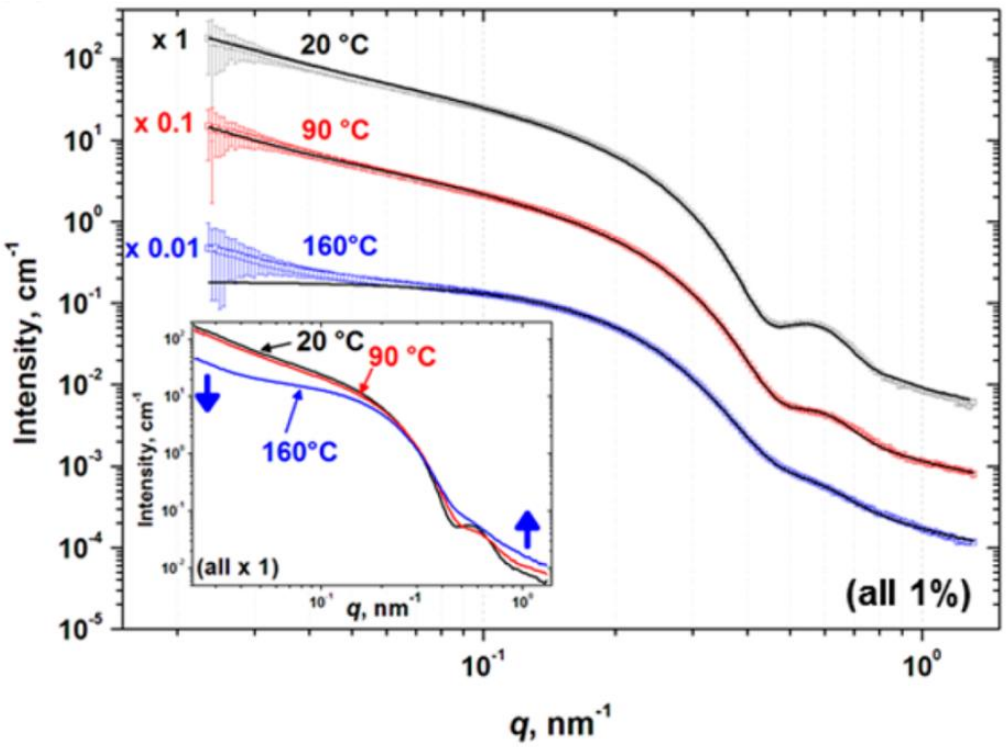

Figure 1.21. SAXS patterns recorded for a 1.0 % w/w dispersion of $PLMA_{16}$–$PBzMA_{37}$ nanoparticles in *n*-dodecane on heating from 20°C to 160°C. Patterns are offset by a factor of 0.1 (90°C) and 0.01 (160°C) for clarity; fits to the data (solid lines) are shown as black lines. Inset shows all three scattering patterns plotted on the same scale.[159]

These SAXS experiments yielded the mean worm core cross-section, worm contour length and solvent fraction in the particle core.[159] In a typical I(q) versus q plot (see Figure 1.21), the low q (Guinier) region is particularly useful for assessing particle morphology. A gradient of zero in this region indicates a spherical morphology, whereas a gradient of negative unity is characteristic of anisotropic particles (rods).[160] In the study by Fielding *et al.*,[159] the $PLMA_{16}$–$PBzMA_{37}$ worms were found to be highly anisotropic but relatively flexible, so a gradient close to (but less than) negative unity was obtained in this region.

Detailed SAXS analysis requires relatively low copolymer concentrations to avoid inter-particle interactions, which otherwise suppress the scattering intensity at low q.[161, 162] Scattering patterns can be fitted to established models available in the literature. The scattering patterns shown in Figure 1.21 were analysed using a worm model.[163, 164] The

total worm cross-section was calculated to be 15.4 nm and the worm contour length exceeded 600 nm, indicating highly anisotropic particles.[159] These values are consistent with TEM observations (see Figure 1.22).

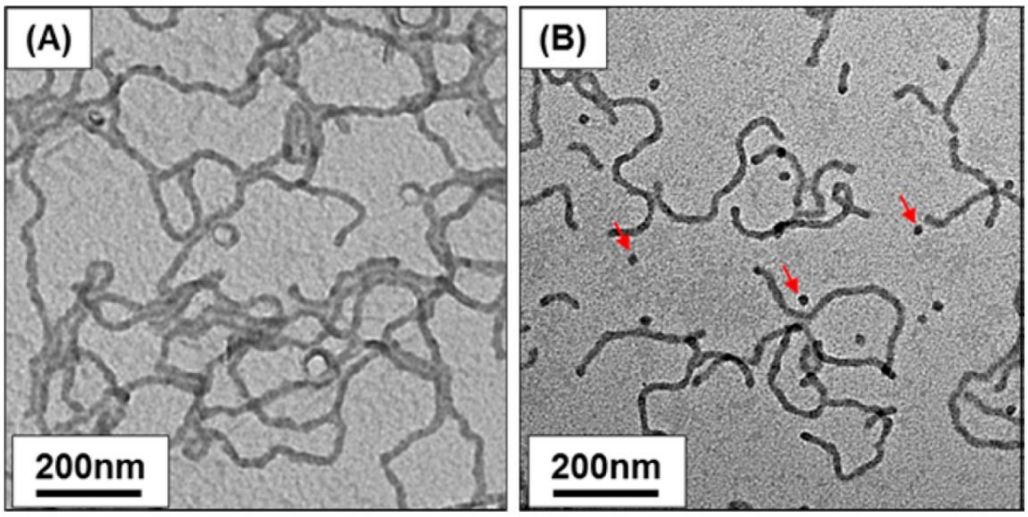

Figure 1.22. TEM images recorded for a 20% w/w $PLMA_{16}$–$PBzMA_{37}$ worm gel. Initially, highly anisotropic worms are observed at 20°C on dilution to 0.01% w/w solids [see image (A)]. On heating this 20% w/w gel to 90°C, degelation occurs. Allowing the hot 20% w/w worm gel to cool from 90 to 20°C (followed by dilution to 0.01% w/w solids prior to preparing a TEM grid) revealed mainly a worm phase [see image (B)], with a minor population of isolated spheres (see red arrows).[159]

Another important finding from this SAXS study was that these $PLMA_{16}$– $PBzMA_{37}$ worms are relatively stiff, because their Kuhn length (160 nm) was an order of magnitude greater than the mean worm cross-section. Also, SAXS studies indicated that there was little/no solvation of the core-forming PBzMA block at 20 °C in *n*-alkanes.[159] SAXS was also used to calculate a radius of gyration of 1.3 nm for the coronal PLMA block. This value is close to that estimated from the mean degree of polymerisation of the PLMA block. On heating to 90°C, the mean worm cross-section remained constant, but the worm contour length was reduced from 600 to ≈350 nm, which indicated partial worm disintegration. SAXS also showed that the degree of core solvation increased at this temperature (suggesting ingress of *n*-dodecane into the PBzMA core). On further heating to 160°C, the SAXS pattern could only be satisfactorily fitted to a model for isotropic particles (total worm cross-section = 15.1 nm, worm contour length = 17.3 nm, and worm Kuhn length = 16.8 nm). This indicated that the original worm-like particles

in the dispersion had been transformed into spherical micelles (see the upturn in the scattering curve at very low *q*, Figure 1.21). Overall, this study highlighted the wealth of knowledge that can be gleaned from SAXS analysis. A similar thermally-induced diblock copolymer morphology has been characterised by DLS, TEM and SAXS in Chapter 2.

The study of fractal and aggregate morphologies of carbon blacks and soots via SAXS is also well documented. The structural morphology of both soot and carbon black particles is best described as a hierarchy composed of five species: fractal agglomerates at the micron length scale, both aggregates and primary particles at the nm scale, sub-units (a turbostratic structure formed by carbon graphite-like layers) at the sub-nm scale and finally the carbon graphite-like layers at the atomic scale.[165, 166, 167, 168, 169] A schematic cartoon depicting the three largest structures is shown in Figure 1.23.

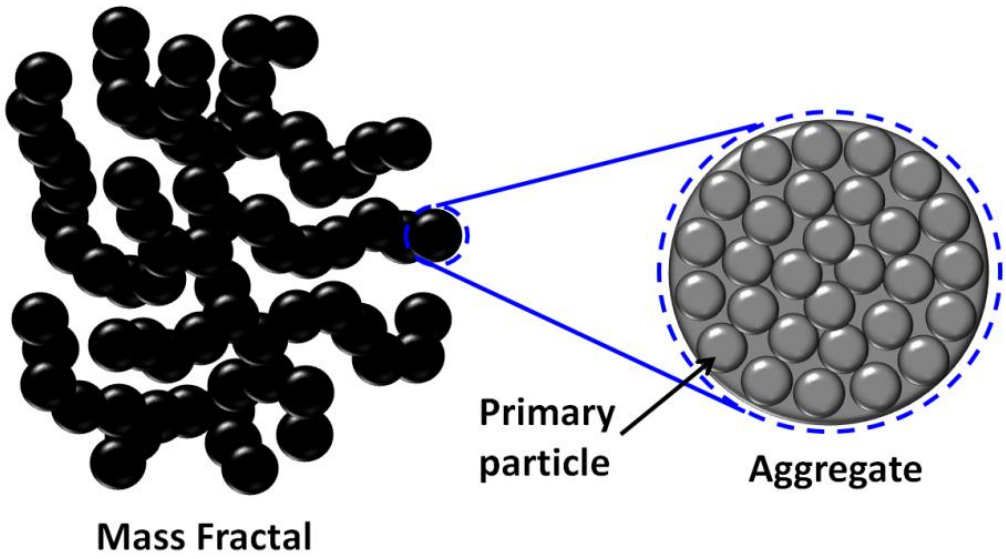

Figure 1.23. Schematic cartoon representing the hierarchical structure of a typical carbon black mass fractal. SAXS patterns obtained from this material are described in Chapter 3.

The study of copolymer-coated carbon black particles by SAXS is rather less well documented. Carbon blacks are often used as fillers within polymers, as they improve the mechanical and electrical properties of the host material.[141, 170] Rieker *et al.* concluded that, on loading carbon black into polymer matrices, the processing of the resulting composites has a strong influence on the extent of interpenetration of carbon

black mass fractals.[141] It was also found that the arrangement of aggregates can be controlled by the loading of carbon black in carbon black/polymer composites. The use of SAXS in this study was invaluable, since it revealed how the degree of interpenetration dramatically changed for a given composite by either changing the method of dispersion or the choice of matrix.[141] In the current work, a direct study of the adsorption of a poly(styrene-*b*-hydrogenated isoprene) star diblock copolymer onto the surface of a commercial carbon black has been studied (see Chapter 3).

1.9 Engine oils

1.9.1 Diesel engines

Over the past two decades, the use of diesel engines for both commercial and domestic vehicles has increased dramatically as a result of greater fuel efficiency (due to higher thermal efficiency[171]), as well as lower engine running costs. With the current increase in the cost of fuel, the case for the diesel engine is becoming even more apparent, since it enables greater fuel economy, whilst providing similar performance to the more traditional spark-ignition petrol engine. However, although more fuel-efficient, particulate emissions from diesel engines can be up to 80 times greater.[172] This results in a number of problems, not least of which being the negative impact on air quality. Although this problem can be minimised by using a diesel particulate filter (DPF)[173] integrated into the engine gas exhaust system, the particulate matter also causes problems elsewhere, specifically within the engine itself. This problem is accentuated by the use of exhaust gas recirculation (EGR).[171, 172, 174] This system is fitted to most modern diesel engines in order to reduce the emission of oxides of nitrogen (NO_x).[172] In EGR, a small proportion of exhaust gas is fed back into the engine intake, which dilutes the fresh air mixture entering the engine prior to combustion.[174] Although beneficial in terms of harmful emission reduction, the process re-introduces organic particulate matter at the beginning of the engine cycle, which in turn has adverse long-term effects on the engine itself.[174]

The primary component of diesel engine particulate matter is soot, which forms colloidal aggregates of approximately 500 nm in diameter.[174] When introduced to the internal components of the engine, these aggregates have the potential to dramatically

increase abrasion between component surfaces and in turn produce mechanical wear within the engine. This reduces engine efficiency (due to frictional power loss), and ultimately prevents the engine from functioning as intended. Furthermore, soot increases the viscosity of the engine oil. This also accelerates component wear, as the lubricant becomes too viscous for efficient flow and hence fails to adequately penetrate precisely engineered low tolerance components.[171] Esangbedo *et al*. investigated the effect of diesel soot concentration on engine oil viscosity, see Figure 1.24.[175] A rapid increase in viscosity with soot concentration occurred; the explanation for this observation was excessive soot agglomeration within the engine oil. This phenomenon was found to be dependent on the nature of the soot, with lower surface functionalisation leading to poorer dispersion efficiencies (presumably as a result of weaker dispersant-soot interactions).[175]

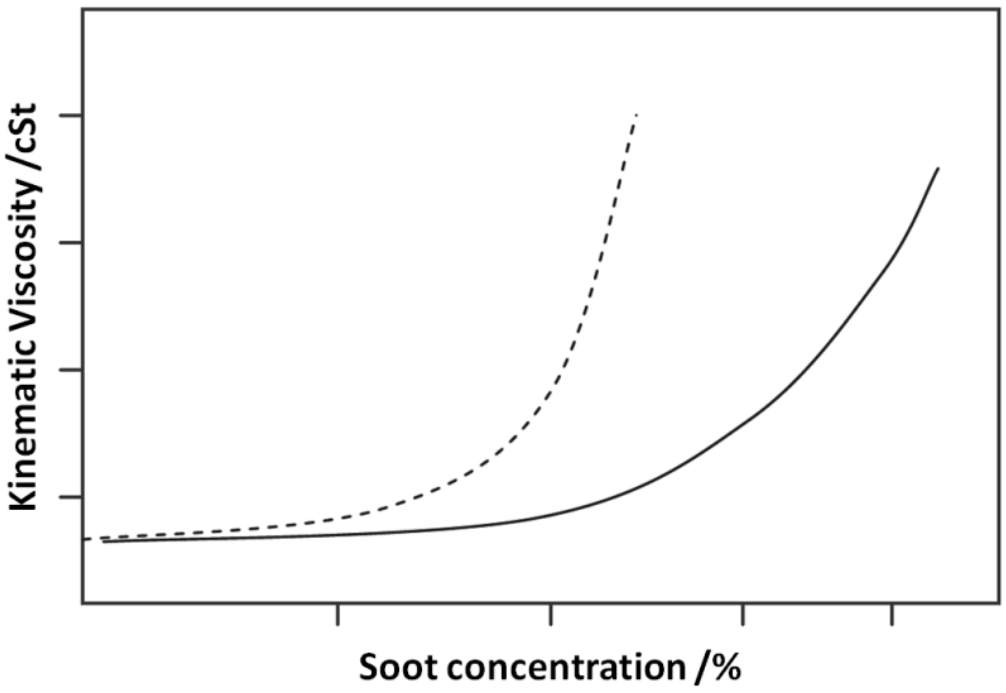

Figure 1.24. Representation of the rapid increase (----) in oil viscosity in a heavy duty diesel engine test compared to a more desirable viscosity profile (—).[175]

1.9.2 Engine component wear

The five major wear mechanisms in a diesel engine are abrasion, adhesion, fatigue, corrosion and lubricant breakdown.[171] Abrasion, adhesion and fatigue are physical processes in which metal surface contact and bridging of surfaces by colloidal particles leads to damage of engine components. Lubricant breakdown and corrosion are processes that involve a series of *chemical* reactions leading to wear. For the above five forms of wear, lubricant contamination is the predominant factor for component degradation. This involves loss of oil formulation properties such as viscosity, plus the accumulation of side-products from the degradation process.[171] Soot particles that are transported into the lubricant with blow-by gases (gasses that pass between the piston and the bore) combine in situ with anti-wear and viscosity modifiers, in turn reducing wear tolerance and adversely affecting engine oil viscosity. Figure 1.25 shows an SEM image of a typical wear scar caused by a 3% soot in oil blend.[172]

Figure 1.25. SEM image of a typical wear scar on a three-body wear machine caused by a 3% soot in oil blend.[172]

1.9.3 Engine oil formulations

In order to combat the adverse effects of internal damage and engine component wear, a high-performance lubricant is essential. This component has a number of functions, including separation of moving parts, neutralising acids to prevent corrosion, dissipating heat, protecting wear surfaces, and suspending/dispersing contaminants, thus allowing the engine to run as smoothly and efficiently as possible.[174]

To overcome such challenges, various functional additives must be included in an engine oil formulation. Such additives are split into two groups.[176] Firstly, viscosity modifiers, which are designed to maintain a relatively constant viscosity by reducing the base oil viscosity at lower temperatures and increasing it at higher temperatures. Such additives also adsorb onto metal surfaces, in turn acting as boundary lubricants. Figure 1.26 shows a schematic cartoon of such a process.[177, 178]

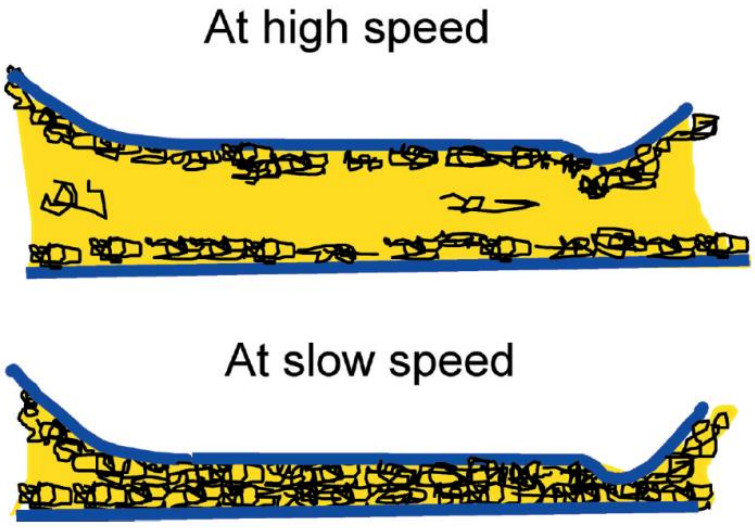

Figure 1.26. Schematic cartoon showing the nature of an adsorbed polymer film and its resulting influence under thin film lubrication conditions (where the blue line indicates a metal surface). High engine speed causes greater oil flow.[177]

The second group of additives are known as performance additives. This group can be divided into six categories: Antiwear agents (such as zinc dithiophosphate (ZDP)) form wear-resistant coatings on the surface of metal parts. Detergents and dispersants prevent hard deposits from forming on engine parts and keep sludge precursors suspended in the oil, which can then be removed when the oil is changed. Antioxidants are used to prevent oxidation of formulation components, hence extending the service interval. Rust and corrosion inhibitors protect the engine against moisture and from acids in the exhaust gases. Friction reducers help to maximise the energy efficiency from the combustion of a given quantity of fuel. Finally, defoamants displace air from oil to protect the integrity of the lubricant.[145, 172]

Further additives are also incorporated in specific formulations, including seal conditioners (which cause seals and gaskets to swell, hence preventing oil leaks where gaps and joints between components might otherwise exist), metal deactivators to prevent oxidation on component surfaces, pour point depressants, which ensure that the desired viscosity/pourability of the oil is maintained at lower temperatures, extreme pressure agents (enhancing the pressure resistance of the oil), and wax crystal modifiers (dewaxing aids), which prevent oil filter blockages at lower temperatures.[179] It is imperative that each additive does not adversely affect the functions of other additives in the formulation, thus inter-additive interactions are an important consideration when optimising formulations.[180]

During its life cycle, an engine lubricant undergoes extensive chemical changes as a result of oxidative high temperature degradation, as well as contamination by water, fuel, wear materials, ethylene glycol and soot.[181] Ultimately, engine oil reaches the end of its life as a result of this contamination and degradation. This leads to inferior performance as a result of, for example, changes in viscosity (which increases because of particulate matter and additive degradation[171]). Contaminated dispersants also cease to function efficiently under such conditions.[171, 172] At this point, the oil needs to be changed, which removes the internal contamination from the engine and allows a fresh allocation of engine oil lubricant to prolong the lifespan of the engine.[181]

1.9.4 Soot dispersion and copolymer dispersants

The dispersion of soot is a major consideration in engine wear reduction. Extensive internal damage can result from abrasion caused by soot aggregates located between moving parts in the engine.[172, 174] As a consequence, the development of dispersion additives for use in engine oils has been at the forefront of lubricant-based research for the last few decades.[10, 11, 182] These additives must not only disperse soot aggregates, but also work harmoniously with other additives present in the engine oil.[12] For this reason, there is usually a set limit to the amount of dispersant that can be added to a given formulation. For example, too much dispersant additive can actually accentuate the problem of internal corrosion, due to the free amines generally associated with such olefin copolymer dispersants.[174]

Dispersant OCPs

The most common, cheap and readily available engine oil additives used for the dispersion of soot are derivatives of linear olefin copolymers (OCPs).[12] These generally contain pendant succinimides, which promote adsorption onto the soot surface (see Figure 1.27). The long-chain OCP backbone can also act as a viscosity modifier in the oil formulation.[12] Careful consideration must be given with regard to the proportion of dispersant used, hence allowing an appropriate balance between adequate dispersion and minimal corrosion.[174] Physical and chemical interactions with other engine oil additives can adversely affect OCP dispersant efficiency and function and intermolecular association of such additives can also produce unwanted gels.[12]

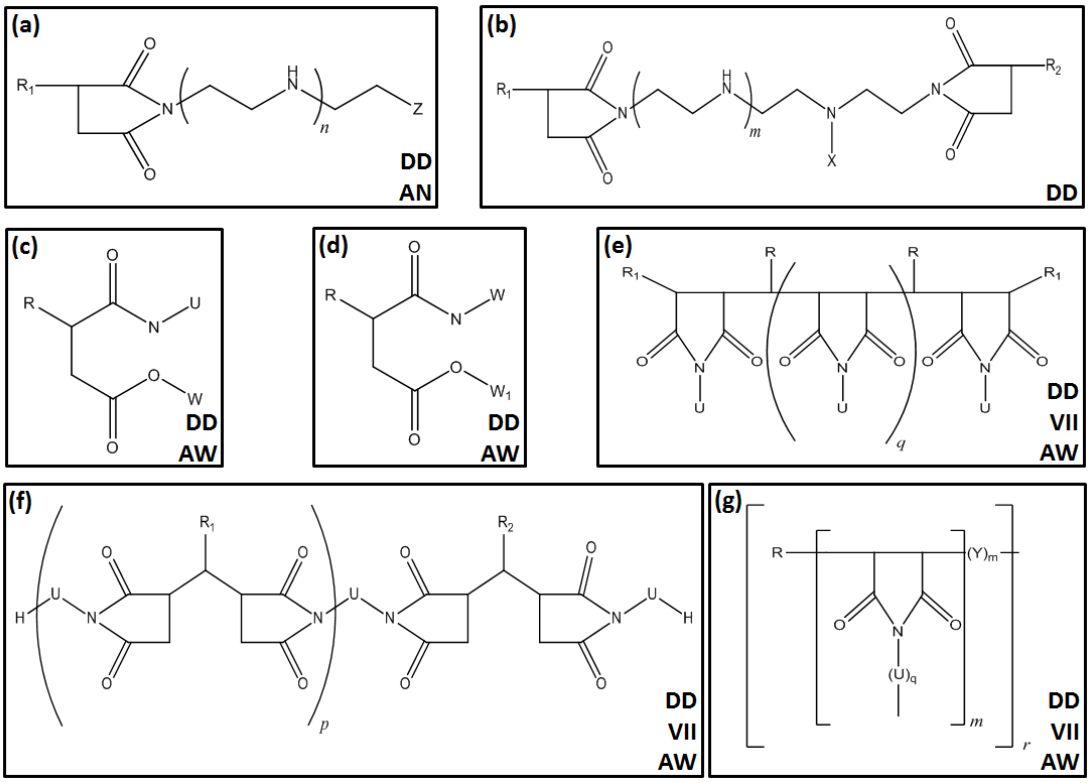

Figure 1.27. Seven of the main polyolefin succinimides and derivatives used as engine oil additives, where (a) is a mono-succinimide, (b) is a bis-succinimide, (c) is a succinic ester amide, (d) is a succinic ester, and (e), (f) and (g) are polysuccinimides. DD = detergent-dispersant, AN = acid neutraliser, AW = antiwear, VII = viscosity index improver. U = polyamine group or their modified derivatives, W,W_1 = polyol group or other oleophilic group, R, R_1, R_2 = polyalkenylor polyolefin or other oleophilic group, X, Z = H or B-, S-, Mo-, Zn-, or O- containing group. *n, m, p, q, r* = integer **>** 1.[12]

Studies of the mechanism of operation of succinimide-based OCPs revealed the molecular architecture and chemical composition to be equally important for the efficiency of soot dispersion.[183] However, the molecular level process by which these additives actually function is presently rather poorly understood. Current literature suggests that the additives rely on anchoring of a hydrophilic end-group (the succinimide for the additives shown in Figure 1.27) to the surface of the soot particles, with the hydrophobic moiety extending into the base oil in a "tail-like" structure.[183] This adsorbed conformation confers enhanced colloidal stability via steric stabilisation.[52] Succinimide-based OCPs are usually preferred to a second class of *metal*-based dispersant additives (for example, Ca, Mg or Ba). The latter additives cause problems, since they form insoluble solids in the engine oil formulation. Fully organic

succinimide-based OCPs are preferred, as no such insoluble solids formed; hence they are sometimes known as 'ashless detergents'.[183]

Diblock copolymers

Although succinimide-based OCP statistical copolymers are one of the cheapest and most widely used soot dispersant additives, alternative copolymer architectures have proven more successful soot dispersants in engine oil. Such additives tend to be more expensive since they require a more complex synthetic route.[34] As a result, they tend to be used in the higher end/performance lubricants.[34] One such additive is linear poly(styrene-*b*-hydrogenated isoprene).[34] It has been suggested by Shar *et al*.[34] that such block copolymers adsorb onto the surface of soot deposits with the polystyrene block acting as a 'head' group whilst the hydrogenated polyisoprene block forms a 'tail', preventing further aggregation.[34] For this particular study, carbon black was used as a model colloidal substrate. This is represented schematically in Figure 1.28. In this thesis, this simplistic hypothesis has been critically assessed (see Chapter 2).

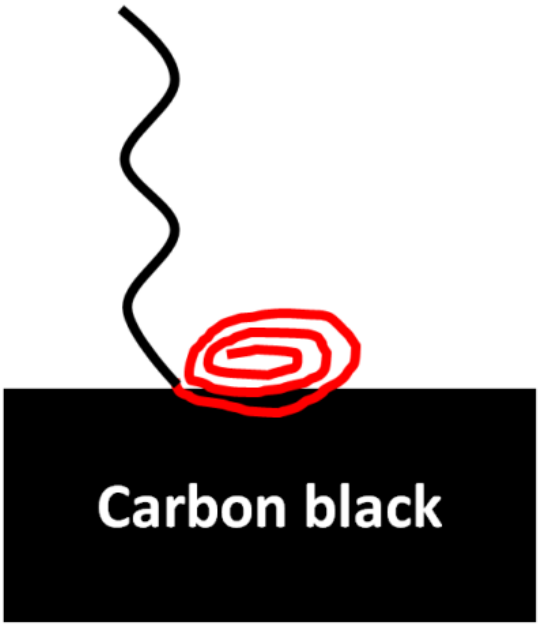

Figure 1.28. Schematic representation of the proposed mode of adsorption of poly(styrene-*b*-hydrogenated isoprene) diblock copolymer onto soot particles, where the red block illustrates polystyrene and the black block denotes hydrogenated polyisoprene.[34]

The extent of copolymer adsorption onto carbon black/soot is strongly dependent on the overall copolymer molecular weight and the block copolymer composition.[34] A selection of block copolymers studied by Shar *et al*.[34] are summarised in Table 1.1. Empirically, it was found that the longer the polystyrene anchor block, the stronger the copolymer adsorption on the carbon black surface from cyclohexane. Moreover, it was observed that the greater the anchor fraction, the greater the adsorbed amount of block copolymer, but only for block copolymers with molecular weights up to ≈ 20,000 g mol^{-1}. Higher molar mass copolymers exhibited a maximum in the adsorbed amount. More generally, it is believed that the poor solvency of the polystyrene block in cyclohexane aids in the adsorption of the copolymer onto the surface of the carbon black.[34]

Polymer	**M_w**	**M_w PS**	**mol% PS**	**M_w HPIP**	**mol% HPIP**	**M_w/M_n**
10K0.82	10,000	9,000		1,000	18	N/A
10K0.06	10,000	1,000		9,000	94	N/A
17K1.00	17,000	17,000	100		0	1.08
15K0.85	14,000	13,500	85	1,000	15	1.07
7K0.57	7,000	5,000	57	2,000	43	1.65
12K0.56	12,000	8,000	56	3,500	44	1.11
9.5K0.44	9,500	6,000	44	4,000	56	1.14
100K0.24	100,000	35,000	24	65,000	76	N/A
7.5K0.21	7,500	2,500	22	5,000	78	1.80
153K0.20	153,000	48,000	20	105,000	80	N/A

Table 1.1. Polystyrene-*b*-hydrogenated isoprene (PS-HPIP) diblock copolymers examined by Shar *et al*.[34] Molecular weights have been rounded up and column 6 has been rectified due to an apparent error in the original data. Polymer codes denote the overall copolymer molecular weight followed by the polystyrene content in mol %.

An earlier study of poly(styrene-*b*-isoprene) assessed the solution behaviour of this type of block copolymer in *n*-alkanes, which may well affect their dispersant performance at elevated temperatures.[106] The polystyrene contents and molecular weights of diblock copolymers studied in this work are shown in Table 1.2. According to ^{1}H NMR analysis, all block copolymers formed polystyrene-core micelles in *n*-alkanes, which

then became molecularly dissolved at elevated temperature. Aromatic signals from the polystyrene block were initially invisible at 30 ˚C but became visible on heating to 90 ˚C.[106] Shar *et al*. suggested that the poor solvency of the polystyrene block in *n*-alkanes drives block copolymer adsorption onto the carbon black surface.[34] If polystyrene solvency increases at high temperatures, it is conceivable that the poly(styrene-*b*-hydrogenated isoprene) chains desorb from the surface of soot/carbon black at normal operating temperatures for diesel engines.

Sample	M_n x10^{-3} (g mol^{-1})	wt% styrene	mol% styrene
SA-3	29	31	23
SA-4	36	45	35
SA-5	39	49	39
SA-6	49	59	49
SA-7	53	62	53

Table 1.2. Molecular weights and block copolymer compositions of the various PS-PIP diblock copolymers examined by Bahadur *et al*. Each copolymer contains a polyisoprene sequence of 20,000 g mol^{-1}.[106] The polystyrene content (in mol %) has been calculated for each copolymer to allow direct comparison with the data presented in Table 1.1.

An extensive study conducted by Stejskal *et al*. examined both equilibrium and non-equilibrium copolymer micelles, specifically poly(styrene-*b*-[ethylene-co-propylene]) copolymers in both *n*-decane and diisopropyl ether (DIPE).[104] It was concluded that the solid-state structure of such copolymer micelles was partly preserved on dissolution in selective solvents. Poly(styrene-*b*-[ethylene-co-propylene]) formed metastable non-equilibrium micellar aggregates with polystyrene cores at 20 ˚C. A transformation to smaller stable equilibrium micelles with lower aggregation numbers was observed after heat treatment (10 mins at 100 ˚C for *n*-decane; 10 mins at 70 ˚C for diisopropyl ether).[104]

The observed change in structure after heat treatment was explained by the kinetically frozen state of the micellar cores at room temperature.[104] Differential scanning calorimetry, small-angle X-ray scattering, static and dynamic light scattering and viscometry experiments were used to characterise the equilibrium and non-equilibrium micelles. Light scattering revealed a pronounced mutual interaction between micelles, even at concentrations as low as of 5 x 10^{-4} g cm $^{-3}$. The concept of 'sticky chains' was introduced by Stejskal *et al*. to explain the inter-micelle association.[104] Surprisingly, the behaviour of poly(styrene-*b*-[ethylene-co-propylene]) micelles in DIPE ether was less complex, with both effects observed in *n*-decane being absent in this solvent. SAXS confirmed this finding, with differing scattering patterns being observed in *n*-decane on varying the temperature, but not in DIPE (see Figure 1.29).[104] Figure 1.30 shows a schematic representation of the colloidal structures formed by an AB diblock copolymer in a selective solvent, as described by Stejskal *et al*.[104]

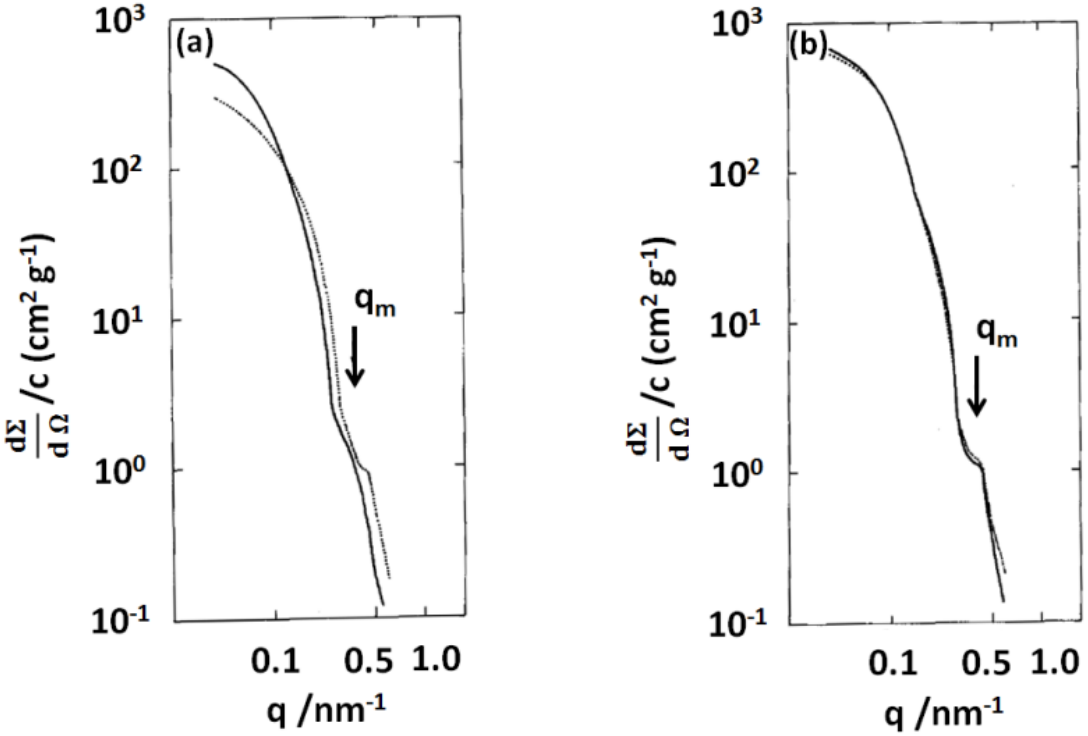

Figure 1.29. SAXS curves for poly(styrene-*b*-[ethylene-co-propylene]) in (a) *n*-decane and (b) DIPE measured at room temperature (dotted lines) and after heating (solid line).[104]

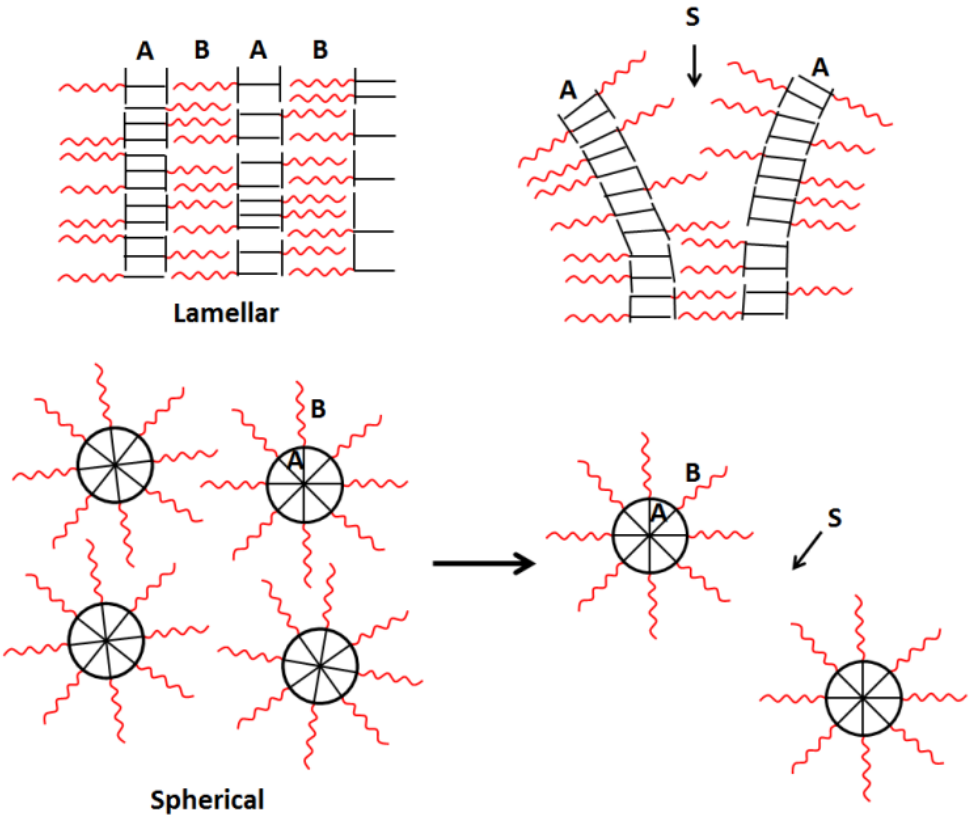

Figure 1.30. Schematic representation of the solid-state structure of an AB diblock copolymer and its selective dissolution by the penetration of solvent 'S', a selective solvent for the B block.[104]

Similar solution behaviour has been found for various related copolymers. For example, Stacy and Kraus[114] examined poly(styrene-*b*-butadiene) (PS-PB) micelles in *n*-hexane, *n*-heptane and *n*-decane. In many cases, a substantial reduction in the micelle aggregation number after heating and cooling in comparison with micellar solutions prepared directly at room temperature was observed. A reduction in solution turbidity from opaque, milky-white to transparent on heating to ~ 50°C and cooling to 20°C is also documented by Tsunashima *et al.* for similar diblocks in *n*-decane.[184]

Schouten and co-workers studied the effect of temperature on a poly(styrene-*b*-isoprene) diblock copolymer with a styrene content of ~ 37 wt%.[113] Gel permeation chromatography measurements in tetrahydrofuran (vs. polystyrene calibration standards), showed an M_w of (1.26 ± 0.05) x 10^5 g mol^{-1} and an M_w/M_n of 1.07. A similar transition to relatively small micelles/unimers at elevated temperatures (up to

140^{o}C) with a concomitant reduction in viscosity was observed in this case. Mandema *et al*. also described the same transition for two poly(styrene-*b*-hydrogenated isoprene) diblock copolymers (38 wt% PS; either 48 000 or 80 000 g mol^{-1}) in *n*-decane and *trans*-decalin.[112] Viscosity, diffusion and light scattering measurements were used in this study. Such a reduction in viscosity was not expected for this system, since micellar dissociation into individual copolymer chains usually causes an increase in viscosity. To explain such behaviour, Mandema *et al*. speculate that the block copolymer micelles associate at higher temperatures to form cylinders or lamellae.[112] However, this hypothesis is contrary to most literature in this area. For example, Stejskal *et al*. suggest that lamellar-type structures *dissociate* at high temperature to form spherical micelles and, once such spherical micelles are formed, they show no tendency to revert back to the original lamella structures.[104] Clearly, the solution behaviour of such block copolymers in selective non-polar solvents can be complex. Some of the apparent discrepancies in the literature may be ascribed to subtle differences in copolymer composition, copolymer molecular weight and thermal history.

Star copolymers

Star diblock copolymers are widely used in engine oils, but their function is mainly that of a viscosity modifier, rather than a soot dispersant.[35, 185, 186] The desired performance of such additives is a reduction in engine oil viscosity at ambient temperature and an increase in viscosity at engine operating temperature (~110^{o}C). Star diblock copolymers can fulfil such requirements, as their structure remains unchanged at elevated temperature (although a change in solvation may become apparent). Such copolymers are also used for improving the viscosity index in other lubricant applications, for example gear oils.[187] The potential for star copolymers to act as soot dispersants is largely undocumented in the literature, but is examined in Chapter 3.

Temperature effects

The effect of temperature on carbon black/soot dispersion stability in an *n*-alkane solvent is extremely important in the context of engine oil formulation. A typical light duty engine operates between 20^{o}C and 110^{o}C, meaning that any difference in the

thermal stability of soot deposits between these temperatures may have a detrimental effect on oil viscosity. This has been investigated in some detail by Won *et al.*[188] The effect of temperature on both a carbon black (Vulcan XC72R, a soot model) alone in SN150N base oil and the same carbon black coated with polyisobutylene succinimide (PIBSI) dispersant additive was assessed, and two important conclusions were drawn. First, rheology studies showed that carbon black particles in base oil in the absence of dispersant are highly aggregated and exhibit no temperature-dependent behaviour. Thus it is unlikely that heating induces a significant increase in the van der Waals interaction between the carbon black particles. Secondly, a study of carbon black particles coated with PIBSI dispersant revealed a significant change in suspension rheology on heating. At 20^{o}C, primary carbon black aggregates were well dispersed, resulting in a low fluid-like rheology. However, at 100^{o}C, such primary aggregates formed agglomerates, producing a 3D gel network with a more solid-like suspension rheology. It was concluded that the temperature-dependent solution viscosity was the result of the hydrocarbon chain of the PIBSI dispersant becoming gradually desolvated at higher temperatures. Hence, its ability to inhibit agglomeration via a steric stabilisation mechanism is diminished, so carbon black aggregates combine to form larger agglomerates. Figure 1.31 shows optical micrographs reported by Won *et al.*[188] that indicate weakening of the aggregate network structure on addition of dispersant, and the effect of temperature on such samples.[188]

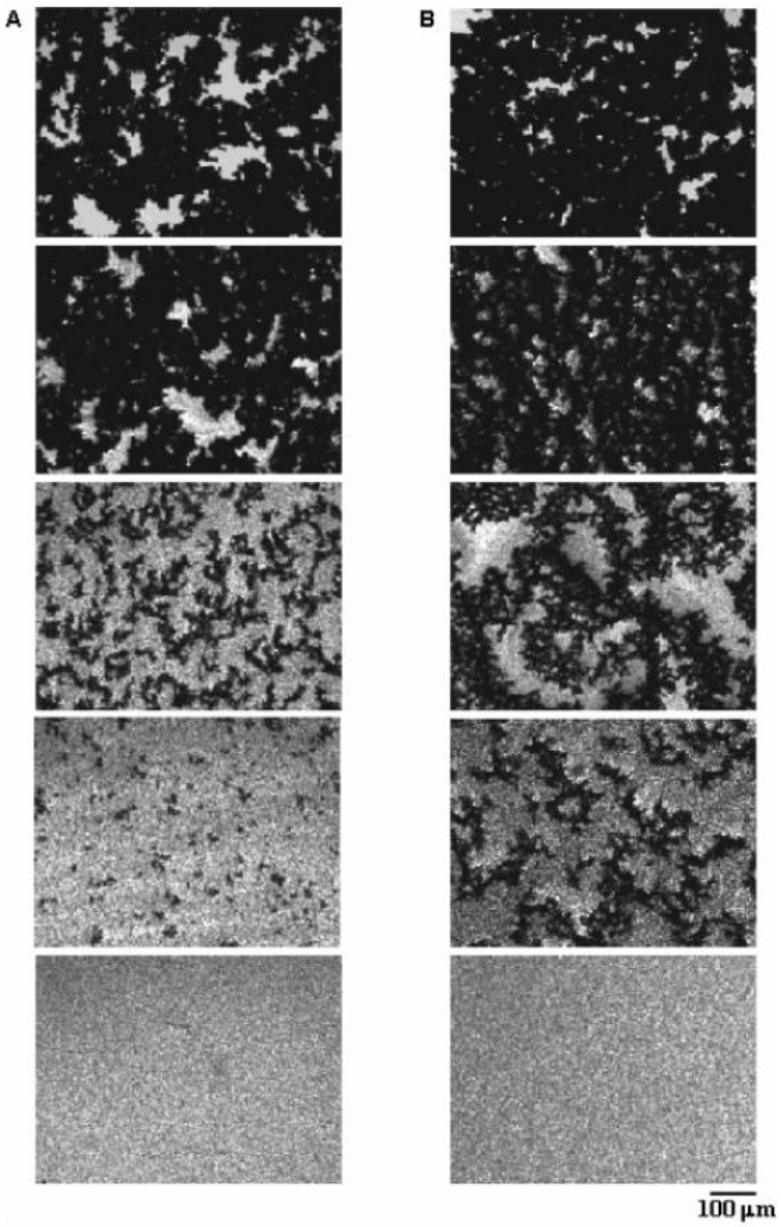

Figure 1.31. Optical micrographs recorded for 4.0 wt% carbon black dispersions at (A) 25ºC and (B) 100ºC, showing a reduced network structure in either the presence of dispersant or an increase in temperature. The dispersant concentrations are (A) 0, 0.5, 0.7, 1.0, 1.2 wt% and (B) 0, 0.5, 1.0, 1.5 and 1.9 wt% from top to bottom. All images were recorded at the same magnification.[188]

Figure 1.32 depicts a schematic cartoon of the mechanism of PIBSI chain collapse at elevated temperatures, as proposed by Won *et al*. A reduction in hydrocarbon solvation at elevated temperature induces collapse, hence reducing steric stabilisation.[188]

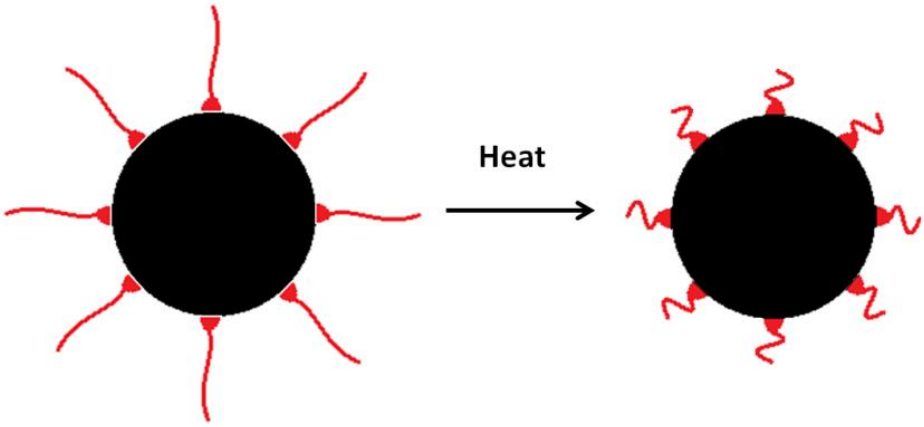

Figure 1.32. Schematic cartoon showing the mechanism of PIBSI collapse as proposed by Won *et al*.[188]

1.9.5 Carbon black: a model colloidal substrate for diesel soot?

Because of the inherent high cost of generating genuine engine soot (which involves running an engine to destruction at the cost of ~£80,000), carbon blacks are commonly used as model colloidal substrates instead of genuine soot.[34, 188, 189] For this reason, it is important to compare and contrast the properties of commercially available carbon blacks in order to ensure their similarity to genuine diesel soot. Clague *et al*. used a range of analytical techniques to characterise both the chemistry and morphology of a diesel engine soot and an exhaust soot. In addition, a comparison was made between these soots and a range of commercial carbon blacks.[145] Significant differences were observed by TGA between the chemical compositions of exhaust and engine soots (see Figure 1.33 and Table 1.3).[145] In Table 1.3, it is shown that the carbon content in exhaust soot is lower than that in engine soot, while the ash content is significantly higher (~ 30% vs. ~2%). Engine soot typically has a slightly higher volatile content than exhaust soot, while furnace black and channel black exhibit consistently low ash and volatile contents. It is also noteworthy that extraction of both engine and exhaust soot affects their carbon, ash and volatile contents. In Figure 1.33, there is a strong IR absorption in the exhaust soot at ~1700 cm^{-1}. This corresponds to a C=O stretch, providing good evidence for more extensive oxidation than in the engine soot. In contrast, the engine soot IR spectrum indicates higher concentrations of aromatic groups and alkyl chains than that of the exhaust soot. These differences are expected, as exhaust gas (and therefore exhaust soot) travel directly from the combustion chamber of

the engine to the exhaust manifold, whereas engine soot is exposed to both the engine oil and other engine-based wear particulates prior to its extraction and examination. Significant differences were found in their surface chemistries and the presence of adsorbed lubricant components on the engine soot was also observed. For example, polyisobutylene signals were observed when analysing dichloromethane extracts of engine soot by ^{13}C NMR spectroscopy, see Figure 1.34.

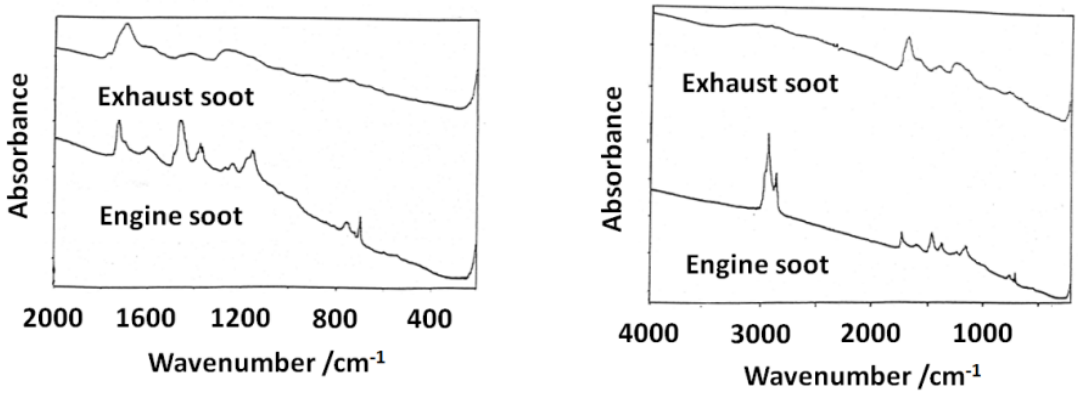

Figure 1.33. IR spectra of dichloromethane extracts of engine and exhaust soots.[145]

Sample	Carbon content (%)	Ash content (%)	Volatile content (%)
Engine soot A	75.6	2.2	22.2
Extracted A	86.7	1.8	11.5
Engine soot B	79.8	1.8	18.4
Extracted B	88.4	1.2	10.4
Exhaust soot	57.7	27.1	15.2
Extracted	35.1	53	11.9
Furnace black XC72R	98.8	0.9	0.3
Channel black: S170*	94.8	0.02	5

Table 1.3. Thermogravimetric analysis of various soots and carbon blacks.[145]

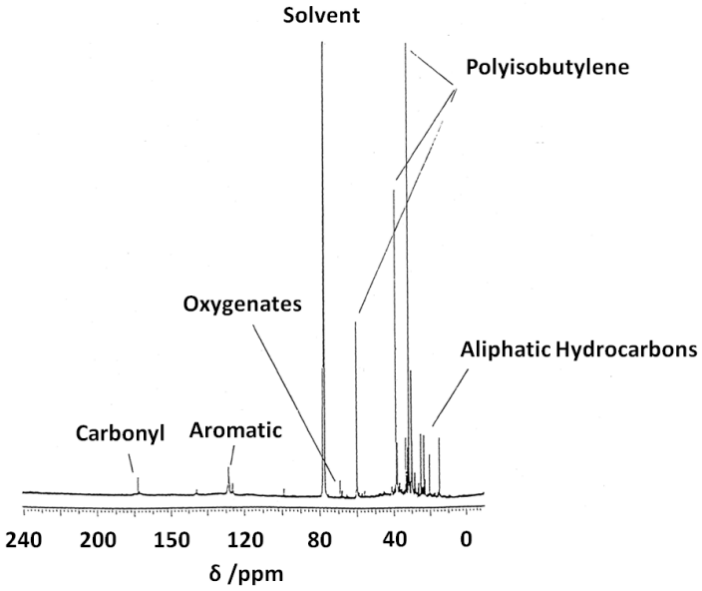

Figure 1.34. ^{13}C NMR solution spectrum recorded for DCM-extracted engine soot.[145]

Regardless of its origin, each form of soot differed from carbon black, particularly in their elemental compositions and surface chemistry (see Table 1.3). However, both forms of soot and typical carbon blacks exhibited very similar primary particle sizes and fractal morphologies, as well as virtually indistinguishable perturbed graphitic or turbostratic internal structures (the latter is defined as a crystal structure in which basal planes have slipped out of alignment). Figure 1.35 illustrates the morphological similarities between diesel soot and Vulcan XC72R carbon black.[145]

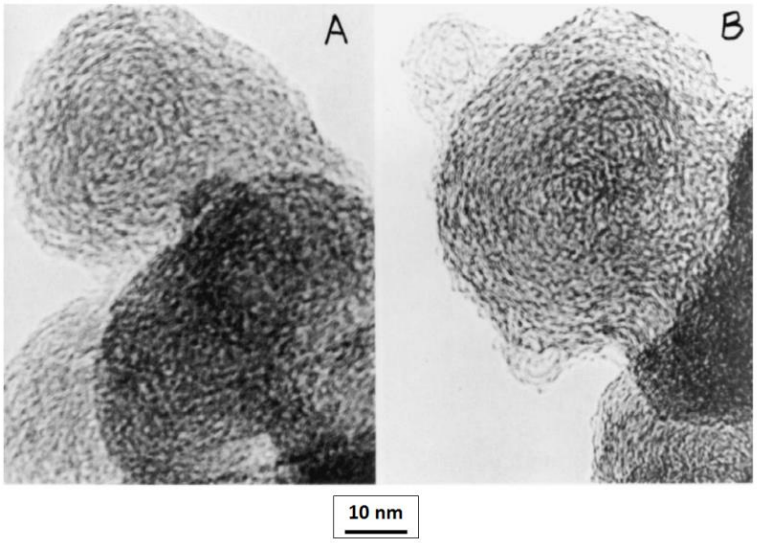

Figure 1.35. Phase contrast transmission electron micrographs of diesel soot (A) and Vulcan XC72R carbon black (B).[145]

A hypothesis was proposed by Clague *et al*. to account for the various differences that are observed. These workers note the similarities in soot and carbon black generation, but emphasise differences between the quenching and post-quenching environments.[145] Nevertheless, it was concluded that certain carbon blacks are reasonably good mimics for understanding the aggregation behaviour of soots in spent lubricating oils.[145]

1.9.6 Block copolymer adsorption

To optimise engine oil formulations, it is important to understand and quantify copolymer adsorption onto soot particles. For example, the adsorption of diblock copolymers such as poly(styrene-*b*-hydrogenated isoprene) onto carbon black from cyclohexane has been investigated by Shar *et al*.[34] The aromatic polystyrene component provides a useful UV spectroscopy chromophore at 262 nm, see Section 1.2.2 of this Introduction. The depletion assay method is the general protocol used for such copolymer adsorption studies, in which the adsorbed amount of additive is determined indirectly from the reduction in copolymer concentration of additive remaining in solution after adsorption.[59, 190] According to Shar and co-workers, poly(styrene-*b*-hydrogenated isoprene) exhibited a strong block composition-dependent adsorption profile when added to carbon black in cyclohexane. Furthermore, the interaction of the polystyrene block with the carbon black surface was proposed to be the likely mode of adsorption.[34] However, it is emphasised that the effect of temperature was not considered in this study; all analyses were conducted at 20^{o}C. Similar depletion assay studies have been conducted in the current work; see Chapters 2, 3 4 and 5.

Computer simulation studies of poly(styrene-*b*-hydrogenated isoprene) tethered to a cyclohexane-carbon black interface were also performed.[34] The self-consistent field (SCF) theory of Evers[118] and Fleer[191] was used to estimate the relative adsorption affinities of the polystyrene anchor and the hydrogenated polyisoprene buoy block at the interface. This approach gave good, albeit only qualitative, agreement with the experimental data. Adsorption isotherms obtained by this group are shown in Figures 1.36, 1.37 and 1.38. At the cyclohexane/carbon black interface, the polystyrene block adsorbed preferentially compared to the hydrogenated polyisoprene, with the poor

solvency of the former block aiding its adsorption.[34] This is as expected, with a π-π stacking interaction to be expected. The polymers denoted as 10K0.82 and 10K0.06 (see Table 1.1), had equivalent molar masses but differing polystyrene contents and hence behaved differently when adsorbed onto the surface of carbon black.[34] The 10K0.06 sample had a very low polystyrene content and so behaved like a hydrogenated polyisoprene homopolymer, showing only relatively weak affinity for the carbon black surface. However, as the polystyrene block content was increased, a significant increase in surface affinity was observed.[34]

Furthermore, it was found that copolymers with similar polystyrene contents but different molar masses (for example copolymers 100K0.22 and 153K0.20 in Table 1.1) adsorbed at slightly different levels, indicating a weak dependence of adsorbed amount on copolymer molar mass.[34] Dependence of the adsorbed amount of copolymer on polystyrene content (determined via computer simulations) for copolymers of varying compositions (M_w ~ 5,000 to 150,000) revealed higher adsorbed amounts with greater polystyrene block contents for low molar mass copolymers (up to M_w ~ 20,000). For higher molar mass copolymers, a maximum in the adsorbed amount was observed, shifting from high to low polystyrene contents and becoming more pronounced as the overall copolymer molar mass was increased.[34] Shar *et al*. concluded that the adsorbed amount of poly(styrene-*b*-hydrogenated isoprene) diblock copolymer depended strongly on the overall copolymer molar mass, but the block composition was just as important.[34] This study is also in good agreement with various theoretical predictions and experimental data published for similar systems.[117, 119, 120, 192, 193, 194]

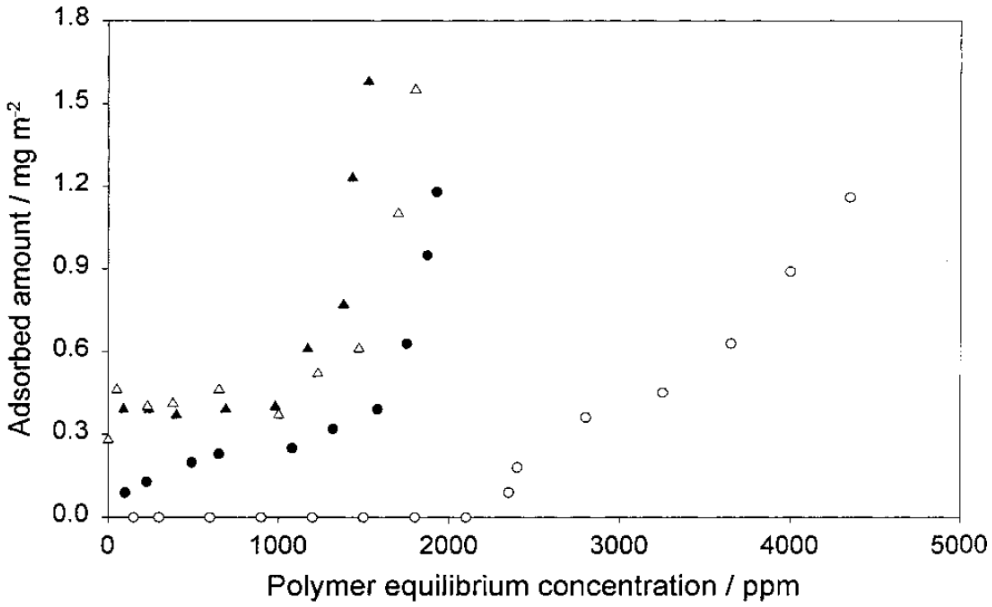

Figure 1.36. Adsorption isotherms determined for various copolymers adsorbed at the cyclohexane/carbon black interface: Black triangle - 17K1.0; open triangle - 14.7K0.85; black circle - 10K0.82; open circle - 10K0.06, where sample codes denote the overall copolymer molecular weight, followed by the polystyrene mol fraction, see Table 1.1.[34]

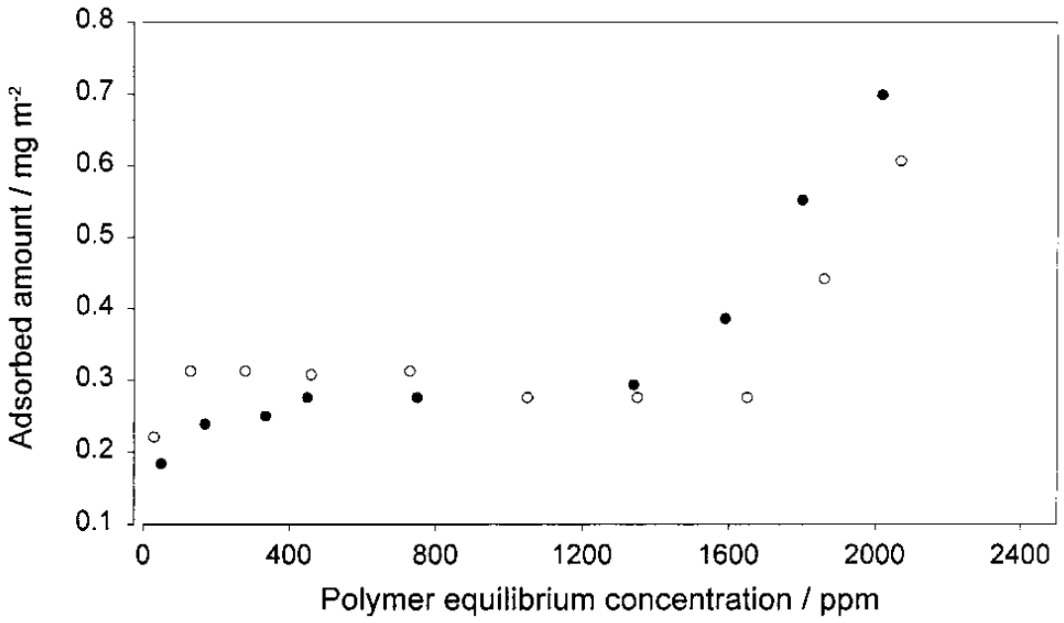

Figure 1.37. Adsorption isotherms for copolymers: Black circles - 7K0.57 and open circles - 11.8K0.56 adsorbed on carbon black as a function of copolymer equilibrium concentration, where sample codes denote the overall copolymer molecular weight, followed by the polystyrene mol fraction, see Table 1.1.[34]

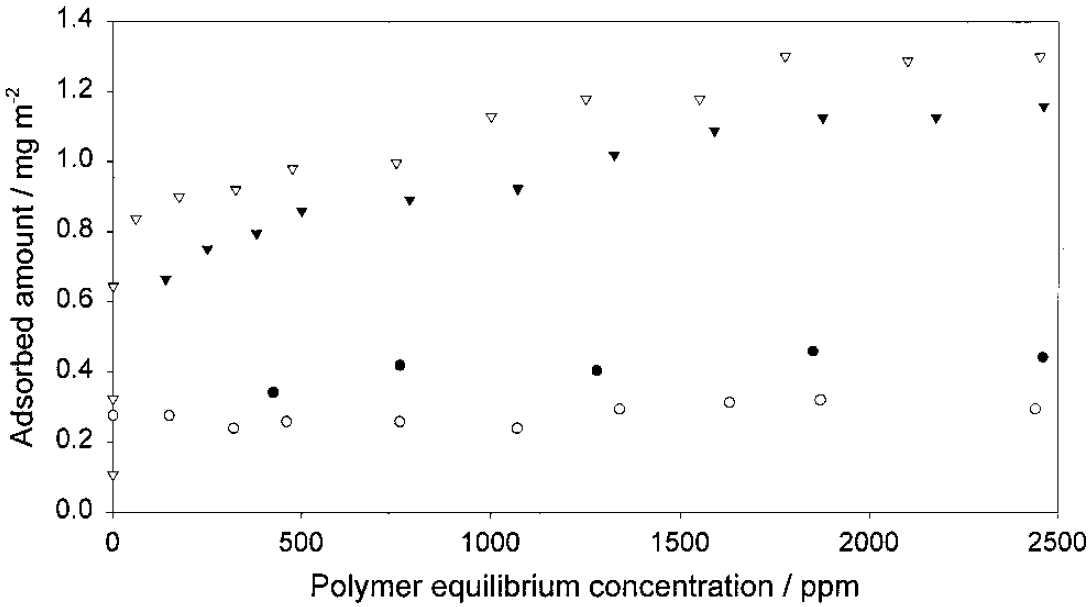

Figure 1.38. Langmuir-type adsorption isotherms observed for two pairs of more soluble copolymers: Open circle - 7.5K0.21, black circle - 9.5K0.44; Black triangle - 100K0.24, open triangle - 153K0.20, where sample codes denote the overall copolymer molecular weight, followed by the polystyrene mol fraction, see Table 1.1.[34]

Project motivation and overview

The motivation for this PhD project was to investigate six diblock copolymer diesel engine oil additives with different architectures and functional groups in order to assess their efficacy at maintaining a stable diesel soot dispersion in *n*-alkanes. An improved understanding of the effects of dispersant type, copolymer architecture and copolymer concentration on soot dispersion performance should allow further optimisation of oil formulation performance. One of the fundamental questions at the start of this project was whether copolymer chains adsorb onto diesel soot particles as micelles or as individual copolymer chains. Chapter 2 addresses this question directly by constructing adsorption isotherms in both selective and non-selective solvents for a commercial linear poly(styrene-*b*-hydrogenated isoprene) copolymer.

In Chapter 3, a commercial poly(styrene-*b*-hydrogenated isoprene) star diblock copolymer that is primarily added to engine oil formulations as a viscosity modifier[35] is

assessed for its carbon black dispersion performance. This work has the potential to inform future engine oil formulation optimisation, as possible soot interactions have not previously been considered for such copolymer additives. Analytical centrifugation has been used to assess the degrees of carbon black dispersion and how this is affected by temperature, solvent and copolymer concentration. It is essential to determine the effective particle density when using this technique; this parameter can be calculated for sterically-stabilised carbon black particles using Stokes' law. SAXS has also been used to assess the colloidal structure of carbon black and how this changes as star diblock copolymer is adsorbed on its surface.

In Chapter 4, carbon black dispersion stabilities are critically compared for three commercial linear diblock copolymer additives. Each copolymer has a different polystyrene content, and hence produces micelles of varying size in selective *n*-alkanes. The effective particle density (introduced in Chapter 3) is more critically evaluated here, including an assessment of errors in such calculations. In principle, micelles with a larger core-forming polystyrene block should confer a thicker stabiliser layer and hence a lower effective particle density.

A comparison between carbon black and genuine diesel soot is made in Chapter 5. Physical parameters such as specific surface area and density are determined, followed by a detailed comparison of the relative degrees of dispersion that can be achieved for carbon black and genuine diesel soot particles when using two commercial copolymers, namely a linear poly(styrene-*b*-hydrogenated isoprene) copolymer and a poly(ethylene-co-propylene) dispersant OCP. SAXS is also used to compare and contrast the fractal morphology and surface characteristics of the two colloidal substrates.

Finally, Chapter 6 details a brief summary of all the work covered in this thesis and suggests possible future areas of research in the context of soot dispersion by diblock copolymer engine oil additives.

References

1. Furrer, W. W.; Bose, A. K. High molecular weight, linear low density, and low density thermoplastic resin blend; bags; high strength, softness. US Patent 4,770,912, 1988.
2. Ferngren, E. T. Flexible bottle. US Patent 2,099,055, 1937.
3. Evans, C. H. Hydrogel contact lens. US Patent 4,199,231, 1980.
4. Galaev, I. Y.; Mattiasson, B. 'Smart' polymers and what they could do in biotechnology and medicine. *Trends in Biotechnology* **1999,** *17*, 335-340.
5. Hoffman., A. J. W. R. P. B. M. J. Assessment of strength and toughness of modified PVC pipes. *Plastics, Rubber and Composites* **2001,** *30*, 434-440.
6. John, F. M.; John, K. W.; Thomas, R. S. Insulated electric cable. US Patent 2,304,210, 1942.
7. Brabec, C. J.; Sariciftci, N. S.; Hummelen, J. C. Plastic solar cells. *Advanced functional materials* **2001,** *11*, 15-26.
8. Walkowiak, M.; Podszun, W.; Leusner, B.; Suling, C.; Schulz, H. H. Dental materials based on organic plastics in paste form. US Patent 4308190, 1981.
9. Hamana, I.; Fujiwara, Y.; Kumakawa, S. Novel naphthalate polyester fibers, and their end uses. US Patent 4,001,479, 1977.
10. Little, R. Q.; Traise, T. P.; Watson, R. W. Lubricating oil additives. US Patent 3,442,808, 1969.
11. Gutierrez, A.; Song, W. R.; Lundberg, R. D.; Kleist, R. A. Novel ethylene alpha-olefin copolymer substituted Mannich base lubricant dispersant additives. US Patent 5017299, 1991.
12. Bartha, L.; Deák, Y. G.; Hancsók, J.; Baladincz, J.; Auer, J.; Kocsis, Z. Polyfunctional PIB succinimide type engine oil additives. *Lubrication Science* **2001,** *13*, 313-328.
13. Carothers, W. H. Studies on polymerization and ring formation. I. An introduction to the general theory of condensation polymers. *Journal of the American Chemical Society* **1929,** *51*, 2548-2559.
14. Odian, G. G.; Odian, G. *Principles of polymerization*; New York: Wiley-Interscience, 2004; Vol. 3.
15. Lovell, P. A.; El-Aasser, M. S. *Emulsion polymerization and emulsion polymers*; Wiley, 1997.
16. Kim, J. H.; Chainey, M.; El-Aasser, M. S.; Vanderhoff, J. W. Preparation of highly sulfonated polystyrene model colloids. *Journal of Polymer Science Part A: Polymer Chemistry* **1989,** *27*, 3187-3199.
17. Lok, K. P.; Ober, C. K. Particle size control in dispersion polymerization of polystyrene. *Canadian Journal of Chemistry* **1985,** *63*, 209-216.
18. O'Neill, M. L.; Yates, M. Z.; Harrison, K. L.; Johnston, K. P.; Canelas, D. A.; Betts, D. E.; DeSimone, J. M.; Wilkinson, S. P. Emulsion stabilization and flocculation in CO_2. 1. turbidimetry and tensiometry. *Macromolecules* **1997,** *30*, 5050-5059.
19. Richez, A. P.; Yow, H. N.; Biggs, S.; Cayre, O. J. Dispersion polymerization in non-polar solvent: evolution toward emerging applications. *Progress in Polymer Science* **2013,** *38*, 897-931.
20. Armes, S. P.; Aldissi, M. Preparation and characterization of colloidal dispersions of polypyrrole using poly(2-vinyl pyridine)-based steric stabilizers. *Polymer* **1990,** *31*, 569-574.

21. Au, K. M.; Armes, S. P. Heterocoagulation as a facile route to prepare stable serum albumin-nanoparticle conjugates for biomedical applications: synthetic protocols and mechanistic insights. *ACS Nano* **2012,** *6,* 8261-8279.
22. Simmons, M. R.; Patrickios, C. S. Synthesis and aqueous solution characterization of catalytically active block copolymers containing imidazole. *Macromolecules* **1998,** *31,* 9075-9077.
23. Baines, F. L.; Billingham, N. C.; Armes, S. P. Synthesis and solution properties of water-soluble hydrophilic−hydrophobic block copolymers. *Macromolecules* **1996,** *29,* 3416-3420.
24. Wilhelm, M.; Zhao, C. L.; Wang, Y.; Xu, R.; Winnik, M. A.; Mura, J. L.; Riess, G.; Croucher, M. D. Poly (styrene-ethylene oxide) block copolymer micelle formation in water: a fluorescence probe study. *Macromolecules* **1991,** *24,* 1033-1040.
25. Dawkins, J. V.; Maghami, G. G.; Shakir, S. A.; Higgins, J. S. Non-aqueous polymer dispersions: radical dispersion polymerization in the presence of the diblock copolymer poly(styrene-b-[ethylene-co-propylene]). *Colloid Polym Sci* **1986,** *264,* 616-618.
26. Vincent, B.; Waterson, J. Colloidal dispersions of electrically-conducting, spherical polyaniline particles. *J. Chem. Soc., Chem. Commun.* **1990,** 683-684.
27. Hadjichristidis, N.; Pispas, S.; Floudas, G. *Block copolymers: synthetic strategies, physical properties, and applications*: John Wiley & Sons, 2003.
28. Hadjichristidis, N.; Pitsikalis, M.; Pispas, S.; Iatrou, H. Polymers with complex architecture by living anionic polymerization. *Chemical Reviews* **2001,** *101,* 3747-3792.
29. Burguiere, C.; Dourges, M. A.; Charleux, B.; Vairon, J. P. Synthesis and characterization of omega-unsaturated poly(styrene-b-n-butyl methacrylate) block copolymers using TEMPO-mediated controlled radical polymerization. *Macromolecules* **1999,** *32,* 3883-3890.
30. Higginson, W.; Wooding, N. 138. Anionic polymerisation. Part I. The polymerisation of styrene in liquid ammonia solution catalysed by potassium amide. *J. Chem. Soc.* **1952,** 760-774.
31. Harries, C. Hydrocarbons of the butadiene series and artificial caoutchoucs prepared from them. *Ann* **1911,** *383,* 157-227.
32. Ziegler, K.; Jakob, L. Alkali organic compounds. XII." Catalysis" of the polymerization of unsaturated hydrocarbons by alkali organic compounds. *Justus Liebigs Annalen der Chemie* **1934,** *511,* 45.
33. Ziegler, K.; Jakob, L.; Wollthan, H.; Wenz, A. Alkali organic compounds. XIII. The first reaction products of alkali metals upon butadiene. *Justus Liebigs Annalen der Chemie* **1934,** *511,* 64.
34. Shar, J. A.; Cosgrove, T.; Obey, T. M.; Warne, M. R.; Wedlock, D. J. Adsorption studies of diblock copolymers at the cyclohexane/carbon black interface. *Langmuir* **1999,** *15,* 7688-7694.
35. Eckert, R. J. Hydrogenated star-shaped polymer. US Patent 4116917, 1978.
36. Lam, W. Y. Lubricating oil composition for improved oxidation, viscosity increase, oil consumption, and piston deposit control. US Patent 11/691,246, 2007.
37. Al-Sabagh, A. M.; Noor El-Din, M. R.; Morsi, R. E.; Elsabee, M. Z. Styrene-maleic anhydride copolymer esters as flow improvers of waxy crude oil. *Journal of Dispersion Science and Technology* **2009,** *30,* 420-426.
38. Mach, H.; Rath, P. Highly reactive polyisobutene as a component of a new generation of lubricant and fuel additives. *Lubrication Science* **1999,** *11,* 175-185.

39. Szwarc, M.; Levy, M.; Milkovich, R. Polymerization initiated by electron transfer to monomer. A new method of formation of block polymers1. *Journal of the American Chemical Society* **1956,** *78,* 2656-2657.
40. Killian, C. M.; Tempel, D. J.; Johnson, L. K.; Brookhart, M. Living polymerization of α-olefins using NiII-α-diimine catalysts. Synthesis of new block polymers based on α-olefins. *Journal of the American Chemical Society* **1996,** *118,* 11664-11665.
41. Shaw, D. J.; Costello, B. Introduction to colloid and surface chemistry: Butterworth-Heinemann, Oxford, 1991, ISBN 0 7506 1182 0, 306 pp,£ 14.95. Elsevier, 1993.
42. Ruehrwein, R. A.; Ward, D. W. Mechanism of clay aggregation by polyelectrolytes. *Soil Science* **1952,** *73,* 485-492.
43. Biggs, S.; Habgood, M.; Jameson, G. J.; Yan, Y.-d. Aggregate structures formed via a bridging flocculation mechanism. *Chemical Engineering Journal* **2000,** *80,* 13-22.
44. Yan, Y.-d.; Burns, J. L.; Jameson, G. J.; Biggs, S. The structure and strength of depletion force induced particle aggregates. *Chemical Engineering Journal* **2000,** *80,* 23-30.
45. Glover, S. M.; Yan, Y.-d.; Jameson, G. J.; Biggs, S. Bridging flocculation studied by light scattering and settling. *Chemical Engineering Journal* **2000,** *80,* 3-12.
46. Gregory, J. Monitoring particle aggregation processes. *Advances in Colloid and Interface Science* **2009,** *147–148,* 109-123.
47. Heller, W.; Pugh, T. L. "Steric" stabilization of colloidal solutions by adsorption of flexible macromolecules. *Journal of Polymer Science* **1960,** *47,* 203-217.
48. Hiemenz, P. C.; Vold, R. D. Rates of flocculation and deflocculation in dispersions of carbon black in hydrocarbons. *Journal of Colloid Science* **1965,** *20,* 635-649.
49. Napper, D. H. *Polymeric stabilization of colloidal dispersions*; Academic Press London, 1983; Vol. 7.
50. Vincent, B.; Edwards, J.; Emmett, S.; Jones, A. Depletion flocculation in dispersions of sterically-stabilised particles ("soft spheres"). *Colloids and Surfaces* **1986,** *18,* 261-281.
51. Feigin, R. I.; Napper, D. H. Depletion stabilization and depletion flocculation. *Journal of Colloid and Interface Science* **1980,** *75,* 525-541.
52. Napper, D. H. Steric stabilization. *Journal of Colloid and Interface Science* **1977,** *58,* 390-407.
53. Jenkins, P.; Snowden, M. Depletion flocculation in colloidal dispersions. *Advances in Colloid and Interface Science* **1996,** *68,* 57-96.
54. Tadros, T. F. Steric stabilisation and flocculation by polymers. *Polym J* **1991,** *23,* 683-696.
55. Scheutjens, J. M. H. M.; Fleer, G. J. Statistical theory of the adsorption of interacting chain molecules. 2. Train, loop, and tail size distribution. *The Journal of Physical Chemistry* **1980,** *84,* 178-190.
56. Barnett, K. G.; Cosgrove, T.; Vincent, B.; Cohen-Stuart, M.; Sissons, D. S. The measurement of the polymer-bound fraction at the solid-liquid interface by pulsed nuclear magnetic resonance. *Macromolecules* **1981,** *14,* 1018-1020.
57. Cohen Stuart, M. A.; Fleer, G. J.; Bijsterbosch, B. H. Adsorption of poly(vinyl pyrrolidone) on silica. II. The fraction of bound segments, measured by a variety of techniques. *Journal of Colloid and Interface Science* **1982,** *90,* 321-334.

58. Howard, G. J.; McConnell, P. Adsorption of polymers at the solution-solid interface. I. Polyethers on silica. *Journal of Physical Chemistry* **1967,** *71,* 2974-2981.
59. van den Boomgaard, T.; King, T. A.; Tadros, T. F.; Tang, H.; Vincent, B. The influence of temperature on the adsorption and adsorbed layer thickness of various molecular weight fractions of poly(vinyl alcohol) on polystyrene latex particles. *Journal of Colloid and Interface Science* **1978,** *66,* 68-76.
60. Langmuir, I. The constitution and fundamental properties of solids and liquids. Part 1. Solids. *Journal of the American Chemical Society* **1916,** *38,* 2221-2295.
61. Ho, Y.-S. Isotherms for the sorption of lead onto peat: comparison of linear and non-linear methods. *Polish Journal of Environmental Studies* **2006,** *15,* 81-86.
62. Cosgrove, T.; Mears, S. J.; Obey, T.; Thompson, L.; Wesley, R. D. Polymer, particle, surfactant interactions. *Colloids and Surfaces A: Physicochemical and Engineering Aspects* **1999,** *149,* 329-338.
63. Thies, C. The adsorption of polystyrene-poly(methyl methacrylate) mixtures at a solid-liquid interface 1. *Journal of Physical Chemistry* **1966,** *70,* 3783-3790.
64. Im, D. H.; Park, S. Y.; Hyun, S. H.; Lee, B. Y.; Kim, Y. H. Aqueous dispersion stability of nickel powders prepared by a chemical reduction method. *J Mater Sci* **2004,** *39,* 3629-3633.
65. Growney, D. J.; Mykhaylyk, O. O.; Armes, S. P. Micellization and adsorption behavior of a near-monodisperse polystyrene-based diblock copolymer in nonpolar media. *Langmuir* **2014,** *30,* 6047-6056.
66. Ma, S.-H.; Matrick, H.; Shor, A. C.; Spinelli, H. J. Aqueous pigmented inks for ink jet printers. US Patent 5,085,698, 1992.
67. Croll, S. DLVO theory applied to TiO_2 pigments and other materials in latex paints. *Progress in Organic Coatings* **2002,** *44,* 131-146.
68. Reuter, E.; Silber, S.; Psiorz, C. The use of new block copolymeric dispersing agents for waterborne paints — theoretical and practical aspects. *Progress in Organic Coatings* **1999,** *37,* 161-167.
69. Cawdery, N.; Obey, T. M.; Vincent, B. Colloidal dispersions of electrically conducting polypyrrole particles in various media. *Journal of the Chemical Society, Chemical Communications* **1988,** 1189-1190.
70. Whipple, W. L.; Maltesh, C. Adsorption of cationic flocculants to paper slurries. *Journal of Colloid and Interface Science* **2002,** *256,* 33-40.
71. Zeng, D.; Wu, J.; Kennedy, J. F. Application of a chitosan flocculant to water treatment. *Carbohydrate Polymers* **2008,** *71,* 135-139.
72. Singh, R.; Nayak, B.; Biswal, D.; Tripathy, T.; Banik, K. Biobased polymeric flocculants for industrial effluent treatment. *Mat Res Innovat* **2003,** *7,* 331-340.
73. Weissenborn, P. K.; Warren, L. J.; Dunn, J. G. Optimisation of selective flocculation of ultrafine iron ore. *International Journal of Mineral Processing* **1994,** *42,* 191-213.
74. Bolto, B. A. Soluble polymers in water purification. *Progress in Polymer Science* **1995,** *20,* 987-1041.
75. Pelton, R. H. A model for flocculation in turbulent flow. *Colloids and Surfaces* **1981,** *2,* 259-275.
76. Alonzo, J.; Hinestrosa, J. P.; Mays, J. W.; Kilbey, S. M. Kinetics of preferential adsorption of amphiphilic star block copolymers that tether by their corona blocks at the solid/fluid interface. *Macromolecules* **2014,** *47,* 4048–4055.

77. Stoll, S.; Buffle, J. Computer simulation of bridging flocculation processes: the role of colloid to polymer concentration ratio on aggregation kinetics. *Journal of Colloid and Interface Science* **1996,** *180,* 548-563.
78. Lu, C.; Pelton, R. PEO flocculation of polystyrene-core poly(vinylphenol)-shell latex: an example of ideal bridging. *Langmuir* **2001,** *17,* 7770-7776.
79. McFarlane, N. L.; Wagner, N. J.; Kaler, E. W.; Lynch, M. L. Poly(ethylene oxide) (PEO) and poly(vinyl pyrolidone) (PVP) induce different changes in the colloid stability of nanoparticles. *Langmuir* **2010,** *26,* 13823-13830.
80. Santore, M. M.; Russel, W. B.; Prud'homme, R. K. Experimental and theoretical study of phase transitions induced in colloidal dispersions by associative polymers. *Faraday Discussions of the Chemical Society* **1990,** *90,* 323-333.
81. Hoogeveen, N. G.; Cohen Stuart, M. A.; Fleer, G. J. Can charged (block co)polymers act as stabilisers and flocculants of oxides? *Colloids and Surfaces A: Physicochemical and Engineering Aspects* **1996,** *117,* 77-88.
82. Snowden, M. J.; Clegg, S. M.; Williams, P. A.; Robb, I. D. Flocculation of silica particles by adsorbing and non-adsorbing polymers. *J. Chem. Soc., Faraday Trans.* **1991,** *87,* 2201-2207.
83. Solberg, D.; Wågberg, L. Adsorption and flocculation behavior of cationic polyacrylamide and colloidal silica. *Colloids and Surfaces A: Physicochemical and Engineering Aspects* **2003,** *219,* 161-172.
84. Overbeek, J. T. G. Colloid stability in aqueous and non-aqueous media. Introductory paper. *Discuss. Faraday Soc.* **1966,** *42,* 7-13.
85. Bhattacharjee, S.; Paria, M. K.; Maiti, H. S. Polyvinyl butyral as a dispersant for barium titanate in a non-aqueous suspension. *J Mater Sci* **1993,** *28,* 6490-6495.
86. Mao, Y.; Cates, M. E.; Lekkerkerker, H. N. W. Depletion force in colloidal systems. *Physica A: Statistical Mechanics and its Applications* **1995,** *222,* 10-24.
87. Zhang, X.; Servos, M. R.; Liu, J. Ultrahigh nanoparticle stability against salt, pH, and solvent with retained surface accessibility via depletion stabilization. *Journal of the American Chemical Society* **2012,** *134,* 9910-9913.
88. Asakura, S.; Oosawa, F. Interaction between particles suspended in solutions of macromolecules. *Journal of Polymer Science* **1958,** *33,* 183-192.
89. Newman, S. Note on colloidal dispersions from block copolymers. *J. Appl. Polym. Sci.* **1962,** *6,* S15-S16.
90. Krause, S. Dilute solution properties of a styrene - methyl methacrylate block copolymer. *J. Phys. Chem.* **1964,** *68,* 1948-1955.
91. Tuzar, Z.; Kratochvíl, P. Block and graft copolymer micelles in solution. *Adv. Colloids Interface Sci.* **1976,** *6,* 201-232.
92. Gao, Z.; Eisenberg, A. A model of micellization for block copolymers in solutions. *Macromolecules* **1993,** *26,* 7353-7360.
93. Noolandi, J.; Hong, K. M. Theory of block copolymer micelles in solution. *Macromolecules* **1983,** *16,* 1443-1448.
94. Förster, S.; Antonietti, M. Amphiphilic block copolymers in structure-controlled nanomaterial hybrids. *Adv. Mater.* **1998,** *10,* 195-217.
95. Vagberg, L. J. M.; Cogan, K. A.; Gast, A. P. Light-scattering study of starlike polymeric micelles. *Macromolecules* **1991,** *24,* 1670-1677.
96. Zhang, L.; Eisenberg, A. Multiple morphologies and characteristics of "crew-cut" micelle-like aggregates of polystyrene-b-poly(acrylic acid) diblock copolymers in aqueous solutions. *Journal of the American Chemical Society* **1996,** *118,* 3168-3181.

97. Gao, Z.; Varshney, S. K.; Wong, S.; Eisenberg, A. Block copolymer "crew-cut" micelles in water. *Macromolecules* **1994,** *27,* 7923-7927.
98. Qin, A.; Tian, M.; Ramireddy, C.; Webber, S. E.; Munk, P.; Tuzar, Z. Polystyrene-poly(methacrylic acid) block copolymer micelles. *Macromolecules* **1994,** *27,* 120-126.
99. Baines, F. L.; Armes, S. P.; Billingham, N. C.; Tuzar, Z. Micellization of poly(2-(dimethylamino)ethyl methacrylate-block-methyl methacrylate) copolymers in aqueous solution. *Macromolecules* **1996,** *29,* 8151-8159.
100. Xu, R.; Winnik, M. A.; Hallett, F.; Riess, G.; Croucher, M. D. Light-scattering study of the association behavior of styrene-ethylene oxide block copolymers in aqueous solution. *Macromolecules* **1991,** *24,* 87-93.
101. Moffitt, M.; Khougaz, K.; Eisenberg, A. Micellization of ionic block copolymers. *Acc. Chem. Res.* **1996,** *29,* 95-102.
102. Burnett, G.; Meares, P.; Paton, C. Styrene+ methyl methacrylate block copolymers. Part 2.—Behaviour in dilute solutions. *Transactions of the Faraday Society* **1962,** *58,* 737-746.
103. Higgins, J. S.; Dawkins, J. V.; Maghami, G. G.; Shakir, S. A. Study of micelle formation by the diblock copolymer polystyrene—b-(ethylene-co-propylene) in dodecane by small-angle neutron scattering. *Polymer* **1986,** *27,* 931-936.
104. Stejskal, J.; Hlavatá, D.; Sikora, A.; Konňák, Č.; Pleštil, J.; Kratochvíl, P. Equilibrium and non-equilibrium copolymer micelles: polystyrene-block-poly (ethylene-co-propylene) in decane and in diisopropylether. *Polymer* **1992,** *33,* 3675-3685.
105. Hlavatá, D.; Stejskal, J.; Pleštil, J.; Koňák, Č.; Kratochvíl, P.; Helmstedt, M.; Mio, H.; Laggner, P. Heat-induced transition of polystyrene- block-poly(ethylene-co-propylene) micelles in decane and in dioxane. *Polymer* **1996,** *37,* 799-805.
106. Bahadur, P.; Sastry, N. V.; Marti, S.; Riess, G. Micellar behaviour of styrene—isoprene block copolymers in selective solvents. *Colloids Surf.* **1985,** *16,* 337-346.
107. Bang, J.; Viswanathan, K.; Lodge, T. P.; Park, M. J.; Char, K. Temperature-dependent micellar structures in poly(styrene-b-isoprene) diblock copolymer solutions near the critical micelle temperature. *J. Chem. Phys.* **2004,** *121,* 11489-11500.
108. McConnell, G. A.; Gast, A. P. Melting of ordered arrays and shape transitions in highly concentrated diblock copolymer solutions. *Macromolecules* **1997,** *30,* 435-444.
109. Szwarc, M.; Levy, M.; Milkovich, R. Polymerization initiated by electron transfer to monomer-a new method of formation of block polymers. *Journal of the American Chemical Society* **1956,** *78,* 2656-2657.
110. Szwarc, M. Living Polymers. *Nature* **1956,** *178,* 1168-1169.
111. Mountrichas, G.; Mpiri, M.; Pispas, S. Micelles of star block (PSPI)8 and PSPI diblock copolymers (PS = polystyrene, PI = polyisoprene): structure and kinetics of micellization. *Macromolecules* **2005,** *38,* 940-947.
112. Mandema, W.; Zeldenrust, H.; Emeis, C. A. Association of block copolymers in selective solvents, 1. Measurements on hydrogenated poly(styrene-isoprene) in decane and in trans-decalin. *Die Makromolekulare Chemie* **1979,** *180,* 1521-1538.
113. Schouten, M.; Dorrepaal, J.; Stassen, W. J. M.; Vlak, W. A. H. M.; Mortensen, K. Thermal stability of polystyrene-b-poly(ethylene/propylene) diblock copolymer micelles in paraffinic solvents. *Polymer* **1989,** *30,* 2038-2046.
114. Stacy, C. J.; Kraus, G. Micelle formation by butadiene-styrene block polymers in n-alkanes. *Polym. Eng. Sci.* **1977,** *17,* 627-633.

115. Bang, J.; Jain, S.; Li, Z.; Lodge, T. P.; Pedersen, J. S.; Kesselman, E.; Talmon, Y. Sphere, cylinder, and vesicle nanoaggregates in poly(styrene-b-isoprene) diblock copolymer solutions. *Macromolecules* **2006,** *39,* 1199-1208.
116. D'Oliveira, J. M. R.; Xu, R.; Jensma, T.; Winnik, M. A.; Hruska, Z.; Hurtrez, G.; Riess, G.; Martinho, J. M. G.; Croucher, M. D. Direct adsorption of polystyrene-poly(ethylene oxide) micelles in water onto polystyrene latex particles. *Langmuir* **1993,** *9,* 1092-1097.
117. Kayes, J. B.; Rawlins, D. A. Adsorption characteristics of certain polyoxyethylene-polyoxypropylene block co-polymers on polystyrene latex. *Colloid & Polymer Science* **1979,** *257,* 622-629.
118. Evers, O. A.; Scheutjens, J. M. H. M.; Fleer, G. J. Statistical thermodynamics of block copolymer adsorption. Part 2. Effect of chain composition on the adsorbed amount and layer thickness. *Journal of the Chemical Society, Faraday Transactions* **1990,** *86,* 1333-1340.
119. Awan, M. A.; Dimonie, V. L.; Filippov, L. K.; El-Aasser, M. S. Adsorption kinetics of amphipathic polystyrene-block-polybutadiene onto silicon wafer and polystyrene planar surfaces. *Langmuir* **1997,** *13,* 130-139.
120. Marques, C.; Joanny, J. F.; Leibler, L. Adsorption of block copolymers in selective solvents. *Macromolecules* **1988,** *21,* 1051-1059.
121. Doliveira, J. M. R.; Xu, R. L.; Jensma, T.; Winnik, M. A.; Hruska, Z.; Hurtrez, G.; Riess, G.; Martinho, J. M. G.; Croucher, M. D. Direct adsorption of polystyrene poly(ethylene oxide) micelles in water onto polystyrene latex-particles. *Langmuir* **1993,** *9,* 1092-1097.
122. Lin, Y.; Alexandridis, P. Temperature-dependent adsorption of pluronic F127 block copolymers onto carbon black particles dispersed in aqueous media. *Journal of Physical Chemistry B* **2002,** *106,* 10834-10844.
123. Sarkar, B.; Venugopal, V.; Tsianou, M.; Alexandridis, P. Adsorption of pluronic block copolymers on silica nanoparticles. *Colloids and Surfaces A: Physicochemical and Engineering Aspects* **2013,** *422,* 155-164.
124. An, S. W.; Su, T. J.; Thomas, R. K.; Baines, F. L.; Billingham, N. C.; Armes, S. P.; Penfold, J. Neutron reflectivity of an adsorbed water-soluble block copolymer: a surface transition to micelle-like aggregates at the air/water interface. *The Journal of Physical Chemistry B* **1998,** *102,* 387-393.
125. Webber, G. B.; Wanless, E. J.; Armes, S. P.; Baines, F. L.; Biggs, S. Adsorption of amphiphilic diblock copolymer micelles at the mica/solution interface. *Langmuir* **2001,** *17,* 5551-5561.
126. Webber, G. B.; Wanless, E. J.; Armes, S. P.; Tang, Y. Q.; Li, Y. T.; Biggs, S. Nano-anemones: Stimulus-responsive copolymer-micelle surfaces. *Advanced Materials* **2004,** *16,* 1794-1798.
127. Lin, Y.; Alexandridis, P. Temperature-dependent adsorption of pluronic F127 block copolymers onto carbon black particles dispersed in aqueous media. *Journal of Physical Chemistry B* **2002,** *106,* 10834-10844.
128. Quaglia, F.; Ostacolo, L.; De Rosa, G.; La Rotonda, M. I.; Ammendola, M.; Nese, G.; Maglio, G.; Palumbo, R.; Vauthier, C. Nanoscopic core-shell drug carriers made of amphiphilic triblock and star-diblock copolymers. *International Journal of Pharmaceutics* **2006,** *324,* 56-66.
129. Li, Y.; Narain, R.; Ma, Y.; Lewis, A. L.; Armes, S. P. Biomimetic thermo-responsive star diblock gelators. *Chem. Comm.* **2004,** 2746-2747.

130. Xia, J.; Zhang, X.; Matyjaszewski, K. Synthesis of star-shaped polystyrene by atom transfer radical polymerization using an "arm first" approach. *Macromolecules* **1999,** *32,* 4482-4484.
131. Gao, H.; Matyjaszewski, K. Synthesis of star polymers by a combination of ATRP and the "click" coupling method. *Macromolecules* **2006,** *39,* 4960-4965.
132. Haddleton, D. M.; Crossman, M. C. Synthesis of methacrylic multi-arm star copolymers by "arm-first" group transfer polymerisation. *Macromolecular Chemistry and Physics* **1997,** *198,* 871-881.
133. Coessens, V.; Pintauer, T.; Matyjaszewski, K. Functional polymers by atom transfer radical polymerization. *Progress in Polymer Science* **2001,** *26,* 337-377.
134. Chong, Y.; Le, T. P.; Moad, G.; Rizzardo, E.; Thang, S. H. A more versatile route to block copolymers and other polymers of complex architecture by living radical polymerization: the RAFT process. *Macromolecules* **1999,** *32,* 2071-2074.
135. Li, Y.; Tang, Y.; Narain, R.; Lewis, A. L.; Armes, S. P. Biomimetic stimulus-responsive star diblock gelators. *Langmuir* **2005,** *21,* 9946-9954.
136. Crossland, R. K.; Clair, D. J. S. Lubricating compositions containing hydrogenated block copolymers as viscosity index improvers. US Patent 3,965,019, 1976.
137. LaRiviere, D.; Asfour, A. F. A.; Hage, A.; Gao, J. Viscometric properties of viscosity index improvers in lubricant base oil over a wide temperature range. Part I: group II base oil. *Lubrication Science* **2000,** *12,* 133-143.
138. Donnet, J.-B. *Carbon black: science and technology*; CRC Press, 1993.
139. Ezquerra, T. A.; Connor, M. T.; Roy, S.; Kulescza, M.; Fernandes-Nascimento, J.; Baltá-Calleja, F. J. Alternating-current electrical properties of graphite, carbon-black and carbon-fiber polymeric composites. *Composites Science and Technology* **2001,** *61,* 903-909.
140. Sahouli, B.; Blacher, S.; Brouers, F.; Darmstadt, H.; Roy, C.; Kaliaguine, S. Surface morphology and chemistry of commercial carbon black and carbon black from vacuum pyrolysis of used tyres. *Fuel* **1996,** *75,* 1244-1250.
141. Rieker, T. P.; Hindermann-Bischoff, M.; Ehrburger-Dolle, F. Small-angle X-ray scattering study of the morphology of carbon black mass fractal aggregates in polymeric composites. *Langmuir* **2000,** *16,* 5588-5592.
142. Rieker, T. P.; Misono, S.; Ehrburger-Dolle, F. Small-angle X-ray scattering from carbon blacks: crossover between the fractal and porod regimes. *Langmuir* **1999,** *15,* 914-917.
143. Adams, C. E.; Belmont, J. A.; Johnson, J. E. Ink jet ink formulations containing carbon black products. US Patent 5,571,311, 1996.
144. Koga, T.; Takenaka, M.; Aizawa, K.; Nakamura, M.; Hashimoto, T. Structure factors of dispersible units of carbon black filler in rubbers. *Langmuir* **2005,** *21,* 11409-11413.
145. Clague, A. D. H.; Donnet, J. B.; Wang, T. K.; Peng, J. C. M. A comparison of diesel engine soot with carbon black. *Carbon* **1999,** *37,* 1553-1565.
146. Soenen, S. J. H.; Himmelreich, U.; Nuytten, N.; Pisanic, T. R.; Ferrari, A.; De Cuyper, M. Intracellular nanoparticle coating stability determines nanoparticle diagnostics efficacy and cell functionality. *Small* **2010,** *6,* 2136-2145.
147. Heuer, A. H.; Claussen, N.; Kriven, W. M.; Ruhle, M. Stability of tetragonal ZrO_2 particles in ceramic matrices. *Journal of the American Ceramic Society* **1982,** *65,* 642-650.

148. Guaratini, T.; Gianeti, M. D.; Campos, P. M. B. G. M. Stability of cosmetic formulations containing esters of vitamins E and A: chemical and physical aspects. *International Journal of Pharmaceutics* **2006,** *327,* 12-16.
149. Rosen, J.; Gothard, L. Q. *Encyclopedia of Physical Science*; Infobase Publishing, 2010.
150. Detloff, T.; Sobisch, T.; Lerche, D. Particle size distribution by space or time dependent extinction profiles obtained by analytical centrifugation. *Particle & Particle Systems Characterization* **2006,** *23,* 184-187.
151. Detloff, T.; Sobisch, T.; Lerche, D. Particle size distribution by space or time dependent extinction profiles obtained by analytical centrifugation (concentrated systems). *Powder Technology* **2007,** *174,* 50-55.
152. Vamvakaki, M.; Billingham, N. C.; Armes, S. P.; Watts, J. F.; Greaves, S. J. Controlled structure copolymers for the dispersion of high-performance ceramics in aqueous media. *Journal of Materials Chemistry* **2001,** *11,* 2437-2444.
153. Colard, C. A. L.; Teixeira, R. F. A.; Bon, S. A. F. Unraveling mechanistic events in solids-stabilized emulsion polymerization by monitoring the concentration of nanoparticles in the water phase. *Langmuir* **2010,** *26,* 7915-7921.
154. Nadler, M.; Mahrholz, T.; Riedel, U.; Schilde, C.; Kwade, A. Preparation of colloidal carbon nanotube dispersions and their characterisation using a disc centrifuge. *Carbon* **2008,** *46,* 1384-1392.
155. Fielding, L. A.; Mykhaylyk, O. O.; Armes, S. P.; Fowler, P. W.; Mittal, V.; Fitzpatrick, S. Correcting for a density distribution: particle size analysis of core–shell nanocomposite particles using disk centrifuge photosedimentometry. *Langmuir* **2012,** *28,* 2536-2544.
156. Ballauff, M. SAXS and SANS studies of polymer colloids. *Current Opinion in Colloid & Interface Science* **2001,** *6,* 132-139.
157. Pedersen, J. S.; Svaneborg, C.; Almdal, K.; Hamley, I. W.; Young, R. N. A small-angle neutron and X-ray contrast variation scattering study of the structure of block copolymer micelles: corona shape and excluded volume interactions. *Macromolecules* **2002,** *36,* 416-433.
158. Di Cola, E.; Lefebvre, C.; Deffieux, A.; Narayanan, T.; Borsali, R. Micellar transformations of poly (styrene-b-isoprene) block copolymers in selective solvents. *Soft Matter* **2009,** *5,* 1081-1090.
159. Fielding, L. A.; Lane, J. A.; Derry, M. J.; Mykhaylyk, O. O.; Armes, S. P. Thermo-responsive diblock copolymer worm gels in non-polar solvents. *Journal of the American Chemical Society* **2014,** *136,* 5790-5798.
160. Glatter, O.; Kratky, O. *Small angle X-ray scattering*; Academic Press London, 1982; Vol. 66.
161. Garamus, V. M.; Pedersen, J. S.; Kawasaki, H.; Maeda, H. Scattering from polymerlike micelles of TDAO in salt/water solutions at semidilute concentrations. *Langmuir* **2000,** *16,* 6431-6437.
162. Arleth, L.; Bergström, M.; Pedersen, J. S. Small-angle neutron scattering study of the growth behavior, flexibility, and intermicellar interactions of wormlike SDS micelles in NaBr aqueous solutions. *Langmuir* **2002,** *18,* 5343-5353.
163. Pedersen, J. S. Form factors of block copolymer micelles with spherical, ellipsoidal and cylindrical cores. *Journal of Applied Crystallography* **2000,** *33,* 637-640.
164. Pedersen, J. S.; Schurtenberger, P. Scattering functions of semiflexible polymers with and without excluded volume effects. *Macromolecules* **1996,** *29,* 7602-7612.

165. Braun, A.; Huggins, F. E.; Seifert, S.; Ilavsky, J.; Shah, N.; Kelly, K. E.; Sarofim, A.; Huffman, G. P. Size-range analysis of diesel soot with ultra-small angle X-ray scattering. *Combustion and Flame* **2004,** *137*, 63-72.
166. di Stasio, S.; Mitchell, J. B. A.; LeGarrec, J. L.; Biennier, L.; Wulff, M. Synchrotron SAXS (in situ) identification of three different size modes for soot nanoparticles in a diffusion flame. *Carbon* **2006,** *44*, 1267-1279.
167. Hessler, J. P.; Seifert, S.; Winans, R. E.; Fletcher, T. H. Small-angle X-ray studies of soot inception and growth. *Faraday Discussions* **2001,** *119*, 395-407.
168. Koga, T.; Hashimoto, T.; Takenaka, M.; Aizawa, K.; Amino, N.; Nakamura, M.; Yamaguchi, D.; Koizumi, S. New insight into hierarchical structures of carbon black dispersed in polymer matrices: A combined small-angle scattering study. *Macromolecules* **2008,** *41*, 453-464.
169. Sorensen, C. M.; Oh, C.; Schmidt, P. W.; Rieker, T. P. Scaling description of the structure factor of fractal soot composites. *Physical Review E* **1998,** *58*, 4666-4672.
170. Ehrburger-Dolle, F.; Hindermann-Bischoff, M.; Livet, F.; Bley, F.; Rochas, C.; Geissler, E. Anisotropic ultra-small-angle X-ray scattering in carbon black filled polymers. *Langmuir* **2000,** *17*, 329-334.
171. George, S.; Balla, S.; Gautam, V.; Gautam, M. Effect of diesel soot on lubricant oil viscosity. *Tribology International* **2007,** *40*, 809-818.
172. Gautam, M.; Chitoor, K.; Durbha, M.; Summers, J. C. Effect of diesel soot contaminated oil on engine wear — investigation of novel oil formulations. *Tribology International* **1999,** *32*, 687-699.
173. Biswas, S.; Verma, V.; Schauer, J. J.; Sioutas, C. Chemical speciation of PM emissions from heavy-duty diesel vehicles equipped with diesel particulate filter (DPF) and selective catalytic reduction (SCR) retrofits. *Atmospheric Environment* **2009,** *43*, 1917-1925.
174. Green, D. A.; Lewis, R. The effects of soot-contaminated engine oil on wear and friction: A review. *Proceedings of the Institution of Mechanical Engineers, Part D: Journal of Automobile Engineering* **2008,** *222*, 1669-1689.
175. Esangbedo, C.; Boehman, A. L.; Perez, J. M. Characteristics of diesel engine soot that lead to excessive oil thickening. *Tribology International* **2012,** *47*, 194-203.
176. Rudnick, L. R. *Lubricant additives: chemistry and applications*; CRC Press, 2009.
177. Müller, M.; Topolovec-Miklozic, K.; Dardin, A.; Spikes, H. A. The design of boundary film-forming PMA viscosity modifiers. *Tribology Transactions* **2006,** *49*, 225-232.
178. Smeeth, M.; Spikes, H. A.; Gunsel, S. The formation of viscous surface films by polymer solutions: boundary or elastohydrodynamic lubrication? *Tribology Transactions* **1996,** *39*, 720-725.
179. Bartels, T.; Bock, W.; Braun, J.; Busch, C.; Buss, W.; Dresel, W.; Freiler, C.; Harperscheid, M.; Heckler, R.-P.; Hörner, D.; Kubicki, F.; Lingg, G.; Losch, A.; Luther, R.; Mang, T.; Noll, S.; Omeis, J. Lubricants and Lubrication. In *Ullmann's Encyclopedia of Industrial Chemistry*; Wiley-VCH Verlag GmbH & Co. KGaA, 2000.
180. Inoue, K.; Watanabe, H. Interactions of Engine Oil Additives. *A S L E Transactions* **1983,** *26*, 189-199.
181. Lvovich, V. F.; Smiechowski, M. F. Impedance characterization of industrial lubricants. *Electrochimica Acta* **2006,** *51*, 1487-1496.
182. Palmer, J. J. F. Preparation of alkenyl succinic anhydrides. US Patent 3,912,764, 1975.

183. Tomlinson, A.; Scherer, B.; Karakosta, E.; Oakey, M.; Danks, T. N.; Heyes, D. M.; Taylor, S. E. Adsorption properties of succinimide dispersants on carbonaceous substrates. *Carbon* **2000,** *38,* 13-28.
184. Tsunashima, Y.; Hirata, M.; Kawamata, Y. Diffusion motions and microphase separation of styrene-butadiene diblock copolymer in solution. 1. Extremely dilute solution region. *Macromolecules* **1990,** *23,* 1089-1096.
185. Lariviere, D.; Asfour, A.-F. A.; Hage, A.; Gao, J. Z. Viscometric properties of viscosity index improvers in lubricant base oil over a wide temperature range. Part I: Group II base oil. *Lubrication Science* **2000,** *12,* 133-143.
186. Kiovsky, T. E. Star-shaped polymer reacted with dicarboxylic acid and amine as dispersant viscosity index improver. US Patent 4,141,847, 1979.
187. Rhodes, R. B.; Eckert, R. J.; Loeffler, D. E. Gear oil viscosity index improvers. US Patent 5,070,131, 1991.
188. Won, Y.-Y.; Meeker, S. P.; Trappe, V.; Weitz, D. A.; Diggs, N. Z.; Emert, J. I. Effect of temperature on carbon-black agglomeration in hydrocarbon liquid with adsorbed dispersant. *Langmuir* **2004,** *21,* 924-932.
189. Kozak, D.; Moreton, D.; Vincent, B. The adsorption of non-ionic surfactants on carbon black particles in hydrocarbon media. *Colloids and Surfaces A: Physicochemical and Engineering Aspects* **2009,** *347,* 245-250.
190. Garvey, M. J.; Tadros, T. F.; Vincent, B. A comparison of the volume occupied by macromolecules in the adsorbed state and in bulk solution: adsorption of narrow molecular weight fractions of poly(vinyl alcohol) at the polystyrene/water interface. *Journal of Colloid and Interface Science* **1974,** *49,* 57-68.
191. Stuart, M. A. C.; Waajen, F. H. W. H.; Cosgrove, T.; Vincent, B.; Crowley, T. L. Hydrodynamic thickness of adsorbed polymer layers. *Macromolecules* **1984,** *17,* 1825-1830.
192. Shar, J. A.; Obey, T. M.; Cosgrove, T. Adsorption studies of polyethers Part 1. adsorption onto hydrophobic surfaces. *Colloids and Surfaces A: Physicochemical and Engineering Aspects* **1998,** *136,* 21-33.
193. Killmann, E.; Maier, H.; Baker, J. A. Hydrodynamic layer thicknesses of various adsorbed polymers on precipitated silica and polystyrene latex. *Colloids and Surfaces* **1988,** *31,* 51-71.
194. Baker, J. A.; Pearson, R. A.; Berg, J. C. Influence of particle curvature on polymer adsorption layer thickness. *Langmuir* **1989,** *5,* 339-342.

Chapter 2

Micellisation and adsorption behaviour of a near-monodisperse polystyrene-based diblock copolymer in non-polar media

Introduction

It is well-documented that AB diblock copolymers form well-defined colloidal aggregates when dissolved in a solvent that is selective for one of the two blocks.[1, 2] In general, if the volume fraction of the soluble block is greater than that of the insoluble block, then well-defined spherical micelles are usually obtained.[3, 4, 5, 6] Over the last 20 years there have been many examples of *amphiphilic* AB diblock copolymers that form spherical micelles in aqueous solution,[7, 8, 9, 10, 11, 12] but there is also a considerable volume of older literature describing the micellisation behaviour of *wholly hydrophobic* AB diblock copolymers in organic solvents.[3, 13] In particular, there are many studies of polystyrene-based AB diblock copolymers that form polystyrene-core micelles in non-polar solvents such as *n*-alkanes.[14, 15, 16, 17, 18, 19] Such diblock copolymers are readily prepared using classical anionic polymerisation,[20, 21] with the soluble block typically being based on either polybutadiene, polyisoprene or their hydrogenated derivatives.[15, 16, 17, 22, 23, 24, 25, 26]

Over the last fifteen years or so, there have been a number of reports describing the interfacial adsorption of block copolymer micelles.[27, 28, 29, 30, 31, 32] For example, Thomas and co-workers used neutron reflectivity to deduce the presence of cationic diblock copolymer micelles adsorbed at the planar air-water interface.[33] Webber *et al*. showed that similar copolymers also adsorb at the planar mica/water interface to produce ordered micelle monolayers that can be visualised directly by atomic force microscopy.[34, 35] Winnik *et al*. reported the adsorption of poly(ethylene oxide)-polystyrene diblock copolymer micelles onto polystyrene latex particles from aqueous solution,[36] while Alexandridis and co-workers found that even rather weakly hydrophobic anchor blocks based on poly(propylene oxide) are sufficient to ensure adsorption of Pluronic block copolymer micelles onto either silica at low pH[37] or carbon black at pH 7.[38] Such adsorbed micelle layers can confer effective steric stabilisation,[39] which may offer technological advantages for aqueous ink dispersions based on carbon black particles.[40]

In this Chapter, the micellisation behaviour of a commercially-available poly(styrene-*b*-hydrogenated isoprene) (PS-PEP) diblock copolymer in two *n*-alkanes has been assessed using a range of techniques, including transmission electron microscopy (TEM), small-angle X-ray scattering (SAXS), dynamic light scattering (DLS), and variable temperature ^{1}H NMR spectroscopy. The adsorption of this diblock copolymer onto a model colloidal substrate, carbon black, is confirmed by X-ray photoelectron spectroscopy (XPS). The adsorbed amount of copolymer is determined indirectly via a supernatant depletion assay based on UV spectroscopy and compared to that obtained via a direct method based on thermogravimetry. In particular, the experimental evidence for micellar adsorption onto carbon black (as opposed to the adsorption of individual copolymer chains, or unimers) is critically examined.

Experimental

Materials

The PS-PEP diblock copolymer used in this work is a commercial product obtained from BP Formulated Products Technology, and was used as received. It was prepared by living anionic polymerisation, which usually ensures good blocking efficiency and a relatively narrow molecular weight distribution.[21] Chloroform, *n*-heptane and *n*-dodecane solvents were obtained from Fisher Scientific UK Ltd and were used as received. Deuterated solvents for NMR studies were obtained from Goss Scientific Ltd, UK and were used as received. The carbon black (Regal 250 R grade) was supplied by Cabot Corporation (Billerica, MA, USA) and was used as received.

Gel permeation chromatography. The molecular weight distribution of the PS-PEP diblock copolymer was assessed by gel permeation chromatography (GPC) using THF eluent. The THF GPC set-up was equipped with two 5 μm 'Mixed C' 30 cm columns, a Varian 290-LC pump and a WellChrom K-2301 refractive index detector operating at 950 ± 30 nm. The THF mobile phase contained 2.0 v/v% triethylamine and 0.05 w/v% butylhydroxytoluene (BHT) and the flow rate was fixed at 1.0 mL min^{-1}. A series of ten near-monodisperse polystyrene standards (M_n = 580 to 552,500 g mol^{-1}) were used for calibration.

Dynamic light scattering. Hydrodynamic diameters were determined by DLS at 25°C using a Malvern Zetasizer NanoZS model ZEN 3600 instrument equipped with a 4 mW He−Ne solid-state laser operating at 633 nm. Back-scattered light was detected at 173°, and the mean particle diameter was calculated from the quadratic fitting of the correlation function over 30 runs of 10 seconds duration. All measurements were performed three times and data were analysed using CONTIN software.

Transmission electron microscopy. Studies were conducted using a Phillips CM100 microscope operating at 100 kV on unstained samples prepared by drying a drop of dilute sample (approximately 0.01 wt%) on a carbon-coated copper grid.

Small-angle X-ray scattering. SAXS patterns were recorded at a synchrotron source (ESRF, station ID02, Grenoble, France) using monochromatic X-ray radiation (wavelength λ = 0.0995 nm) and a 2D FReLoN Kodak CCD detector (frame exposure time 0.1 s). Camera lengths of either 9.1 m or 3 m were utilised for data collection, which correspond to a q range of 0.01 nm^{-1} to 0.2 nm^{-1} (where $q = \frac{4\pi \sin\theta}{\lambda}$ is the scattering vector and 2θ is the scattering angle). Dilute (1.0% w/w) PS-PEP diblock copolymer micellar dispersions or solutions in various solvents were injected into a thin-walled flow-through quartz capillary cell (1.4 mm diameter; wall thickness ~ 10 μm). Scattering data were reduced using a SAXS utilities software package (which allows integration, normalisation, background subtraction and merging of scattering patterns) and were further analysed using Irena SAS macros for Igor Pro[41].

Model used for SAXS analysis

TEM and DLS studies (see Figures 1.3-1.5) suggest that dispersions prepared via direct dissolution of the PS-PEP diblock copolymer in *n*-alkanes at 20ºC comprise a mixture of large spheres and worm-like particles, whereas only relatively small spheres were observed after heating such dispersions at 90°C (Figure 2.5). Given the relatively low polystyrene content of the copolymer (28 mol%), these spheres are best described as star-like micelles with relatively small PS cores and relatively thick brush-like PEP coronas.[44] Such structures are readily amenable to SAXS analysis. A structural model

has already been developed for star-like micelles[44] and is briefly summarised here. The general equation for the scattering intensity, *I*, of interacting micelles is expressed as[56]

$$I = F_{mic}(q) + F_{mic}^{av}(q)[S_{PY}(q, R_{PY}, f_{PY}) - 1] \quad (1)$$

where the star-like micelle form factor is represented as[44]

$$F_{mic}(q) = N_{agg}^2 \beta_s^2 A_s^2(q, R_s) + N_{agg} \beta_c^2 F_c(q, R_g) + N_{agg}[N_{agg} - F_c(0)] \beta_c^2 A_c^2(q) + 2N_{agg}^2 \beta_s \beta_c A_s A_c(q) \quad (2)$$

and R_s is the micelle core radius and R_g is the radius of gyration of the PEP coronal block. The X-ray scattering length contrast between the core block and the coronal block is $\beta_s = V_s(\xi_s - \xi_{sol})$ and $\beta_c = V_c(\xi_c - \xi_{sol})$, respectively, where ξ_s, ξ_c, and ξ_{sol} are the X-ray scattering length densities of the core block (ξ_{PS} = 9.58 × 10^{10} cm^{-2}), the coronal block (ξ_{PEP} = 8.81 × 10^{10} cm^{-2}) and solvent ($\xi_{heptane}$ = 6.68 × 10^{10} cm^{-2} or $\xi_{dodecane}$ = 7.63 × 10^{10} cm^{-2}), respectively. V_s and V_c are the volumes of the PS core block and the PEP coronal block, respectively. Expressing the diblock copolymer composition in terms of mol fractions (0.28 for PS and 0.72 for PEP) and estimating the molecular weights of each block to be 44.3 kg mol^{-1} for PS and 76.7 kg mol^{-1} for PEP, the mean number of monomer repeat units is calculated to be 426 for the core block and 1094 for the coronal block, respectively. Assuming reasonable values for the mass densities of each block (ρ_{PS} = 1.051 g cm^{-3} and ρ_{PEP} = 0.91 g cm^{-3}) the core block and the coronal block volumes can be calculated using $V = \frac{M_w}{N_A \rho}$ to be 70 nm^3 and 140 nm^3, respectively. The mean micelle aggregation number, N_{agg}, is given by $N_{agg} = (1 - x_{sol})\frac{4\pi R_s^3}{3V_s}$, where x_{sol} is the concentration of *n*-alkane solvent in the PS-based micelle core. The amplitude of the core self-term is given by: $A_s(q, R_s) = \Phi(qR_s)\exp\left(-\frac{q^2\sigma^2}{2}\right)$, where $\Phi(qR_s) = \frac{3[\sin(qR_s) - qR_s\cos(qR_s)]}{(qR_s)^3}$ is the amplitude of the form factor for a sphere. The exponent term represents a sigmoidal interface between the blocks of width σ that describes a decaying scattering length density at the core surface. The self-correlation term of the corona block is given by the effective single-chain form factor

$F_c(q,R_g)=\frac{F_{exv}(q,R_g)}{1+\nu F_{exv}(q,R_g)}$, where $F_{exv}(q, R_g)$ is the form factor for self-avoiding chains[57] (we use equation 13 in this reference and the formalism therein is also adopted) and ν is a parameter related to the chain-chain interaction within the corona. The effective forward scattering is $F_c(0)=\frac{1}{1+\nu}$. For these star-like micelles, the contribution of the coronal blocks to the scattering signal is comparable to that from the micelle core [$(\beta_c/\beta_s)^2 \approx 2.2$ in *n*-heptane and ≈ 1.5 in *n*-dodecane]. Thus the amplitude of the corona chain form factor is obtained from a normalised Fourier transform of the radial density distribution function of the corona chains:

$$A_c(q)=\frac{\int_{R_s}^{R_s+2s}\mu_c(r)\frac{\sin(qr)}{qr}r^2dr}{\int_{R_s}^{R_s+2s}\mu_c(r)r^2dr}\exp\left(-\frac{q^2\sigma^2}{2}\right) \quad (3)$$

The radial profile, $\mu_c(r)$, can be expressed by a linear combination of two cubic b splines, with two fitting parameters *s* and *a* corresponding to the width of the profile and the weight coefficient, respectively. This information can be found elsewhere,[44, 58] as can the approximate integrated form of equation 3. The form factor of the average radial scattering length density distribution of micelles in equation 1 is used as

$$F_{mic}^{av}(q)=N_{agg}^2[\beta_s A_s(q,R_s)+\beta_c A_c(q)]^2 \quad (4)$$

Use of equation 1 implicitly assumes that interactions between star-like micelles can be described by a structure factor based on the Percus-Yevick approximation $S_{PY}(q,R_{PY},f_{PY})$,[59] where $R_{PY} = R_s + \Delta R$ is the interaction radius and f_{PY} is the hard-sphere volume fraction. In this model, the size polydispersity for the star-like micelles can be calculated by assuming a normal distribution of the micelle core radius R_s with a standard deviation σ_{Rs}. Thus the total number of fitting parameters is ten (R_s, σ_{Rs}, R_g, x_{sol}, σ, *s*, *a*, ν, ΔR and f_{PY}). General parameters such as the copolymer volume fraction and various parameters related to the SAXS measurement geometry are not included in this list. Irena SAS Igor Pro macros were used for model fitting. During the SAXS studies, air bubbles were observed in some of the copolymer dispersions during their

injection into the glass capillary cell. This artefact most likely explains the upturn in scattering intensity observed at very low q (q < 0.03 nm^{-1}) in the resulting SAXS patterns. A unified fit approach[60] incorporated in the Irena SAS programme was used to account for this effect.

Sample/solvent	Thermal history	R_s (σ_{Rs}) /nm	s /nm	ΔR /nm	f_{PY}
PS-PEP in *n*-heptane	as-prepared at 20°C	15.1 (1.3)	36.1	38.5	0.15
	annealed at 90°C	10.7 (1.0)	29.3	31.7	0.21
PS-PEP in *n*-dodecane	as-prepared at 20°C	n.d.	n.d.	n.d.	n.d.
	annealed at 110°C	9.5 (0.9)	28.6	28.6	0.19

Table 2.1. Structural parameters obtained from SAXS data fitting: radius of the star-like micelle core (R_s, nm), standard deviation of the radius (σ_{Rs}, nm), width of the corona electron density profile (s, nm), the interaction distance between the star-like micelle core boundaries ($\Delta R = R_{PY} - R_s$, nm) and the hard-sphere volume fraction (f_{PY}). n.d. stands for no data.

^{1}H NMR spectroscopy. The mean polystyrene content of the PS-PEP diblock copolymer dissolved in a non-selective solvent ($CDCl_3$) was determined using a Bruker AV1-250 MHz NMR spectrometer (64 scans per spectrum). Variable temperature spectra were recorded between 25°C and 110°C using either d_{16}-heptane or d_{26}-dodecane using a Bruker AV1-400 MHz NMR spectrometer (32 scans per spectrum).

Helium pycnometry. The solid-state density of the Regal 250R carbon black was measured using a Micrometrics AccuPyc 1330 helium pycnometer at 20°C.

Surface area analysis. BET surface area measurements were performed using a Quantachrome Nova 1000e instrument with dinitrogen gas (mean area per molecule = 16.2 Å^2) as an adsorbate at 77 K. Samples were degassed under vacuum at 100°C for at least 15 h prior to analysis. The particle diameter, d, was calculated using the formula $d = 6/(\rho.A_s)$, where A_s is the BET specific surface area in m^2 g^{-1} and ρ is the carbon black density in g m^{-3} obtained from helium pycnometry.

UV spectroscopy. UV spectra were recorded at 20°C for the PS-PEP diblock copolymer dissolved in 1:1 chloroform/*n*-heptane mixtures (i.e. the *n*-heptane supernatant diluted with an equal volume of chloroform) using a Perkin Elmer Lambda

25 instrument operating between 200 and 500 nm. A calibration curve was constructed for the same copolymer dissolved in pure chloroform and gave a molar extinction coefficient of 222 ± 2 mol^{-1} dm^3 cm^{-1}, which is close to the literature value reported for polystyrene.[42]

Copolymer adsorption onto carbon black via supernatant depletion assay using UV spectroscopy. The desired mass of PS-PEP (3.0 – 90.0 mg) was weighed into a glass vial and carbon black (300.0 mg) was weighed into a separate vial. Then *n*-heptane (5.00 mL) was added to the PS-PEP. This suspension was stirred at 20^{o}C (Turrax stirrer, 1 minute) then heated up to 90^{o}C for 1 h. The resulting copolymer micelle dispersion was added to the pre-weighed carbon black, stirred (Turrax stirrer, 1 minute), sonicated for 1 h, then left on a roller mill for 16 h overnight. The resulting dispersion was centrifuged for 4 h at 18,000 rpm in a centrifuge rotor that was pre-cooled to 15^{o}C so as to minimise solvent evaporation. Taking care not to disturb the sedimented carbon black particles, the supernatant was decanted into an empty vial and then 0.40 mL of this solution was diluted with an equal volume of pure chloroform to ensure molecular dissolution of the copolymer chains prior to analysis by UV spectroscopy. The aromatic chromophore at 262 nm due to the polystyrene block was used to quantify the copolymer concentration remaining in the supernatant after exposure to the carbon black, thus enabling the adsorbed amount to be determined by difference.

Thermogravimetric analysis. Analyses were conducted on the pristine diblock copolymer, carbon black alone and copolymer-coated carbon black particles. Each sample was heated under a nitrogen atmosphere up to 800^{o}C at a heating rate of 20^{o}C min^{-1} using a Q500 TGA instrument (TA Instruments). The mass loss observed between 300 and 500^{o}C was attributed to complete pyrolysis of the diblock copolymer, with the remaining incombustible residue being attributed to carbon black.

X-ray photoelectron spectroscopy. Studies were conducted on carbon black dispersion samples pressed onto indium foil using a Kratos Axis Ultra DLD X-ray photoelectron spectrometer equipped with a monochromatic Al X-ray source ($h\nu$ = 1486.6 eV) operating at 6.0 mA and 15 kV at a typical base pressure of 10^{-8} torr. The step size was

1.0 eV for all survey spectra (pass energy = 160 eV). Spectra were typically acquired from at least two separate sample areas.

Results and Discussion

Copolymer Characterisation

The commercial PS-PEP diblock copolymer used in this work can be prepared by sequential monomer addition using anionic polymerisation. It had a relatively narrow molecular weight distribution (M_w/M_n = 1.04) and an apparent M_n of 117,000 g mol^{-1} as judged by gel permeation chromatography in tetrahydrofuran (THF) using a series of near-monodisperse polystyrene calibration standards. ^{1}H NMR spectroscopy analysis indicated a polystyrene content of 28 mol % (see Figure 2.1).

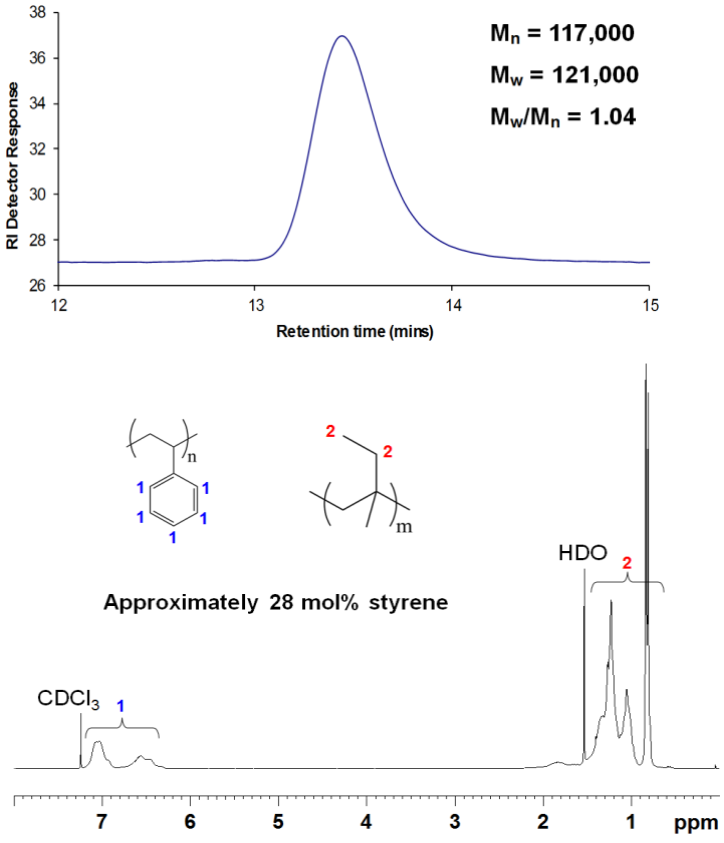

Figure 2.1. ^{1}H NMR spectrum ($CDCl_3$) and THF GPC curve obtained for PS-PEP diblock copolymer obtained for PS-PEP diblock copolymer. The molecular weight data are expressed relative to polystyrene standards. A comparison between the integrated aromatic signals and those of the aliphatic backbone indicate a polystyrene content of 28 mol % via ^{1}H NMR.

Copolymer Self-Assembly

The micellisation of PS-PEP diblock copolymers of comparable molecular weight and polystyrene content (1.05 x 10^5 g mol^{-1}; 34% by mass) was studied by Stejskal *et al.*, who found that direct dissolution in *n*-decane at 20^{o}C invariably led to the formation of ill-defined relatively large micellar aggregates.[15, 16] However, heating such colloidal dispersions up to a minimum of 90^{o}C produced smaller, well-defined micelles of relatively low polydispersity, which remained stable on cooling to 20^{o}C. Similar observations were also reported by Price and co-workers for the same class of diblock copolymer.[43] These two scenarios are depicted in Figure 2.2 for the specific diblock copolymer used in the present work, along with the molecular dissolution that occurs when dissolving such PS-PEP diblock copolymers in non-selective solvents such as chloroform (this work) or THF.[15] In the present study, the PS-PEP diblock copolymer/*n*-alkane system described by Stejskal *et al.*[15, 16] and others[44] has been revisited (see Figure 2.2) to gain further physical insights by utilising modern instrumentation techniques such as transmission electron microscopy, ^{1}H NMR spectroscopy and a synchrotron source to substantially extend the accessible *q* range in small-angle X-ray scattering (SAXS) experiments. In addition, preliminary copolymer adsorption studies using carbon black have also been conducted. This model colloidal substrate is generally considered to be an appropriate mimic for diesel soot particulates, see Chapters 1 and 5.[32, 45, 46, 47, 48]

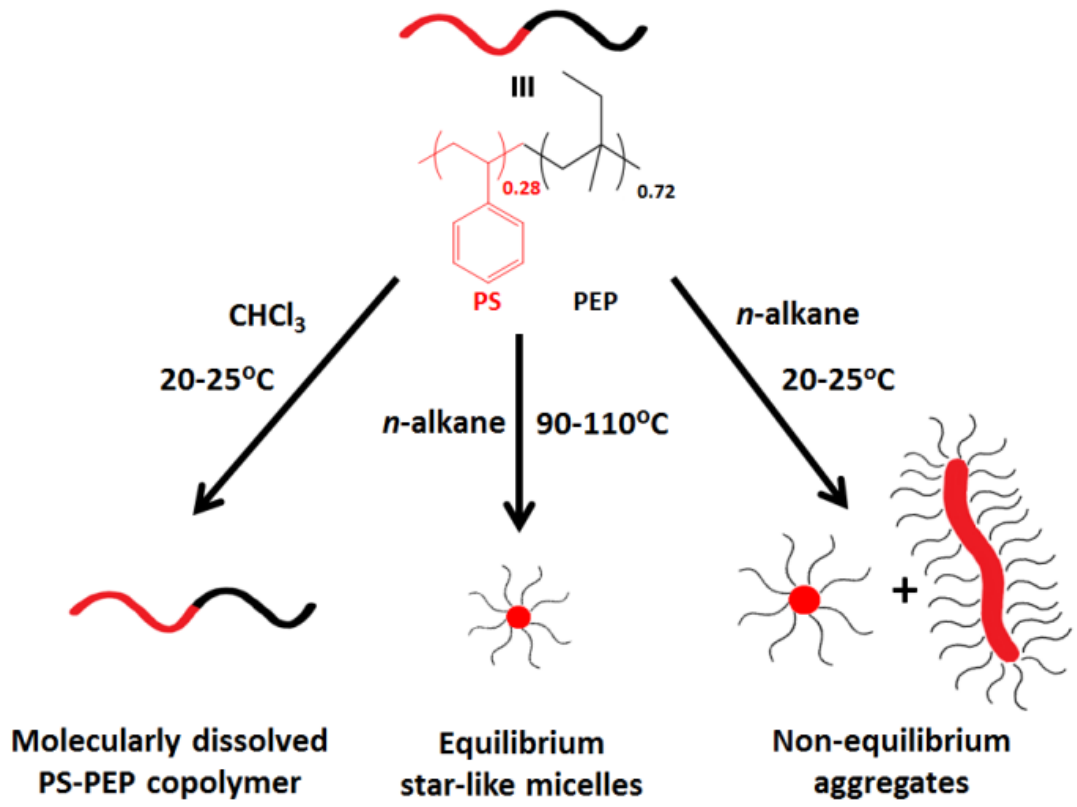

Figure 2.2. Schematic overview depicting the three states of the PS-PEP diblock copolymer: (a) molecularly dissolved in chloroform, (b) small well-defined micelles when dispersed in either *n*-heptane or *n*-dodecane followed by a thermal cycle and (c) large ill-defined colloidal aggregates when dispersed in either *n*-heptane or *n*-dodecane with no thermal cycle.

Effect of Solvent Quality on Copolymer Self-Assembly

Figure 2.3 depicts the intensity-average diameter of PS-PEP chains obtained when this copolymer is first molecularly dissolved in chloroform and then diluted using various amounts of *n*-heptane to produce a final fixed copolymer concentration of 1.0 % w/w.

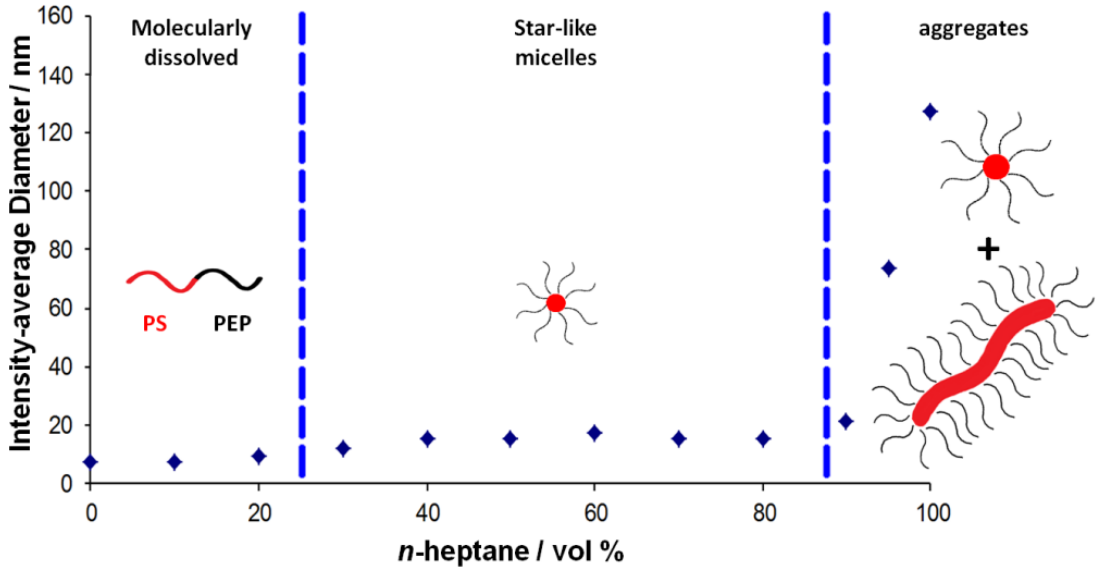

Figure 2.3. DLS intensity-average diameter vs. volume fraction of *n*-heptane for PS-PEP diblock copolymer at 20ºC. In each case (apart from 100 vol % *n*-heptane), the copolymer was first dissolved in chloroform, followed by dilution with the desired amount of *n*-heptane.

Initially, molecular dissolution occurs up to around 25 vol % added *n*-heptane. Then small well-defined micelles of 15-20 nm diameter are produced for solvent compositions containing up to around 85-90 vol% *n*-heptane, followed by the formation of much larger aggregates of more than 70 nm diameter at 95 vol% *n*-heptane. Direct dissolution in pure *n*-heptane leads to polydisperse colloidal aggregates of around 128 nm diameter. However, this value was derived using the Stokes-Einstein equation, which assumes perfectly monodisperse, non-interacting spheres. Stejskal and co-workers showed such ill-defined dispersions can be readily converted into well-defined micelles via a single thermal cycle.[15, 16] This is illustrated in Figure 2.4, which shows representative transmission electron micrographs of the mixture of copolymer morphologies (spheres plus cylinders) that are present when the PS-PEP diblock copolymer is dissolved directly in (a) *n*-heptane and (c) *n*-dodecane. The latter solvent was generally preferred to *n*-heptane since its higher boiling point minimises evaporative losses and allows access to higher temperatures. Small well-defined spherical micelles are produced on heating these initial ill-defined copolymer dispersions for 1 h up to 90ºC in (b) *n*-heptane or 110ºC in (d) *n*-dodecane. Digital photographs depicting the visual appearance of the corresponding copolymer dispersions before and after this thermal cycle are also shown.

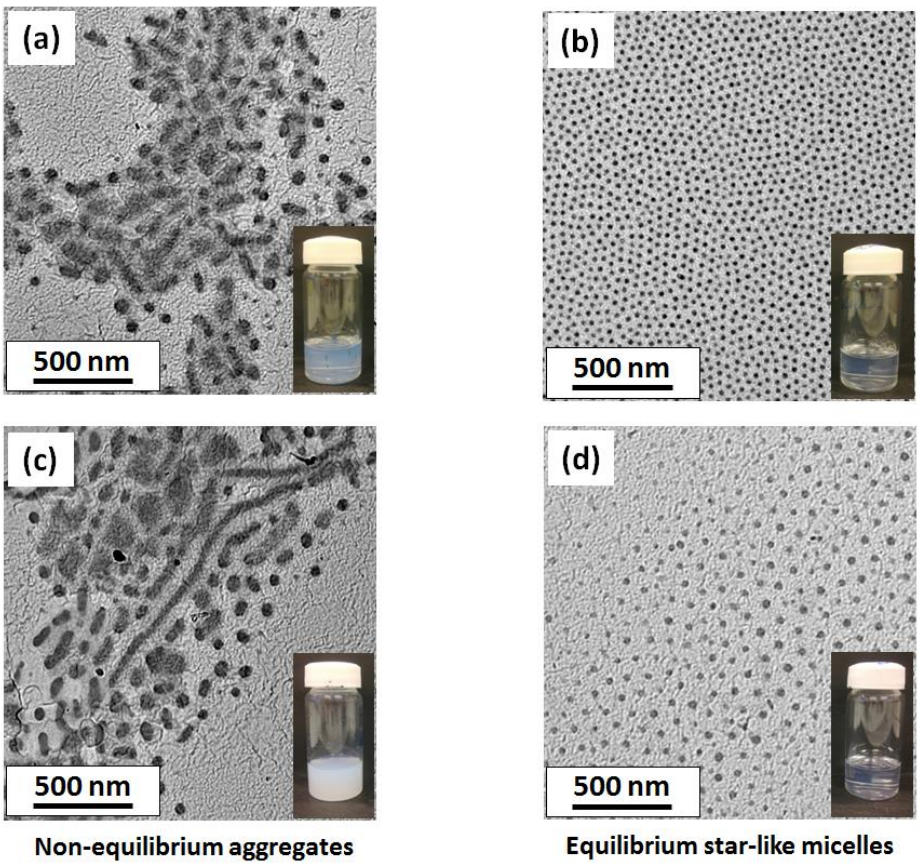

Figure 2.4. TEM images obtained for the PS-PEP diblock copolymer used in this study. (a) Large ill-defined colloidal aggregates formed via direct dispersion at 20°C in *n*-heptane and (b) the much smaller spherical star-like micelles formed at 20°C on heating this initial dispersion to 90°C for 1 h in *n*-heptane. (c) and (d) show the same copolymer dispersed in *n*-dodecane at 20°C and after heating to 110°C prior to cooling to 20°C, respectively. The corresponding digital photographs recorded for these four dispersions are also shown as insets; these images confirm that much less turbid dispersions are observed for both solvents after the thermal cycle.

As expected, the dispersions containing the larger, more polydisperse aggregates are significantly more turbid than the micellar dispersion obtained after the thermal treatment. According to Stejskal *et al.*, the larger particles are most likely an artefact of the solid-state copolymer morphology.[15, 16] This seems to be a reasonable explanation. Since the PS block is the minor component, the PS-PEP diblock copolymer is expected to form mainly spherical PS domains embedded in a PEP matrix in the solid state.[49]

Under these conditions the PEP chains are in their unperturbed dimensions, which leads to a relatively large aggregation number and micelle domain size. On direct dissolution in an *n*-alkane at 20^{o}C, the frozen, non-equilibrium nature of the glassy PS cores prevents any structural arrangement (see later discussion). Thus, the original relatively large kinetically-trapped micelles persist, despite the better-than-θ-solvent environment for the PEP coronal chains (which favours the formation of smaller micelles of lower aggregation number). This subtle change in copolymer morphology can only occur if the frozen micelles are subjected to sufficient thermal energy via a subsequent heating cycle. Such experiments are described below.

Effect of Thermal Cycling on Copolymer Morphology

The pronounced reduction in copolymer dimensions that occurs on increasing the solution temperature is shown in Figure 2.5 for a 20^{o}C – 90^{o}C – 20^{o}C thermal cycle conducted using *n*-heptane. The apparent 'sphere-equivalent' diameter of 128 nm observed at 20^{o}C is physically rather meaningless, since TEM studies indicate the presence of a significant fraction of polydisperse cylinders under these conditions. On heating up to 70-80^{o}C, the mean size of the colloidal aggregates is dramatically reduced and TEM studies confirm the formation of well-defined spherical micelles, which makes the DLS data rather more reliable and easier to interpret. Moreover, analysis of the DLS data using CONTIN software reveals bimodal size distributions (see, for example, inset (b) recorded at 80^{o}C), with the smaller population at around 5-6 nm corresponding to molecularly dissolved copolymer chains (or unimers).

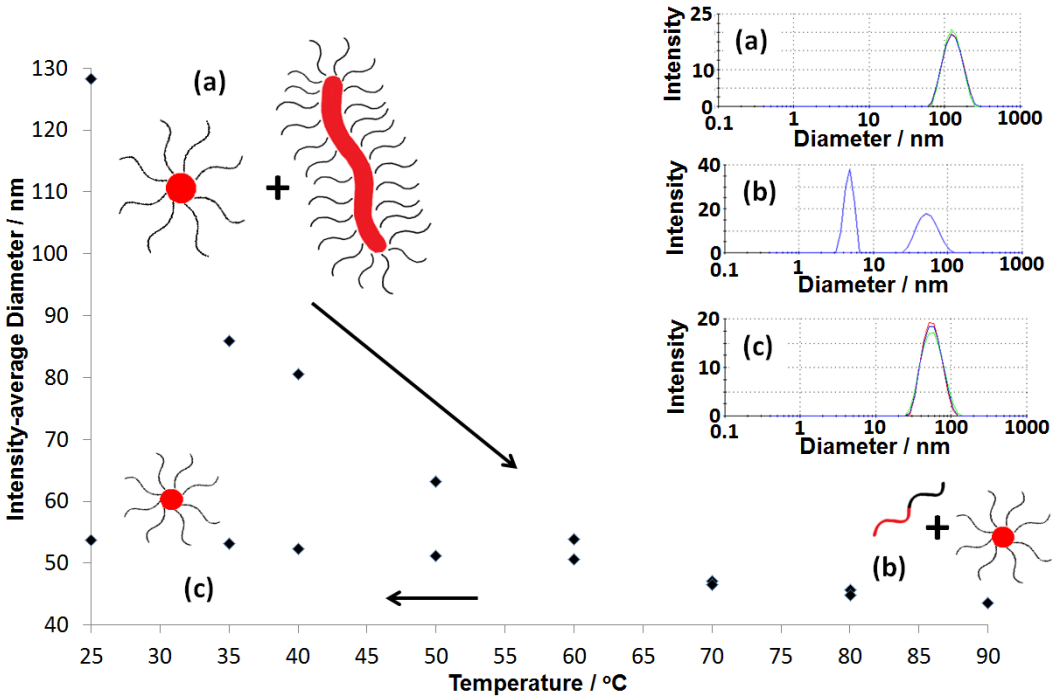

Figure 2.5. DLS intensity-average diameter obtained for (a) the PS-PEP diblock copolymer dispersed directly in *n*-heptane at 25ºC, (b) the gradual reduction in colloidal dimensions on heating up to 90ºC, producing relatively small star-like micelles that are in equilibrium with molecularly dissolved copolymer chains (unimers), (c) the star-like micelles that are formed on cooling to 25ºC. The inset DLS size distributions confirm the presence of unimers in (b).

Presumably, the initial cylinders are converted into spheres on heating via a 'budding' process. This interpretation is supported by the observation that the intensity-average diameter of the small spheres is comparable to the mean width of the original cylinders. Similar observations were recently reported by Blanazs *et al.*,[50] but in this latter case a worm-to-sphere transition occurred on *cooling* an aqueous dispersion of methacrylic diblock copolymer worms, rather than on heating. This qualitative difference is attributed to the inverse temperature-solubility often exhibited by water-soluble polymers.[51]

SAXS Studies of Diblock Copolymer Micelles

The model used to fit the four SAXS patterns shown in Figure 2.6 is described in the experimental section. A pronounced peak at $q < 0.08$ nm^{-1} indicates structure factor effects resulting from inter-micelle interactions. These interactions are attributed to the relatively long highly swollen PEP corona block and occur even at relatively low

volume fractions.[44] Thus, a suitable form factor and structure factor were incorporated into the SAXS model chosen to analyse this system (see experimental section). After consideration of a preliminary analysis using this structural model, and bearing in mind previous literature data obtained for a similar PS-PEP diblock copolymer dispersion in *n*-decane,[44] some parameters were fixed at estimated physically realistic values (e.g. ν = 2, σ = 5 nm and a = 0) prior to fitting. The sigmoidal interface width, σ, was taken to be equal to the projected contour length of the PEP repeat unit (i.e. four all-*trans* C-C bonds). It was also assumed that two parameters associated with the corona dimensions, ΔR and s, (see experimental section) could be related to the radius of gyration of the corona block, R_g such that $\Delta R \approx 2R_g$ and $s \approx 2R_g$. After incorporating these physical constraints within the model, the mixing parameter, a, which describes the radial profile of the corona scattering length density, tended to zero. This enabled the overall number of fitting parameters for equation 1 to be reduced from ten (see experimental section) to seven, thus simplifying the model.

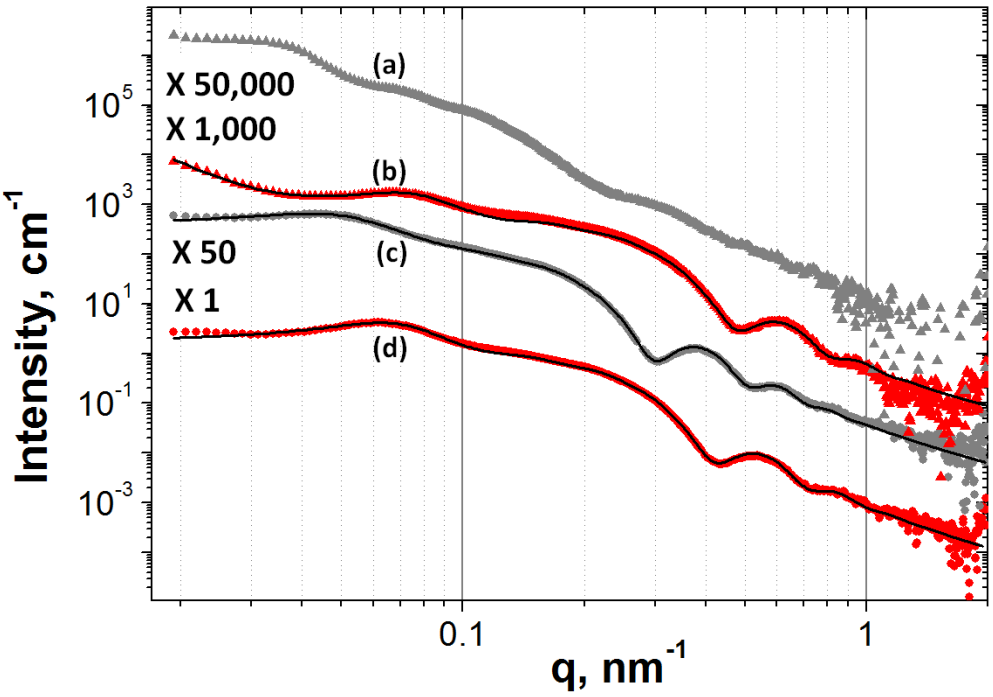

Figure 2.6. SAXS patterns obtained for PS-PEP diblock copolymer dispersions: (a) as-prepared in *n*-dodecane at 20°C; (b) after thermal annealing in *n*-dodecane at 110°C; (c) as-prepared in *n*-heptane at 20°C; (d) after thermal annealing in *n*-heptane at 90°C. The data in each SAXS pattern are multiplied by an appropriate coefficient for the sake of clarity. The solid lines represent fittings to the SAXS data obtained using the star-like micelle model.

The star-like micelle model produced a good fit to the SAXS data for PS-PEP diblock copolymer dispersions in *n*-heptane both before and after thermal cycling (see Figure 2.6 and Table 2.1). This suggests that star-like micelles are the dominant morphology in these samples, which is in good agreement with TEM observations (see Figure 2.4). However, an appropriate structural model could not be identified for the as-prepared PS-PEP diblock copolymer dispersion in *n*-dodecane. In this case, neither the star-like micelle model nor a worm-like micelle model produced a satisfactory fit to the observed SAXS pattern. This finding also correlates with TEM studies, which indicate an ill-defined mixed copolymer morphology for this sample (see Figure 2.4). Detailed SAXS analysis indicated a relatively low volume fraction of the *n*-alkane solvent in the micelle cores (x_{sol}). More specifically, it is estimated that $x_{sol} \approx 0.10$ for *n*-heptane and *n*-dodecane, which is close to values reported by Pedersen and co-workers for a related system.[44] This is consistent with the fact that *n*-alkanes are non-solvents for the PS block at room temperature. SAXS studies also confirm that the large polydisperse colloidal aggregates initially produced via direct dissolution in *n*-heptane or *n*-dodecane at 20^{o}C are transformed into smaller well-defined star-like micelles after heating up to 90^{o}C (*n*-heptane) or 110^{o}C (*n*-dodecane). For example, the mean micelle core radius of as-prepared PS-PEP aggregates in *n*-heptane is reduced from 15.1 to 10.7 nm after such a thermal cycle (see Table 2.1). In addition, SAXS analyses demonstrate that thermal cycling in both solvents yielded analogous star-like micelles with a mean radius for the PS-core micelles (R_s) of approximately 10 nm and a PEP corona thickness (s or ΔR) of around 30 nm, giving an overall particle radius of 40 nm, see Table 2.1. Thus these observations are similar to those reported by Pedersen and co-workers: [44] appropriate heat treatment generates star-like PS-PEP micelles (with a co-existing population of molecularly dissolved copolymer chains) which are frozen on cooling to 20^{o}C. In the present study, SAXS analyses indicated an R_g of 15.5 nm for the PEP corona block. This is in good agreement with Monte Carlo simulations performed by Pedersen and co-workers for a similar diblock copolymer (with PS and PEP block molecular weights of 40 kg mol^{-1} and 80 kg mol^{-1}, respectively) in *n*-decane.[44] Such star-like PS-PEP micelles were estimated to have an $R_g \sim 15.0$ nm.

Variable Temperature ^{1}H NMR Studies

Variable temperature ^{1}H NMR studies were conducted in order to gain some spectroscopic insights into the break-up of the large polydisperse aggregates and formation of well-defined micelles during the thermal cycle. Both d_{16}-heptane and d_{26}-dodecane were utilised for these experiments, with the much higher b.p. of the latter solvent allowing a wider temperature range to be accessed. Figure 2.7a shows the partial ^{1}H NMR spectra recorded for the copolymer dispersion in d_{26}-dodecane on heating up to 110^{o}C. Initially, no NMR signals were observed (see spectra recorded at 25^{o}C and 55^{o}C). In contrast, broad aromatic signals that are characteristic of the core-forming PS block are observed in the 70^{o}C to 110^{o}C range, which disappear completely on cooling to 25^{o}C. Similar observations were made for the copolymer dispersion in d_{16}-heptane, although 80^{o}C was the limit of this particular study due to the relatively low solvent boiling point (~ 98^{o}C), see Figure 2.7b. This indicates significant swelling of the micelle cores by the hot *n*-alkane solvent. This is perfectly understandable given that polystyrene is insoluble in cyclohexane at 20^{o}C, but becomes completely soluble when heated above 34^{o}C.[52]

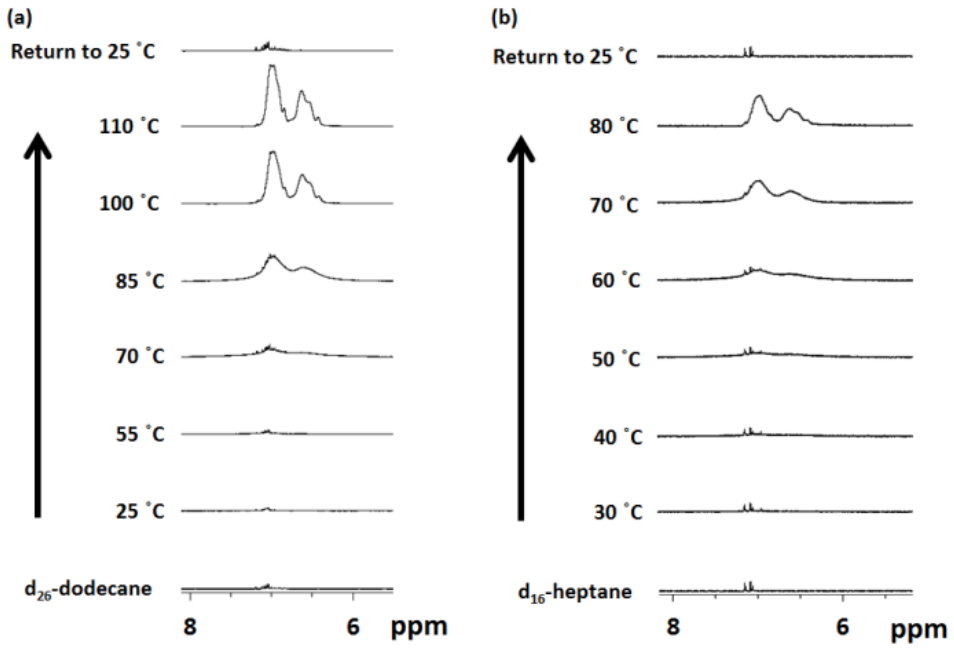

Figure 2.7. Partial ^{1}H NMR spectra recorded for the PS-PEP diblock copolymer in d_{16}-heptane on gradual heating from 30^{o}C to 80^{o}C, and d_{26}-dodecane on gradual heating from 25^{o}C to 110^{o}C, followed by cooling to 25^{o}C. The appearance of aromatic signals is attributed to increasing solvation of the polystyrene chains within the micelle cores at higher temperatures.

Such solvent plasticisation leads to a much lower effective T_g for the core-forming PS block (DSC analysis of the solid PS-PEP copolymer indicates a T_g of 107ºC, see Figure 2.8), which becomes increasingly mobile at elevated temperatures. However, if these integrated aromatic signals are compared to signals assigned to the PEP stabiliser block (not shown), the degree of solvation of the PS chains is always significantly lower than the actual polystyrene content of the PS-PEP diblock copolymer (28 mol%), see Figure 2.9. This is consistent with highly swollen micelle cores, but does not necessarily mean micelle dissolution. On the other hand, a high degree of core swelling causes a shift from non-ergodic, frozen micelles[4, 15, 16, 43] towards micelles that are in equilibrium with dissolved copolymer chains, with the presence of the latter component being already confirmed by the DLS studies shown in Figure 2.5. These variable temperature ^{1}H NMR spectra also suggest that *n*-dodecane is a marginally worse solvent for the PS block than *n*-heptane, since the latter leads to a greater degree of solvation at 60-70ºC (see Figure 2.9).

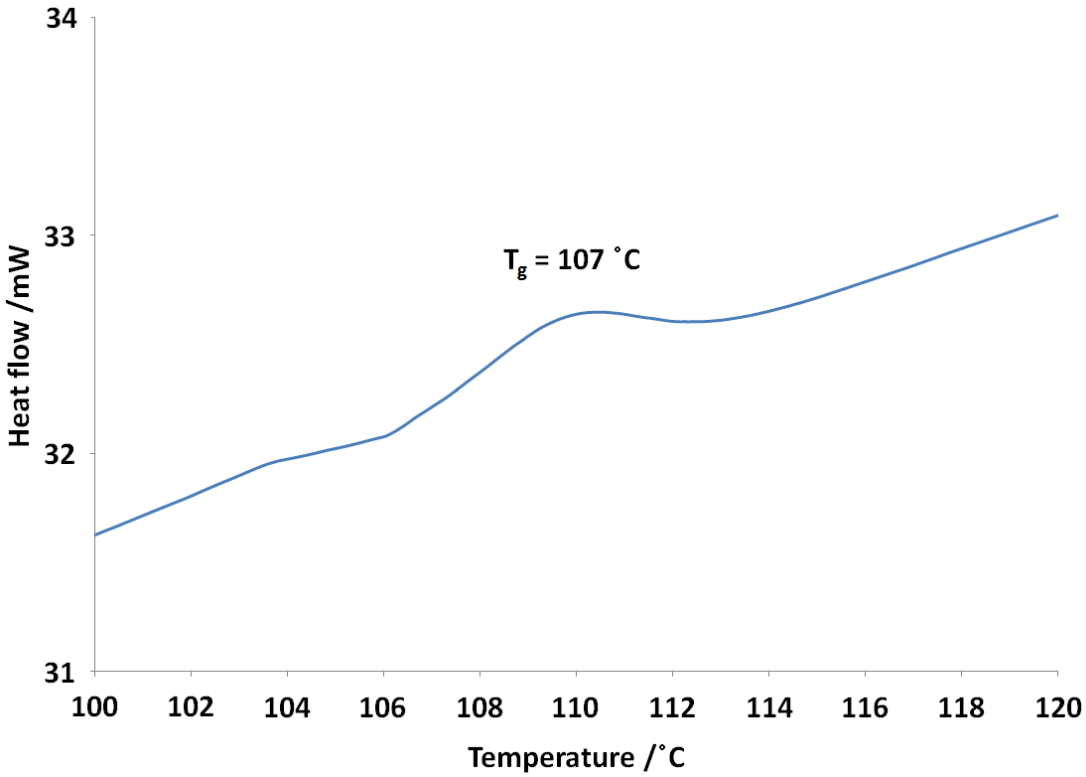

Figure 2.8. DSC curve recorded for the PS-PEP diblock copolymer. The observed onset glass transition temperature of 107ºC relates to the glassy polystyrene block.

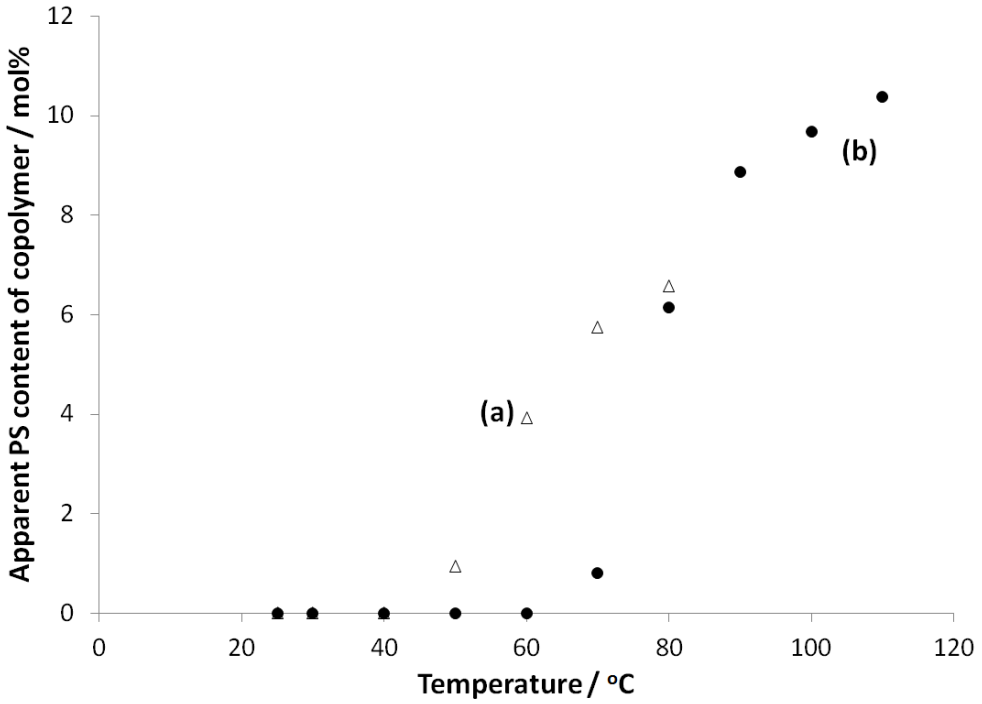

Figure 2.9. Apparent polystyrene content of the PS-PEP diblock copolymer with increasing temperature as judged by ^{1}H NMR studies performed in (a) d_{16}-heptane and (b) d_{26}-dodecane. The actual polystyrene content of this PS-PEP diblock copolymer is 28 mol%, as judged by ^{1}H NMR analysis in $CDCl_3$. Thus the polystyrene-based micelle cores never become fully solvated even at 110°C.

Block Copolymer Adsorption onto Carbon Black Particles

The adsorption of PS-PEP diblock copolymers onto carbon black from cyclohexane has been reported by Cosgrove and co-workers.[32] Such model formulations are of interest, since carbon black is believed to be a useful mimic for understanding the behaviour of diesel engine soot, which must be well dispersed within the engine oil in order to minimize engine wear (see Chapters 1 and 5).[45] Surface-active copolymers such as succinimide-capped polyisobutylenes are also known to act as effective soot dispersants in engine oil formulations.[46, 53] In the present work, a commercial carbon black (Regal 250R, kindly provided by Cabot Corporation) was chosen as a model colloidal substrate. A representative transmission electron micrograph of these particles reveals the characteristic fractal morphology normally associated with this material, see Figure

2.10a. BET surface area measurements (N_2 adsorbate at 77 K) gave a linear plot (see Figure 2.10b) and indicated a specific surface area of 43 m^2 g^{-1}. Combined with a carbon black density of 1.89 g cm^{-3} determined by helium pycnometry this suggests a mean sphere-equivalent diameter of approximately 74 nm, which corresponds to the primary grain size of this material.

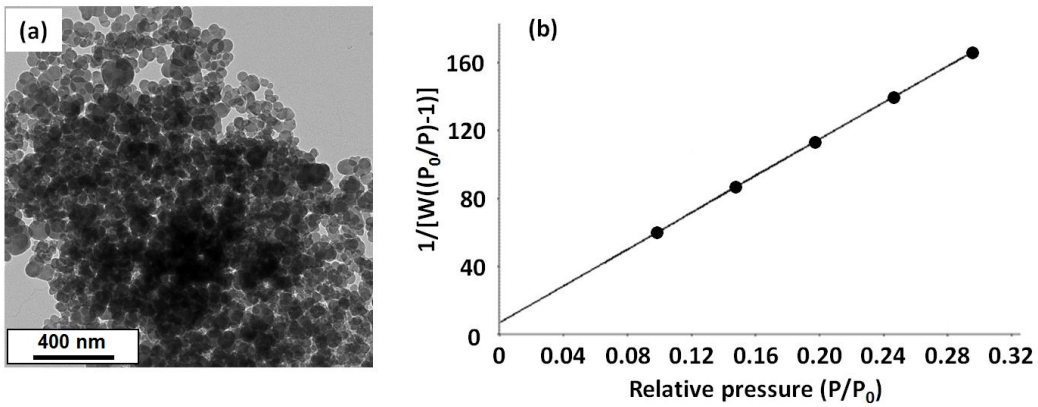

Figure 2.10. (a) TEM image and (b) BET surface area measurements for Regal 250 R carbon black, which is utilised as a model colloidal substrate for adsorption of the PS-PEP diblock copolymer. The carbon black has a characteristic fractal morphology and a primary grain size (number-average diameter) of approximately 74 nm. Analysis of the BET data indicates a specific surface area, $A_{s,}$ of 43 m^2 g^{-1}.

Direct spectroscopic evidence for the presence of the copolymer chains on the surface of the carbon black particles can be obtained using X-ray photoelectron spectroscopy (XPS). This technique has excellent inter-element resolution and a typical sampling depth of just a few nm.[54] However, normally it would be extremely difficult to detect a carbon-rich copolymer such as PS-PEP adsorbed onto carbon black. Fortuitously, the Regal 250R grade of carbon black contains a significant surface sulphur signal. This elemental impurity is obscured as the copolymer micelles adsorb onto the carbon black surface, as evidenced by the gradual attenuation of the S2p signal (see Figure 2.11).

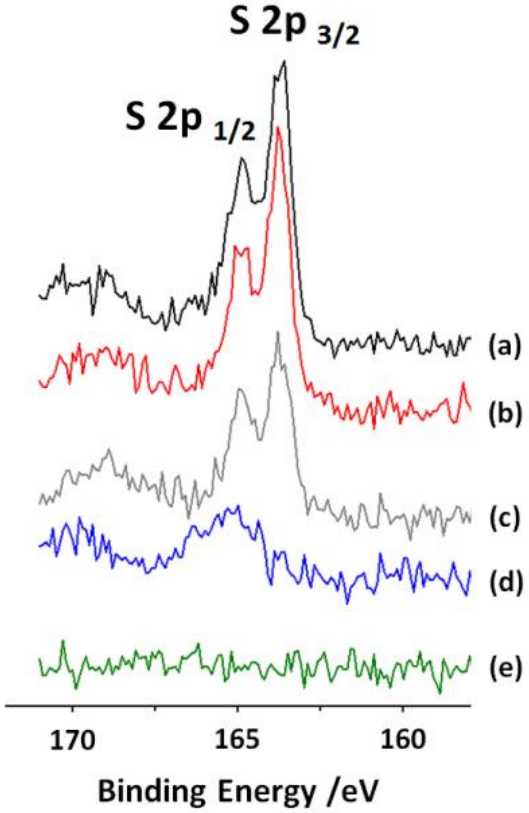

Figure 2.11. XPS S2p core-line spectra recorded for the PS-PEP diblock copolymer adsorbed onto carbon black from *n*-heptane at 20°C. The sulphur signal is due to an impurity in the carbon black surface and this feature is gradually obscured by the adsorbed copolymer: (a) carbon black alone, (b) 5% w/w PS-PEP copolymer adsorbed onto carbon black, (c) 10% w/w PS-PEP copolymer adsorbed onto carbon black, (d) 15% w/w PS-PEP copolymer adsorbed onto carbon black (e) 20% w/w PS-PEP copolymer adsorbed onto carbon black.

The extent of copolymer adsorption onto this carbon black from *n*-heptane at 20°C was initially examined indirectly by using a supernatant depletion assay based on UV spectroscopy, after sedimentation of the relatively dense carbon black particles using high speed centrifugation. Here the polystyrene block acts as a convenient aromatic UV chromophore, since it gives rise to a strong signal at 262 nm and a highly linear Beer-Lambert law plot (see Figure 2.12). However, it is perhaps worth emphasising that this supernatant assay cannot be performed directly in *n*-alkane solvents: the UV radiation is strongly scattered by the micellar aggregates with a $1/\lambda^4$ wavelength dependence, which leads to a rapidly rising baseline at shorter wavelengths. Instead, an aliquot of the

copolymer dispersion in the *n*-alkane is first diluted into an equal volume of chloroform. This is sufficient to cause micellar dissociation to form individual copolymer chains: SAXS analysis confirms much weaker X-ray scattering and the presence of random coils with a mean radius of gyration of around 6.5 nm, suggesting molecular dissolution of the PS-PEP diblock copolymer in chloroform. An adsorption isotherm was constructed using this protocol and is depicted in Figure 2.13. Classical Langmuir-type adsorption is observed, which indicates monolayer coverage and is generally expected for polymer adsorption.[55] The adsorbed amount at the 'knee' of the isotherm is approximately 3.5 mg m^{-2}, which is a relatively high plateau value for simple physical adsorption.

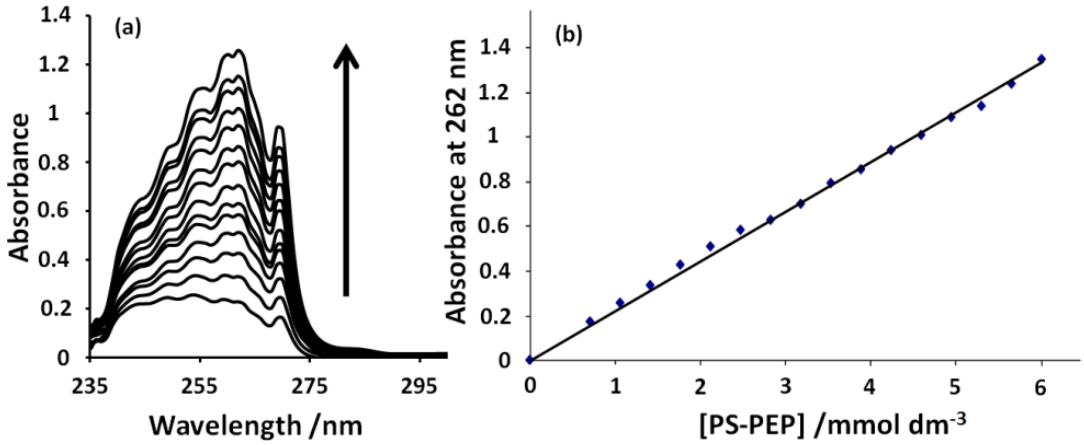

Figure 2.12. UV absorption spectra (arrow indicates increasing copolymer concentration) and corresponding Beer-Lambert plot for the aromatic chromophore at 262 nm assigned to the polystyrene component of the PS-PEP diblock copolymer dissolved in chloroform at 20°C.

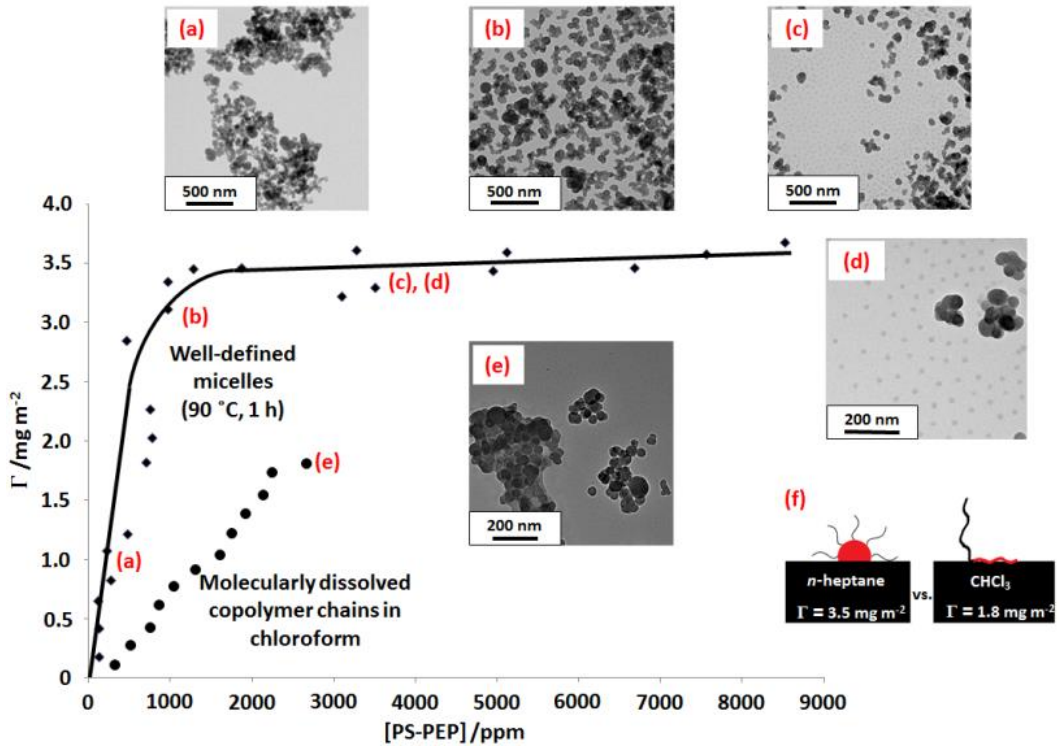

Figure 2.13. Adsorption isotherms obtained for PS-PEP diblock copolymer adsorbed onto carbon black from chloroform and *n*-heptane (after heating to 90ºC for 1 h) at 20ºC, as determined using a UV spectroscopy-based supernatant depletion assay. The copolymer is molecularly dissolved in chloroform and thus only weakly adsorbed onto carbon black from this good solvent. In contrast, the copolymer is present as micelles in *n*-heptane, and strong adsorption is observed from this solvent. The TEM images indicate the degree of dispersion of the carbon black particles at various points on the adsorption isotherm obtained for copolymer adsorption from *n*-heptane: (a) at submonolayer coverage; (b) at approximately monolayer coverage; (c) above monolayer coverage. Image (d) also shows that the copolymer micelles are clearly present in co-existence with the carbon black particles. Image (e) shows the aggregation state of the carbon black particles at high copolymer concentration (2670 ppm) in chloroform. (f) Cartoon schematic to illustrate the strong micellar adsorption (Γ = 3.5 mg m^{-2}) that occurs in *n*-heptane and the significantly weaker unimer (single chain) adsorption (Γ = 1.8 mg m^{-2}) that occurs in chloroform.

An obvious explanation is micellar adsorption from *n*-alkanes, rather than the adsorption of individual copolymer chains. This hypothesis is supported by the much weaker adsorption observed from chloroform under the same conditions (only ~ 0.80 mg m^{-2} at around 1000 ppm, which corresponds to the 'knee' of the Langmuir isotherm observed for copolymer adsorption from *n*-heptane). Even at a relatively high copolymer concentration of 2660 ppm, only an adsorbed amount of ~ 1.8 mg m^{-2} is

observed, which is around half of that obtained for adsorption from *n*-heptane. Furthermore, the copolymer-coated carbon black particles prepared below, at and above the 'knee' of the Langmuir isotherm were studied by TEM (see the four inset images shown in Figure 2.13). Below the maximum adsorbed amount of copolymer, the carbon black particles still appear to be somewhat aggregated (see inset image a), but a significantly higher degree of dispersion is achieved either at or above the 'knee' of the isotherm (see inset images b, c). Moreover, close inspection of the TEM image corresponding to the latter condition reveals the presence of PS-PEP diblock copolymer micelles in co-existence with the carbon black particles (see inset image d). The aggregation state of the carbon black particles at high copolymer concentration in chloroform is shown in image (e). A schematic cartoon illustrating the difference between micellar and unimer adsorption is also provided as inset (f) in Figure 2.13.

Finally, thermogravimetric analysis was used to directly determine the adsorbed amount of copolymer on the carbon black particles from *n*-heptane at 20^{o}C (after a 20^{o}C – 90^{o}C – 20^{o}C thermal cycle to ensure the formation of well-defined micelles). A control experiment confirmed minimal mass loss (~ 0.6%) occurred for carbon black alone on heating up to 500^{o}C under nitrogen, see Figure 2.14. In contrast, the PS-PEP diblock copolymer was fully pyrolysed under these conditions (see inset thermogram in the same Figure). Thus pyrolysis of the copolymer-coated carbon black particles (isolated as sediments after high speed centrifugation) under carefully controlled conditions allowed the adsorbed amount of copolymer to be determined. A series of thermograms are shown in Figure 2.14 with higher mass losses being observed at 500^{o}C as the initial copolymer concentration is gradually increased. In particular, the 8.75 % mass loss corresponds to an adsorbed amount, Γ, of 2.0 mg m^{-2}, which is close to that determined by UV spectroscopy under the same conditions (2.1 mg m^{-2}).

There is a general caveat to consider when using both of the above techniques to measure copolymer adsorbed amount. First of all, TGA will tend to *overestimate* the adsorbed amount of copolymer when this is present in excess. This is due to a minor fraction of the star diblock copolymer sedimenting under the centrifugation conditions used to isolate the carbon black particles prior to TGA analysis (as confirmed using

control experiments). Thus this technique will only be reliable below (and up to) monolayer coverage, since there is essentially no excess copolymer in the supernatant in this regime. Similarly, the supernatant depletion assay based on UV spectroscopy must *underestimate* the adsorbed amount above monolayer coverage for the same reason. In summary, these two techniques report consistent data for adsorbed amounts up to monolayer coverage, but necessarily diverge thereafter.

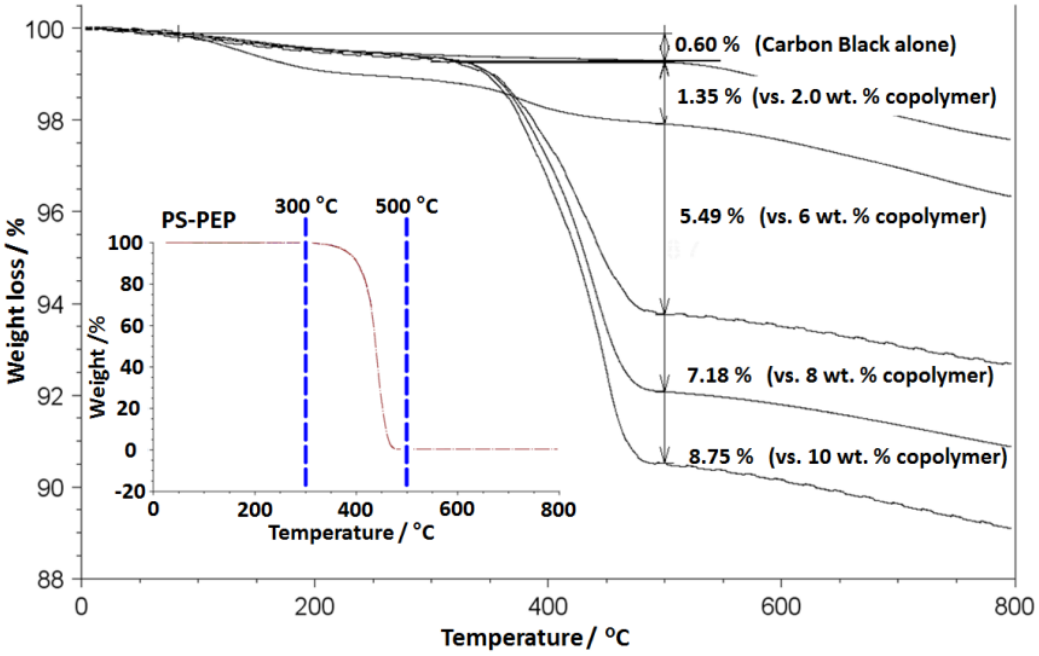

Figure 2.14. Thermogravimetric curves obtained for increasing amounts of PS-PEP diblock copolymer adsorbed onto carbon black. Analyses were performed under a nitrogen atmosphere at a heating rate of 20°C per min. Under these conditions, carbon black alone loses only 0.60% mass when heated up to 500°C. In contrast, the copolymer alone (inset curve) is completely pyrolysed. Thus the observed mass loss at 500°C for the copolymer-coated carbon black particles can be attributed to the copolymer content (after a small correction for the carbon black mass loss). This direct method for determining the adsorbed amount of copolymer is in good agreement with the indirect method based on UV spectroscopy (see Figure 2.13).

In summary, it is clear that, after a suitable thermal cycle, the PS-PEP diblock copolymer forms small, well-defined micelles in *n*-alkanes at 20°C and that such micelles adsorb onto carbon black particles under these conditions. This behaviour offers a benefit since it is likely to enhance the degree of dispersion of any diesel soot

that may be present in the engine oil. However, it is emphasised that this situation might not necessarily be the case at the typical diesel engine operating temperature of 100-110^{o}C, since under these conditions a significant proportion of molecularly-dissolved copolymer chains appear to be present, in addition to solvent-swollen micelles. This latter scenario may well favour unimer adsorption over micelle adsorption, but the high temperature adsorption studies required to explore this hypothesis are beyond the scope of the present work.

Conclusions

TEM studies confirm that the commercial PS-PEP diblock copolymer used in this work forms large polydisperse colloidal aggregates when dissolved directly in *n*-alkanes at 20^{o}C. However, a single heating cycle breaks up these ill-defined aggregates, leading to the formation of well-defined, near-monodisperse spherical micelles on cooling. DLS studies provide good evidence for the co-existence of micelles and dissolved copolymer chains (unimers) at elevated temperature. Variable temperature ^{1}H NMR studies are consistent with the latter observations, since partial solvation of the core-forming polystyrene chains is observed above 50^{o}C. These results are also consistent with SAXS studies, which indicate the presence of molecularly dissolved copolymer chains in chloroform (data not shown), formation of well-defined spherical star-like micelles in either *n*-heptane or *n*-dodecane after a single heating cycle and large, mixed morphology aggregates when the PS-PEP diblock copolymer is dissolved directly in such *n*-alkanes without any thermal conditioning. Moreover, a pronounced broad feature at low q is consistent with weakly interacting micelles, as previously suggested by Stejskal and co-workers.[15] This interaction is most likely to be the result of interpenetration of the star-like micelles above their critical overlap concentration, rather than being due to inter-micelle attractive forces.[44]

XPS studies confirm that the PS-PEP diblock copolymer adsorbs onto carbon black particles at 20^{o}C. The extent of adsorption can be assessed using a UV spectroscopy-based supernatant depletion assay. If a non-selective solvent such as chloroform is utilised, then the adsorbed amount is relatively low ($\Gamma \sim 1.8$ mg m^{-2}). However, significantly higher adsorbed amounts ($\Gamma \sim 3.5$ mg m^{-2}) are obtained for copolymer

adsorption from *n*-heptane and a classical Langmuir-type isotherm is observed. This suggests micellar adsorption, rather than unimer adsorption, and is consistent with direct determination of the adsorbed copolymer content by thermogravimetry. These results are consistent with TEM observations of copolymer micelles in co-existence with carbon black particles when working above the 'knee' of the adsorption isotherm. It is also noteworthy that the original fractal morphology of the carbon black substrate is substantially disrupted under these optimised conditions: its degree of dispersion is close to its primary grain size indicated by BET surface area measurements. This study has enhanced our understanding of the performance of this commercial diblock copolymer when it is utilised as a diesel soot dispersant in engine oil formulations.

References

1. Newman, S. Note on colloidal dispersions from block copolymers. *J. Appl. Polym. Sci.* **1962,** *6*, S15-S16.
2. Krause, S. Dilute Solution Properties of a Styrene—Methyl Methacrylate Block Copolymer. *J. Phys. Chem.* **1964,** *68*, 1948-1955.
3. Tuzar, Z.; Kratochvíl, P. Block and graft copolymer micelles in solution. *Adv. Colloids Interface Sci.* **1976,** *6*, 201-232.
4. Gao, Z.; Eisenberg, A. A model of micellization for block copolymers in solutions. *Macromolecules* **1993,** *26*, 7353-7360.
5. Noolandi, J.; Hong, K. M. Theory of block copolymer micelles in solution. *Macromolecules* **1983,** *16*, 1443-1448.
6. Förster, S.; Antonietti, M. Amphiphilic block copolymers in structure-controlled nanomaterial hybrids. *Adv. Mater.* **1998,** *10*, 195-217.
7. Gao, Z.; Varshney, S. K.; Wong, S.; Eisenberg, A. Block Copolymer "Crew-Cut" Micelles in Water. *Macromolecules* **1994,** *27*, 7923-7927.
8. Qin, A.; Tian, M.; Ramireddy, C.; Webber, S. E.; Munk, P.; Tuzar, Z. Polystyrene-poly(methacrylic acid) block copolymer micelles. *Macromolecules* **1994,** *27*, 120-126.
9. Baines, F. L.; Armes, S. P.; Billingham, N. C.; Tuzar, Z. Micellization of Poly(2-(dimethylamino)ethyl methacrylate-block-methyl methacrylate) Copolymers in Aqueous Solution. *Macromolecules* **1996,** *29*, 8151-8159.
10. Wilhelm, M.; Zhao, C. L.; Wang, Y.; Xu, R.; Winnik, M. A.; Mura, J. L.; Riess, G.; Croucher, M. D. Poly (styrene-ethylene oxide) block copolymer micelle formation in water: a fluorescence probe study. *Macromolecules* **1991,** *24*, 1033-1040.
11. Xu, R.; Winnik, M. A.; Hallett, F.; Riess, G.; Croucher, M. D. Light-scattering study of the association behavior of styrene-ethylene oxide block copolymers in aqueous solution. *Macromolecules* **1991,** *24*, 87-93.
12. Moffitt, M.; Khougaz, K.; Eisenberg, A. Micellization of ionic block copolymers. *Acc. Chem. Res.* **1996,** *29*, 95-102.
13. Burnett, G.; Meares, P.; Paton, C. Styrene+ methyl methacrylate block copolymers. Part 2.—Behaviour in dilute solutions. *Transactions of the Faraday Society* **1962,** *58*, 737-746.
14. Higgins, J. S.; Dawkins, J. V.; Maghami, G. G.; Shakir, S. A. Study of micelle formation by the diblock copolymer polystyrene—b-(ethylene-co-propylene) in dodecane by small-angle neutron scattering. *Polymer* **1986,** *27*, 931-936.
15. Stejskal, J.; Hlavatá, D.; Sikora, A.; Konňák, Č.; Pleštil, J.; Kratochvíl, P. Equilibrium and non-equilibrium copolymer micelles: polystyrene-block-poly (ethylene-co-propylene) in decane and in diisopropylether. *Polymer* **1992,** *33*, 3675-3685.
16. Hlavatá, D.; Stejskal, J.; Pleštil, J.; Koňák, Č.; Kratochvíl, P.; Helmstedt, M.; Mio, H.; Laggner, P. Heat-induced transition of polystyrene- block-poly(ethylene-co-propylene) micelles in decane and in dioxane. *Polymer* **1996,** *37*, 799-805.
17. Bahadur, P.; Sastry, N. V.; Marti, S.; Riess, G. Micellar behaviour of styrene—isoprene block copolymers in selective solvents. *Colloids Surf.* **1985,** *16*, 337-346.

18. Bang, J.; Viswanathan, K.; Lodge, T. P.; Park, M. J.; Char, K. Temperature-dependent micellar structures in poly(styrene-b-isoprene) diblock copolymer solutions near the critical micelle temperature. *J. Chem. Phys.* **2004,** *121*, 11489-11500.
19. McConnell, G. A.; Gast, A. P. Melting of Ordered Arrays and Shape Transitions in Highly Concentrated Diblock Copolymer Solutions. *Macromolecules* **1997,** *30*, 435-444.
20. Szwarc, M.; Levy, M.; Milkovich, R. Polymerization initiated by electron transfer to monomer-a new method of formation of block polymers. *Journal of the American Chemical Society* **1956,** *78*, 2656-2657.
21. Szwarc, M. Living Polymers. *Nature* **1956,** *178*, 1168-1169.
22. Mountrichas, G.; Mpiri, M.; Pispas, S. Micelles of Star Block (PSPI)8 and PSPI Diblock Copolymers (PS = Polystyrene, PI = Polyisoprene): Structure and Kinetics of Micellization. *Macromolecules* **2005,** *38*, 940-947.
23. Mandema, W.; Zeldenrust, H.; Emeis, C. A. Association of block copolymers in selective solvents, 1. Measurements on hydrogenated poly(styrene-isoprene) in decane and in trans-decalin. *Die Makromolekulare Chemie* **1979,** *180*, 1521-1538.
24. Schouten, M.; Dorrepaal, J.; Stassen, W. J. M.; Vlak, W. A. H. M.; Mortensen, K. Thermal stability of polystyrene-b-poly(ethylene/propylene) diblock copolymer micelles in paraffinic solvents. *Polymer* **1989,** *30*, 2038-2046.
25. Stacy, C. J.; Kraus, G. Micelle formation by butadiene-styrene block polymers in n-alkanes. *Polym. Eng. Sci.* **1977,** *17*, 627-633.
26. Bang, J.; Jain, S.; Li, Z.; Lodge, T. P.; Pedersen, J. S.; Kesselman, E.; Talmon, Y. Sphere, Cylinder, and Vesicle Nanoaggregates in Poly(styrene-b-isoprene) Diblock Copolymer Solutions. *Macromolecules* **2006,** *39*, 1199-1208.
27. D'Oliveira, J. M. R.; Xu, R.; Jensma, T.; Winnik, M. A.; Hruska, Z.; Hurtrez, G.; Riess, G.; Martinho, J. M. G.; Croucher, M. D. Direct adsorption of polystyrene-poly(ethylene oxide) micelles in water onto polystyrene latex particles. *Langmuir* **1993,** *9*, 1092-1097.
28. Kayes, J. B.; Rawlins, D. A. Adsorption characteristics of certain polyoxyethylene-polyoxypropylene block co-polymers on polystyrene latex. *Colloid & Polymer Science* **1979,** *257*, 622-629.
29. Evers, O. A.; Scheutjens, J. M. H. M.; Fleer, G. J. Statistical thermodynamics of block copolymer adsorption. Part 2.-Effect of chain composition on the adsorbed amount and layer thickness. *Journal of the Chemical Society, Faraday Transactions* **1990,** *86*, 1333-1340.
30. Awan, M. A.; Dimonie, V. L.; Filippov, L. K.; El-Aasser, M. S. Adsorption Kinetics of Amphipathic Polystyrene-block-polybutadiene onto Silicon Wafer and Polystyrene Planar Surfaces. *Langmuir* **1997,** *13*, 130-139.
31. Marques, C.; Joanny, J. F.; Leibler, L. Adsorption of block copolymers in selective solvents. *Macromolecules* **1988,** *21*, 1051-1059.
32. Shar, J. A.; Cosgrove, T.; Obey, T. M.; Warne, M. R.; Wedlock, D. J. Adsorption Studies of Diblock Copolymers at the Cyclohexane/Carbon Black Interface. *Langmuir* **1999,** *15*, 7688-7694.
33. An, S. W.; Su, T. J.; Thomas, R. K.; Baines, F. L.; Billingham, N. C.; Armes, S. P.; Penfold, J. Neutron Reflectivity of an Adsorbed Water-Soluble Block Copolymer: A Surface Transition to Micelle-like Aggregates at the Air/Water Interface. *The Journal of Physical Chemistry B* **1998,** *102*, 387-393.

34. Webber, G. B.; Wanless, E. J.; Armes, S. P.; Baines, F. L.; Biggs, S. Adsorption of amphiphilic diblock copolymer micelles at the mica/solution interface. *Langmuir* **2001,** *17*, 5551-5561.
35. Webber, G. B.; Wanless, E. J.; Armes, S. P.; Tang, Y. Q.; Li, Y. T.; Biggs, S. Nano-anemones: Stimulus-responsive copolymer-micelle surfaces. *Advanced Materials* **2004,** *16*, 1794-1798.
36. Doliveira, J. M. R.; Xu, R. L.; Jensma, T.; Winnik, M. A.; Hruska, Z.; Hurtrez, G.; Riess, G.; Martinho, J. M. G.; Croucher, M. D. Direct adsorption of polystyrene poly(ethylene oxide) micelles in water onto polystyrene latex-particles. *Langmuir* **1993,** *9*, 1092-1097.
37. Sarkar, B.; Venugopal, V.; Tsianou, M.; Alexandridis, P. Adsorption of Pluronic block copolymers on silica nanoparticles. *Colloids and Surfaces A: Physicochemical and Engineering Aspects* **2013,** *422*, 155-164.
38. Lin, Y.; Alexandridis, P. Temperature-Dependent Adsorption of Pluronic F127 Block Copolymers onto Carbon Black Particles Dispersed in Aqueous Media. *The Journal of Physical Chemistry B* **2002,** *106*, 10834-10844.
39. Napper, D. H. *Polymeric stabilization of colloidal dispersions*; Academic Press London1983; Vol. 7.
40. Lin, Y.; Alexandridis, P. Temperature-Dependent Adsorption of Pluronic F127 Block Copolymers onto Carbon Black Particles Dispersed in Aqueous Media. *The Journal of Physical Chemistry B* **2002,** *106* (42), 10834-10844.
41. Ilavsky, J.; Jemian, P. R. Irena: tool suite for modeling and analysis of small-angle scattering. *Journal of Applied Crystallography* **2009,** *42*, 347-353.
42. Scares, B. G.; de Souza Gomes, A. Spectrophotometric determination of the styrene content of alpha-methylstyrene—styrene copolymers. *Polymer Bulletin* **1988,** *20*, 543-548.
43. Price, C. Micelle formation by block copolymers in organic solvents. *Pure and Applied Chemistry* **1983,** *55*, 1563-1572.
44. Pedersen, J. S.; Svaneborg, C.; Almdal, K.; Hamley, I. W.; Young, R. N. A small-angle neutron and X-ray contrast variation scattering study of the structure of block copolymer micelles: Corona shape and excluded volume interactions. *Macromolecules* **2003,** *36* (2), 416-433.
45. Clague, A. D. H.; Donnet, J. B.; Wang, T. K.; Peng, J. C. M. A comparison of diesel engine soot with carbon black. *Carbon* **1999,** *37*, 1553-1565.
46. Won, Y.-Y.; Meeker, S. P.; Trappe, V.; Weitz, D. A.; Diggs, N. Z.; Emert, J. I. Effect of Temperature on Carbon-Black Agglomeration in Hydrocarbon Liquid with Adsorbed Dispersant. *Langmuir* **2004,** *21*, 924-932.
47. Pugh, R. J.; Matsunaga, T.; Fowkes, F. M. The dispersibility and stability of carbon black in media of low dielectric constant. 1. Electrostatic and steric contributions to colloidal stability. *Colloids and Surfaces* **1983,** *7*, 183-207.
48. Pugh, R. J.; Fowkes, F. M. The dispersibility and stability of carbon black in media of low dielectric constant. 2. Sedimentation volume of concentrated dispersions, adsorption and surface calorimetry studies. *Colloids and Surfaces* **1984,** *9*, 33-46.
49. Khandpur, A. K.; Foerster, S.; Bates, F. S.; Hamley, I. W.; Ryan, A. J.; Bras, W.; Almdal, K.; Mortensen, K. Polyisoprene-Polystyrene Diblock Copolymer Phase Diagram near the Order-Disorder Transition. *Macromolecules* **1995,** *28*, 8796-8806.

50. Blanazs, A.; Verber, R.; Mykhaylyk, O. O.; Ryan, A. J.; Heath, J. Z.; Douglas, C. W. I.; Armes, S. P. Sterilizable Gels from Thermoresponsive Block Copolymer Worms. *Journal of the American Chemical Society* **2012,** *134*, 9741-9748.
51. Molyneux, P. *Water-soluble synthetic polymers: properties and behavior*; CRC Press. Inc.1983.
52. Thompson, K. L.; Armes, S. P.; Howse, J. R.; Ebbens, S.; Ahmad, I.; Zaidi, J. H.; York, D. W.; Burdis, J. A. Covalently Cross-Linked Colloidosomes. *Macromolecules* **2010,** *43*, 10466-10474.
53. Bezot, P.; Hesse-Bezot, C.; Diraison, C. Aggregation kinetics of colloidal suspensions of engine soots. Influence of polymeric lubricant additives. *Carbon* **1997,** *35*, 53-60.
54. Beamson, G.; Briggs, D. *High resolution XPS of organic polymers: the Scienta ESCA300 database*; Wiley, Chichester1992; Vol. 4.
55. Cohen Stuart, M. A.; Cosgrove, T.; Vincent, B. Experimental aspects of polymer adsorption at solid/solution interfaces. *Advances in Colloid and Interface Science* **1985,** *24*, 143-239.
56. Pedersen, J. S. Structure factors effects in small-angle scattering from block copolymer micelles and star polymers. *Journal of Chemical Physics* **2001,** *114* (6), 2839-2846.
57. Pedersen, J. S.; Schurtenberger, P. Scattering functions of semiflexible polymers with and without excluded volume effects. *Macromolecules* **1996,** *29* (23), 7602-7612.
58. Pedersen, J. S.; Gerstenberg, M. C. The structure of P85 Pluronic block copolymer micelles determined by small-angle neutron scattering. *Colloids and Surfaces a-Physicochemical and Engineering Aspects* **2003,** *213* (2-3), 175-187.
59. Kinning, D. J.; Thomas, E. L. Hard-Sphere Interactions Between Spherical Domains in Diblock Copolymers. *Macromolecules* **1984,** *17* (9), 1712-1718.
60. Beaucage, G. Approximations leading to a unified exponential power-law approach to small-angle scattering. *Journal of Applied Crystallography* **1995,** *28*, 717-728.

Chapter 3

Star diblock copolymer concentration dictates the degree of dispersion of carbon black particles in non-polar media: bridging flocculation versus steric stabilisation

Introduction

It is well-documented that soluble polymers can influence the stability of colloidal dispersions *via* four different mechanisms: bridging flocculation, steric stabilisation, depletion stabilisation and depletion flocculation.[1, 2, 3, 4, 5, 6, 7, 8, 9, 10, 11, 12] The mechanism depends on the precise system and also on the polymer concentration. For example, bridging flocculation is normally associated with a relatively low polymer concentration, whereas steric stabilisation or depletion effects are usually observed at higher polymer concentrations.[11, 13, 14] The first two mechanisms are particularly pertinent to the present study.

Ruehrwein and Ward first proposed the principle of bridging flocculation in 1952.[1] This phenomenon is now widely used for papermaking,[15] water treatment,[16] industrial effluent treatment,[17] and mining industries[18] to obtain efficient solid–liquid separations.[19] High molecular weight polymers have been shown to be particularly efficient bridging flocculants.[20] If the dimensions of the polymer chains are sufficiently large, then adsorption onto two or more particles can occur, see Figure 3.3a. This bridging aids particle aggregation, with strong kinetic effects being well-documented.[7, 21, 22] La Mer and Healy[23] reported that the degree of flocculation depended on both polymer molecular weight and dosage for the adsorption of polyacrylamides on calcium phosphate particles in aqueous media. Specific interactions such as hydrogen bonding have been demonstrated to enhance the extent of bridging flocculation.[24, 25] It is also well-documented that increasing the polymer concentration can lead to initial bridging flocculation being superseded by steric stabilisation.[26, 27] There are many literature reports of bridging flocculation based on the addition of high molecular weight water-soluble polymers such as poly(ethylene oxide) or polyacrylamide or poly(*N*-vinylpyrrolidone) to either silica sols or polystyrene latex in *aqueous* media.[4, 25, 28, 29] However, there appear to be rather few studies of bridging flocculation in *non-aqueous* media.[30, 31] A rare example here is an early study by Hiemenz *et al.*, who examined the kinetics of flocculation resulting from the adsorption of polystyrene onto carbon black particles from either toluene or cyclohexane.[7]

Steric stabilisation is an important, generic and highly versatile colloidal stabilisation mechanism that is applicable for both aqueous and non-aqueous dispersions.[11] It has been widely utilised for many applications, including the preparation of inks,[32] latex paints[33] and coatings,[34] the efficient dispersion of diesel soot in engine oils,[35] and for the preparation of electrically conducting polymer particles.[36, 37, 38, 39, 40] The appropriate design of effective steric stabilisers requires an understanding of the interaction of the polymeric stabiliser with the particle surface, the continuous phase, and also the conformation that the adsorbed polymer chain adopts at the solid/liquid interface.[9, 14] In particular, the polymeric stabiliser should be strongly adsorbed, provide high coverage of the particles and form a thick, well-solvated steric barrier in order to offset the ever-present attractive van der Waals forces operating between colloidal particles.

Many different copolymer architectures are now accessible via so-called 'living' polymerisation chemistry, including homopolymers,[41, 42] macromonomers,[43, 44] statistical copolymers,[13, 45, 46] block copolymers,[47, 48, 49] graft copolymers[50] and star copolymers.[51, 52, 53] All of these copolymer architectures have been examined as putative steric stabilisers for latex syntheses. The star diblock copolymer architecture is particularly relevant to the present study. Such copolymers have been utilised as drug carriers,[54] thermo-responsive gelators,[55,56, 57, 58] or as viscosity modifiers in engine oil formulations.[59, 60] The synthesis of star diblock copolymers has been achieved using anionic polymerisation,[52] atom transfer radical polymerisation[61] and reversible addition-fragmentation chain transfer (RAFT) polymerisation.[62] Alonzo *et al.*,[21] recently reported the kinetics of adsorption of PS-PVP star diblocks onto a planar silicon surface from toluene. In the present study, we examine the influence of a commercial star diblock copolymer on the colloidal stability of carbon black particles in non-polar media (e.g. *n*-dodecane). This copolymer comprises relatively long hydrogenated polyisoprene blocks as the inner cross-linked core, with relatively short polystyrene chains as the outer block. The adsorbed amount of copolymer, Γ, on the carbon black particles was determined indirectly *via* a supernatant depletion assay based on UV spectroscopy and also assessed directly by thermogravimetric analysis. Subsequently, the degree of dispersion of the carbon black particles was assessed as a function of copolymer

concentration using analytical centrifugation, optical microscopy (OM), transmission electron microscopy (TEM) and small angle x-ray scattering (SAXS).

Experimental

Materials

The star diblock copolymer used in this work is a commercial product that was supplied by BP Formulated Products Technology and was used as received. PAO2 base oil was provided by BP Formulated Products Technology and both *n*-dodecane and *n*-heptane were obtained from Fisher Scientific UK Ltd. Each solvent was used as received. Deuterated solvents for NMR studies were obtained from Goss Scientific Ltd, UK and were used as received. The carbon black (Regal 250R grade) was kindly supplied by Cabot Corporation (Billerica, MA, USA) and was used as received.

Gel permeation chromatography. The molecular weight distribution of the star diblock copolymer was assessed by gel permeation chromatography (GPC) using THF eluent. The THF GPC set-up was equipped with two 5 μm 'Mixed C' 30 cm columns, a Varian 290-LC pump and a WellChrom K-2301 refractive index detector operating at 950 ± 30 nm. The THF mobile phase contained 2.0 v/v% triethylamine and 0.05 w/v% butylhydroxytoluene (BHT) and the flow rate was fixed at 1.0 mL min^{-1}. A series of ten near-monodisperse polystyrene standards (M_n = 580 to 552,500 g mol^{-1}) were used for calibration.

Dynamic Light Scattering (DLS). Hydrodynamic diameters were measured at 25°C using a Malvern Zetasizer NanoZS model ZEN 3600 instrument equipped with a 4 mW He−Ne solid-state laser operating at 633 nm. Back-scattered light was detected at 173°, and the mean particle diameter was calculated from the quadratic fitting of the correlation function over 30 runs of 10 seconds duration. All measurements were performed three times and data were analysed using cumulants analysis of the experimental correlation function using Dispersion Technology Software version 6.20. Sample dilution of 0.01 wt% used throughout..

Transmission electron microscopy. Studies were conducted using a Phillips CM100 microscope operating at 100 kV on unstained samples prepared by drying a drop of dilute sample (approximately 0.01 wt%) on a carbon-coated copper grid.

Small-angle X-ray scattering (SAXS) studies

SAXS patterns were collected at a synchrotron source (Diamond Light Source, station I22, Didcot, UK) using monochromatic X-ray radiation and a 2D Pilatus 2M CCD detector (wavelength λ = 0.10 nm, camera length = 10 m, which gives a q range from 0.011 nm^{-1} to 1.33 nm^{-1}, where $q = \frac{4\pi \sin\theta}{\lambda}$ is the length of the scattering vector and θ is half of the scattering angle). A liquid cell comprising two mica windows each of 25 μm thickness attached by an adhesive double-sided tape to both sides of a polycarbonate washer of 1 mm thickness was used as a sample holder. The carbon black dispersions were loaded to the partially assembled cell (a mica window attached to one side of the washer) and then the dispersion was sealed in the cell by attaching the second mica window to the washer. In order to avoid sedimentation of the carbon black on the time scale of the SAXS experiments, the loaded liquid cell was continuously rotated by a motor. Scattering data were reduced (i.e., integrated, normalized and background-subtracted) by Dawn software developed at Diamond Light Source and were further analysed using Irena SAS macros for Igor Pro[63].

^{1}H NMR spectroscopy. The mean polystyrene content of the diblock copolymer dissolved in a non-selective solvent ($CDCl_3$) was determined using a Bruker AV1-250 MHz NMR spectrometer (64 scans per spectrum). Variable temperature spectra were recorded between 25^{o}C and 100^{o}C using d_{26}-dodecane using a Bruker AV1-400 MHz NMR spectrometer (32 scans per spectrum).

UV spectroscopy. UV spectra were recorded at 20^{o}C for the diblock copolymer dissolved in *n*-dodecane using a Perkin Elmer Lambda 25 instrument operating between 200 and 500 nm. A linear calibration curve was constructed for the same copolymer dissolved in pure chloroform at a fixed wavelength of 262 nm, which corresponds to the aromatic chromophore of the polystyrene block. This gave a molar extinction

coefficient of 222 ± 2 mol^{-1} dm^3 cm^{-1}, which is close to the literature value reported for polystyrene.[64]

Copolymer adsorption onto carbon black via supernatant depletion assay using UV spectroscopy. The desired mass of diblock copolymer (3.0-90.0 mg) was weighed into a glass vial and carbon black (300.0 mg) was weighed into a separate vial. Then *n*-dodecane (5.00 mL) was added, following by stirring at 20ºC (Turrax stirrer, 1 minute, 2500 rpm). The resulting star copolymer dispersion was added to the pre-weighed carbon black, stirred (Turrax stirrer, 1 minute, 2500 rpm), sonicated for 1 h, then left on a roller mill for 16 h overnight. The resulting dispersion was centrifuged for 4 h at 18,000 rpm in a centrifuge rotor that was pre-cooled to 15ºC so as to minimise solvent evaporation. Taking care not to disturb the sedimented carbon black particles, the supernatant was decanted into an empty vial and then 0.80 mL of this solution was analysed by UV spectroscopy. The aromatic chromophore at 262 nm due to the polystyrene block was used to quantify the copolymer concentration remaining in the supernatant after exposure to the carbon black, thus enabling the adsorbed amount to be determined by difference.

Thermogravimetric analysis. Analyses were conducted on the pristine star diblock copolymer, carbon black alone and star copolymer-coated carbon black particles. Each sample was heated under a nitrogen atmosphere up to 800ºC at a heating rate of 10ºC min^{-1} using a Q500 TGA instrument (TA Instruments). The mass loss observed between 300 and 500ºC was attributed to complete pyrolysis of the diblock copolymer, with the remaining incombustible residue being attributed to carbon black.

Analytical centrifugation. Carbon black aggregate diameters were determined using a LUMiSizer® analytical photocentrifuge (LUM GmbH, Berlin, Germany) at 20ºC. Measurements were conducted on 10 wt% carbon black dispersions in either *n*-dodecane or d_{26}-dodecane at 200-4000 rpm using 2 mm path length polyamide cells. The particle density is an essential input parameter for analytical centrifugation studies. In the present case, the effective carbon black density is significantly reduced because of the presence of the adsorbed star copolymer. Thus this parameter was determined

using Stokes' law by performing LUMiSizer® analyses in both *n*-dodecane and d_{26}-dodecane (see later for further details). The LUMiSizer® is a microprocessor-controlled analytical centrifuge and is particularly convenient for the analysis of diblock copolymer-stabilised carbon black dispersions described in this work, since it allows simultaneous characterisation of multiple dispersions in organic solvents over a wide range of operating temperature (4^{o}C to 60^{o}C). The LUMiSizer® employs STEP™-Technology (Space- and Time-resolved Extinction Profiles) allowing the measurement of the intensity of transmitted light as a function of time and position over the entire cell length simultaneously. The progression of these transmission profiles contains information on the rate of sedimentation and, given knowledge of the particle density, enables assessment of the particle size distribution.

Optical Microscopy. 10 wt% carbon black dispersions were placed on a microscope slide and covered with a cover slip. Digital images were recorded using a Motic DMBA300 digital biological microscope equipped with a built-in camera and Motic Images Plus 2.0 ML software.

Viscometry. These studies were conducted using an Ostwald viscometer immersed in a water bath at 20^{o}C. Each measurement was repeated five times and the data were averaged. The solution viscosity was calculated from the viscosity of a known solvent.

Results and Discussion

Star Diblock Copolymer Characterisation

THF GPC analysis of the commercial star diblock copolymer used in this study indicated an M_n of 384,000 g mol^{-1} and an M_w/M_n of approximately 1.40 (expressed relative to a series of near-monodisperse polystyrene calibration standards) (see Figure 3.1). Such copolymers can be prepared by anionic polymerisation via the 'arm-first method' using sequential monomer addition.[60] Thus styrene was polymerised first, followed by isoprene and the divinylbenzene cross-linker. Based on formulations disclosed in the patent literature,[60] it is estimated that each star comprises approximately eight diblock copolymer arms. According to ^{1}H NMR analysis conducted in $CDCl_3$ (see

Figure 3.1), there was little or no evidence for unsaturated vinyl groups on the polyisoprene chains, which suggests that the copolymer had been subjected to catalytic hydrogenation.[65]

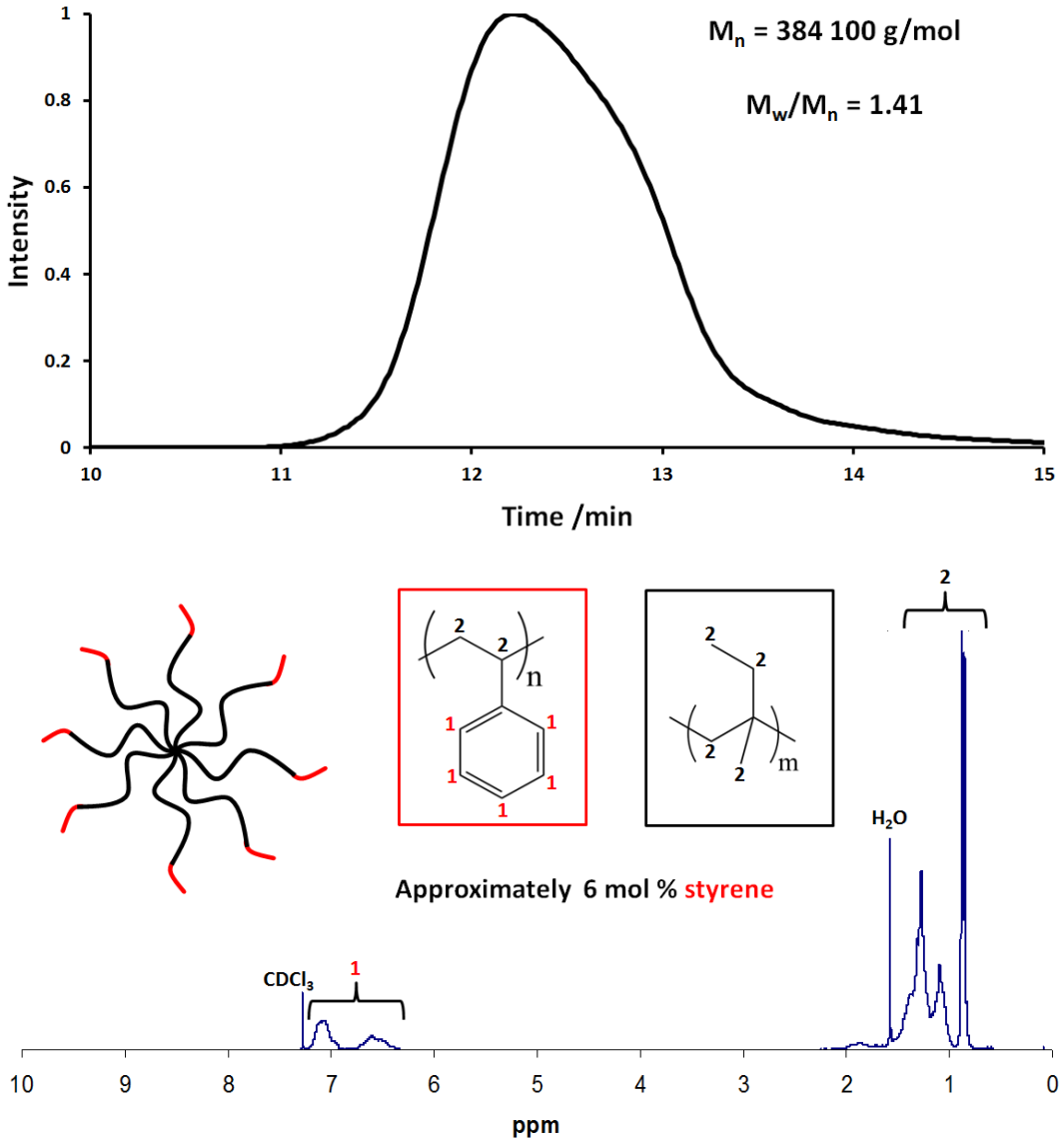

Figure 3.1. GPC analysis (20°C in THF, calibration with monodisperse polystyrene standards, RI detector) and ^{1}H NMR analysis of star diblock copolymer ($CDCl_3$, 20°C) to determine a polystyrene content of approximately 6 mol%.

Integrating the assigned signals in the same ^{1}H NMR spectrum enables the mean polystyrene content of this star diblock copolymer to be calculated as approximately 6 mol%. These relatively short blocks comprise the outer arms of the star copolymer and are expected to be rather poorly solvated in *n*-alkanes.[66] Hence a micellar gel network is formed at relatively high copolymer concentrations (see Figure 3.2). At lower copolymer concentrations, this star copolymer acts as a viscosity modifier (or thickener), which is its primary function as an additive in commercial engine oils.[60] In the context of the present work, when the star copolymer is added to carbon black particles in *n*-alkanes, it is assumed that the polystyrene blocks act as 'stickers' that aid copolymer adsorption onto the carbon black (see Figure 3.3), which is known to be a useful mimic for diesel engine soot (see Chapters 1 and 5).[35, 67, 68, 69, 70]

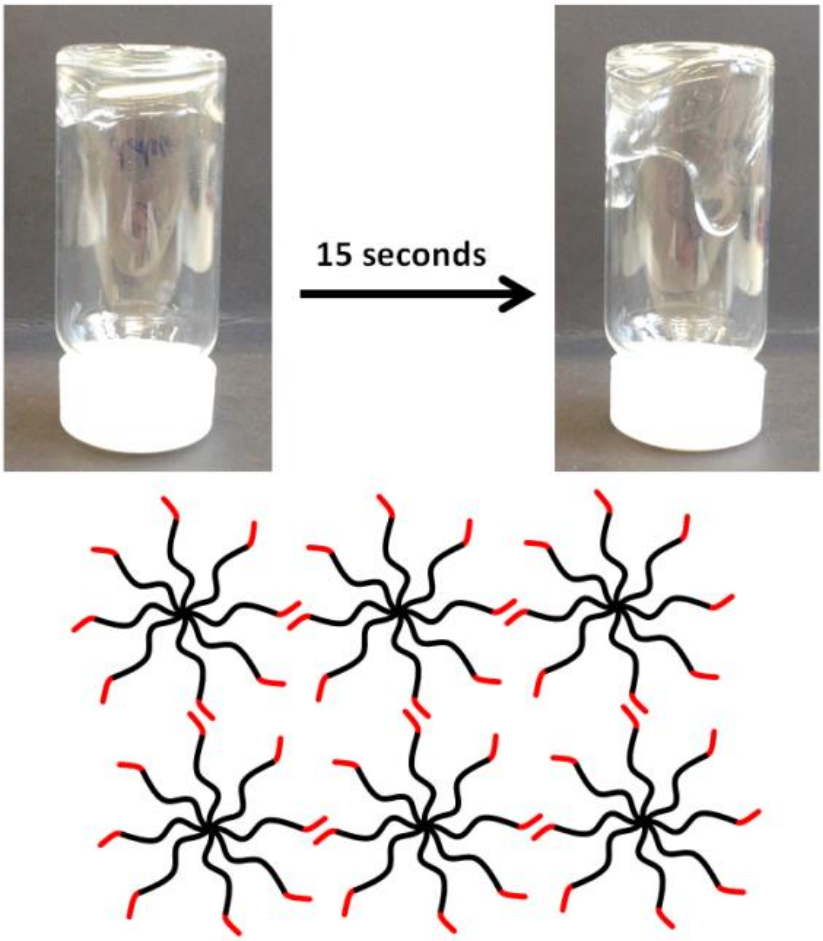

Figure 3.2. Digital images and schematic cartoon depicting the gel network formation of star diblock copolymer at high concentration (20 wt%, *n*-dodecane, 20^{o}C).

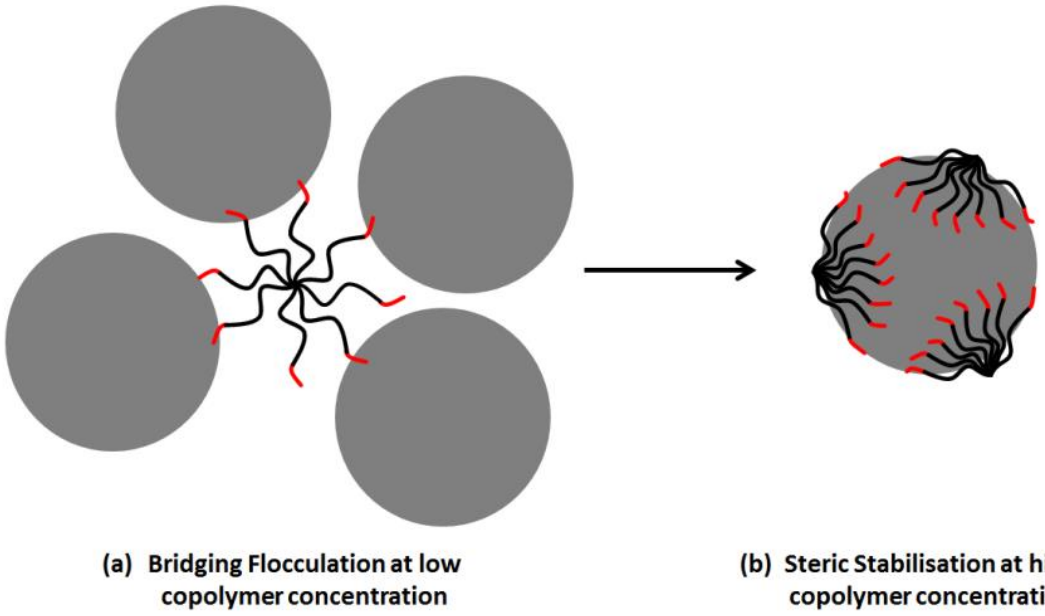

Figure 3.3. Schematic representation of the two roles played by the star diblock copolymer in the presence of a model colloidal substrate in non-polar media: (a) bridging flocculant and (b) steric stabiliser. In practice, the carbon black particles utilised in this study exhibit a complex fractal morphology, rather than the simple spherical morphology depicted in this Figure.

Star Diblock Copolymer Adsorption onto Carbon Black Particles

As outlined in Chapter 2, BET surface area analysis (N_2 adsorbate at 77 K) indicated a specific surface area of 43 m g^{-1} for carbon black. Combined with a solid-state density of 1.89 g cm^{-3} determined by helium pycnometry, this suggests a mean sphere-equivalent diameter of approximately 74 nm, which corresponds to the mean grain size for this particular carbon black. As in Chapter 2, the extent of copolymer adsorption onto this model colloidal substrate from *n*-dodecane at 20^{o}C was examined indirectly using a supernatant depletion assay based on UV spectroscopy, after centrifugal sedimentation of the relatively dense carbon black particles. Here the polystyrene block acts as a convenient aromatic UV chromophore, since it gives rise to a strong signal at 262 nm and a highly linear Beer-Lambert law plot (see inset in Figure 3.4). In this case, and in contrast to the method used in Chapter 2, the supernatant assay was performed directly in *n*-dodecane since there was negligible scattering from the molecularly

dissolved copolymer. An adsorption isotherm was constructed using this protocol, see Figure 3.4.

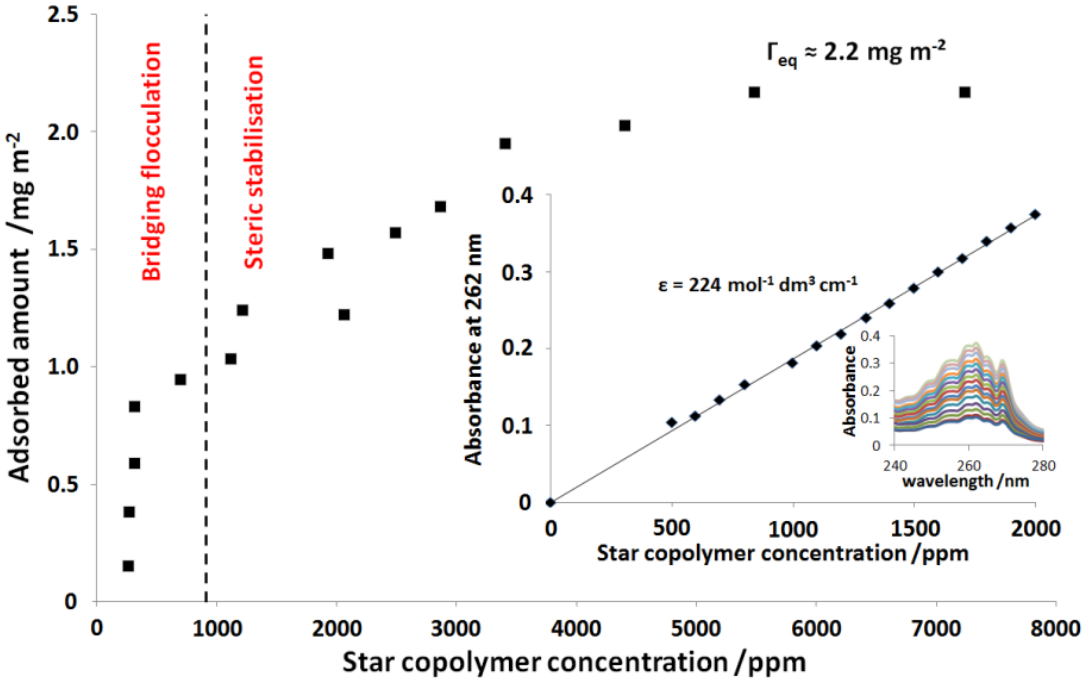

Figure 3.4. Low-affinity Langmuir-type adsorption isotherm obtained at 20°C for the star diblock copolymer adsorbed onto carbon black from *n*-dodecane, as determined using a supernatant depletion assay based on UV spectroscopy. The insets show the Beer-Lambert calibration plot used to determine the star copolymer concentration in each supernatant and the original UV spectra used to construct this calibration plot.

Langmuir-type adsorption is observed, as generally expected for polymer adsorption.[71] The maximum adsorbed amount of copolymer, Γ, (corresponding to monolayer coverage) can be calculated from the linear form of the Langmuir equation.[72] This parameter was found to be somewhat solvent-dependent, with Γ values of 2.2 ± 0.1, 3.1 ± 0.1 and 2.1 ± 0.1 mg m^{-2} being obtained for *n*-dodecane, *n*-heptane and PAO2 base oil respectively, see Figure 3.5. These adsorbed amounts are relatively high for merely physical adsorption.[73]

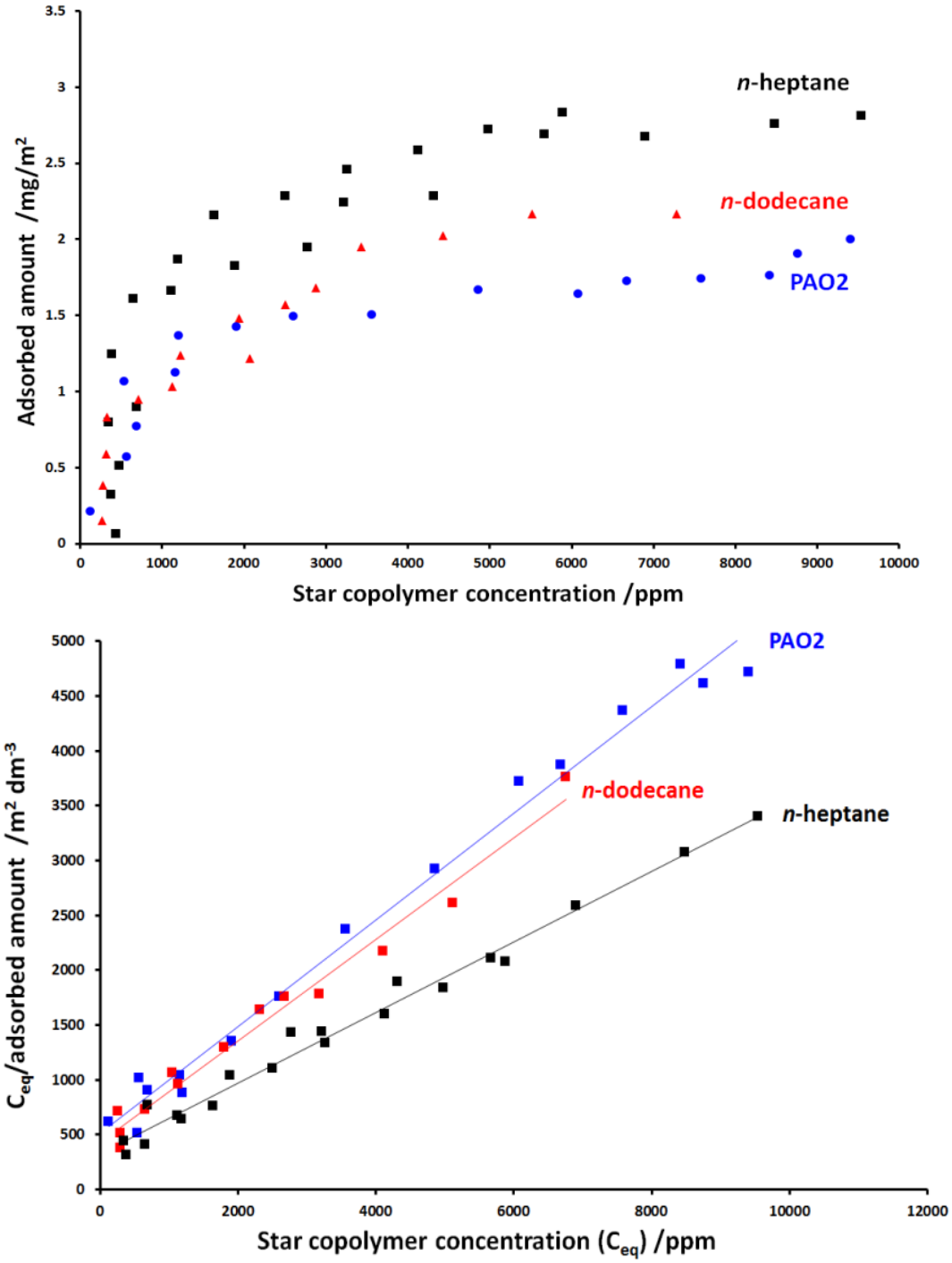

Figure 3.5. Adsorption isotherms obtained for star diblock copolymer adsorbed onto carbon black from *n*-heptane, *n*-dodecane and PAO2 base oil (after heating to 90°C for 1 h) at 20°C, as determined using a UV spectroscopy-based supernatant depletion assay. Adsorbed amounts determined via gradients from linear isotherms. A higher affinity isotherm is observed in *n*-heptane (Γ = 3.1 ± 0.1 mg m^{-2}) versus *n*-dodecane (Γ = 2.2 ± 0.1 mg m^{-2}) and PAO2 base oil (Γ = 2.1 ± 0.1 mg m^{-2}).

In addition, thermogravimetric analysis (TGA) was used to determine the amount of adsorbed copolymer on the carbon black surface from *n*-dodecane (see Figure 3.6). A control experiment confirmed that minimal mass loss (~ 0.73%) occurred for carbon black particles alone on heating up to 500°C under an inert atmosphere. In contrast, the star diblock copolymer was fully pyrolysed under these conditions (see inset thermogram in the same Figure). Thus pyrolysis of the copolymer-coated carbon black particles (isolated as compacted sediments after centrifugation) allowed the adsorbed amount of copolymer to be determined. A series of thermograms are shown in Figure 3.6; higher mass losses are observed at 500°C as the initial copolymer concentration is gradually increased.

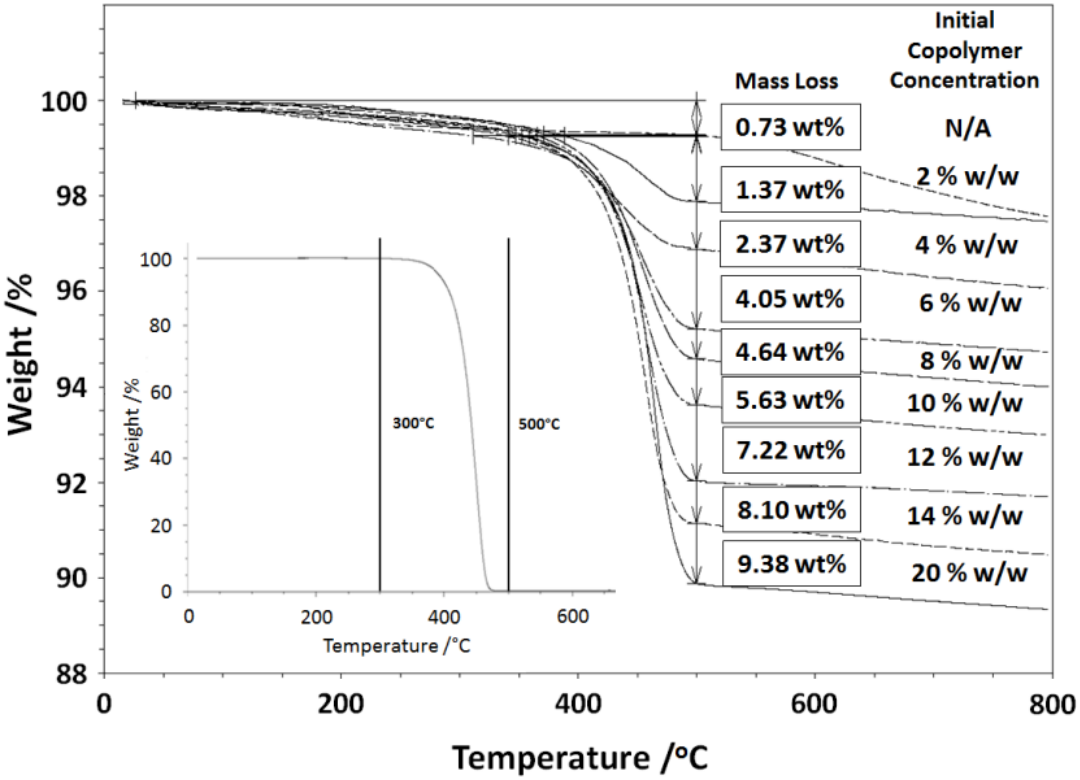

Figure 3.6. Thermogravimetric curves obtained for the adsorption of increasing amounts of star diblock copolymer onto carbon black particles from *n*-dodecane at 20°C. Analyses were performed under a nitrogen atmosphere at a heating rate of 10°C per min. Under these conditions, carbon black loses only 0.73% by mass when heated up to 500°C. In contrast, the star diblock copolymer (see inset curve) is completely pyrolysed under these conditions. Thus the observed mass loss at 500°C for star diblock copolymer-coated carbon black particles can be attributed to the copolymer content (after correcting for the carbon black mass loss). This direct method for determining the adsorbed amount of star diblock copolymer is in reasonably good agreement with the indirect supernatant assay method based on UV spectroscopy (see isotherm, Figure 3.7).

Adsorption isotherms constructed using each technique are shown in Figure 3.7. When assessed using TGA, the apparent adsorbed amount continues to increase beyond the monolayer coverage value indicated by UV spectroscopy. This is because the star diblock copolymer is not completely molecularly dissolved in *n*-dodecane. Indeed, DLS studies indicate some degree of self-association occurs in dilute solution under these conditions, which is presumably mediated by attractive forces between the partially solvated polystyrene chains. As discussed in Chapter 2, control experiments confirm that a minor fraction of the star diblock copolymer can be sedimented under the centrifugation conditions used to isolate the carbon black particles. This means that the technique should be reliable below (and up to) monolayer coverage, since there is essentially no excess copolymer in the supernatant in this regime. However, it will tend to *overestimate* the adsorbed amount of copolymer when this is present in excess. Similarly, the supernatant depletion assay based on UV spectroscopy must *underestimate* the adsorbed amount above monolayer coverage.

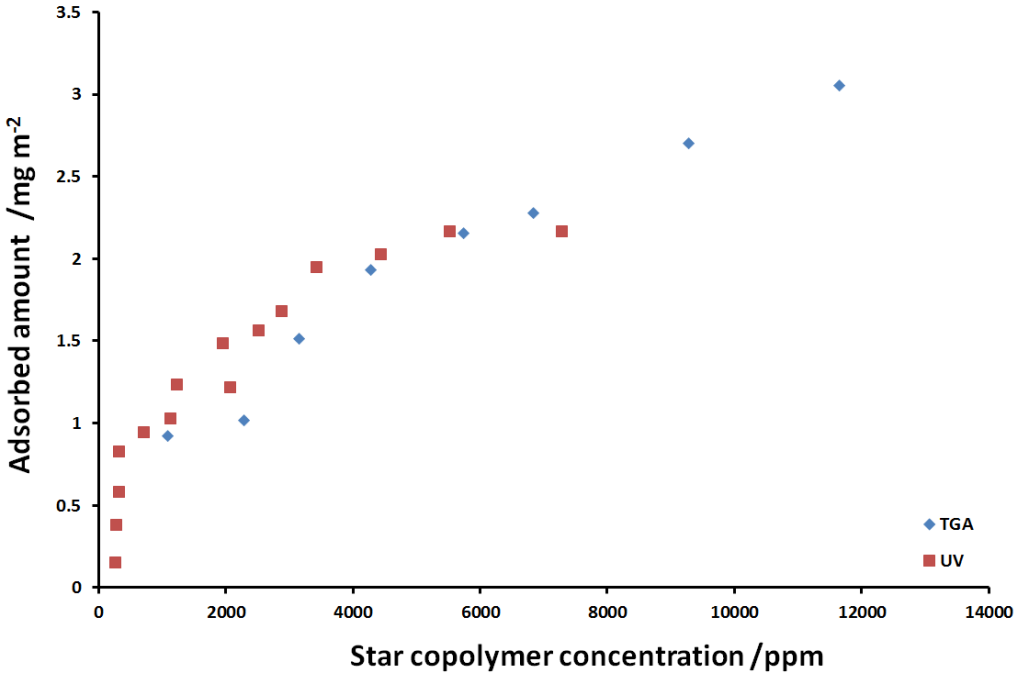

Figure 3.7. Adsorption isotherms obtained for star diblock copolymer adsorbed onto carbon black from *n*-dodecane (after heating to 110°C for 1 h) at 20°C, as determined using a UV spectroscopy-based supernatant depletion assay (red) and directly via TGA analysis (blue).

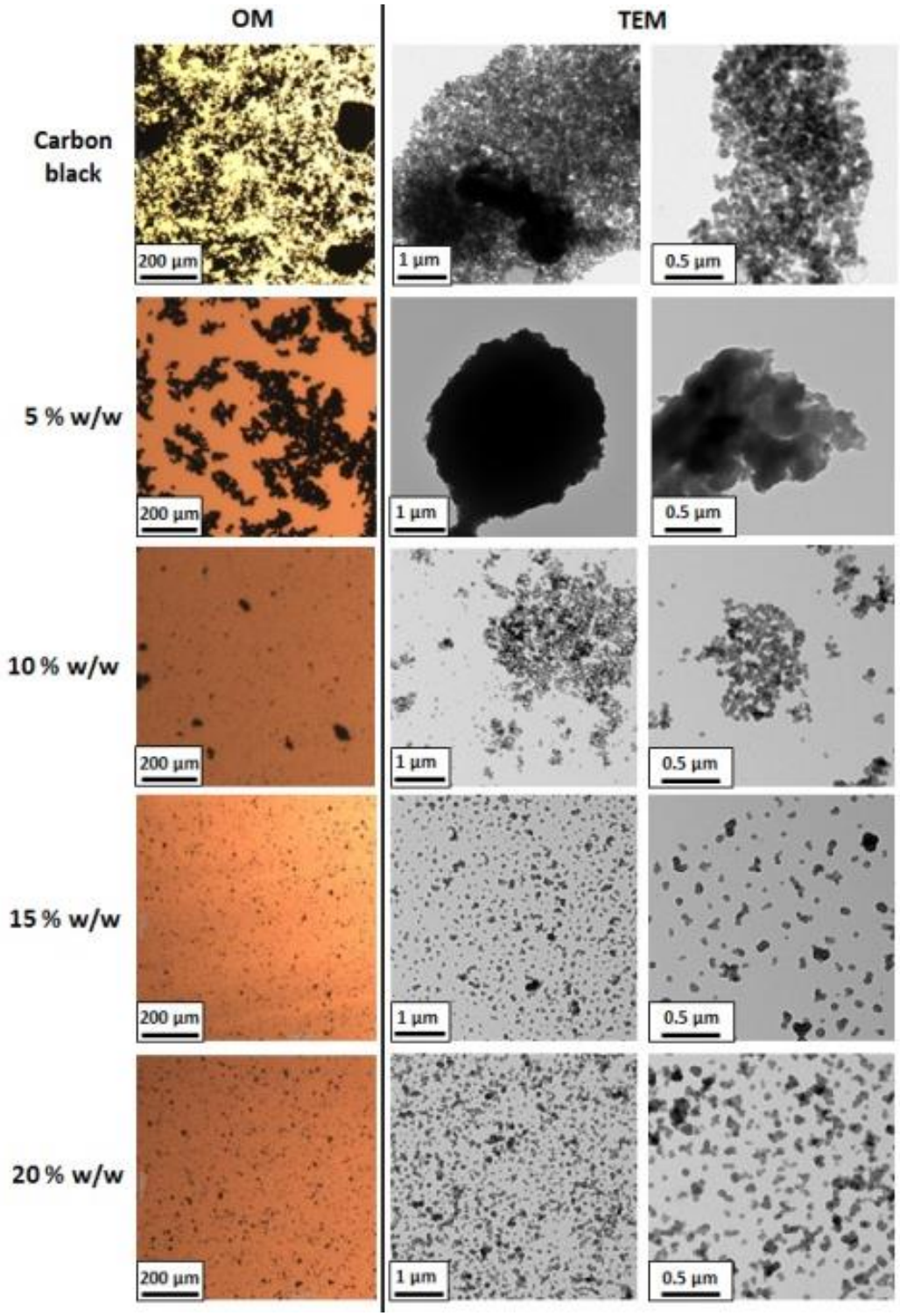

Figure 3.8. Representative TEM images obtained for carbon black particles in the presence of 5-20% w/w star diblock copolymer in *n*-dodecane. The corresponding optical microscopy images recorded for these four dispersions are also shown; these images confirm that a much greater degree of dispersion is obtained at higher copolymer concentration. This is because the star diblock copolymer switches from acting as a bridging flocculant to acting as an effective steric stabiliser at a certain critical concentration (see Figure 3.3).

Star Diblock Copolymer Adsorbed Carbon Black particles

Optical microscopy, TEM and analytical centrifugation were used to determine the boundary between bridging flocculation and steric stabilisation of the carbon black particles as a function of copolymer concentration (see Figures 3.8 and 3.9). Inspecting Figure 3.8, large agglomerates can be observed at 5.0 % w/w copolymer based on carbon black. OM and TEM are sensitive to different length scales: the former technique is sensitive to the presence of strongly light-absorbing micron-sized carbon black mass fractals, whereas the latter technique enables the population of well-dispersed submicron-sized carbon black 'fines' to be visualised. At (or above) 10 % w/w copolymer, a few large agglomerates are still present, but mainly smaller aggregates are observed along with some primary particles, suggesting reasonably stable dispersions.

At lower copolymer concentrations, it is postulated that the star copolymer adsorbs simultaneously onto multiple carbon black particles *via* its outer polystyrene blocks, thus promoting bridging flocculation.[74] At higher copolymer concentrations, the star copolymer instead acts as a steric stabiliser, resulting in colloidally stable carbon black dispersions (see Figure 3.3b). This behaviour differs qualitatively from that reported to a hydrogenated polyisoprene-polystyrene *linear* diblock copolymer, for which only steric stabilisation is observed via micellar adsorption (see Chapter 2). However, it can be dangerous to infer too much regarding the apparent degree of dispersion of particles using *post mortem* TEM studies, because drying artefacts can sometimes occur. Thus selected carbon black dispersions were also characterised using analytical centrifugation (see below) and SAXS (see later).

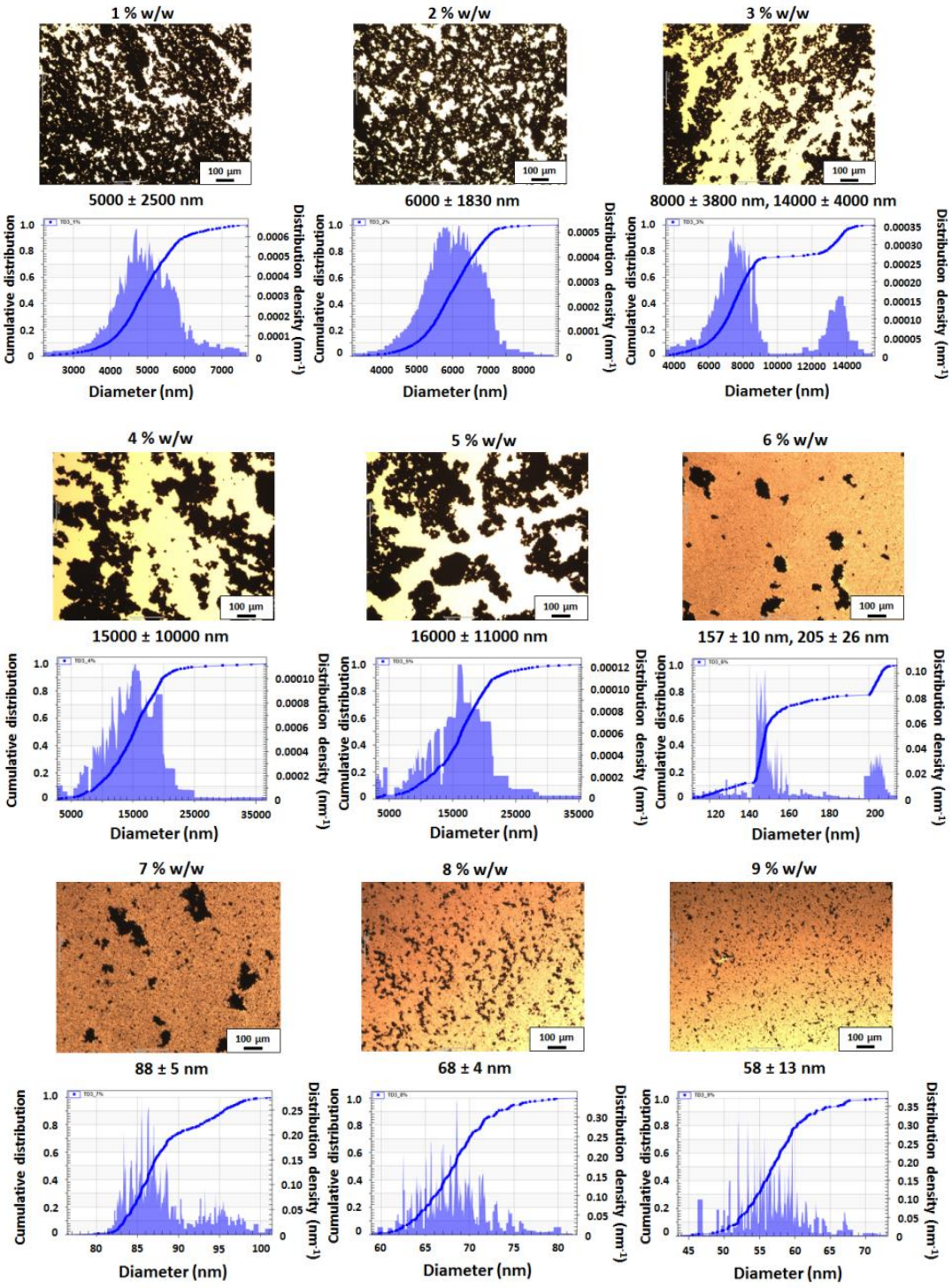

Figure 3.9. Representative optical microscopy images obtained for carbon black dispersions prepared using 1-9 % w/w star diblock copolymer in *n*-dodecane at 20^{o}C. The corresponding particle size distributions (and mean volume-average particle diameters) determined via analytical centrifugation (LUMiSizer® instrument) are also shown for each dispersion.

Effective Density

In order to calculate a particle size distribution *via* analytical centrifugation, an accurate particle density is required. Details of the calculation of such an *effective* particle density for copolymer-adsorbed carbon black particles, plus errors associated with such a calculation are covered in Chapter 4, but are also briefly covered here for reference. The solid-state density of carbon black has been determined to be 1.89 g cm^{-3}, as judged by helium pycnometry, see Chapter 2. However, its *effective* particle density in the present case is significantly reduced, because the density of the solvated layer of adsorbed copolymer chains is comparable to that of the solvent, which is much less dense than carbon black. Thus Stokes' law was utilised in order to determine the effective particle density.[75] In principle, centrifugation of two copolymer-adsorbed carbon black dispersions prepared in two comparable solvents with differing densities and viscosities (in this case, *n*-dodecane and d_{26}-dodecane) should produce two different particle velocities v_1 (or v_2), see equations 1 and 2 below.

$$v_1 = \frac{\left(\rho_p - \rho_{F,1}\right).X^2.\omega^2}{18\,.\eta_1}\,.r \qquad (1)$$

$$v_2 = \frac{\left(\rho_p - \rho_{F,2}\right).X^2.\omega^2}{18\,.\eta_2}\,.r \qquad (2)$$

Here ρ_P is the effective particle density, $\rho_{F,1}$ is the fluid (solvent) density, η_1 (or η_2) is the viscosity of the continuous phase, ω is the angular velocity, X is the diameter of the particles and r is the position of the measurement taken. Combining equations 1 and 2 to eliminate the experimental constants X, ω, r and rearranging terms leads to an expression for the effective density of the copolymer-coated carbon black particles, ρ_p, see equation 3.

$$\rho_P = \frac{\left(v_1\,\eta_1\rho_2 - v_2\,\eta_2\rho_1\right)}{\left(v_1\,\eta_1 - v_2\,\eta_2\right)} \qquad (3)$$

Unfortunately, the solution dynamic viscosity of d_{26}-dodecane (in this formalism, η_2) is not available in the literature. Thus Ostwald (capillary) viscometry was used to determine the kinematic viscosity, υ, of d_{26}-dodecane relative to that of *n*-dodecane at

20ºC (see Table 3.1). The kinematic viscosity was converted to the corresponding dynamic viscosity using equation 4.

$$\upsilon = \frac{\mu}{\rho} \quad (4)$$

Here υ is the kinematic viscosity, μ is the dynamic viscosity and ρ is the solvent density. Using this approach, the dynamic viscosity of d_{26}-dodecane was calculated to be 1.44 mPa.s. This experimental value agrees exceptionally well with that determined using an empirical relationship derived by Lutskii for the relative viscosities of deuterated *n*-alkanes compared to the equivalent protonated compounds (1.44 mPa.s).[76, 77]

Measurement Number	Time taken for *n*-dodecane descent (s)	Time taken for d_{26}-dodecane descent (s)
1	189	177
2	190	177
3	189	178
4	189	180
5	189	178
Mean time	**189**	**178**

Table 3.1. Ostwald viscometry measurements for *n*-dodecane and d_{26}-dodecane at 20ºC. The ratio of these mean times indicates a d_{26}-dodecane/*n*-dodecane kinematic viscosity ratio of 0.94. Given a kinematic viscosity of 1.78×10^{-6} m^2/s for *n*-dodecane, this suggests a kinematic viscosity of 1.67×10^{-6} m^2/s for d_{26}-dodecane.

Using equation 3, an effective particle density, ρ_p, of 0.98 ± 0.01g cm^{-3} was estimated for star copolymer-stabilised carbon black particles dispersed in *n*-dodecane at 20ºC prepared using 10 % w/w copolymer based on carbon black (see below for details; these conditions were selected since they correspond to approximately monolayer coverage of the carbon black particles – see Figure 3.4).

$$\frac{(0.3407 \text{ x } 0.00134 \text{ x } 864) - (0.1801 \text{ x } 0.00145 \text{ x } 781)}{(0.3407 \text{ x } 0.00134) - (0.1801 \text{ x } 0.00145)} = 975\ kg\ m^{-3}$$

$$= 0.98\ g\ cm^{-3}$$

This appears to be a reasonable value, since it enables a mean volume-average diameter of 70-75 nm to be calculated for these sterically-stabilised carbon black particles via analytical centrifugation. This size appears to be physically realistic because it is close

to the mean grain size for carbon black, which is estimated to be around 74 nm by BET surface area analysis (see Chapter 2). All particle size distributions determined by analytical centrifugation in this study were calculated using the above effective particle density. Clearly, this approximation most likely introduces systematic errors when working in solvents other than *n*-dodecane, especially at temperatures other than 20ºC and copolymer concentrations other than 10 % w/w. However, determination of effective particle densities under all of these conditions was beyond the scope of this work.

To assess the precise location of the flocculation/dispersion boundary in a given solvent, analytical centrifugation was used to determine mean diameters for the carbon black aggregates. In this context, a smaller apparent size indicates a higher degree of dispersion. In principle, analytical centrifugation can be used to assess the relative populations of both the micron-sized agglomerates (mass fractals) and also the submicron-sized aggregates/primary particles. Figure 3.9 compares the optical micrographs obtained for copolymer-stabilised carbon black dispersions in *n*-dodecane with the equivalent analytical centrifugation particle size distribution plots. The flocculation/dispersion boundary is discernible at around 5-6 % w/w copolymer for both techniques. The average floc size increases as this critical concentration is approached, presumably as initial aggregates combine to form larger agglomerates. Indeed, the bimodal distribution observed at 3 % w/w copolymer via analytical centrifugation provides some evidence for the co-existence of these two species. Similarly, the bimodal size distribution observed at 6.0 % w/w copolymer (i.e. just beyond the flocculation/dispersion boundary) indicates the presence of a few remaining carbon black agglomerates together with a major population of rather smaller aggregates. Finally, at 8-9 % w/w copolymer, the mean carbon black particle size is close to the mean grain size of 74 nm indicated by BET studies (see Chapter 2).

Compared to related techniques such as disk centrifuge photosedimentometry, one important advantage of the LUMiSizer® instrument is that it enables experiments to be performed over a wide range of temperature, rather than just ambient temperature. Accordingly, similar copolymer concentration-dependent studies were conducted using

n-heptane, *n*-dodecane or PAO2 base oil at 4, 20 and 60^{o}C. Inspecting Figure 3.10, the critical copolymer concentration corresponding to the flocculation/dispersion phase boundary is more or less independent of temperature. However, this parameter is clearly solvent-dependent, being around 7-8 % w/w for *n*-heptane, 5-6 % w/w for *n*-dodecane and approximately 6-7 % w/w for PAO2 base oil. As stated above, a somewhat higher affinity adsorption isotherm is observed for *n*-heptane compared to that found for *n*-dodecane and PAO2 base oil (see Figure 3.5). Using these three Γ values, the critical fractional coverage, θ_c, corresponding to the flocculation/dispersion boundary was calculated for each solvent. For *n*-heptane, *n*-dodecane and PAO2, θ_c is estimated to be 0.48 ± 0.01, 0.45 ± 0.02 and 0.60 ± 0.02, respectively. The difference in θ_c for the first two solvents is within experimental error, whereas the higher fractional coverage observed for the PAO2 suggests a somewhat higher degree of solvation for the star copolymer in this base oil. Returning to Figure 3.10, higher dispersion stabilities (as judged by smaller apparent particle diameters) were always observed at 4^{o}C compared to those at 20^{o}C, whereas poorer stabilities were universally obtained at 60^{o}C. To examine whether the star diblock copolymer *alone* exhibits temperature sensitivity, variable temperature ^{1}H NMR studies were performed from 25^{o}C to 100^{o}C for this copolymer dissolved in d_{26}-dodecane (Figure 3.11). An apparent polystyrene content of 3.2 ± 0.2 mol% was observed at 25^{o}C. As stated earlier, ^{1}H NMR analysis in $CDCl_3$, which is a good solvent for both the polystyrene and hydrogenated polyisoprene blocks, indicates that the actual polystyrene content of this copolymer is 6 mol %. This observation indicates that the outer polystyrene blocks of the star copolymer are only *partially* solvated (see Figure 3.1). This is consistent with the ability of this non-linear copolymer to act as an effective bridging flocculant. However, there is surprisingly little change in the apparent polystyrene content of this copolymer with temperature.

The temperature-dependent intrinsic viscosity of a polyisobutylene succinimide (PIBSI) dispersant was studied by Won *et al*.[68] These authors found that raising the temperature caused a reduction in solvation of the PIBSI chains. This compromises the efficiency of this dispersant in preventing the agglomeration of carbon blacks in *n*-alkanes at elevated temperature. In the context of the present work, it is hypothesised that hydrogenated polyisoprene chains may also become less solvated at higher temperatures, which would

account for the inferior dispersion stability observed in the LUMiSizer® experiments performed at 60°C.

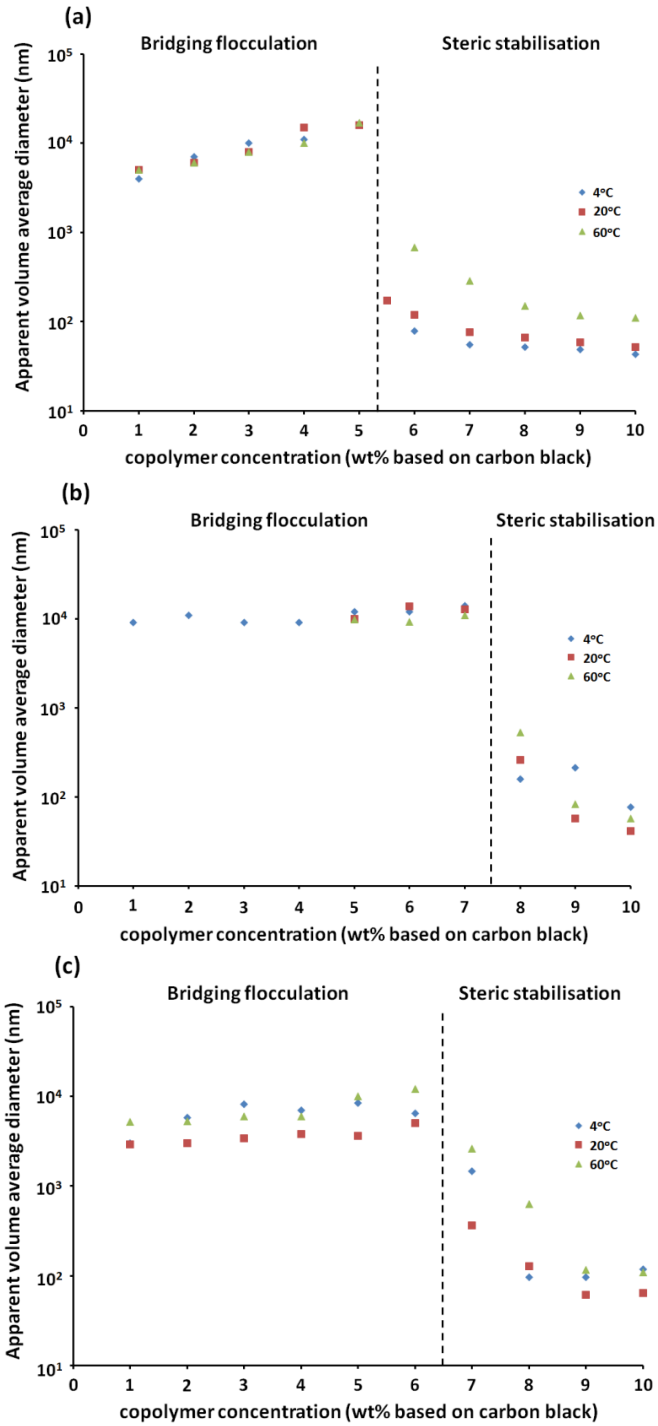

Figure 3.10. Concentration dependence of the mean volume-average diameter for dispersions of carbon black particles dispersed in (a) *n*-dodecane, (b) *n*-heptane and (c) PAO2 base oil in the presence of star diblock copolymer, as determined via analytical centrifugation (LUMiSizer® instrument) at 4°C, 20°C and 60°C.

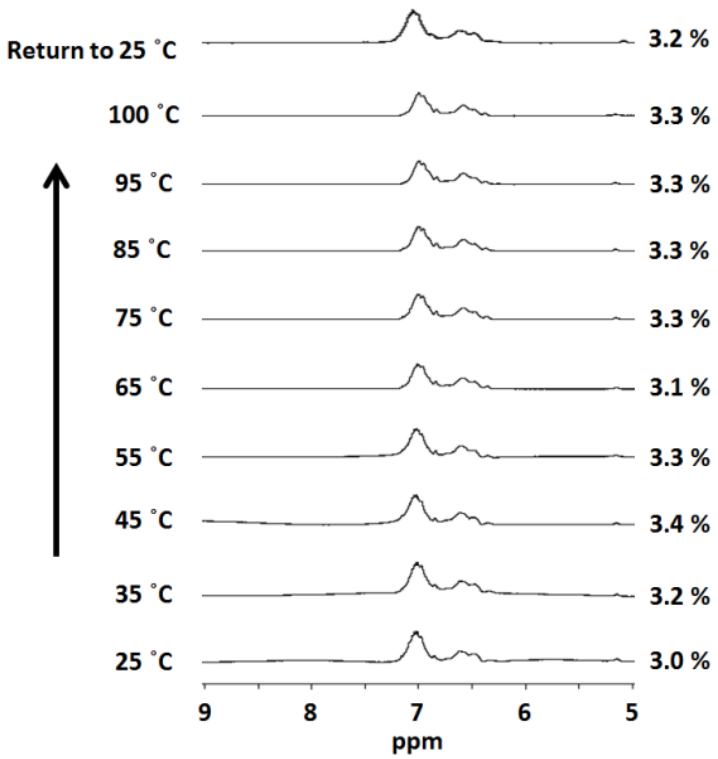

Figure 3.11. Partial ^{1}H NMR spectra recorded for the star diblock copolymer in d_{26}-dodecane on heating from 25ºC to 100ºC, followed by cooling to 25ºC. The appearance of aromatic signals is attributed to partial solvation of the polystyrene outer arms of the star diblock copolymer. The *apparent* polystyrene content (in mol %) of the star diblock copolymer is indicated at the right-hand side of each spectrum; the actual polystyrene content is ~ 6 mol %.

SAXS analysis

It is well known that the structural morphology of carbon black (and diesel soot) particles can be described as a complex hierarchy composed of five species: fractal agglomerates (1) at the micron length scale, aggregates (2) and primary particles (3) at the nm scale, sub-units (4) (a turbostratic structure comprising graphite-like layers arranged in non-aligned basal planes) at the sub-nm scale, and finally graphite-like carbon layers (5) at the atomic scale.[78, 79, 80, 81, 82] The first three structural levels can be analysed by SAXS/USAXS (ultrasmall-angle X-ray scattering), while the other two levels can be characterised using wide-angle X-ray scattering (WAXS). The primary particles are fused together to form aggregates that are considered to be unbreakable via

dispersion processes,[81] but the larger hierarchical structures can be affected by the processing conditions.[78, 83, 84] Thus SAXS/USAXS measurements are often employed for characterisation of carbon black/soot dispersions in order to obtain structural information about organisation of the aggregated particles.[81, 84, 85] In this context, the unified Guinier plus power law approach proposed by Beaucage is commonly employed,[86, 87, 88] since it enables an arbitrary number of interrelated structural features at various length scales to be described.[81, 89] The scattering profile is decomposed into the scattering intensity, $I(q)$, arising from each structural element comprising the hierarchical structures. It can be expressed analytically as follows:

$$I(q) \cong \sum_{i=1}^{N} \left[G_i \exp\left(-\frac{q^2 R_{g,i}^2}{3} \right) + \exp\left(-\frac{q^2 R_{g,i+1}^2}{3} \right) B_i \left(\frac{[\mathrm{erf}(q k_i R_{g,i} / \sqrt{6}]^3}{q} \right)^{P_i} \right] S_i(q) \qquad (5)$$

where N is the number of structural elements/levels, and the scattering intensity originating from each structural element/level (i.e., the expression enclosed by the square brackets) is represented as the sum of two components describing the Guinier and power laws, respectively. G_i is the Guinier pre-exponential factor of the i^{th} structural element and B_i is a constant that is characteristic of the type of power-law scattering, as defined by the regime in which the exponent P_i falls. $R_{g,\,i}$ and $R_{g,\,i+1}$ are radii of gyration of a large-scale structure and a small-scale substructure, respectively. The exponent term associated with $R_{g,\,i+1}$ provides a high q cut-off for the power law component, which is incorporated into equation 5 in order to describe scattering from a system with inter-related multi-scale features. This factor is commonly used for mass fractals.[63, 87] If the latter is not required, the exponent term is assumed to be unity. P_i is a scaling exponent of the power law assigned to the larger structure $R_{g,\,i}$. Generally, the value of the exponent enables the structural morphology to be classified. Thus for mass fractals $P_i < 3$, for surface fractals $3 < P_i < 4$, for Porod's law (smooth surface with a sharp interface) $P_i = 4$ and for diffuse interfaces $P_i > 4$ (negative Porod's law deviation). k_i is an empirical constant that has either a value of unity for steep power law decays ($P_i > 3$) or 1.06 for mass fractals ($1.5 < P_i < 3$).[87] Weakly-correlated particles can also be

considered using equation 5 by incorporating a structure factor, $S_i(q)$,[88, 90] which comprises a damped spherical correlation of colloidal particles:

$$S_i(q) = [1 + \eta_i f(qR_{c,i})]^{-1} \quad (6)$$

where $f(qR_{c,i}) = 3[\sin(qR_{c,i}) - qR_{c,i}\cos(qR_{c,i})]/(qR_{c,i})^3$ is the form factor for spherical interactions correlated over a distance R_c and η describes the degree of correlation, which is assumed to be weak if $\eta < 3$. If no correlations are present for the i[th] structural element/level then $S_i(q) = 1$. The multi-level unified fit, equation 5, is implemented as a routine in the SAXS data analysis software Irena SAS macros for Igor Pro.[63]

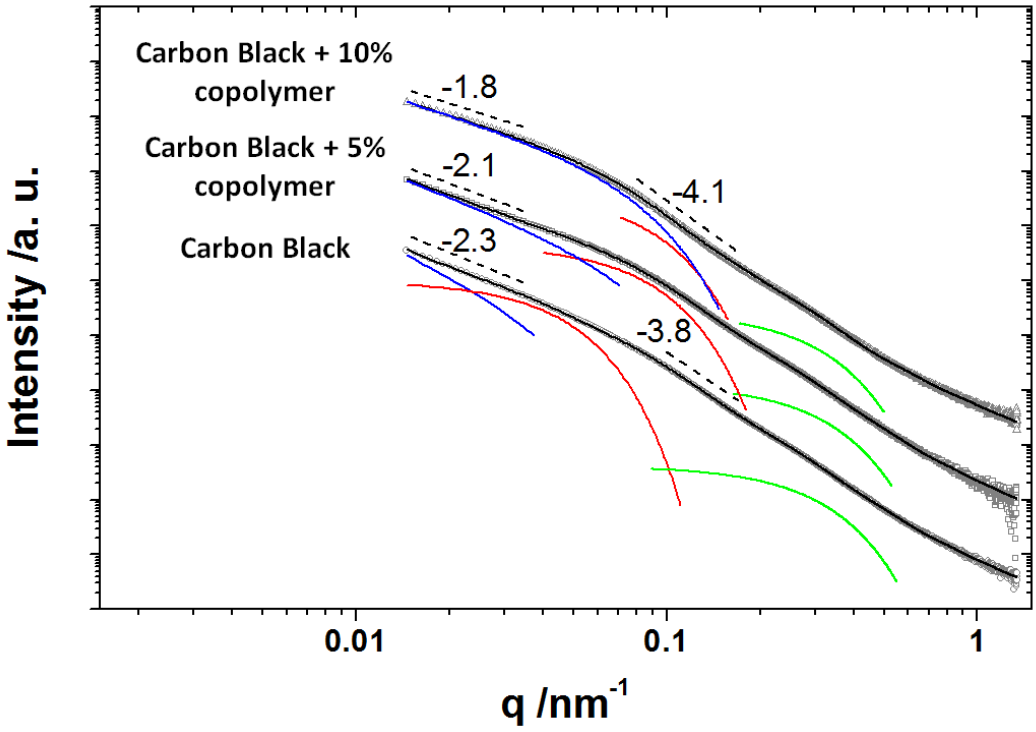

Figure 3.12. Representative SAXS patterns recorded for a 1.0 % w/w carbon black dispersion in *n*-dodecane alone (circles), in *n*-dodecane at two star diblock copolymer concentrations (5.0 % w/w based on carbon black, squares; 10.0 % w/w based on carbon black, triangles). Dashed lines indicate the power law gradient of the scattering intensity. Solid black lines show multi-level unified fits to the data. Coloured lines indicate unified fits to the mass fractals (blue), and the Guinier components of the unified fits to both the agglomerates (red) and the primary particles (green).

Three hierarchical structures can be identified in the SAXS pattern recorded for the original carbon black dispersed in *n*-dodecane (see Figure 3.12, the lowest pattern). By analogy with previous work,[85] the SAXS intensity gradient of -2.3 for $q < 0.03$ nm^{-1} is associated with mass fractals formed by carbon black aggregates and the corresponding gradient of -3.8 for 0.1 nm^{-1} $< q <$ 0.2 nm^{-1} is assigned to surface fractals of the aggregates. Primary particles can be clearly identified as an upturn in SAXS intensity at $q \sim 0.3$ nm^{-1} via a Porod plot (see lowest pattern in Figure 3.13). Thus SAXS patterns obtained for the original carbon black dispersion in *n*-dodecane can be interpreted in terms of scattering from primary particles (level 3), aggregates of these primary particles (level 2) and mass fractals of the aggregates (level 1), see Table 3.2.

Star diblock copolymer added (copolymer mass based on mass of carbon black)	**Level 1 (fractals)**	**Level 2 (aggregates)**		**Level 3 (primary particles)**			
	P_1	**$2R_{g,2}$ /nm**	**P_2**	**$2R_{g,3}$ /nm**	**P_3**	**$R_{c,3}$**	**η_3**
Carbon black alone	2.6	96	4.0	13.8	1.9	23	2.0
1.0 % w/w	2.5	92	4.0	13.4	1.5	23	2.1
2.0 % w/w	2.6	86	4.0	13.8	1.9	23	2.2
3.0 % w/w	2.3	42	4.0	14.4	1.8	26	2.2
4.0 % w/w	2.2	46	4.0	14.8	2.0	24	1.3
5.0 % w/w	2.2	50	4.1	13.6	2.1	23	1.8
7.0 % w/w	2.2	56	4.1	14.0	1.8	23	1.4
8.0 % w/w	2.2	56	4.2	14.8	2.2	23	1.0
9.0 % w/w	1.9	62	4.3	14.0	2.0	23	1.6
10.0 % w/w	1.7	52	4.3	14.2	2.1	20	1.8

Table 3.2. Calculated parameters for three hierarchical structures (levels) derived from multi-level unified fits to the experimental SAXS patterns recorded for 1.0 % w/w carbon black dispersions; the relevant power law exponent (P_1, P_2 or P_3), the size of the structural element ($2R_{g,2}$ or $2R_{g,3}$), the correlation distance ($R_{c,3}$) and the degree of correlation (η). N.B. Errors in the fitted parameters shown in this Table are within a unit of the last digit of the values given.

Structural characteristics of the carbon black can be determined by fitting the unified model to the scattering patterns (see equation 5). A multi-level unified fit described in a previous study[81] has been employed for the SAXS analysis in this work. The SAXS pattern for the initial dispersion of carbon black in *n*-dodecane is reasonably well described by this model (see the lowest patterns in Figures 3.12 and 3.13). The mean primary particle size, $2R_{g,3}$, is 13.8 nm (see Table 3.2, level 3) ,which is comparable to data reported in other studies.[78, 81, 85] The aggregate size, $2R_{g,2}$ = 96 nm (see Table 3.2, level 2) is within the size range observed previously.[78] The power law exponent for these aggregates, P_2 = 4.0 (see Table 3.2) (rather than the value of 3.8 estimated directly from the SAXS pattern, Figure 3.12), indicates a smooth electron density distribution at the aggregate surface, suggesting that the primary particles that make up these aggregates have a relatively smooth interface. It is usually found that the power law exponent for the aggregates ranges from 3.4 to 4.0,[78, 81, 82, 84, 89] indicating that the electron density distribution at the primary particle surface can vary according to the synthesis method and processing conditions. The power law exponent of the mass fractals formed by the aggregates (see Table 3.2, level 1) corresponds to a fractal dimension D_m (or P_1) of 2.6. A similar fractal dimension was observed for a diesel soot dispersed in acetone.[85] Thus the structural morphology of the carbon black particles dispersed in *n*-dodecane can be described as relatively compact mass fractals (see Figure 3.14a). It was also found that incorporating an appropriate structure factor into the model produced a better fit to the SAXS pattern recorded for the primary particles (level 3). Further analysis revealed a weak correlation between the primary particles (η_3 < 3, see Table 3.2). The power law exponent calculated for the primary particles, P_3, is also given in Table 3.2. This parameter is based on the scattering at high *q*. However, it is difficult to interpret such exponents as this region of the scattering pattern is also influenced by excess scattering from a smaller hierarchical carbon structure (sub-units of ~ 1.5 - 2.0 nm) and also by internal inhomogeneities of carbon particles comprising crystalline and amorphous phases.[79, 81, 89]

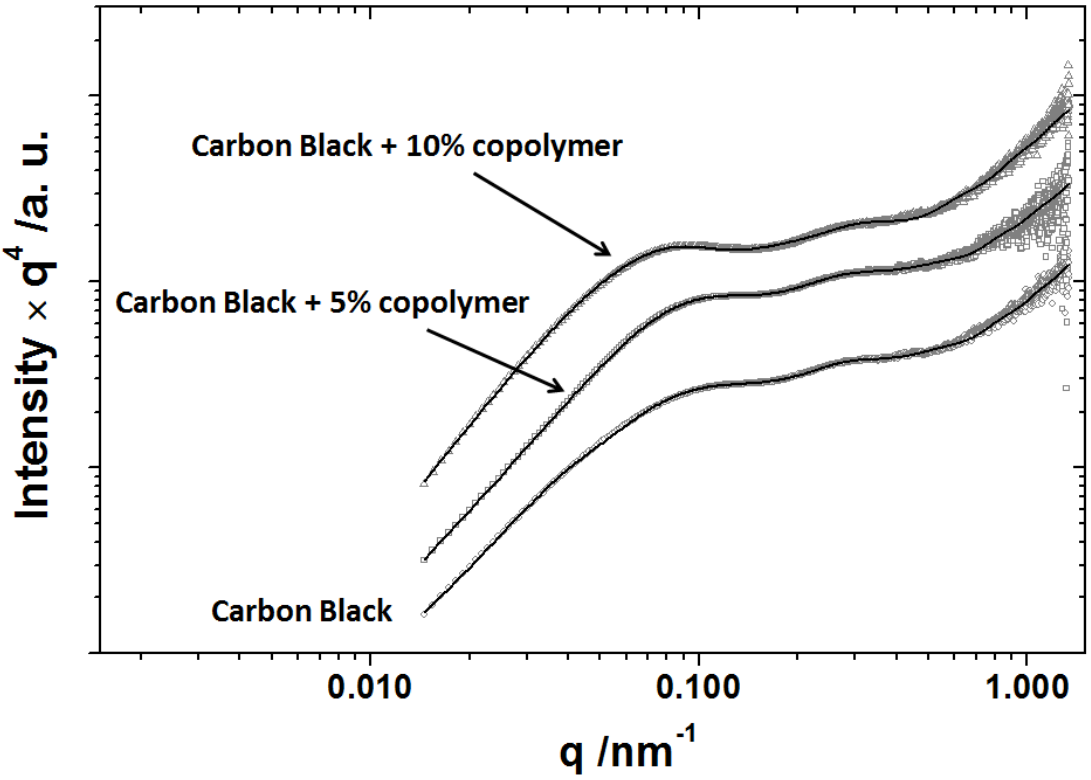

Figure 3.13. Porod law plots of representative SAXS patterns recorded for 1.0 % w/w carbon black dispersions in *n*-dodecane alone (circles), and in *n*-dodecane at two star diblock copolymer concentrations (5.0 % w/w based on carbon black, squares; 10.0 % w/w based on carbon black, triangles). Solid lines indicate multi-level unified fits to the experimental data.

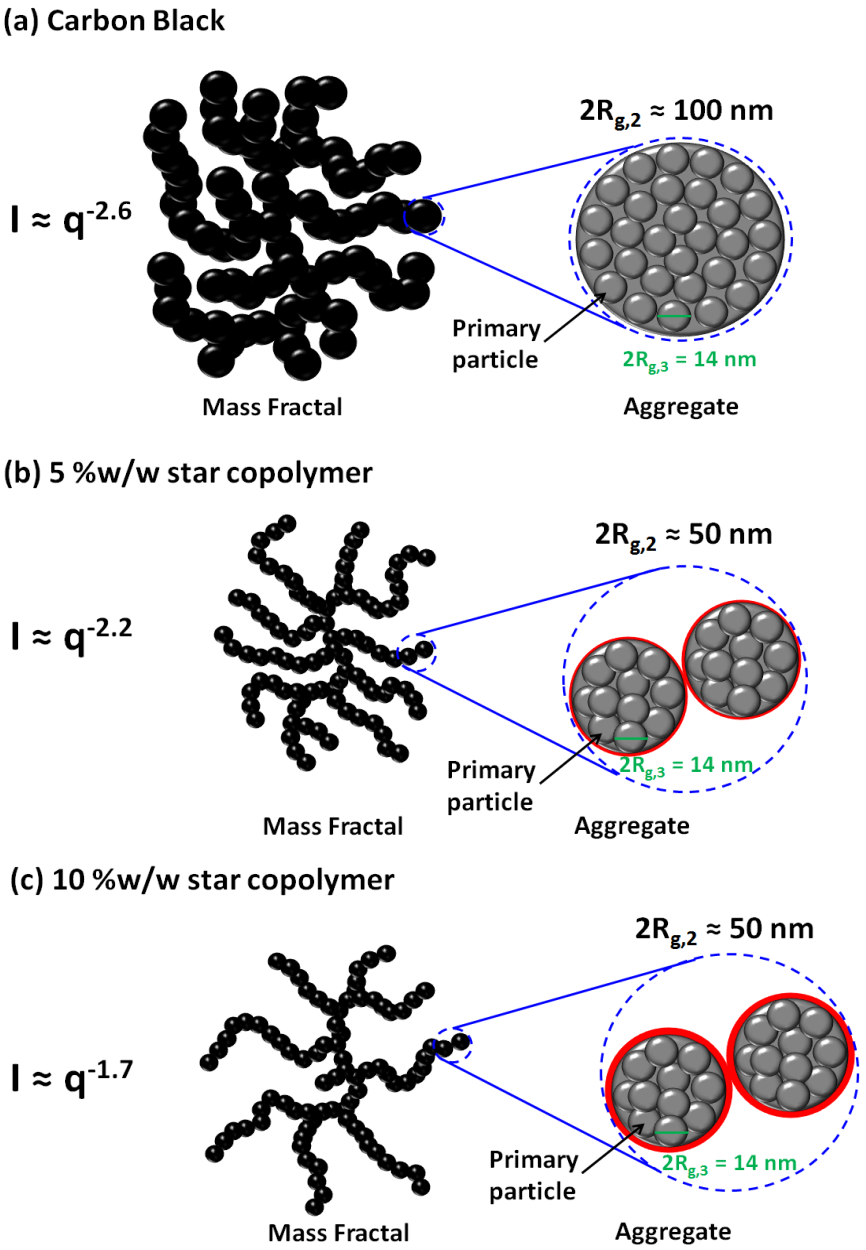

Figure 3.14. Structural morphologies and associated power law exponents for carbon black dispersions: (a) in *n*-dodecane alone, (b) in *n*-dodecane plus 5.0 % w/w star diblock copolymer, (c) in *n*-dodecane plus 10.0 % w/w star diblock copolymer. The red shell surrounding the aggregates depicts the likely location of the copolymer.

SAXS patterns recorded for the carbon black dispersion in *n*-dodecane in the presence of varying concentrations of the star diblock copolymer differ significantly compared to that observed for poorly dispersed carbon black particles alone in this solvent (Figure 3.12 and Figure 3.13). On increasing the copolymer concentration, the gradient of the

scattering intensity associated with the mass fractal dimension increases from -2.3 to -1.8, while that associated with the aggregate surface structure is reduced from -3.8 to -4.1 (Figure 3.12). Further structural information is obtained from detailed SAXS analysis. The multi-level unified model described by equation 5 produced reasonable fits to scattering patterns of the carbon black dispersions containing copolymer (Figure 3.12 and Figure 3.13). Inspecting Table 3.2, the primary particle size remains approximately 14 nm (as found for the carbon black particles alone), with insignificant deviations in the other parameters associated with this structural level. These data suggest that addition of this copolymer to the carbon black essentially does not affect structural morphology associated with the primary particles. In contrast, pronounced changes are revealed in the other two structural levels on increasing the copolymer concentration. The mean aggregate size is reduced to 40-60 nm (Table 3.2 and Figure 3.15), which is comparable to the size of the aggregates observed for carbon black dispersions in toluene after being subjected to prolonged ultrasonic treatment.[81]

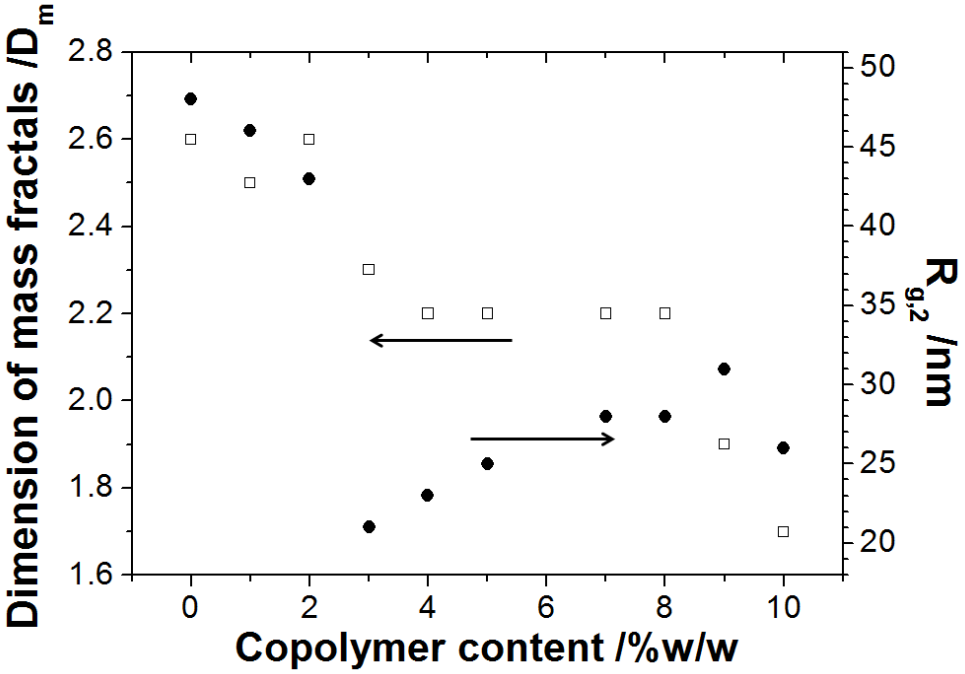

Figure 3.15. Change in mass fractal dimension, D_m ($D_m = P_1$, Table 3.2) (open squares) and radius of gyration of the carbon black aggregates, $R_{g,2}$ (filled circles) with increasing star diblock copolymer concentration for 1.0 % w/w carbon black dispersions in *n*-dodecane.

The characteristic mass fractal dimension is gradually reduced from 2.6 to 1.7 (Table 3.2 and Figure 3.15). There is also a discernible increase in the power law exponent for the aggregates from 4.0 to 4.3 (P_2, Table 3.2). This observation is consistent with copolymer adsorption (see Figures 3.14b and 3.14c). In this case a copolymer shell of relatively low electron density covering electron-dense carbon black aggregates produces a diffuse interface between the aggregates and the surrounding environment, causing a negative deviation of the scattering intensity gradient from Porod's law, for which the gradient is equal to -4.0. Ruland's sigmoidal gradient model can be used in order to estimate the diffuse interface thickness associated with a negative deviation from Porod's law:[91, 92]

$$I(q) = \frac{K}{q^4}\exp(\sigma^2 q^2) \qquad (7)$$

where σ is the standard deviation of the Gaussian smoothing function related to the width of the transition zone, where K is a constant.[91] The interface thickness, t, can be calculated using $t = \sqrt{2\pi}\sigma$.[92] SAXS analysis suggests that the most sensitive part of the scattering patterns related to the negative deviation of level 2 (Table 3.2, $P_2 > 4$) is in the q range from 0.1 nm^{-1} to 0.2 nm^{-1} (Figure 3.13). Fitting Ruland's model to a power law function with an exponent of -4.3 within this q range indicates a negative deviation corresponding to an interface thickness of approximately 7.5 nm. The radius of gyration (R_g) of the star diblock copolymer can be estimated mathematically. The projected contour length for both polystyrene and 1,2-polyisoprene repeat units is 0.255 nm (i.e., two C–C bonds in an *all-trans* conformation), the total contour length of one arm of the star diblock copolymer (M_n = 384 K, ~ eight arms per star) = 666 × 0.255 nm = 170 nm. A mean Kuhn length of 1.72 nm (based on the known literature value for polyisoprene[93]) indicates an unperturbed radius of gyration, $R_g = (170 \times 1.72/6)^{0.5}$, or ~7 nm. Thus the above adsorbed copolymer layer thickness of 7.5 nm suggests some degree of flattening of the star diblock copolymer when adsorbed onto the carbon black particles.

The observed changes in structural morphology with increasing copolymer concentration can be combined in the following model (see Figure 3.14). Adding $\geq$ 3.0 % w/w star diblock copolymer breaks up the carbon black aggregates into smaller

aggregates (see Figures 3.14b, 3.14c and 3.15). Simultaneously, the mass fractal dimension, D_m, is reduced from 2.6 to 1.7 (see Figure 3.15), suggesting the transformation of initially compact carbon black aggregates (see Figure 3.14a) into relatively loose aggregates (see Figure 3.14c). Moreover, a thicker adsorbed layer of copolymer is clearly formed on the latter aggregates when employing higher copolymer concentrations (Figures 3.14b and 3.14c).

Conclusions

In summary, this study demonstrates the value of utilising a range of complementary characterisation techniques that offer structural information over a range of length scales. Optical microscopy, TEM and analytical centrifugation studies indicate that the star diblock copolymer acts as a flocculant for carbon black in *n*-dodecane at relatively low copolymer concentrations, since bridging of the copolymer chains between multiple carbon black particles leads to the formation of aggregates and larger agglomerates. However, above a certain critical concentration (corresponding to a fractional surface coverage of 0.45 to 0.60), bridging is no longer favoured; the star diblock copolymer acts as a steric stabiliser for the carbon black particles under these conditions. In this latter regime, analytical centrifugation requires knowledge of the effective density of the sterically-stabilised carbon black particles, but fortunately this parameter can be calculated via Stokes' law (although not for all experimental conditions studied herein). The critical copolymer concentration required for steric stabilisation was found to be somewhat solvent-dependent, but surprisingly independent of temperature.

SAXS studies enable three hierarchical structures to be identified for the carbon black used in this study. Scattering patterns obtained in *n*-dodecane can be interpreted in terms of scattering from primary particles, aggregates of these primary particles and mass fractals of such aggregates. Furthermore, addition of the star diblock copolymer does not affect the primary structural morphology associated with the carbon black particles. However, pronounced changes are revealed in the other two structural levels on increasing the copolymer concentration. The mean aggregate size is reduced along with the characteristic mass fractal dimension. There is also an increase in the power

law exponent for the aggregates from 4.0 to 4.3. This is consistent with a shell of relatively low electron density covering electron-dense carbon black aggregates, which hence offers direct evidence for copolymer adsorption. The observed changes in structural morphology with increasing copolymer concentration indicate that adding at least 3.0 % w/w star diblock copolymer breaks up the carbon black aggregates into smaller aggregates, while concomitantly transforming the initially compact carbon black aggregates into relatively loose aggregates. Furthermore, SAXS provides direct evidence for copolymer adsorption on the carbon black and allows an estimate of the adsorbed layer thickness.

References

1. Ruehrwein, R. A.; Ward, D. W. Mechanism of Clay Aggregation By Polyelectrolytes. *Soil Science* **1952,** *73,* 485-492.
2. Biggs, S.; Habgood, M.; Jameson, G. J.; Yan, Y.-d. Aggregate structures formed via a bridging flocculation mechanism. *Chemical Engineering Journal* **2000,** *80,* 13-22.
3. Yan, Y.-d.; Burns, J. L.; Jameson, G. J.; Biggs, S. The structure and strength of depletion force induced particle aggregates. *Chemical Engineering Journal* **2000,** *80,* 23-30.
4. Glover, S. M.; Yan, Y.-d.; Jameson, G. J.; Biggs, S. Bridging flocculation studied by light scattering and settling. *Chemical Engineering Journal* **2000,** *80,* 3-12.
5. Gregory, J. Monitoring particle aggregation processes. *Advances in Colloid and Interface Science* **2009,** *147–148,* 109-123.
6. Heller, W.; Pugh, T. L. "Steric" stabilization of colloidal solutions by adsorption of flexible macromolecules. *Journal of Polymer Science* **1960,** *47,* 203-217.
7. Hiemenz, P. C.; Vold, R. D. Rates of flocculation and deflocculation in dispersions of carbon black in hydrocarbons. *Journal of Colloid Science* **1965,** *20,* 635-649.
8. Napper, D. H. *Polymeric stabilization of colloidal dispersions*; Academic Press London1983; Vol. 7.
9. Vincent, B.; Edwards, J.; Emmett, S.; Jones, A. Depletion flocculation in dispersions of sterically-stabilised particles ("soft spheres"). *Colloids and Surfaces* **1986,** *18,* 261-281.
10. Feigin, R. I.; Napper, D. H. Depletion stabilization and depletion flocculation. *Journal of Colloid and Interface Science* **1980,** *75,* 525-541.
11. Napper, D. H. Steric stabilization. *Journal of Colloid and Interface Science* **1977,** *58,* 390-407.
12. Jenkins, P.; Snowden, M. Depletion flocculation in colloidal dispersions. *Advances in Colloid and Interface Science* **1996,** *68,* 57-96.
13. Armes, S. P.; Aldissi, M. Preparation and characterization of colloidal dispersions of polypyrrole using poly(2-vinyl pyridine)-based steric stabilizers. *Polymer* **1990,** *31,* 569-574.
14. Tadros, T. F. Steric Stabilisation and Flocculation by Polymers. *Polym J* **1991,** *23,* 683-696.
15. Whipple, W. L.; Maltesh, C. Adsorption of Cationic Flocculants to Paper Slurries. *Journal of Colloid and Interface Science* **2002,** *256,* 33-40.
16. Zeng, D.; Wu, J.; Kennedy, J. F. Application of a chitosan flocculant to water treatment. *Carbohydrate Polymers* **2008,** *71,* 135-139.
17. Singh, R.; Nayak, B.; Biswal, D.; Tripathy, T.; Banik, K. Biobased polymeric flocculants for industrial effluent treatment. *Mat Res Innovat* **2003,** *7,* 331-340.
18. Weissenborn, P. K.; Warren, L. J.; Dunn, J. G. Optimisation of selective flocculation of ultrafine iron ore. *International Journal of Mineral Processing* **1994,** *42,* 191-213.
19. Bolto, B. A. Soluble polymers in water purification. *Progress in Polymer Science* **1995,** *20,* 987-1041.
20. Pelton, R. H. A model for flocculation in turbulent flow. *Colloids and Surfaces* **1981,** *2,* 259-275.

21. Alonzo, J.; Hinestrosa, J. P.; Mays, J. W.; Kilbey, S. M. Kinetics of Preferential Adsorption of Amphiphilic Star Block Copolymers that Tether by Their Corona Blocks at the Solid/Fluid Interface. *Macromolecules* **2014**.
22. Stoll, S.; Buffle, J. Computer Simulation of Bridging Flocculation Processes: The Role of Colloid to Polymer Concentration Ratio on Aggregation Kinetics. *Journal of Colloid and Interface Science* **1996,** *180,* 548-563.
23. Healy, T. W.; La Mer, V. K. The energetics of flocculation and redispersion by polymers. *Journal of Colloid Science* **1964,** *19,* 323-332.
24. Lu, C.; Pelton, R. PEO Flocculation of Polystyrene-Core Poly(vinylphenol)-Shell Latex: An Example of Ideal Bridging. *Langmuir* **2001,** *17,* 7770-7776.
25. McFarlane, N. L.; Wagner, N. J.; Kaler, E. W.; Lynch, M. L. Poly(ethylene oxide) (PEO) and Poly(vinyl pyrolidone) (PVP) Induce Different Changes in the Colloid Stability of Nanoparticles. *Langmuir* **2010,** *26,* 13823-13830.
26. Santore, M. M.; Russel, W. B.; Prud'homme, R. K. Experimental and theoretical study of phase transitions induced in colloidal dispersions by associative polymers. *Faraday Discussions of the Chemical Society* **1990,** *90,* 323-333.
27. Hoogeveen, N. G.; Cohen Stuart, M. A.; Fleer, G. J. Can charged (block co)polymers act as stabilisers and flocculants of oxides? *Colloids and Surfaces A: Physicochemical and Engineering Aspects* **1996,** *117,* 77-88.
28. Snowden, M. J.; Clegg, S. M.; Williams, P. A.; Robb, I. D. Flocculation of silica particles by adsorbing and non-adsorbing polymers. *J. Chem. Soc., Faraday Trans.* **1991,** *87,* 2201-2207.
29. Solberg, D.; Wågberg, L. Adsorption and flocculation behavior of cationic polyacrylamide and colloidal silica. *Colloids and Surfaces A: Physicochemical and Engineering Aspects* **2003,** *219,* 161-172.
30. Overbeek, J. T. G. Colloid stability in aqueous and non-aqueous media. Introductory paper. *Discuss. Faraday Soc.* **1966,** *42,* 7-13.
31. Bhattacharjee, S.; Paria, M. K.; Maiti, H. S. Polyvinyl butyral as a dispersant for barium titanate in a non-aqueous suspension. *J Mater Sci* **1993,** *28,* 6490-6495.
32. Ma, S.-H.; Matrick, H.; Shor, A. C.; Spinelli, H. J. Aqueous pigmented inks for ink jet printers. 1992.
33. Croll, S. DLVO theory applied to TiO2 pigments and other materials in latex paints. *Progress in Organic Coatings* **2002,** *44,* 131-146.
34. Reuter, E.; Silber, S.; Psiorz, C. The use of new blockcopolymeric dispersing agents for waterborne paints — theoretical and practical aspects. *Progress in Organic Coatings* **1999,** *37,* 161-167.
35. Shar, J. A.; Cosgrove, T.; Obey, T. M.; Warne, M. R.; Wedlock, D. J. Adsorption Studies of Diblock Copolymers at the Cyclohexane/Carbon Black Interface. *Langmuir* **1999,** *15,* 7688-7694.
36. Cawdery, N.; Obey, T. M.; Vincent, B. Colloidal dispersions of electrically conducting polypyrrole particles in various media. *Journal of the Chemical Society, Chemical Communications* **1988,** 1189-1190.
37. Armes, S. P.; Vincent, B. Dispersions of electrically conducting polypyrrole particles in aqueous media. *J. Chem. Soc., Chem. Commun.* **1987,** 288-290.
38. Armes, S. P.; Aldissi, M. Novel colloidal dispersons of polyaniline. *Journal of the Chemical Society, Chemical Communications* **1989,** 88-89.

39. Simmons, M. R.; Chaloner, P. A.; Armes, S. P.; Greaves, S. J.; Watts, J. F. Synthesis and Characterization of Colloidal Polypyrrole Particles Using Reactive Polymeric Stabilizers. *Langmuir* **1998,** *14*, 611-618.
40. Armes, S. P.; Aldissi, M. Preparation and characterization of colloidal dispersions of polypyrrole using poly(2-vinyl pyridine)-based steric stabilizers. *Polymer* **1990,** *31*, 569-574.
41. Kim, J. H.; Chainey, M.; El-Aasser, M. S.; Vanderhoff, J. W. Preparation of highly sulfonated polystyrene model colloids. *Journal of Polymer Science Part A: Polymer Chemistry* **1989,** *27*, 3187-3199.
42. Lok, K. P.; Ober, C. K. Particle size control in dispersion polymerization of polystyrene. *Canadian Journal of Chemistry* **1985,** *63*, 209-216.
43. O'Neill, M. L.; Yates, M. Z.; Harrison, K. L.; Johnston, K. P.; Canelas, D. A.; Betts, D. E.; DeSimone, J. M.; Wilkinson, S. P. Emulsion Stabilization and Flocculation in CO2. 1. Turbidimetry and Tensiometry. *Macromolecules* **1997,** *30*, 5050-5059.
44. Richez, A. P.; Yow, H. N.; Biggs, S.; Cayre, O. J. Dispersion polymerization in non-polar solvent: Evolution toward emerging applications. *Progress in Polymer Science* **2013,** *38*, 897-931.
45. Au, K. M.; Armes, S. P. Heterocoagulation as a Facile Route To Prepare Stable Serum Albumin-Nanoparticle Conjugates for Biomedical Applications: Synthetic Protocols and Mechanistic Insights. *ACS Nano* **2012,** *6*, 8261-8279.
46. Simmons, M. R.; Patrickios, C. S. Synthesis and aqueous solution characterization of catalytically active block copolymers containing imidazole. *Macromolecules* **1998,** *31*, 9075-9077.
47. Baines, F. L.; Billingham, N. C.; Armes, S. P. Synthesis and Solution Properties of Water-Soluble Hydrophilic−Hydrophobic Block Copolymers. *Macromolecules* **1996,** *29*, 3416-3420.
48. Wilhelm, M.; Zhao, C. L.; Wang, Y.; Xu, R.; Winnik, M. A.; Mura, J. L.; Riess, G.; Croucher, M. D. Poly (styrene-ethylene oxide) block copolymer micelle formation in water: a fluorescence probe study. *Macromolecules* **1991,** *24*, 1033-1040.
49. Dawkins, J. V.; Maghami, G. G.; Shakir, S. A.; Higgins, J. S. Non-aqueous polymer dispersions: radical dispersion polymerization in the presence of the diblock copolymer poly(styrene-b-[ethylene-co-propylene]). *Colloid Polym Sci* **1986,** *264*, 616-618.
50. Vincent, B.; Waterson, J. Colloidal dispersions of electrically-conducting, spherical polyaniline particles. *J. Chem. Soc., Chem. Commun.* **1990,** 683-684.
51. Hadjichristidis, N.; Pispas, S.; Floudas, G. *Block copolymers: synthetic strategies, physical properties, and applications*; John Wiley & Sons2003.
52. Hadjichristidis, N.; Pitsikalis, M.; Pispas, S.; Iatrou, H. Polymers with complex architecture by living anionic polymerization. *Chemical reviews* **2001,** *101*, 3747-3792.
53. Burguiere, C.; Dourges, M. A.; Charleux, B.; Vairon, J. P. Synthesis and characterization of omega-unsaturated poly(styrene-b-n-butyl methacrylate) block copolymers using TEMPO-mediated controlled radical polymerization. *Macromolecules* **1999,** *32*, 3883-3890.
54. Quaglia, F.; Ostacolo, L.; De Rosa, G.; La Rotonda, M. I.; Ammendola, M.; Nese, G.; Maglio, G.; Palumbo, R.; Vauthier, C. Nanoscopic core-shell drug carriers made of amphiphilic triblock and star-diblock copolymers. *International Journal of Pharmaceutics* **2006,** *324*, 56-66.

55. Li, Y.; Narain, R.; Ma, Y.; Lewis, A. L.; Armes, S. P. Biomimetic thermo-responsive star diblock gelators. *Chemical communications* **2004,** 2746-2747.
56. Xia, J.; Zhang, X.; Matyjaszewski, K. Synthesis of star-shaped polystyrene by atom transfer radical polymerization using an "arm first" approach. *Macromolecules* **1999,** *32,* 4482-4484.
57. Gao, H.; Matyjaszewski, K. Synthesis of Star Polymers by a Combination of ATRP and the "Click" Coupling Method. *Macromolecules* **2006,** *39,* 4960-4965.
58. Haddleton, D. M.; Crossman, M. C. Synthesis of methacrylic multi-arm star copolymers by "arm-first" group transfer polymerisation. *Macromolecular Chemistry and Physics* **1997,** *198,* 871-881.
59. Li, Y.; Tang, Y.; Narain, R.; Lewis, A. L.; Armes, S. P. Biomimetic Stimulus-Responsive Star Diblock Gelators†. *Langmuir* **2005,** *21,* 9946-9954.
60. Eckert, R. J. Hydrogenated star-shaped polymer. 1978.
61. Coessens, V.; Pintauer, T.; Matyjaszewski, K. Functional polymers by atom transfer radical polymerization. *Progress in Polymer Science* **2001,** *26,* 337-377.
62. Chong, Y.; Le, T. P.; Moad, G.; Rizzardo, E.; Thang, S. H. A more versatile route to block copolymers and other polymers of complex architecture by living radical polymerization: the RAFT process. *Macromolecules* **1999,** *32,* 2071-2074.
63. Ilavsky, J.; Jemian, P. R. Irena: tool suite for modeling and analysis of small-angle scattering. *Journal of Applied Crystallography* **2009,** *42,* 347-353.
64. Scares, B. G.; de Souza Gomes, A. Spectrophotometric determination of the styrene content of alpha-methylstyrene—styrene copolymers. *Polymer Bulletin* **1988,** *20,* 543-548.
65. One method for achieving such a high level of saturation is to use H_2 gas with a mixture of Ni(octanoate)$_2$ catalyst and $AlEt_3$ in cyclohexane at 65^{o}C.[59].
66. Godward, J.; Heatley, F.; Price, C. 1 H Nuclear magnetic relaxation study of the phase structure of polystyrene-block-poly (ethylene/propylene) copolymer micelles. *J. Chem. Soc., Faraday Trans.* **1993,** *89,* 3471-3475.
67. Clague, A. D. H.; Donnet, J. B.; Wang, T. K.; Peng, J. C. M. A comparison of diesel engine soot with carbon black. *Carbon* **1999,** *37,* 1553-1565.
68. Won, Y.-Y.; Meeker, S. P.; Trappe, V.; Weitz, D. A.; Diggs, N. Z.; Emert, J. I. Effect of Temperature on Carbon-Black Agglomeration in Hydrocarbon Liquid with Adsorbed Dispersant. *Langmuir* **2004,** *21,* 924-932.
69. Pugh, R. J.; Matsunaga, T.; Fowkes, F. M. The dispersibility and stability of carbon black in media of low dielectric constant. 1. Electrostatic and steric contributions to colloidal stability. *Colloids and Surfaces* **1983,** *7,* 183-207.
70. Pugh, R. J.; Fowkes, F. M. The dispersibility and stability of carbon black in media of low dielectric constant. 2. Sedimentation volume of concentrated dispersions, adsorption and surface calorimetry studies. *Colloids and Surfaces* **1984,** *9,* 33-46.
71. Cohen Stuart, M. A.; Cosgrove, T.; Vincent, B. Experimental aspects of polymer adsorption at solid/solution interfaces. *Advances in Colloid and Interface Science* **1985,** *24,* 143-239.
72. Ho, Y.-S. Isotherms for the sorption of lead onto peat: comparison of linear and non-linear methods. *Polish Journal of Environmental Studies* **2006,** *15,* 81-86.
73. Fleer, G. *Polymers at interfaces*; Springer Science & Business Media1993.
74. Huang, J.-C. Carbon black filled conducting polymers and polymer blends. *Advances in Polymer Technology* **2002,** *21,* 299-313.

75. Detloff, T.; Sobisch, T.; Lerche, D. Particle Size Distribution by Space or Time Dependent Extinction Profiles obtained by Analytical Centrifugation. *Particle & Particle Systems Characterization* **2006,** *23*, 184-187.
76. Lutskii, A. Molecular constants and the viscosity of liquids. *Zh. Fiz. Khim* **1955,** *29*, 1162-1172.
77. Viswanath, D. S. *Viscosity of liquids: theory, estimation, experiment, and data*; Springer Science & Business Media2007.
78. Braun, A.; Huggins, F. E.; Seifert, S.; Ilavsky, J.; Shah, N.; Kelly, K. E.; Sarofim, A.; Huffman, G. P. Size-range analysis of diesel soot with ultra-small angle X-ray scattering. *Combustion and Flame* **2004,** *137*, 63-72.
79. di Stasio, S.; Mitchell, J. B. A.; LeGarrec, J. L.; Biennier, L.; Wulff, M. Synchrotron SAXS (in situ) identification of three different size modes for soot nanoparticles in a diffusion flame. *Carbon* **2006,** *44*, 1267-1279.
80. Hessler, J. P.; Seifert, S.; Winans, R. E.; Fletcher, T. H. Small-angle X-ray studies of soot inception and growth. *Faraday Discussions* **2001,** *119*, 395-407.
81. Koga, T.; Hashimoto, T.; Takenaka, M.; Aizawa, K.; Amino, N.; Nakamura, M.; Yamaguchi, D.; Koizumi, S. New insight into hierarchical structures of carbon black dispersed in polymer matrices: A combined small-angle scattering study. *Macromolecules* **2008,** *41*, 453-464.
82. Sorensen, C. M.; Oh, C.; Schmidt, P. W.; Rieker, T. P. Scaling description of the structure factor of fractal soot composites. *Physical Review E* **1998,** *58*, 4666-4672.
83. Koga, T.; Takenaka, M.; Aizawa, K.; Nakamura, M.; Hashimoto, T. Structure factors of dispersible units of carbon black filler in rubbers. *Langmuir* **2005,** *21*, 11409-11413.
84. Rieker, T. P.; Hindermann-Bischoff, M.; Ehrburger-Dolle, F. Small-angle X-ray scattering study of the morphology of carbon black mass fractal aggregates in polymeric composites. *Langmuir* **2000,** *16*, 5588-5592.
85. Braun, A.; Ilavsky, J.; Seifert, S.; Jemian, P. R. Deformation of diesel soot aggregates as a function of pellet pressure: A study with ultra-small-angle x-ray scattering. *Journal of Applied Physics* **2005,** *98*.
86. Beaucage, G. Approximations leading to a unified exponential power-law approach to small-angle scattering. *Journal of Applied Crystallography* **1995,** *28*, 717-728.
87. Beaucage, G. Small-angle scattering from polymeric mass fractals of arbitrary mass-fractal dimension. *Journal of Applied Crystallography* **1996,** *29*, 134-146.
88. Beaucage, G.; Schaefer, D. W. Structural studies of complex-systems using small-angle scattering - A unified guinier power-law approach. *Journal of Non-Crystalline Solids* **1994,** *172*, 797-805.
89. Braun, A.; Shah, N.; Huggins, F. E.; Kelly, K. E.; Sarofim, A.; Jacobsen, C.; Wirick, S.; Francis, H.; Ilavsky, J.; Thomas, G. E.; Huffman, G. P. X-ray scattering and spectroscopy studies on diesel soot from oxygenated fuel under various engine load conditions. *Carbon* **2005,** *43*, 2588-2599.
90. Beaucage, G.; Ulibarri, T. A.; Black, E. P.; Schaefer, D. W. Multiple size scale structures in silica-siloxane composites studied by small-angle scattering. In *Hybrid Organic-Inorganic Composites*, 1995; Vol. 585, pp 97-111.

91. Ruland, W. Small-angle scattering of two-phase systems: determination and significance of systematic deviations from Porod's law. *Journal of Applied Crystallography* **1971,** *4*, 70-73.
92. Roe, R.-J.; Roe, R. *Methods of X-ray and neutron scattering in polymer science*; Oxford University Press New York2000; Vol. 554580219.
93. Fetters, L. J.; Lohse, D. J.; Richter, D.; Witten, T. A.; Zirkel, A. Connection between Polymer Molecular Weight, Density, Chain Dimensions, and Melt Viscoelastic Properties. *Macromolecules* **1994,** *27*, 4639-4647.

Chapter 4

Determination of effective particle density for sterically-stabilised carbon black particles: Effect of diblock copolymer stabiliser composition

Introduction

The formation of colloidal aggregates on dissolution of an AB diblock copolymer in a solvent that is selective for one of the two blocks was first reported more than fifty years ago.[1, 2] If the volume fraction of the soluble block is significantly greater than that of the insoluble block, then so-called 'star-like' spherical micelles are formed in solution.[3, 4, 5, 6] On the other hand, if the volume fraction of the soluble block is appreciably less than that of the insoluble block, then so-called 'crew-cut' micelles can be obtained.[7, 8, 9, 10] There are many papers describing the micellar self-assembly of wholly hydrophobic AB diblock copolymers in organic solvents.[3, 11, 12, 13, 14, 15] In particular, polystyrene-based AB diblock copolymers that form polystyrene-core micelles in non-polar solvents such as *n*-alkanes are well documented.[16, 17, 18, 19, 20, 21, 22, 23] These diblock copolymers can be readily prepared using classical anionic polymerisation,[24, 25] with the soluble block typically being based on either polybutadiene, polyisoprene or their hydrogenated derivatives.[17, 18, 19, 26, 27, 28, 29, 30]

The adsorption of diblock copolymer micelles onto colloidal particles is well documented.[31, 32, 33, 34, 35, 36] In Chapter 2 it was shown that a commercial poly(styrene-*b*-hydrogenated isoprene) diblock copolymer adsorbs onto carbon black in the form of micelles from *n*-heptane, but as individual copolymer chains from chloroform (which is a good solvent for both blocks). In Chapter 3, adsorption of a star diblock copolymer onto the same carbon black particles revealed an interesting concentration-dependent flocculation/dispersion boundary, in which bridging flocculation was observed at low copolymer concentration and steric stabilisation occurred at high copolymer concentration. In both cases, carbon black was selected as a colloidal substrate for such studies because this material has been shown to be a convenient mimic for diesel soot particles.[36, 37] The latter are formed during incomplete fuel combustion in diesel engines and are known to lead to long-term engine wear and reduced fuel economy.[38, 39, 40] Thus suitable oil-soluble block copolymers that can minimise diesel soot formation and/or aid its dispersion at the nanometer scale are routinely added to engine oil formulations to address this problem and hence improve performance. In addition, sterically-stabilised carbon black particles are widely used in inkjet formulations[41, 42] and also as coatings.[43] Each of these applications requires fine control over the degree of dispersion of the

carbon black particles, which is best assessed by determining accurate particle size distributions.

In this Chapter, three polystyrene-based diblock copolymers of differing copolymer compositions and molecular weights have been investigated. Their micellar self-assembly behaviour in *n*-dodecane is examined and the adsorption of these micelles onto carbon black particles dispersed in this solvent is studied at 20^{o}C.

The effective densities of the resulting sterically-stabilised carbon black particles are calculated from geometric considerations, assuming (i) a spherical core-shell morphology and (ii) that the diblock copolymer micelles form hemi-micelles on the carbon black surface. Since the micelle layer thickness is relatively large compared to the primary grain size of the carbon black particles, such effective densities are significantly lower than that of carbon black alone. Thus this approach is *essential* for determining accurate particle size distributions via analytical centrifugation, since otherwise substantial experimental errors are incurred. Analytical centrifugation is preferred to traditional particle sizing techniques such as dynamic light scattering: this is because fractionation occurs during the measurement, which leads to significantly higher resolution. In view of this advantage, the former technique has been utilised for the characterisation of a wide range of colloidal dispersions.[44, 45, 46, 47, 48, 49, 50, 51, 52, 53] It has a wide dynamic range and offers much higher resolution than dynamic light scattering or laser diffraction because fractionation occurs during the measurement. Thus high resolution particle size distributions can be obtained provided that the density of the particles and the continuous phase is known. It is particularly effective and convenient for hard spheres such as gold sols,[52, 54] but can also offer useful information for other colloidal particles. For example, analytical centrifugation has been used to characterise polymer-silica nanocomposite particles with framboidal morphologies,[55, 56] sterically-stabilised latexes,[57, 58] protein-coated particles,[59, 60] core-shell latexes, emulsions[61] and various organic/inorganic nanoparticles.[62, 63, 64, 65, 66, 67]

Experimental

Materials

The three commercial polystyrene-based diblock copolymers used in this Chapter were supplied by BP Formulated Products Technology (Pangbourne, UK). Such diblock copolymers can be prepared by living anionic polymerisation of styrene with either butadiene or isoprene followed by catalytic hydrogenation using nickel-based catalysts.[36] This usually ensures well-defined diblock copolymers with minimal homopolymer contamination and relatively narrow molecular weight distributions.[25] Chloroform and *n*-dodecane solvents were obtained from Fisher Scientific UK Ltd and were used as received. Deuterated chloroform for NMR studies was obtained from Goss Scientific Ltd, UK and was used as received. The carbon black (Regal 250R grade) was supplied by the Cabot Corporation (Billerica, MA, USA) and was used as received.

Gel permeation chromatography. The molecular weight distribution of the three diblock copolymers was assessed by gel permeation chromatography (GPC) using THF eluent. The THF GPC set-up comprised two 5 μm 'Mixed C' 30 cm columns, a Varian 290-LC pump and a WellChrom K-2301 refractive index detector operating at 950 ± 30 nm. The THF mobile phase contained 2.0 v/v% triethylamine and 0.05 w/v% butylhydroxytoluene (BHT) and the flow rate was fixed at 1.0 mL min^{-1}. A series of ten near-monodisperse polystyrene standards (M_n = 580 to 552,500 g mol^{-1}) were used for calibration.

Dynamic light scattering (DLS). Temperature-dependent studies were performed using a Malvern Zetasizer NanoZS model ZEN 3600 instrument equipped with a 4 mW He−Ne solid-state laser operating at 633 nm which was equipped with a Peltier cell, at a fixed scattering angle of 173°. Copolymers were diluted in *n*-dodecane (0.01 % w/w) and equilibrated for 5 min at 5ºC intervals in a 25ºC−90ºC−25ºC thermal cycle. The intensity average diameter and polydispersity of the diblock copolymer particles were calculated at a given temperature by cumulants analysis of the experimental correlation function using Dispersion Technology Software version 6.20. Data were averaged over 13 runs each of 30 s duration.

Transmission electron microscopy. Studies were conducted using a Phillips CM100 microscope operating at 100 kV on unstained samples prepared by drying a drop of dilute sample (approximately 0.01 % w/w) on a carbon-coated copper grid.

Small-angle X-ray scattering. SAXS patterns were obtained for 1.0% w/w copolymer dispersions using a modified Bruker AXS Nanostar instrument (camera length = 1.46 m, CuKa radiation) equipped with a 2D HiSTAR multi-wire gas detector. SAXS patterns were recorded over a q range of 0.008 Å $^{-1}$ < q < 0.16 Å^{-1}, where $q = \frac{4\pi \sin\theta}{\lambda}$ is the length of the scattering vector and θ is half of the scattering angle. A glass capillary of 2 mm path length was used as a sample holder and an exposure time of 2.0 h was utilised for each sample.

Model used for SAXS analysis. A structural model has already been developed for star-like micelles[68] and is briefly summarised here. The general equation for the scattering intensity, I, of interacting micelles is expressed as:[69]

$$I = F_{mic}(q) + F_{mic}^{av}(q)[S_{PY}(q, R_{PY}, f_{PY}) - 1] \quad (1)$$

where the star-like micelle form factor is represented as:[68]

$$F_{mic}(q) = N_{agg}^2 \beta_s^2 A_s^2(q, R_s) + N_{agg} \beta_c^2 F_c(q, R_g) + N_{agg}[N_{agg} - F_c(0)]\beta_c^2 A_c^2(q) + 2N_{agg}^2 \beta_s \beta_c A_s A_c(q) \quad (2)$$

Here R_s is the micelle core radius and R_g is the radius of gyration of the coronal block. The X-ray scattering length contrast between the core block and the coronal block is $\beta_s = V_s(\xi_s - \xi_{sol})$ and $\beta_c = V_c(\xi_c - \xi_{sol})$, respectively, where ξ_s, ξ_c, and ξ_{sol} are the X-ray scattering length densities of the core block (ξ_{PS} = 9.63 × 10^{10} cm^{-2}), the coronal block (ξ_{PB} = 8.84 × 10^{10} cm^{-2}, ξ_{PEP} = 8.75 × 10^{10} cm^{-2}) and solvent ($\xi_{dodecane}$ = 7.63 × 10^{10} cm^{-2}), respectively. V_s and V_c are the volumes of the PS core block and the PEP (or PB) coronal block, respectively. Expressing each diblock copolymer composition in terms of its respective mol fractions and estimating the molecular weights of each block, the mean number of monomer repeat units is calculated for each block (see Table 4.1).

Using literature values for the densities of each block, the respective volumes of the core and coronal blocks can be calculated using $V = \frac{M_w}{N_A \rho}$. These values are given in Table 4.1. The mean micelle aggregation number, N_{agg}, is given by $N_{agg} = (1 - x_{sol}) \frac{4\pi R_s^3}{3V_s}$, where x_{sol} is the concentration of *n*-dodecane solvent in the PS micelle cores. The amplitude of the core self-term is given by: $A_s(q, R_s) = \Phi(qR_s) \exp\left(-\frac{q^2\sigma^2}{2}\right)$, where $\Phi(qR_s) = \frac{3[\sin(qR_s) - qR_s \cos(qR_s)]}{(qR_s)^3}$ is the amplitude of the form factor for a sphere. The exponent term represents a sigmoidal interface between the blocks of width σ that describes a decaying scattering length density at the core surface. The self-correlation term of the corona block is given by the effective single-chain form factor $F_c(q, R_g) = \frac{F_{exv}(q, R_g)}{1 + \nu F_{exv}(q, R_g)}$, where $F_{exv}(q, R_g)$ is the form factor for self-avoiding chains[70] (equation 13 is used in this reference and the formalism therein is also adopted) and ν is a parameter related to the chain-chain interaction within the corona. The effective forward scattering is $F_c(0) = \frac{1}{1+\nu}$. For these star-like micelles, the contribution of the coronal blocks to the scattering signal is comparable to that from the micelle core [$(\beta_c / \beta_s)^2 \approx 0.37$-1.2 in *n*-dodecane]. Thus the amplitude of the corona chain form factor is obtained from a normalised Fourier transform of the radial density distribution function of the corona chains:

$$A_c(q) = \frac{\int_{R_s}^{R_s+2s} \mu_c(r) \frac{\sin(qr)}{qr} r^2 dr}{\int_{R_s}^{R_s+2s} \mu_c(r) r^2 dr} \exp\left(-\frac{q^2\sigma^2}{2}\right) \quad (3)$$

The radial profile, $\mu_c(r)$, can be expressed by a linear combination of two cubic b splines, with two fitting parameters *s* and *a* corresponding to the width of the profile and the weight coefficient, respectively. This information can be found elsewhere,[68, 71] as can the approximate integrated form of equation 3. The form factor of the average radial scattering length density distribution of micelles in equation 1 is used as

$$F_{mic}^{av}(q) = N_{agg}^2[\beta_s A_s(q,R_s) + \beta_c A_c(q)]^2 \quad (4)$$

Use of equation 1 implicitly assumes that interactions between star-like micelles can be described by a structure factor based on the Percus-Yevick approximation $S_{PY}(q,R_{PY},f_{PY})$,[72] where $R_{PY} = R_s + \Delta R$ is the interaction radius and f_{PY} is the hard-sphere volume fraction. In this model, the size polydispersity for the star-like micelles can be calculated by assuming a normal distribution of the micelle core radius R_s with a standard deviation σ_{Rs}. Thus the total number of fitting parameters is five (R_s, σ_{Rs}, R_g, s, and ΔR). In addition, the following parameters were fixed: $x_{sol} = 0.10$, $\sigma = 5$, $a = 0$, $\nu = 2$ and $f_{PY} = 0.19$, since these values have been previously determined for PS-PEP28 in *n*-dodecane at a synchrotron source (ESRF, station ID02, Grenoble, France), and are assumed to be very similar for PS-PB20 and PS-PEP35, see Chapter 2. General parameters such as the copolymer volume fraction and various parameters related to the SAXS measurement geometry are not included in this list. Irena SAS Igor Pro macros were used for model fitting.

^{1}H NMR spectroscopy. The mean polystyrene content of each diblock copolymer dissolved in a non-selective solvent ($CDCl_3$) was determined using a Bruker AV1-250 MHz NMR spectrometer (64 scans per spectrum). Variable temperature spectra were recorded between 25^{o}C and 110^{o}C using d_{26}-dodecane using a Bruker AV1-400 MHz NMR spectrometer (32 scans per spectrum).

Helium pycnometry. The solid-state density of the Regal 250R carbon black was determined using a Micrometrics AccuPyc 1330 helium pycnometer at 20^{o}C.

Surface area analysis. BET surface area measurements were performed using a Quantachrome Nova 1000e instrument with dinitrogen gas (mean area per molecule = 16.2 Å^2) as an adsorbate at 77 K. Samples were degassed under vacuum at 100^{o}C for at least 15 h prior to analysis. The particle diameter, d, was calculated using the formula $d = 6/(\rho.A_s)$, where A_s is the BET specific surface area in $m^2\ g^{-1}$ and ρ is the carbon black density in $g\ m^{-3}$ obtained from helium pycnometry.

UV spectroscopy. UV spectra were recorded at 20ºC for the diblock copolymers dissolved in 1:1 chloroform/*n*-dodecane mixtures (i.e. the *n*-dodecane supernatant was diluted with an equal volume of chloroform) using a Perkin Elmer Lambda 25 instrument operating between 200 and 500 nm. A calibration curve was constructed for the same copolymer dissolved in pure chloroform and gave a molar extinction coefficient of 222 ± 2 mol^{-1} dm^3 cm^{-1}, which is close to the literature value reported for polystyrene.[73] In order to determine the extent of copolymer adsorption onto carbon black via a supernatant depletion assay using UV spectroscopy, the following protocol was adopted. The desired mass of diblock copolymer (3.0 – 90.0 mg) was weighed into a glass vial and carbon black (300.0 mg) was weighed into a separate vial. Then *n*-dodecane (5.00 mL) was added to the diblock copolymer and this suspension was stirred at 20ºC (Turrax stirrer, 1 minute) before being heated up to 110ºC for 1 h. The resulting copolymer micelle dispersion was added to the pre-weighed carbon black, stirred (Turrax stirrer, 1 minute), sonicated for 1 h, and left on a roller mill for 16 h overnight. The dispersion was then centrifuged for 4 h at 18,000 rpm in a centrifuge rotor that was pre-cooled to 15ºC so as to minimise solvent evaporation. Taking care not to disturb the sedimented carbon black particles, the supernatant was decanted into an empty vial and then 0.40 mL of this solution was diluted with an equal volume of pure chloroform to ensure molecular dissolution of the copolymer chains prior to analysis by UV spectroscopy. The aromatic chromophore at 262 nm due to the polystyrene block was used to quantify the copolymer concentration remaining in the supernatant after exposure to the carbon black using the Beer-Lambert linear calibration curve described above, thus enabling the adsorbed amount to be determined by difference.

Analytical centrifugation. The LUMiSizer® (LUM GmbH, Berlin, Germany) is a microprocessor-controlled analytical photocentrifuge that is particularly convenient for analysis of the sterically-stabilised carbon black dispersions described in this work. This instrument employs STEP™-Technology (Space- and Time-resolved Extinction Profiles) to enable the measurement of the intensity of transmitted light as a function of time and position simultaneously over the entire cell length. The progression of the transmission profiles contains information on the rate of sedimentation and therefore allows assessment of the particle size distribution.

Measurements were conducted at 20ºC on 1.0 % w/w carbon black dispersions in *n*-dodecane at 3000 rpm using disposable polyamide cells (path length = 2 mm). The theoretical effective particle density of the sterically-stabilised carbon black particles was calculated from geometric considerations (see later) and constant position analysis was used to determine volume-average particle diameters.

Results and Discussion

Copolymer characterisation

The three commercial diblock copolymers used in this Chapter are denoted by the sample codes indicated in Table 4.1. Polystyrene contents were determined to be 20, 28 and 35 mol% for PS-PB20, PS-PEP28 and PS-PEP35 respectively using ^{1}H NMR spectroscopy in $CDCl_3$ at 20ºC (see Figure 4.1 and Table 4.1). Each copolymer had a relatively narrow molecular weight distribution ($M_w/M_n < 1.10$) as judged by THF GPC analysis using a series of near-monodisperse polystyrene calibration standards.

Copolymer Code	**Copolymer Description**	**Polystyrene content[a] / mol%**	M_n [b] /kg mol^{-1}	M_w [b] /kg mol^{-1}	M_w/M_n [b]	**Micelle diameter [c] /nm**		
						TEM	**SAXS**	**DLS**
PS-PB20	Poly(styrene-*b*-hydrogenated butadiene)	20	183	198	1.08	24	71	88
PS-PEP28	Poly(styrene-*b*-hydrogenated isoprene)	28	117	121	1.04	24	68	85
PS-PEP35	Poly(styrene-*b*-hydrogenated isoprene)	35	163	177	1.08	27	65	89

Table 4.1. Summary of copolymer sample codes, copolymer compositions, molecular weight data and micelle diameters for the three diblock copolymers used in this Chapter.

a. ^{1}H NMR spectroscopy studies conducted in $CDCl_3$
b. Determined by gel permeation chromatography (refractive index detector; THF eluent; calibration using a series of near-monodisperse polystyrene standards)
c. Determined at 20ºC after heating the initial copolymer dispersion in *n*-dodecane to 110ºC for 1 h. TEM only 'sees' the micelle cores, whereas SAXS and DLS report the micelle cores plus the solvated micelle coronas.

Unfortunately, each copolymer differs in terms of its copolymer molecular weight and block composition, which makes it impossible to examine the effect of either of these two parameters in isolation. Nevertheless, appropriate consideration of these three copolymers sheds useful light on their performance as dispersants for carbon black particles in non-polar media (see later).

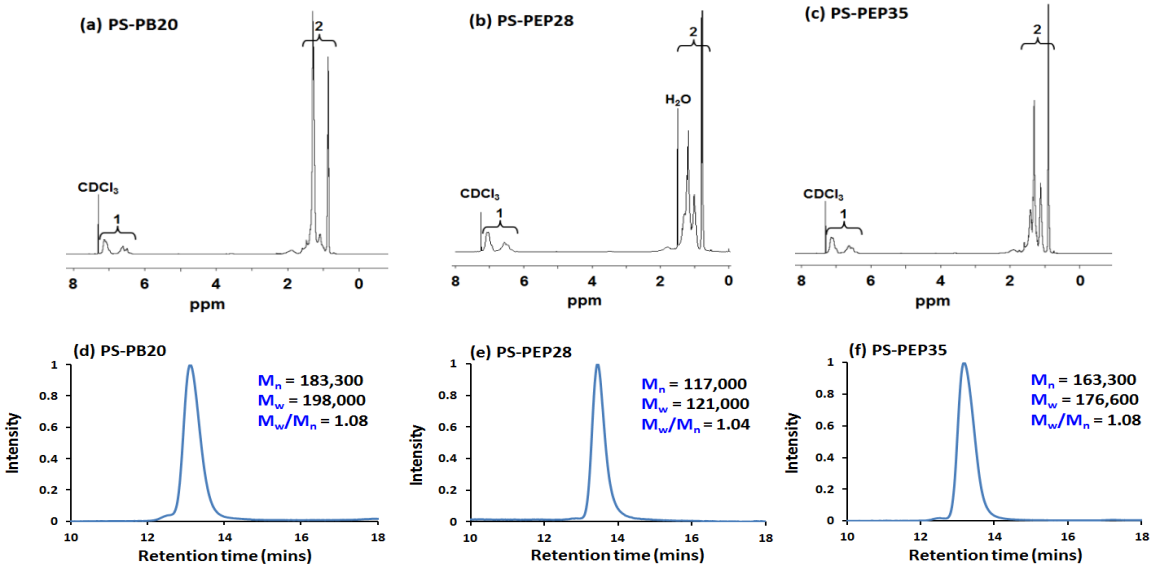

Figure 4.1. ^{1}H NMR spectra ($CDCl_3$) obtained for the three diblock copolymers used in this work. Comparison of the integrated aromatic signals with those of the aliphatic backbone signals indicate mean polystyrene contents of (a) 20 mol % for PS-PB20, (b) 28 mol % for PS-PEP28 and (c) 35 mol % for PS-PEP35. The corresponding THF GPC curves recorded for these three copolymers are also shown [see (d)-(f)]. Molecular weight data are expressed relative to polystyrene standards.

Copolymer self-assembly

The micellisation of the PS-PEP28 diblock copolymer has been extensively discussed in Chapter 2. When dissolved directly in *n*-dodecane at 20^{o}C, ill-defined colloidal aggregates are obtained because the insoluble glassy polystyrene block prevents efficient break-up of the original solid-state morphology of this copolymer. However, heating these aggregates up to 110^{o}C for 1 h followed by cooling to 20^{o}C produces small, well-defined polystyrene-core micelles. This morphological transformation is confirmed by transmission electron microscopy (TEM) studies of each of the three diblock copolymers before and after the 20^{o}C-110^{o}C-20^{o}C thermal cycle, see Figure 4.2.

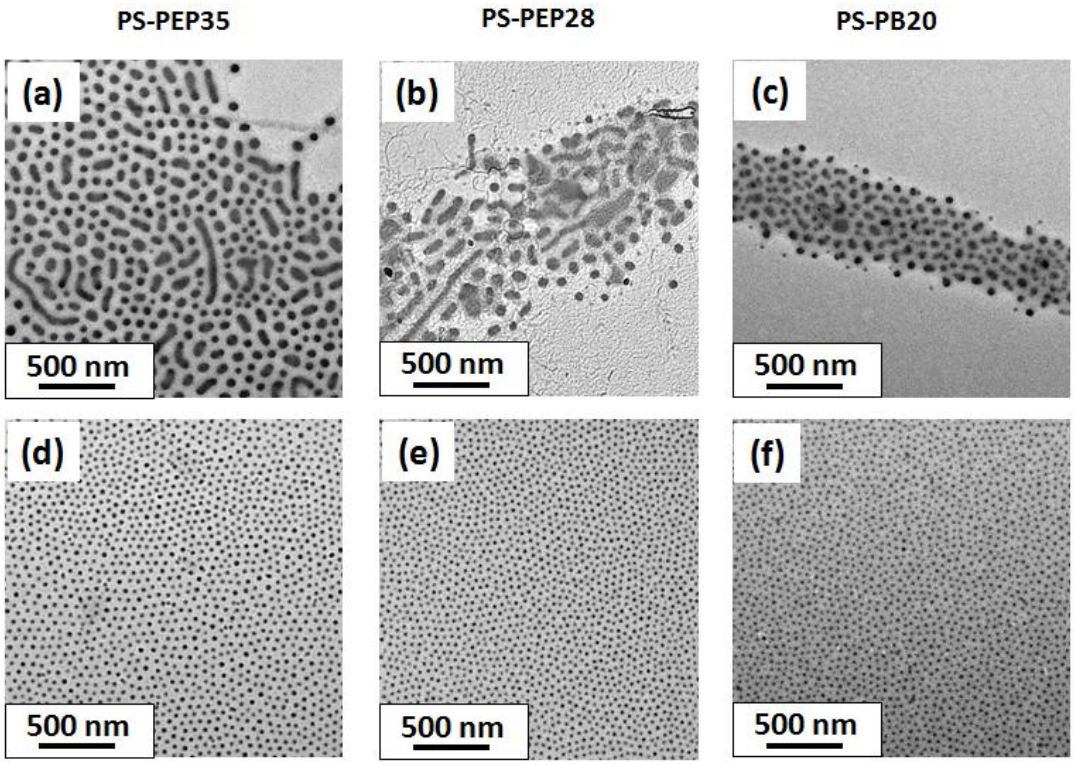

Figure 4.2. TEM images recorded for the colloidal aggregates formed by the three linear polystyrene-based diblock copolymers used in this study. Images (a), (b) and (c) show the relatively large, ill-defined, non-equilibrium aggregates formed via direct dispersion at 20^{o}C in *n*-dodecane. In contrast, images (d), (e) and (f) show the much smaller, well-defined equilibrium spherical micelles formed at 20^{o}C on heating this initial dispersion to 110^{o}C for 1 h in *n*-dodecane.

Variable temperature dynamic light scattering (DLS) was also used to monitor this change in copolymer morphology, see Figure 4.3. The initial 'sphere-equivalent' diameter observed at 25^{o}C should be treated with some caution, since the TEM images reveal the presence of a significant fraction of polydisperse cylinders, see Figure 4.2. On heating to 75^{o}C, the mean particle dimensions are dramatically reduced, which is consistent with the corresponding TEM images indicating the formation of well-defined spherical micelles. It seems likely that the original cylinders are converted into spheres via a 'budding' process, since the intensity-average diameter of the small micelles is roughly comparable to the mean width of the original cylinders indicated by TEM (see Figure 4.2). Similar observations were recently reported by Fielding *et al.*,[12] who observed a worm-to-sphere transition for poly(lauryl methacrylate)-poly(benzyl methacrylate) diblock copolymers on heating above 90^{o}C in *n*-dodecane (as judged by TEM).

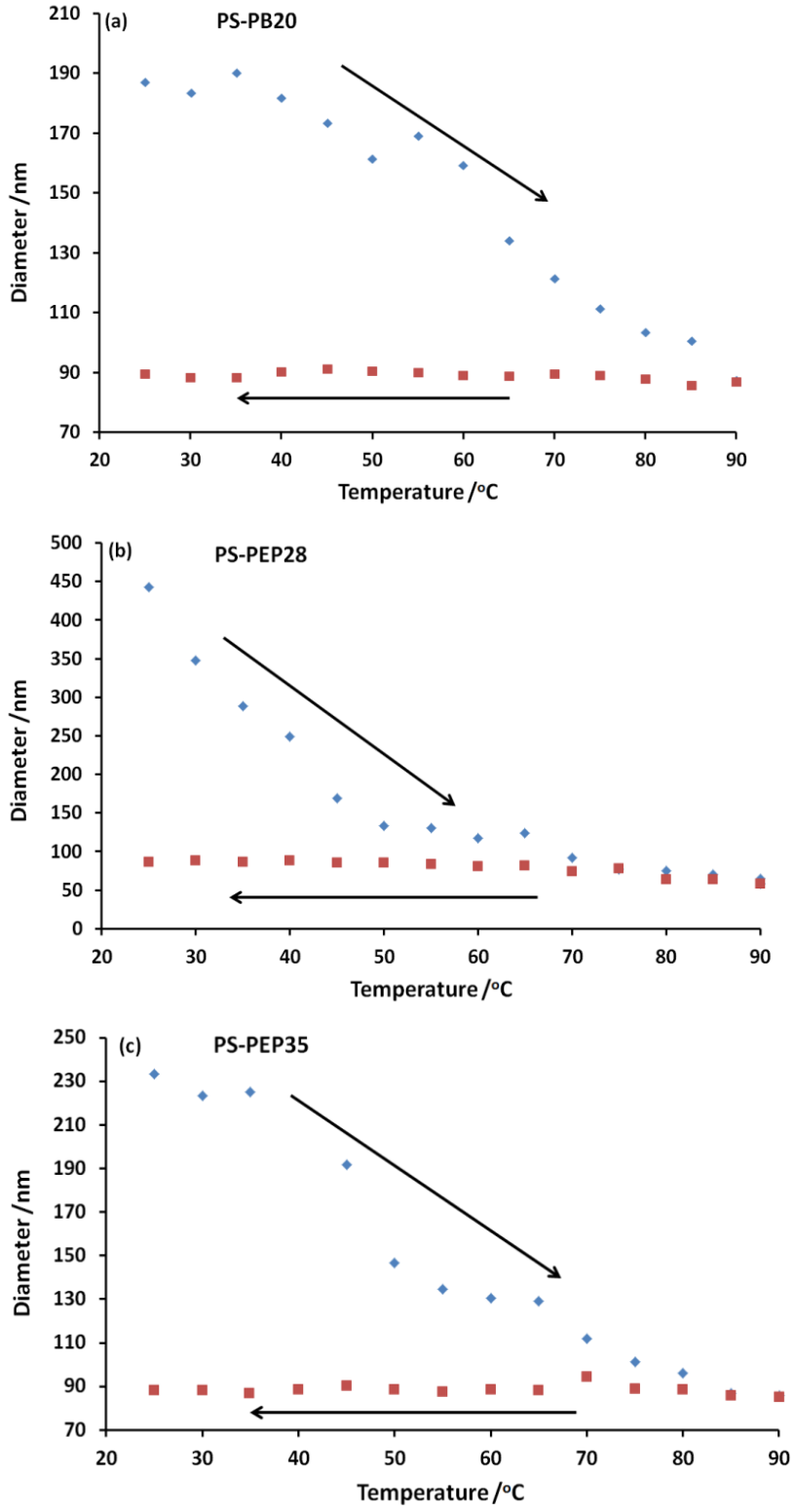

Figure 4.3. Variation in DLS intensity-average diameter observed for (a) PS-PB20, (b) PS-PEP28 and (c) PS-PEP35 diblock copolymer aggregates dispersed directly in *n*-dodecane at 25ºC, followed by heating up to 90ºC (blue points) and cooling to 25ºC (red points). In each case this thermal cycle breaks up the initial large, ill-defined non-equilibrium aggregates and produces small, well-defined equilibrium micelles.

The three copolymers examined in this study form well-defined 'star-like' micelles[21] with relatively constant core diameters of 24 to 27 nm, as judged by TEM, see Table 4.1. After appropriate thermal treatment, DLS studies indicate overall micelle diameters of 85-89 nm. It is emphasised here that TEM reports only the core diameter for the dehydrated micelles, while SAXS and DLS report the overall hydrodynamic diameter of the solvated micelles (i.e. the micelle core plus the micelle corona). SAXS also provides additional structural information, which will be discussed later on in this Chapter. To gain further insight into the mechanism of break-up of the ill-defined non-equilibrium aggregates and subsequent formation of well-defined equilibrium micelles, variable temperature ^{1}H NMR studies were conducted in d_{26}-dodecane. Figure 4.4 shows the partial ^{1}H NMR spectra recorded for PS-PB20 and PS-PEP35 copolymer dispersions in d_{26}-dodecane on heating up to 110^{o}C followed by cooling to 25^{o}C. Initially, no ^{1}H NMR signals were observed between 25^{o}C and 65^{o}C. In contrast, broad aromatic signals characteristic of the core-forming PS block are observed in the 75^{o}C to 110^{o}C temperature range, which subsequently disappeared on cooling back to 25^{o}C. Similar observations were reported for the PS-PEP28 copolymer in Chapter 2.

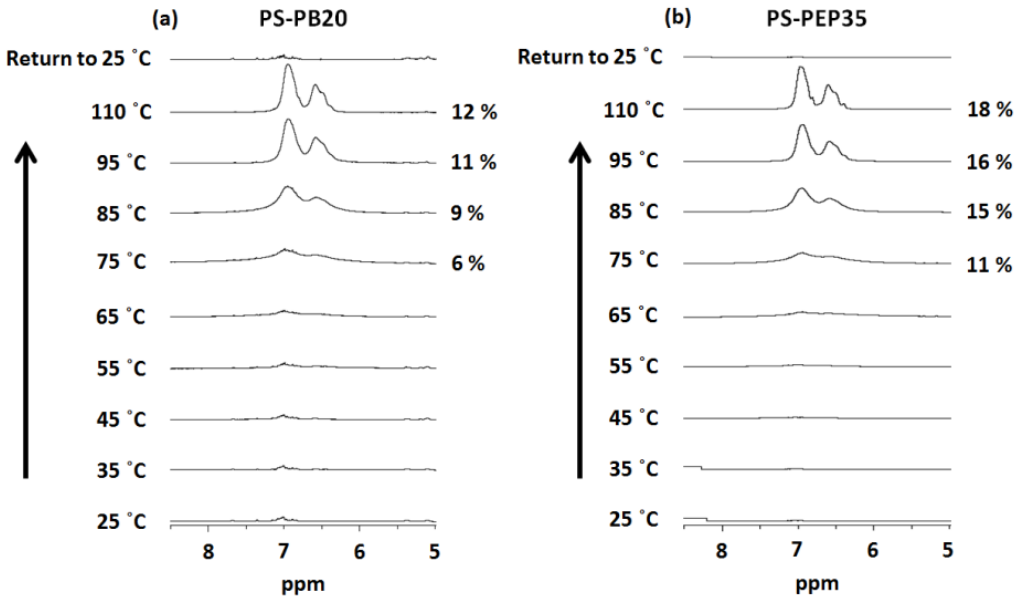

Figure 4.4. Partial ^{1}H NMR spectra recorded for (a) PS-PB20 and (b) PS-PEP35 in d_{26}-dodecane on heating from 25^{o}C to 110^{o}C, followed by cooling to 25^{o}C. The appearance of aromatic signals at 6.5-7.0 ppm is attributed to increasing solvation of the polystyrene chains within the micelle cores at higher temperatures. Apparent polystyrene contents (mol %) are indicated on the right-hand side of each spectrum. The equivalent variable temperature NMR study for PS-PEP28 in d_{26}-dodecane (and d_{16}-heptane) under the same conditions is shown in Chapter 2.

These spectroscopic observations suggest gradual solvent ingress within the micelle cores.[74] Such plasticisation leads to a much lower effective T_g for the core-forming PS chains, which become increasingly mobile at elevated temperature. It is noteworthy that if the apparent polystyrene contents in d_{26}-dodecane are compared to the actual polystyrene contents determined in $CDCl_3$ (which is a good solvent for both blocks), then the degree of solvation of the polystyrene block is never more than approximately 50-60%, see Figure 4.4 and Figure 4.1. Such ^{1}H NMR spectra are therefore consistent with solvent-swollen micelle cores, rather than molecularly dissolved copolymer chains.

SAXS studies of copolymer micelles

The star-like micelle model used to fit the three SAXS patterns shown in Figure 4.5 was the same as that used to model the SAXS data in Chapter 2, and is also detailed here for continuity (see Experimental section). This model produced good fits to the SAXS patterns obtained for the PS-PB20, PS-PEP28 and PS-PEP35 diblock copolymer micelles formed in *n*-dodecane after thermal cycling (see Figure 4.5 and Table 4.2). Detailed SAXS analysis indicated a relatively low volume fraction of the *n*-dodecane solvent within the micelle cores (x_{sol} ~ 0.10). Similar values have been reported by Pedersen *et al*. for a related diblock copolymer system.[75] This relatively low solvent volume fraction is consistent with the fact that *n*-dodecane is a non-solvent for polystyrene at 20^{o}C. Moreover, the star-like micelle model also revealed a mean radius for the PS core (R_s) of 9.3 nm (PS-PB20), 8.9 nm (PS-PEP28), and 9.1 nm (PS-PEP35). The PB (or PEP) corona thicknesses (s) were found to be 26.4 nm (PS-PB20), 25.1 nm (PS-PEP28), and 23.2 nm (PS-PEP35). These data give overall particle diameters of 71 nm (PS-PB20), 68 nm (PS-PEP28), and 65 nm (PS-PEP35) respectively, see Table 4.3. These are within the same size range as those observed via DLS measurements. The largest micelle diameter is observed for PS-PB20, which is not unexpected given that this copolymer also has the highest molecular weight (183 K versus 117 K for PS-PEP28 and 163 K for PS-PEP35, see Table 4.1).

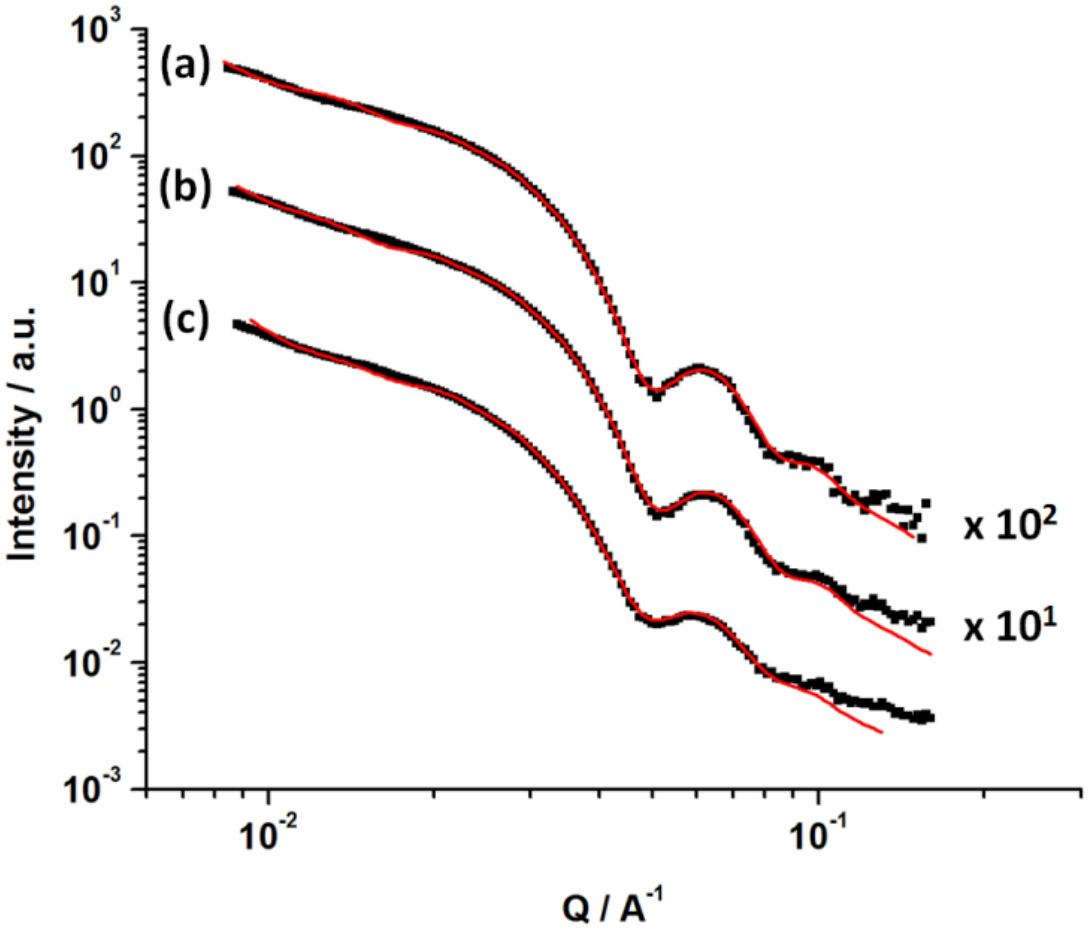

Figure 4.5. SAXS patterns obtained for 1.0 % w/w diblock copolymer micelles in *n*-dodecane at 20°C for (a) PS-PEP35, (b) PS-PEP28 and (c) PS-PB20. In each case well-defined micelles were only obtained after thermal annealing for 1 h at 110°C (see Figure 4.2). The patterns shown in (a) and (b) are multiplied by an appropriate arbitrary coefficient for the sake of clarity. The red lines represent fits to the SAXS data obtained using a star-like micelle model.[68]

Sample ID	(a) Mol fraction (b) Molecular weight /kg mol^{-1}		Number of repeat units		Density /g cm^{-3}		Volume /nm^3		R_s (σ_{Rs}) /nm	s /nm	Overall micelle diameter /nm
PS-PB20	**PS**	**PB**	**PS**	**PB**	**PS**	**PB**	**PS**	**PB**	9.3 (±1.8)	26.4	71
	(a) 0.20	0.80	558	2232	1.05	0.91	91	227			
	(b) 58	125									
PS-PEP28	**PS**	**PEP**	**PS**	**PEP**	**PS**	**PEP**	**PS**	**PEP**	8.9 (±1.3)	25.1	68
	(a) 0.28	0.72	412	1059	1.05	0.90	67	136			
	(b) 43	74									
PS-PEP35	(a) 0.35	0.65	697	1294	1.05	0.90	114	166	9.1 (±1.5)	23.2	65
	(b) 72	91									

Table 4.2. Summary of mol fraction, molecular weight, number of repeat units, density and volume of each block for the three types of star-like micelles, plus the following structural parameters obtained from data fits to SAXS patterns: micelle core radius (R_s, nm), standard deviation of the micelle core radius (σ_{Rs}, nm), width of the micelle corona electron density profile (s, nm) and the overall micelle diameter ($2R_s + 2s$, nm).

Carbon black characterisation

In principle, understanding the adsorption of each commercial diblock copolymer onto carbon black should provide useful physical insights regarding their efficacy as putative diesel soot dispersants in engine oils. In this regard, carbon black acts as a convenient model colloidal substrate for genuine diesel soot, since the latter is prohibitively expensive.[37] The physical properties of the Regal 250R carbon black used in this Chapter are detailed in Chapter 2: it has a distinctive fractal morphology, which is typical of most carbon blacks and also diesel engine soot.[36, 37, 76, 77] BET surface area analysis indicated a specific surface area of 43 m^2 g^{-1}, while helium pycnometry gave a solid-state density of 1.89 g cm^{-3}. Combining these values, the primary grain size for individual carbon black particles is calculated to be approximately 74 nm. This is in fairly good agreement with the number-average diameter of 70 nm estimated from TEM studies, with the BET value being considered to be more statistically robust.

Copolymer adsorption on carbon black

Figure 4.6 (a) shows the isotherms obtained for each diblock copolymer adsorbed as well-defined micelles onto carbon black from *n*-dodecane at 20ºC. PS-PB20 exhibited the highest affinity isotherm with a maximum adsorbed amount, Γ, of 3.31 ± 0.16 mg m^{-2}, whereas PS-PEP28 and PS-PEP35 had Γ values of 2.25 ± 0.07 mg m^{-2} and 1.57 ± 0.06 mg m^{-2}, respectively (as determined from the gradients of the corresponding linear plots, see Figure 4.6 (b)). Thus increasing the polystyrene content of the copolymer leads to progressively weaker adsorption. This finding was not anticipated, because Shar and co-workers[36] had previously reported that the polystyrene component was essential for a strong interaction with the carbon black surface for adsorption from cyclohexane at 20ºC. On this basis, it was predicted that the highest affinity isotherm would be observed for the diblock copolymer with the highest polystyrene content (i.e. PS-PEP35). However, both the copolymer molecular weight and chemical nature of the stabiliser block (PB or PEP) differ for all three copolymers (see Table 4.1), so it is perhaps difficult to examine the effect of varying the polystyrene content under such circumstances. Presumably, subtle differences in the structure of these copolymers (and perhaps also the star-like character of the micelles) influence their adsorption behaviour.

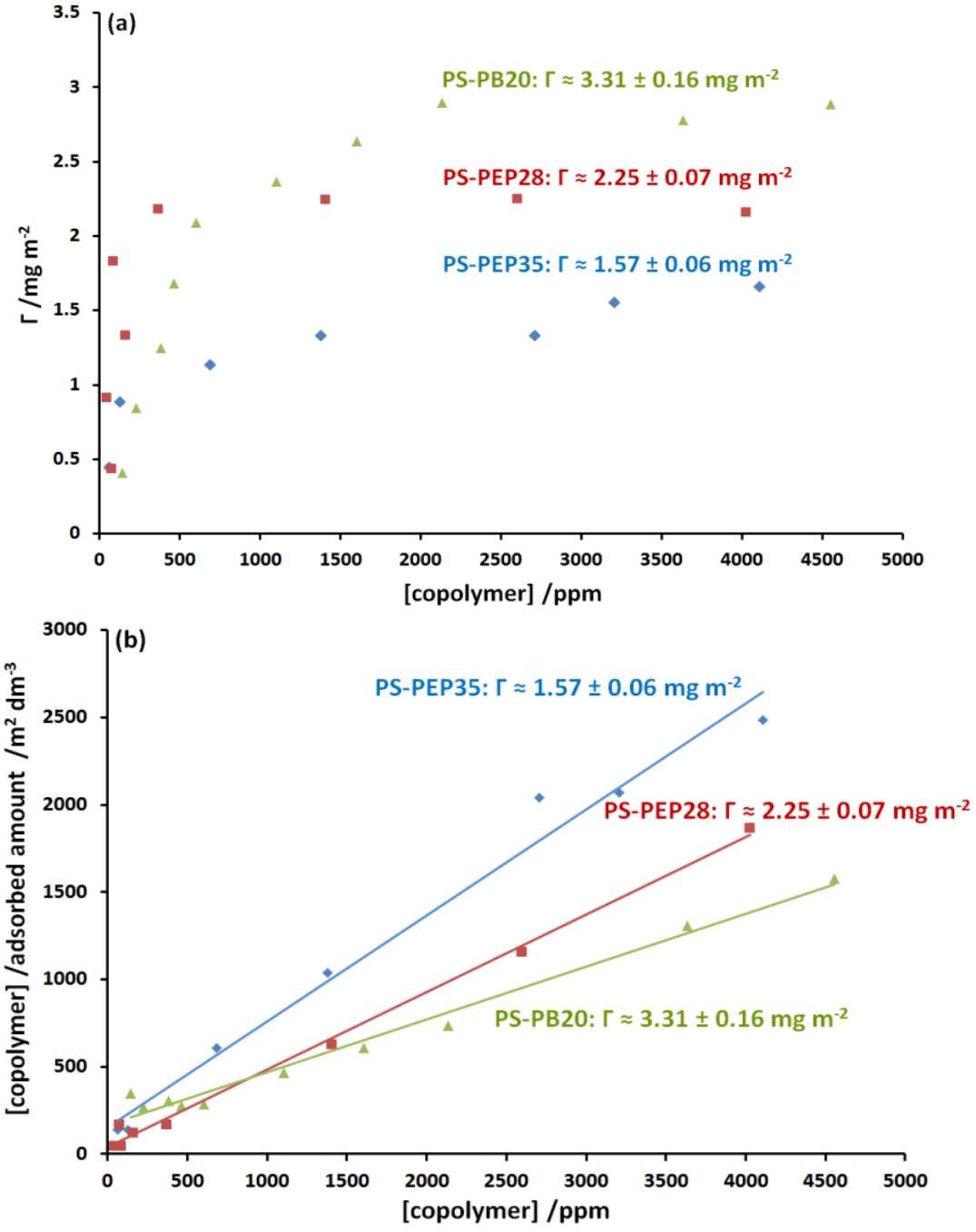

Figure 4.6. (a) Langmuir-like and (b) linear adsorption isotherms obtained for the three polystyrene-based diblock copolymers (PS-PB20, PS-PEP28 and PS-PEP35) adsorbed in the form of well-defined micelles (obtained after heating to 110°C for 1 h) onto carbon black particles from *n*-dodecane at 20°C, as determined using a supernatant depletion assay based on UV spectroscopy.

The resulting sterically-stabilised carbon black dispersions were studied by TEM. Figure 4.7 shows representative images obtained for (a) the pristine carbon black and (b-d) dispersions stabilised using each copolymer in turn (at 10 % copolymer by mass based on carbon black). Significantly smaller, more discrete carbon black particles are observed in the presence of each copolymer than for carbon black alone. Moreover, excess non-adsorbed micelles are observed for the dispersion prepared using PS-PEP35 (see inset in Figure 4.7d). Inspecting the adsorption isotherms constructed for the three diblock copolymers in Figure 4.6, this copolymer exhibited the lowest equilibrium adsorbed amount (Γ = 1.57 ± 0.06 mg m^{-2}) and hence has a lower concentration threshold for the presence of excess micelles in solution. In contrast, PS-PEP28 and PS-PB20 each exhibit a stronger adsorption affinity for carbon black, which means that excess micelles are not present in solution under the same conditions.

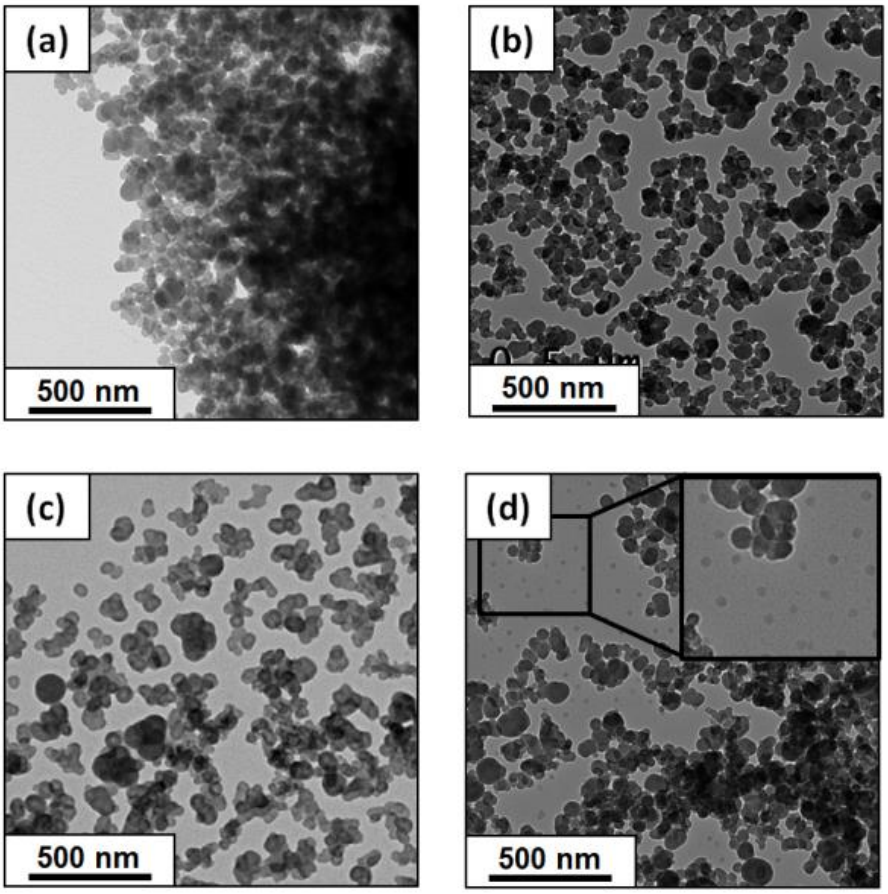

Figure 4.7. Representative TEM images for Regal 250R carbon black particles in *n*-dodecane: (a) no copolymer; (b) PS-PB20, (c) PS-PEP28 and (d) PS-PEP35. For (b) to (d) 10 % w/w copolymer based on carbon black was used in each case. TEM grids were prepared by allowing each copolymer dispersion to dry at 20^{o}C.

Effective densities of sterically-stabilised carbon black particles

In order to assess the degree of dispersion of sterically-stabilised carbon black particles, analytical centrifugation has been used in combination with optical microscopy studies. The latter technique is useful for assessing the presence of micron-sized agglomerates, but is not sensitive to submicron-sized colloidal aggregates. In principle, analytical centrifugation should be capable of reporting high resolution particle size distributions in the colloidal size range. However, the effective particle density must be known accurately for this technique, since it is an important input parameter. One important question here is whether the same effective particle density can be used regardless of the copolymer type. Alternatively, do the subtle differences in dimensions and adsorption behaviour observed for the three types of copolymer micelles examined herein necessitate effective particle densities to be determined for each case? Since sedimentation is proportional to the particle mass, and inversely proportional to the frictional force acting on the particle (which is a function of the particle morphology and size), the correct interpretation of sedimentation data requires knowledge of the density of the sedimenting particle, which may be a complex function for core-shell particles with solvated shells. Furthermore, for core-shell particles comprising differing densities for the core and shell components, it is known that an inherent density distribution is superimposed on particle size distributions determined by analytical centrifugation techniques. In the case where the shell density exceeds the core density, this leads to artifactual *narrowing* of the particle size distribution.[56] On the other hand, if the shell density is less than that of the core, which is the case in the present study, artifactual *broadening* of the particle size distribution is expected. In principle, this problem can be addressed by recalculating the true particle density for each data point of the digitised particle size distribution. For example, Fielding *et al*. reported a corrected particle size distribution obtained by disk centrifuge analysis of well-defined core-shell polystyrene/silica nanocomposite particles.[56] However, given the relatively ill-defined, highly fractal nature of the carbon black particles, such a correction has not been applied to the work in this Chapter.

For perfectly monodisperse spherical particles with a well-defined core-shell morphology, Lascelles and Armes derived a simple geometric relationship for the shell thickness, *d*, in terms of the core radius *R*, and the mass fractions, m_1 and m_2, and densities, ρ_1 and ρ_2, of the core and shell components, see equation 5.[62]

$$d = R\left[\left(\frac{m_2\rho_1}{m_1\rho_2} + 1\right)^{1/3} - 1\right] \quad (5)$$

Considering the relative volumes (v_1 and v_2) and mass fractions (m_1 and m_2) of a two-component composite material (in this case core-shell particles) enables calculation of a composite particle density, ρ_{comp}, using equation 6.

$$\rho_{\text{comp}} = \frac{m_1+m_2}{V_1+V_2} = \frac{m_1+m_2}{\frac{m_1}{\rho_1}+\frac{m_2}{\rho_2}} \quad (6)$$

In the context of the present study, the subscripts '1' and '2' refer to the carbon black core and copolymer micelle shell, respectively. If it is assumed that (i) the density of the copolymer shell is equal to that of the solvent (*n*-dodecane) and (ii) *d* corresponds to the mean *radius* of the star-like micelles calculated from SAXS analysis (see Table 4.3), then a theoretical effective particle density can be calculated for sterically-stabilised carbon black particles. However, we emphasise that this approach is only an approximation since it assumes a monodisperse spherical morphology for carbon black, which is clearly not the case (see Figure 4.7). Moreover, it is additionally assumed that the star-like diblock copolymer micelles form a hemi-micelle at the surface of the carbon black particles whose mean thickness is equal to that of the original micelle radius and that the density of this copolymer stabiliser shell approximates to that of the pure solvent (which is 0.75 g cm^{-3} for *n*-dodecane at 20°C). This situation is depicted schematically in Figure 4.8.

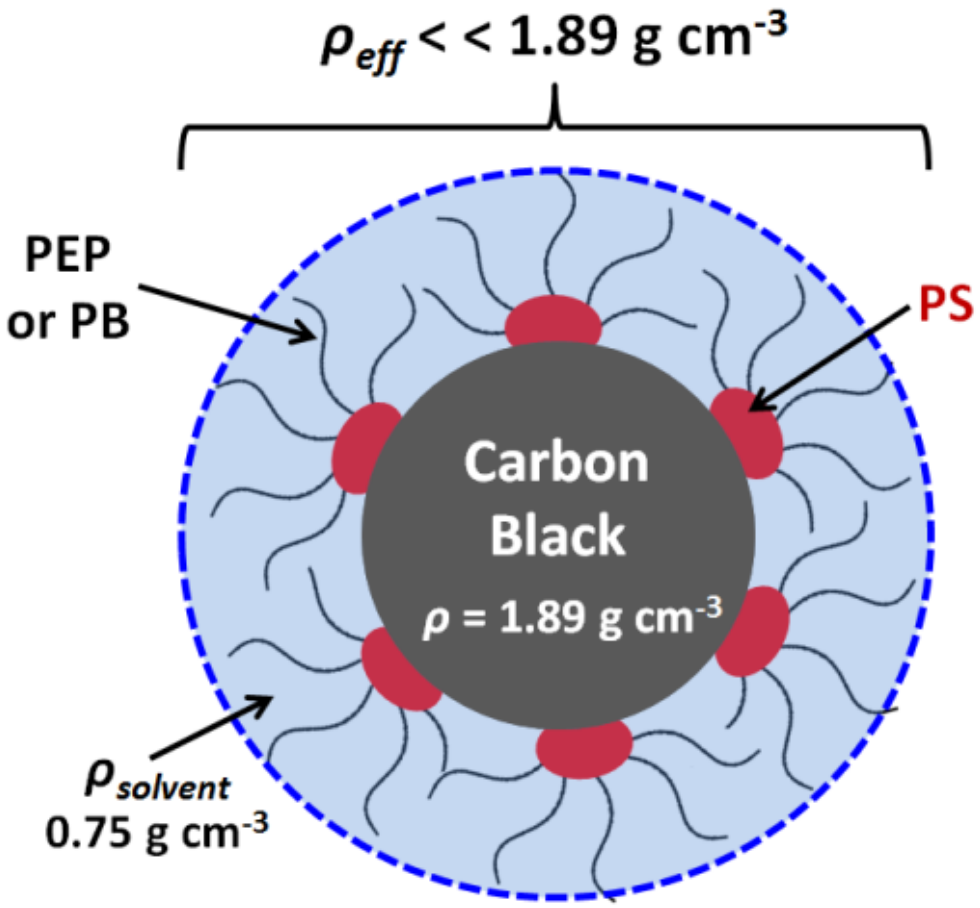

Figure 4.8. Schematic representation of the sterically-stabilised carbon black particles for which the effective particle density, ρ_{eff}, is calculated using simple geometric considerations based on the micelle dimensions as determined by SAXS (see Tables 1 and 2). In reality, the carbon particles exhibit a fractal morphology, rather than the spherical core-shell morphology shown here.

Using equations 5 and 6 in combination with the SAXS micelle dimensions and carbon black primary grain size derived from BET surface area analysis, effective particle densities of 0.90, 0.91 and 0.92 g cm^{-3} were calculated for sterically-stabilised carbon black particles prepared using PS-PB20, PS-PEP28 and PS-PEP35 copolymer micelles, respectively (see Table 4.3). Clearly, these theoretical values are substantially lower than the solid-state density of carbon black indicated by helium pycnometry (1.89 g cm^{-3}). This indicates that the mass fraction of the low-density stabiliser shell (which can be approximated as comprising pure solvent) is significantly larger (~ 70 %) than that of the high-density carbon black cores (see Table 4.3).

Copolymer ID	Steric stabiliser layer thickness, *d* nm	Adsorbed amount on carbon black mg m^{-2}	Mass fraction of carbon black core	Effective particle density, ρ_{eff} g cm^{-3}	Density difference $\Delta\rho$[a] g cm^{-3}	Volume-average particle diameter nm
PS-PB20	35.5	3.31	0.28	0.90	0.15	140 ± 10 163 ± 7 b
PS-PEP28	34.0	2.25	0.29	0.91	0.16	118 ± 15
PS-PEP35	32.5	1.57	0.31	0.92	0.17	117 ± 10

Table 4.3. Summary of steric stabiliser layer thicknesses, equilibrium adsorbed amounts of diblock copolymer micelles on carbon black, calculated mass fraction of the carbon black core, theoretical effective particle densities, density differences ($\Delta\rho$) and volume-average particle diameters determined via analytical centrifugation for 1.0 % w/w carbon black dispersions at 20^{o}C (using 6.0% w/w copolymer based on carbon black). These tabulated data were calculated assuming (i) a perfectly monodisperse spherical core-shell morphology, (ii) a primary grain size of 74 nm diameter for the carbon black particles and (iii) that the density of the steric stabiliser layer is equal to that of the pure solvent.

a**.** $\Delta\rho$ = effective particle density - density of *n*-dodecane.
b, Bimodal size distribution as judged by analytical centrifugation (see Figure 4.10).

Stokes' law can be used to calculate particle velocities for such sterically-stabilised carbon black particles in pairs of similar solvents, such as *n*-dodecane and *n*-decane or *n*-dodecane and deuterated *n*-dodecane. In principle, such particle velocities can be used to calculate the effective particle density. However, in practice this approach is not valid if the shell component dominates over the core component, since the density of the solvent shell necessarily varies with the nature of the solvent, which in turn leads to significantly different effective particle densities. In view of this technical problem, approximate effective particle densities were calculated purely based on geometric considerations.

Particle size analysis via analytical centrifugation using the LUMiSizer instrument utilises equation 7 below.

$$x^2 = \frac{18\eta_F}{(\rho_P - \rho_F)\omega^2 t} \ln\left(\frac{r_m}{r_0}\right) \quad (7)$$

Here x is the particle diameter, η_F is the viscosity of the spin fluid, ρ_P is the density of the sedimenting particles, ρ_F is the density of the spin fluid (in this case *n*-dodecane), ω is the angular velocity, t is the sedimentation time, r_m is an arbitrary (fixed) position of measurement of the light transmission and r_0 is the position of the solvent meniscus.

The form of equation 7 (more specifically, the density difference term, ρ_P - ρ_F) indicates that huge errors (~300 %) are incurred if the solid-state density of carbon black is erroneously used as an input parameter for determining volume-average particle size distributions via analytical centrifugation. This important point is emphasised in Figure 4.10, which shows the apparent and actual volume-average particle size distributions determined for the three types of sterically-stabilised carbon black particles using (a) the density of carbon black alone and (b) the effective particle densities calculated using equations 5 and 6. In the former case, the particle size distributions are clearly too low, since the volume-average diameter is less than the primary grain size of the carbon black particles (74 nm as judged by BET surface area analysis and confirmed by TEM studies). In contrast, physically reasonable volume-average diameters (117 - 140 nm) are obtained when using effective particle densities that account for the relatively high degree of solvation for such particles.

The effect of varying the solvated stabiliser layer thickness (*d*) on the density difference ($\Delta\rho$) between the particles and the solvent for sterically-stabilised carbon black particles dispersed in *n*-dodecane at 20^{o}C is plotted in Figure 4.9. This relationship was calculated using equations 5 and 6 by assuming (i) a perfectly monodisperse spherical core-shell morphology, (ii) a primary grain size of 74 nm diameter for the carbon black particles and (iii) that the density of the steric stabiliser layer is equal to that of the pure solvent. Although changes in $\Delta\rho$ are particularly large for relatively thin stabiliser layers (< 10 nm), it is noteworthy that the density difference ($\mathbf{\Delta}\rho$) remains quite sensitive to the solvated steric stabiliser layer thickness within the range of interest (32.5 – 35.5 nm, see

Table 4.3). This emphasises the importance of calculating accurate effective particle densities for such sterically-stabilised carbon black dispersions.

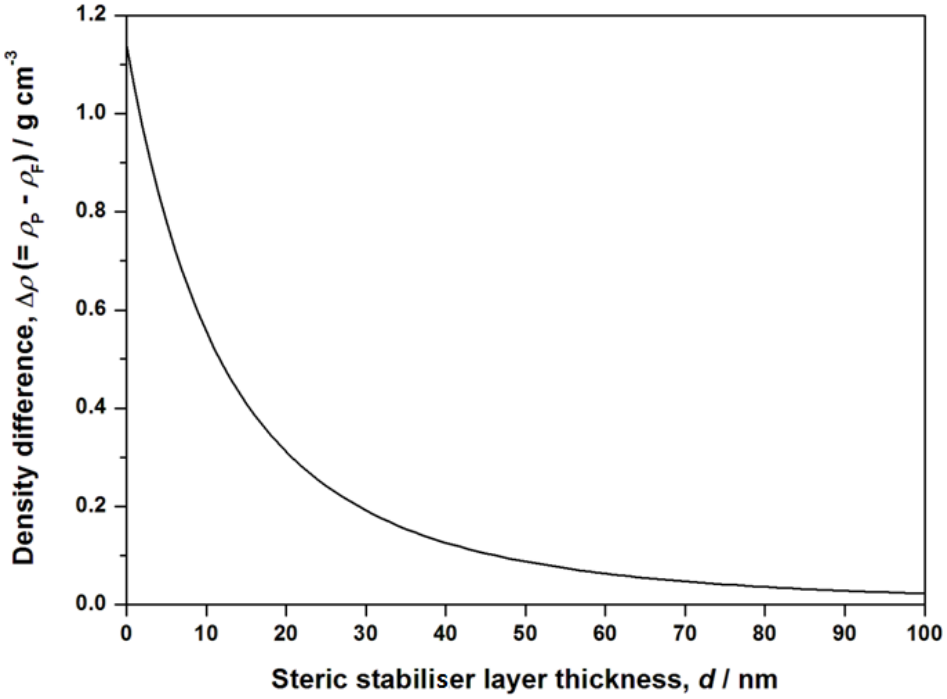

Figure 4.9. Effect of varying the steric stabiliser layer thickness (d) on the density difference ($\Delta\rho$) between the effective particle density (ρ_P) and the solvent density (ρ_F) for sterically-stabilised carbon black particles dispersed in *n*-dodecane at 20°C. This relationship was calculated using equations 5 and 6 by assuming (i) a perfectly monodisperse spherical core-shell morphology, (ii) a primary grain size of 74 nm diameter for the carbon black particles and (iii) that the density of the steric stabiliser layer is equal to that of the pure solvent.

Effect of diblock copolymer composition on carbon black dispersion stability

It is perhaps worth emphasising that, despite the comparable dimensions of the copolymer micelles in solution (see Table 4.1), their differing adsorption behaviour (see Figure 4.6) leads to subtle differences in the effective particle density for the corresponding sterically-stabilised carbon black particles (see Table 4.3). However, the volume-average particle size distributions obtained for these dispersions are broadly comparable (see Figure 4.10). This indicates that each diblock copolymer leads to a similar degree of dispersion for carbon black in *n*-dodecane at 20°C. Hence all three copolymers are expected to be useful dispersants for diesel engine soot in engine oils.

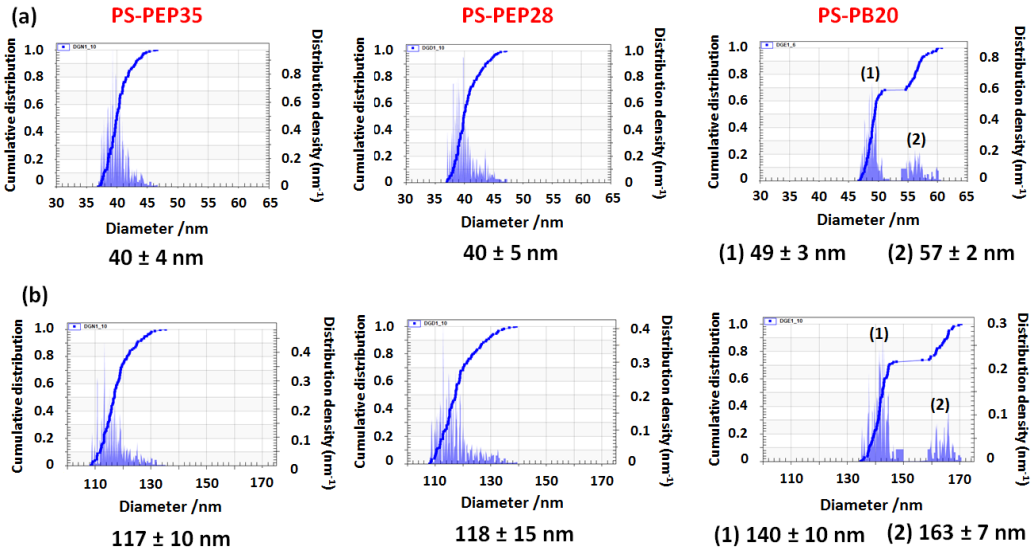

Figure 4.10. Particle size distributions obtained via analytical centrifugation analysis of 1.0 % w/w carbon black particles dispersed in *n*-dodecane at 20°C with the aid of the three diblock copolymers used in this work (PS-PB20, PS-PEP28 and PS-PEP35). Volume-average diameters are calculated (a) using the solid-state density of carbon black (which leads to large experimental errors), (b) using theoretical effective particle densities (see Table 4.3). In each case, 6.0 % w/w copolymer was utilised based on the mass of carbon black. Instrument conditions: 3000 rpm for 166 min.

Effect of temperature on carbon black dispersion stability

It is important to consider the effect of temperature on carbon black dispersion stability, since commercial diesel engines operate anywhere between -10 (cold start) and 110°C. Figure 4.11 contains optical micrographs for carbon black stabilised by each diblock copolymer at both 20°C and 80°C. A *decrease* in mass fractal size is observed on *decreasing* diblock copolymer polystyrene content at 80°C. This is somewhat unexpected, since a higher polystyrene content would be expected to lead to stronger adsorption hence more effective particle stabilisation. However, since PS-PB20 has the highest equilibrium adsorbed amount (Γ, of 3.31 ± 0.16 mg m^{-2}, see Figure 4.6), such a result is not unreasonable.

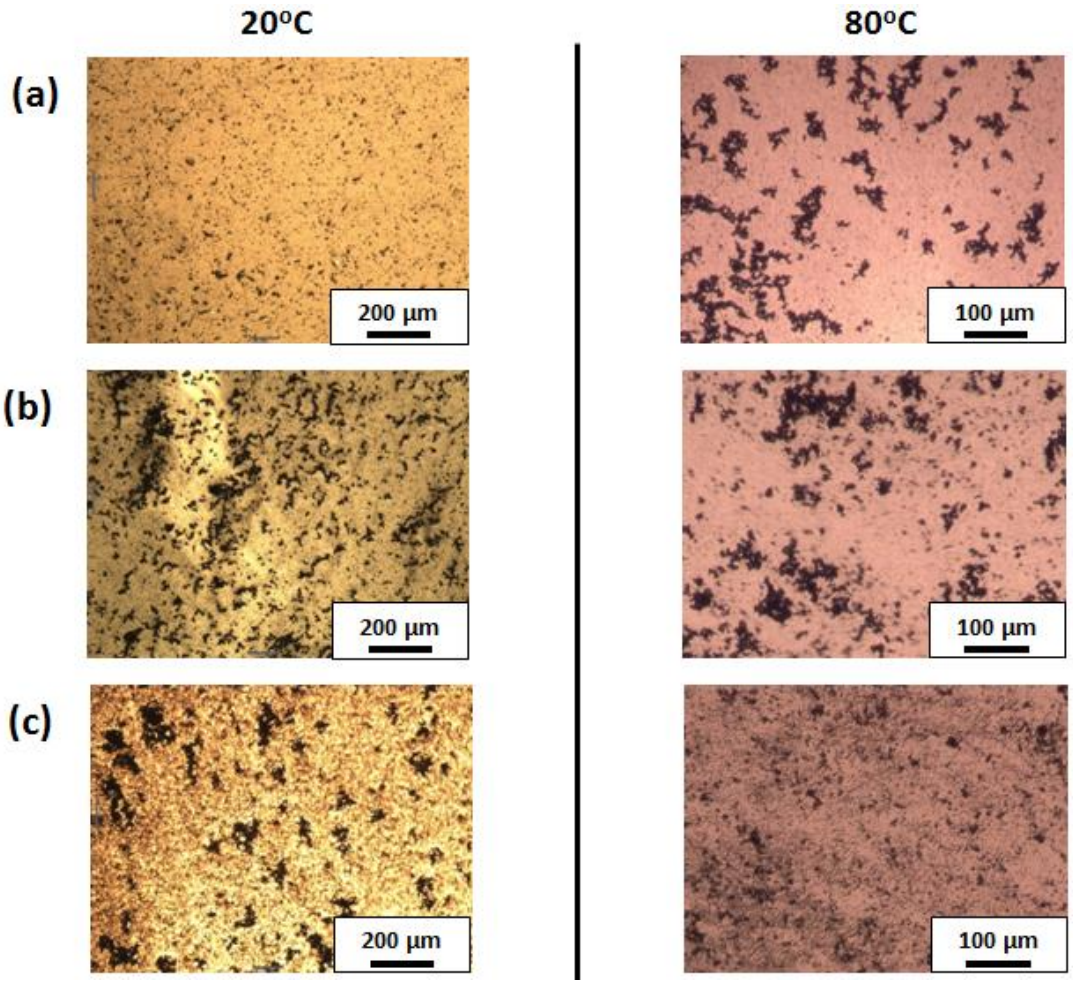

Figure 4.11. Optical microscopy images of carbon black with (a) PS-PEP35, (b) PS-PEP28 and (c) PS-PB20 diblock copolymers adsorbed at 10 % w/w (based on carbon black) in *n*-dodecane. Dispersions assessed at 20°C and 80°C.

Figure 4.12 illustrates the sub-micron scale dispersion stabilities from analytical centrifugation at 4°C, 20°C and 60°C (via sedimentation profiles). Here, each diblock copolymer is at the concentration required for monolayer coverage (~10 % w/w based on carbon black). At 4°C, very little sedimentation occurs, which indicates a relatively stable dispersion. On increasing the temperature to 20°C and then 60°C, carbon black dispersions appear to become less stable, with an increase in the particle sedimentation distance in a given time. Generally, there appears to be relatively little difference in sedimentation distance *between* the three diblock copolymers at a given temperature. It is important to mention that particle size distributions could not be constructed at 4°C

and 60ºC, since the effect of temperature on effective particle density has not been assessed. Since the continuous phase *n*-dodecane forms an integral part of the overall composite structure (see Figure 4.8), and solvent density and viscosity changes with temperature (as does copolymer solvency), particle density will be affected. However, such a study was beyond the scope of the current work. Furthermore, since composite density changes with temperature, the data in Figure 4.12 comes with an important caveat; a change in sedimentation distance may be in part due to a change in composite density.

As mentioned in Chapter 3, The effect of a change in temperature on carbon black dispersion stability has been investigated by Won *et al*.[78] The temperature-dependent intrinsic viscosity of a polyisobutylene succinimide dispersant was studied, and it was suggested that an increase in temperature causes conformational changes in the solvophilic hydrocarbon stabiliser chain of the adsorbed dispersant. This induces collapse, in turn decreasing its efficiency in inhibiting agglomeration. In the same study, the effect of temperature on the rheological properties of carbon black without added dispersant showed virtually no temperature dependence. It was concluded to be unlikely that heating induces a significant increase in the van der Waals interaction between the carbon-black particles.[78]

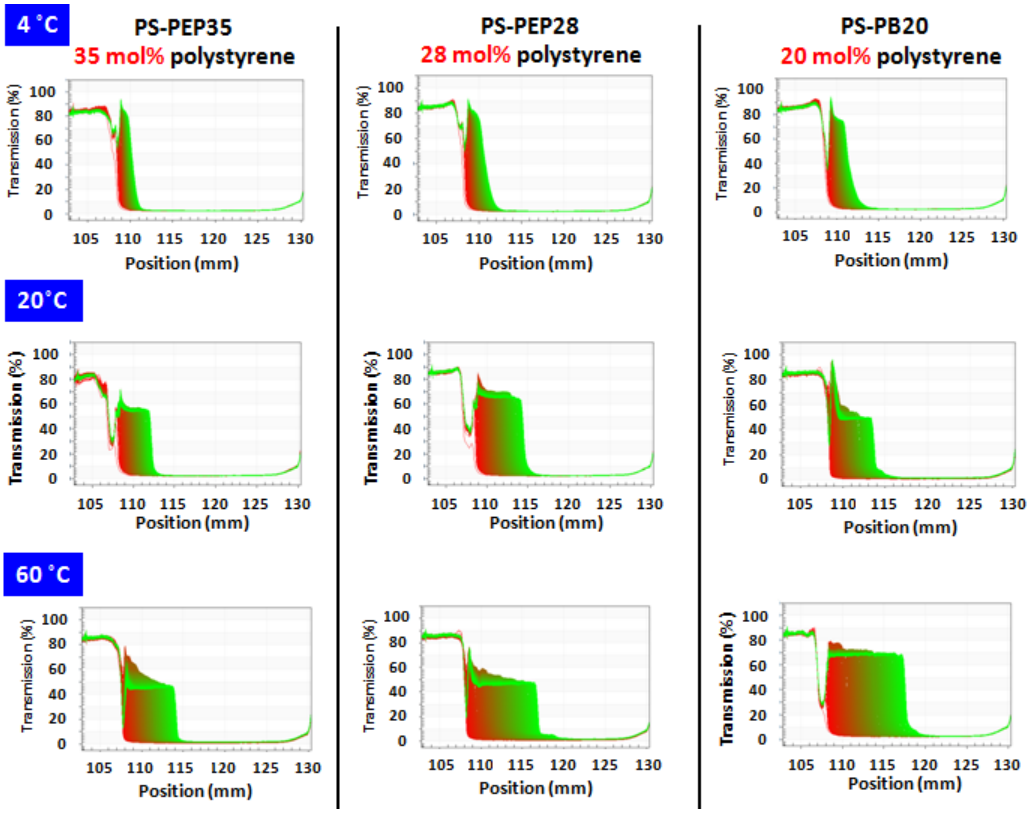

Figure 4.12. Raw profile plots obtained via analytical centrifugation for carbon black dispersed using three diblock copolymers with different polystyrene contents. 10 % w/w copolymer (based on carbon black) in 10 % w/w total solids (based on solvent) in each case, at 4ºC, 20ºC and 60ºC in *n*-dodecane. Instrument run at 3000 rpm for 166 min. Colour indicates time, where red is the first transmission profile and green is the last.

Conclusions

Three near-monodisperse polystyrene-based diblock copolymers each form large, ill-defined polydisperse colloidal aggregates when dissolved directly in *n*-dodecane at 20ºC. However, a single heating cycle (110ºC, 1 h) breaks up such aggregates, leading to the formation of well-defined spherical micelles on cooling to 20ºC. Variable temperature ^{1}H NMR studies conducted in d_{26}-dodecane are consistent with these observations, since partial solvation of the core-forming polystyrene chains is observed above 65ºC. Dynamic light scattering studies also confirmed a gradual reduction in intensity-average diameter at higher temperature for all three diblock copolymers, followed by the formation of small near-monodisperse micelles on cooling to 20ºC. Adsorption of such micelles onto carbon black particles, which serve as a convenient mimic for diesel soot, was quantified using a supernatant depletion assay based on UV

spectroscopy. Maximum adsorbed amounts, Γ, corresponding to micelle monolayer formation, were determined to be 3.31, 2.25 and 1.57 mg m^{-2} for PS-PB20, PS-PEP28 and PS-PEP35. Thus *increasing* the mole fraction of the polystyrene anchor block actually leads to *weaker* micelle adsorption at the surface of the carbon black particles.

Assuming a spherical core-shell morphology, effective particle densities were calculated for the three types of sterically-stabilised carbon black particles using (i) the micelle dimensions derived from SAXS and (ii) the primary grain size of the carbon black determined by BET surface area analysis. This approach yielded effective particle densities of 0.90, 0.91 and 0.92 g cm^{-3} for the sterically-stabilised carbon black particles prepared using the PS-PB20, PS-PEP28 and PS-PEP35 diblock copolymers, respectively. Thus, although these three copolymers form micelles in *n*-dodecane with rather similar dimensions, each copolymer actually leads to a subtly different effective particle density, which is always substantially lower than the solid-state density of carbon black (1.89 g cm^{-3}). Since the rate of sedimentation of the sterically-stabilised carbon black particles depends on the density *difference* between the effective particle density and the *n*-dodecane solvent (density = 0.75 g cm^{-3}), *substantial errors can be incurred in analytical centrifugation studies unless appropriate care is taken to determine an accurate effective particle density*. This is important because analytical centrifugation is a highly convenient technique for assessing the relative degree of dispersion of sterically-stabilised carbon black particles by comparing their volume-average particle size distributions. Temperature has an effect on carbon black dispersion stability; a decrease in stability is observed on increasing temperature for PS-PEP35 and PS-PEP28 at the micron length-scale, while the opposite is observed for PS-PB20. It is assumed the main reason for this is the difference in adsorbed amount for each diblock copolymer. Meanwhile, analytical centrifugation suggests a general decrease in dispersion stability, although these data must be treated with caution due to assumed changes in copolymer-adsorbed particle density with temperature. Overall, the work in this Chapter enhanced understanding of the performance of three commercial diblock copolymers when employed as diesel soot dispersants in engine oil formulations. Given the wide range of applications for sterically-stabilised carbon black dispersions, the results are also likely to have broader implications.

References

1. Newman, S. Note on colloidal dispersions from block copolymers. *J. Appl. Polym. Sci.* **1962,** *6,* S15-S16.
2. Krause, S. Dilute solution properties of a styrene - methyl methacrylate block copolymer. *J. Phys. Chem.* **1964,** *68,* 1948-1955.
3. Tuzar, Z.; Kratochvíl, P. Block and graft copolymer micelles in solution. *Adv. Colloids Interface Sci.* **1976,** *6,* 201-232.
4. Gao, Z.; Eisenberg, A. A model of micellization for block copolymers in solutions. *Macromolecules* **1993,** *26,* 7353-7360.
5. Noolandi, J.; Hong, K. M. Theory of block copolymer micelles in solution. *Macromolecules* **1983,** *16,* 1443-1448.
6. Förster, S.; Antonietti, M. Amphiphilic block copolymers in structure-controlled nanomaterial hybrids. *Adv. Mater.* **1998,** *10,* 195-217.
7. Zhang, L.; Eisenberg, A. Multiple Morphologies of "Crew-Cut" Aggregates of Polystyrene-b-poly(acrylic acid) Block Copolymers. *Science* **1995,** *268,* 1728-1731.
8. Zhang, L.; Eisenberg, A. Multiple Morphologies and Characteristics of "Crew-Cut" Micelle-like Aggregates of Polystyrene-b-poly(acrylic acid) Diblock Copolymers in Aqueous Solutions. *Journal of the American Chemical Society* **1996,** *118,* 3168-3181.
9. Gao, Z.; Varshney, S. K.; Wong, S.; Eisenberg, A. Block Copolymer "Crew-Cut" Micelles in Water. *Macromolecules* **1994,** *27,* 7923-7927.
10. Yu, K.; Eisenberg, A. Bilayer Morphologies of Self-Assembled Crew-Cut Aggregates of Amphiphilic PS-b-PEO Diblock Copolymers in Solution. *Macromolecules* **1998,** *31,* 3509-3518.
11. Burnett, G.; Meares, P.; Paton, C. Styrene+ methyl methacrylate block copolymers. Part 2.—Behaviour in dilute solutions. *Transactions of the Faraday Society* **1962,** *58,* 737-746.
12. Fielding, L. A.; Lane, J. A.; Derry, M. J.; Mykhaylyk, O. O.; Armes, S. P. Thermo-responsive diblock copolymer worm gels in non-polar solvents. *Journal of the American Chemical Society* **2014,** *136,* 5790-5798.
13. Fielding, L. A.; Derry, M. J.; Ladmiral, V.; Rosselgong, J.; Rodrigues, A. M.; Ratcliffe, L. P.; Sugihara, S.; Armes, S. P. RAFT dispersion polymerization in non-polar solvents: facile production of block copolymer spheres, worms and vesicles in n-alkanes. *Chemical Science* **2013,** *4,* 2081-2087.
14. Dan, M.; Huo, F.; Zhang, X.; Wang, X.; Zhang, W. Dispersion RAFT polymerization of 4-vinylpyridine in toluene mediated with the macro-RAFT agent of polystyrene dithiobenzoate: Effect of the macro-RAFT agent chain length and growth of the block copolymer nano-objects. *Journal of Polymer Science Part A: Polymer Chemistry* **2013,** *51,* 1573-1584.
15. Houillot, L.; Bui, C.; Save, M.; Charleux, B.; Farcet, C.; Moire, C.; Raust, J.-A.; Rodriguez, I. Synthesis of Well-Defined Polyacrylate Particle Dispersions in Organic Medium Using Simultaneous RAFT Polymerization and Self-Assembly of Block Copolymers. A Strong Influence of the Selected Thiocarbonylthio Chain Transfer Agent. *Macromolecules* **2007,** *40,* 6500-6509.
16. Higgins, J. S.; Dawkins, J. V.; Maghami, G. G.; Shakir, S. A. Study of micelle formation by the diblock copolymer polystyrene—b-(ethylene-co-propylene) in dodecane by small-angle neutron scattering. *Polymer* **1986,** *27,* 931-936.

17. Stejskal, J.; Hlavatá, D.; Sikora, A.; Konňák, Č.; Pleštil, J.; Kratochvíl, P. Equilibrium and non-equilibrium copolymer micelles: polystyrene-block-poly (ethylene-co-propylene) in decane and in diisopropylether. *Polymer* **1992,** *33,* 3675-3685.
18. Hlavatá, D.; Stejskal, J.; Pleštil, J.; Koňák, Č.; Kratochvíl, P.; Helmstedt, M.; Mio, H.; Laggner, P. Heat-induced transition of polystyrene- block-poly(ethylene-co-propylene) micelles in decane and in dioxane. *Polymer* **1996,** *37,* 799-805.
19. Bahadur, P.; Sastry, N. V.; Marti, S.; Riess, G. Micellar behaviour of styrene—isoprene block copolymers in selective solvents. *Colloids Surf.* **1985,** *16,* 337-346.
20. Bang, J.; Viswanathan, K.; Lodge, T. P.; Park, M. J.; Char, K. Temperature-dependent micellar structures in poly(styrene-b-isoprene) diblock copolymer solutions near the critical micelle temperature. *J. Chem. Phys.* **2004,** *121,* 11489-11500.
21. McConnell, G. A.; Gast, A. P. Melting of ordered arrays and shape transitions in highly concentrated diblock copolymer solutions. *Macromolecules* **1997,** *30,* 435-444.
22. Choi, S.-H.; Bates, F. S.; Lodge, T. P. Structure of Poly(styrene-b-ethylene-alt-propylene) Diblock Copolymer Micelles in Squalane. *The Journal of Physical Chemistry B* **2009,** *113,* 13840-13848.
23. Hillmyer, M. A.; Lodge, T. P. Synthesis and self-assembly of fluorinated block copolymers. *Journal of Polymer Science Part A: Polymer Chemistry* **2002,** *40,* 1-8.
24. Szwarc, M.; Levy, M.; Milkovich, R. Polymerization initiated by electron transfer to monomer-a new method of formation of block polymers. *Journal of the American Chemical Society* **1956,** *78,* 2656-2657.
25. Szwarc, M. Living Polymers. *Nature* **1956,** *178,* 1168-1169.
26. Mountrichas, G.; Mpiri, M.; Pispas, S. Micelles of star block (PSPI)8 and PSPI diblock copolymers (PS = polystyrene, PI = polyisoprene): structure and kinetics of micellization. *Macromolecules* **2005,** *38,* 940-947.
27. Mandema, W.; Zeldenrust, H.; Emeis, C. A. Association of block copolymers in selective solvents, 1. Measurements on hydrogenated poly(styrene-isoprene) in decane and in trans-decalin. *Die Makromolekulare Chemie* **1979,** *180,* 1521-1538.
28. Schouten, M.; Dorrepaal, J.; Stassen, W. J. M.; Vlak, W. A. H. M.; Mortensen, K. Thermal stability of polystyrene-b-poly(ethylene/propylene) diblock copolymer micelles in paraffinic solvents. *Polymer* **1989,** *30,* 2038-2046.
29. Stacy, C. J.; Kraus, G. Micelle formation by butadiene-styrene block polymers in n-alkanes. *Polym. Eng. Sci.* **1977,** *17,* 627-633.
30. Bang, J.; Jain, S.; Li, Z.; Lodge, T. P.; Pedersen, J. S.; Kesselman, E.; Talmon, Y. Sphere, cylinder, and vesicle nanoaggregates in poly(styrene-b-isoprene) diblock copolymer solutions. *Macromolecules* **2006,** *39,* 1199-1208.
31. D'Oliveira, J. M. R.; Xu, R.; Jensma, T.; Winnik, M. A.; Hruska, Z.; Hurtrez, G.; Riess, G.; Martinho, J. M. G.; Croucher, M. D. Direct adsorption of polystyrene-poly(ethylene oxide) micelles in water onto polystyrene latex particles. *Langmuir* **1993,** *9,* 1092-1097.
32. Kayes, J. B.; Rawlins, D. A. Adsorption characteristics of certain polyoxyethylene-polyoxypropylene block co-polymers on polystyrene latex. *Colloid & Polymer Science* **1979,** *257,* 622-629.
33. Evers, O. A.; Scheutjens, J. M. H. M.; Fleer, G. J. Statistical thermodynamics of block copolymer adsorption. Part 2. Effect of chain composition on the adsorbed amount and layer thickness. *Journal of the Chemical Society, Faraday Transactions* **1990,** *86,* 1333-1340.

34. Awan, M. A.; Dimonie, V. L.; Filippov, L. K.; El-Aasser, M. S. Adsorption kinetics of amphipathic polystyrene-block-polybutadiene onto silicon wafer and polystyrene planar surfaces. *Langmuir* **1997,** *13,* 130-139.
35. Marques, C.; Joanny, J. F.; Leibler, L. Adsorption of block copolymers in selective solvents. *Macromolecules* **1988,** *21,* 1051-1059.
36. Shar, J. A.; Cosgrove, T.; Obey, T. M.; Warne, M. R.; Wedlock, D. J. Adsorption studies of diblock copolymers at the cyclohexane/carbon black interface. *Langmuir* **1999,** *15,* 7688-7694.
37. Clague, A. D. H.; Donnet, J. B.; Wang, T. K.; Peng, J. C. M. A comparison of diesel engine soot with carbon black. *Carbon* **1999,** *37,* 1553-1565.
38. Diatto, P.; Anzani, M.; Tinucci, L.; Tripaldi, G.; Vettor, A. Investigation on soot dispersant properties and wear effects in the boundary lubrication regime. *Tribology Series* **1999,** *36,* 809-819.
39. Gautam, M.; Chitoor, K.; Durbha, M.; Summers, J. C. Effect of diesel soot contaminated oil on engine wear — investigation of novel oil formulations. *Tribology International* **1999,** *32,* 687-699.
40. Green, D. A.; Lewis, R. The effects of soot-contaminated engine oil on wear and friction: A review. *Proceedings of the Institution of Mechanical Engineers, Part D: Journal of Automobile Engineering* **2008,** *222,* 1669-1689.
41. Adams, C. E.; Belmont, J. A.; Johnson, J. E. Ink jet ink formulations containing carbon black products. US Patent 5,571,311, 1996.
42. Ma, S.-H.; Matrick, H.; Shor, A. C.; Spinelli, H. J. Aqueous pigmented inks for ink jet printers. US Patent 5,085,698, 1992.
43. Carmine, J.; Ryntz, R. The use of naphthenic acid ester as a dispersing agent in aqueous conductive primers. *JCT, Journal of coatings technology* **1994,** *66,* 93-98.
44. Mächtle, W. Characterization of dispersions using combined H_2O/D_2O ultracentrifuge measurements. *Macromolecular Chemistry* **1984,** *185,* 1025-1039.
45. Lechner, M. D.; Mächtle, W. Determination of the particle size distribution of 5–100-nm nanoparticles with the analytical ultracentrifuge: consideration and correction of diffusion effects. In *Analytical Ultracentrifugation V*, Cölfen, H., Ed.; Springer Berlin Heidelberg, 1999; Vol. 113, pp 37-43.
46. Planken, K. L.; Cölfen, H. Analytical ultracentrifugation of colloids. *Nanoscale* **2010,** *2,* 1849-1869.
47. Cölfen, H.; Pauck, T. Determination of particle size distributions with angström resolution. *Colloid Polym Sci* **1997,** *275,* 175-180.
48. Mächtle, W. High-Resolution, Submicron Particle Size Distribution Analysis Using Gravitational-Sweep Sedimentation. *Biophysical Journal* **1999,** *76,* 1080-1091.
49. Detloff, T.; Sobisch, T.; Lerche, D. Particle Size Distribution by Space or Time Dependent Extinction Profiles obtained by Analytical Centrifugation. *Particle & Particle Systems Characterization* **2006,** *23,* 184-187.
50. Sobisch, T.; Lerche, D. Thickener performance traced by multisample analytical centrifugation. *Colloids and Surfaces A: Physicochemical and Engineering Aspects* **2008,** *331,* 114-118.
51. Demeler, B.; Nguyen, T.-L.; Gorbet, G. E.; Schirf, V.; Brookes, E. H.; Mulvaney, P.; El-Ballouli, A. a. O.; Pan, J.; Bakr, O. M.; Demeler, A. K.; Hernandez Uribe, B. I.; Bhattarai, N.; Whetten, R. L. Characterization of Size, Anisotropy, and Density Heterogeneity of Nanoparticles by Sedimentation Velocity. *Analytical Chemistry* **2014,** *86,* 7688-7695.

52. Carney, R. P.; Kim, J. Y.; Qian, H.; Jin, R.; Mehenni, H.; Stellacci, F.; Bakr, O. M. Determination of nanoparticle size distribution together with density or molecular weight by 2D analytical ultracentrifugation. *Nat Commun* **2011,** *2*, 335.
53. Lerche, D.; Sobisch, T. Consolidation of concentrated dispersions of nano- and microparticles determined by analytical centrifugation. *Powder Technology* **2007,** *174*, 46-49.
54. Krpetić, Ž.; Davidson, A. M.; Volk, M.; Lévy, R.; Brust, M.; Cooper, D. L. High-Resolution Sizing of Monolayer-Protected Gold Clusters by Differential Centrifugal Sedimentation. *ACS Nano* **2013,** *7*, 8881-8890.
55. Balmer, J. A.; Le Cunff, E. C.; Armes, S. P.; Murray, M. W.; Murray, K. A.; Williams, N. S. J. When Does Silica Exchange Occur between Vinyl Polymer−Silica Nanocomposite Particles and Sterically Stabilized Latexes? *Langmuir* **2010,** *26*, 13662-13671.
56. Fielding, L. A.; Mykhaylyk, O. O.; Armes, S. P.; Fowler, P. W.; Mittal, V.; Fitzpatrick, S. Correcting for a Density Distribution: Particle Size Analysis of Core–Shell Nanocomposite Particles Using Disk Centrifuge Photosedimentometry. *Langmuir* **2012,** *28*, 2536-2544.
57. Colard, C. A. L.; Teixeira, R. F. A.; Bon, S. A. F. Unraveling Mechanistic Events in Solids-Stabilized Emulsion Polymerization by Monitoring the Concentration of Nanoparticles in the Water Phase. *Langmuir* **2010,** *26*, 7915-7921.
58. Yow, H. N.; Biggs, S. Probing the stability of sterically stabilized polystyrene particles by centrifugal sedimentation. *Soft Matter* **2013,** *9*, 10031-10041.
59. Monopoli, M. P.; Walczyk, D.; Campbell, A.; Elia, G.; Lynch, I.; Baldelli Bombelli, F.; Dawson, K. A. Physical−Chemical Aspects of Protein Corona: Relevance to in Vitro and in Vivo Biological Impacts of Nanoparticles. *Journal of the American Chemical Society* **2011,** *133*, 2525-2534.
60. Au, K. M.; Armes, S. P. Heterocoagulation as a Facile Route To Prepare Stable Serum Albumin-Nanoparticle Conjugates for Biomedical Applications: Synthetic Protocols and Mechanistic Insights. *ACS Nano* **2012,** *6*, 8261-8279.
61. Detloff, T.; Sobisch, T.; Lerche, D. Particle size distribution by space or time dependent extinction profiles obtained by analytical centrifugation (concentrated systems). *Powder Technology* **2007,** *174*, 50-55.
62. Lascelles, S. F.; Armes, S. P. Synthesis and characterization of micrometre-sized, polypyrrole-coated polystyrene latexes. *J. Mater. Chem.* **1997,** *7*, 1339-1347.
63. Stejskal, J.; Kratochvíl, P.; Armes, S. P.; Lascelles, S. F.; Riede, A.; Helmstedt, M.; Prokeš, J.; Křivka, I. Polyaniline Dispersions. 6. Stabilization by Colloidal Silica Particles. *Macromolecules* **1996,** *29*, 6814-6819.
64. Lovett, J. R.; Fielding, L. A.; Armes, S. P.; Buxton, R. One-Pot Preparation of Conducting Polymer-Coated Silica Particles: Model Highly Absorbing Aerosols. *Advanced functional materials* **2014,** *24*, 1290-1299.
65. Chiu, H.-T.; Chang, C.-Y.; Chiang, T.-Y.; Kuo, M.-T.; Wang, Y.-H. Using analytical centrifugation to characterize the dispersibility and particle size distributions of organic/inorganic composite coatings. *J Polym Res* **2011,** *18*, 1587-1596.
66. Chiu, H.-T.; Chiang, T.-Y.; Huang, Y.-C.; Chang, C.-Y.; Kuo, M.-T. Preparation, Particle Characterizations and Application of Nano-Pigment Suspension. *Polymer-Plastics Technology and Engineering* **2010,** *49*, 1552-1562.
67. Petzold, G.; Goltzsche, C.; Mende, M.; Schwarz, S.; Jaeger, W. Monitoring the stability of nanosized silica dispersions in presence of polycations by a novel centrifugal sedimentation method. *Journal of Applied Polymer Science* **2009,** *114*, 696-704.

68. Pedersen, J. S.; Svaneborg, C.; Almdal, K.; Hamley, I. W.; Young, R. N. A small-angle neutron and X-ray contrast variation scattering study of the structure of block copolymer micelles: corona shape and excluded volume interactions. *Macromolecules* **2002,** *36*, 416-433.
69. Pedersen, J. S. Structure factors effects in small-angle scattering from block copolymer micelles and star polymers. *Journal of Chemical Physics* **2001,** *114*, 2839-2846.
70. Pedersen, J. S.; Schurtenberger, P. Scattering functions of semiflexible polymers with and without excluded volume effects. *Macromolecules* **1996,** *29*, 7602-7612.
71. Pedersen, J. S.; Gerstenberg, M. C. The structure of P85 Pluronic block copolymer micelles determined by small-angle neutron scattering. *Colloids and Surfaces a-Physicochemical and Engineering Aspects* **2003,** *213*, 175-187.
72. Kinning, D. J.; Thomas, E. L. Hard-Sphere Interactions Between Spherical Domains in Diblock Copolymers. *Macromolecules* **1984,** *17*, 1712-1718.
73. Scares, B. G.; de Souza Gomes, A. Spectrophotometric determination of the styrene content of alpha-methylstyrene—styrene copolymers. *Polymer Bulletin* **1988,** *20*, 543-548.
74. Godward, J.; Heatley, F.; Price, C. 1 H Nuclear magnetic relaxation study of the phase structure of polystyrene-block-poly (ethylene/propylene) copolymer micelles. *J. Chem. Soc., Faraday Trans.* **1993,** *89*, 3471-3475.
75. Pedersen, J. S.; Svaneborg, C.; Almdal, K.; Hamley, I. W.; Young, R. N. A small-angle neutron and X-ray contrast variation scattering study of the structure of block copolymer micelles: Corona shape and excluded volume interactions. *Macromolecules* **2003,** *36*, 416-433.
76. Rieker, T. P.; Misono, S.; Ehrburger-Dolle, F. Small-angle X-ray scattering from carbon blacks: crossover between the fractal and porod regimes. *Langmuir* **1999,** *15*, 914-917.
77. Sahouli, B.; Blacher, S.; Brouers, F.; Darmstadt, H.; Roy, C.; Kaliaguine, S. Surface morphology and chemistry of commercial carbon black and carbon black from vacuum pyrolysis of used tyres. *Fuel* **1996,** *75*, 1244-1250.
78. Won, Y.-Y.; Meeker, S. P.; Trappe, V.; Weitz, D. A.; Diggs, N. Z.; Emert, J. I. Effect of temperature on carbon-black agglomeration in hydrocarbon liquid with adsorbed dispersant. *Langmuir* **2004,** *21*, 924-932.

Chapter 5

Is carbon black a suitable model colloidal substrate for diesel engine soot?

Introduction

Diesel engines are widely used in trucks and buses, as well as many cars and light-duty vehicles. Their popularity is in large part due to their high thermal efficiency, which leads to lower fuel consumption compared to petrol engines. It is well-known that fuel combustion in diesel engines leads to the production of nitrogen oxides (NO_x) in the exhaust gas, which are harmful to the environment.[1, 2, 3, 4, 5, 6] In the 1990s, diesel engine manufacturers retarded the fuel injection timing in order to meet legislated NO_x emission targets. However, this approach led to an increase in the amount of soot being transferred into the engine oil.[7] NO_x emission limits have been further tightened within the last fifteen years. Automotive manufacturers met these more stringent emissions targets by recirculating the exhaust gas back into the engine; this approach is commonly known as exhaust gas recirculation (EGR).[8, 9, 10, 11] However, under certain engine operating conditions EGR contributed to the build-up of unwanted soot particles within the engine oil.[12, 13] This accumulation of soot within the engine oil leads to higher viscosity, blockage of oil filters, greater engine wear and sludge formation.[14] Jao et al. reported that oil soot leads to engine wear via an abrasive wear mechanism. Moreover, the same workers showed that higher levels of abrasive contaminants within the oil inhibits boundary film formation.[15, 16, 17] This excessive build-up of soot particles in engine oil is highly undesirable because it accelerates engine wear, which ultimately leads to lower fuel efficiency and reduced engine lifetimes.[18, 19, 20, 21] Fortunately, this soot-related wear problem can be mitigated by the addition of various copolymers to engine oil formulations.[20, 22, 23, 24] Such copolymers can act as dispersants and confer steric stabilisation, thus maximising the degree of dispersion of the diesel soot. However, genuine diesel soot is prohibitively expensive for optimisation studies, because it can only be generated by running an engine over an extended period under sub-optimal conditions. Thus various grades of commercial carbon black particles (prepared via gas phase pyrolysis of either hydrocarbon oil or natural gas) have been suggested as cost-effective mimics for diesel soot.[22, 25, 26, 27, 28] For example, Clague and co-workers utilised a wide range of techniques, including ^{13}C NMR spectroscopy, IR spectroscopy, atomic emission spectroscopy, thermogravimetric analysis, inverse gas chromatography, transmission electron microscopy (TEM) and X-ray photoelectron spectroscopy (XPS), in order to directly compare both soot extracted from diesel engine oil and also an exhaust soot with various commercial carbon blacks. Although various

differences were observed, these authors nevertheless concluded that 'there appears to be potential for certain blacks to mimic the aggregation behaviour of soots for use in lubrication oils'.[27] Similarly, Bezot *et al*. used static and dynamic light scattering in combination with a reaction limited cluster aggregation mechanism to characterise three types of carbon black in terms of their fractal dimensions.[29] However, in a later paper by the same team, only one of these commercial carbon blacks exhibited a similar morphology to that of soot particles isolated from three different drain oils.[30] Moreover, Müller *et al*. compared a commercial carbon black (FR 101 33/D; ex. Degussa) with soot particulates obtained by running a heavy duty diesel engine under 'black smoke' conditions using a range of characterisation techniques and concluded that the former material was a poor surrogate for the latter.[31, 32]

In this Chapter, a specific grade of carbon black is examined to determine its suitability as a mimic for a particular diesel soot. Initially, various physical properties such as specific surface area, density, particle morphology and surface composition are determined for both materials using BET surface area analysis, helium pycnometry, TEM, small-angle X-ray scattering (SAXS), aqueous electrophoresis and XPS, respectively. Subsequently, the adsorption of two commercial copolymer dispersants, namely a poly(ethylene-co-propylene) (dOCP) statistical copolymer and a polystyrene-block-poly(ethylene-co-propylene) diblock copolymer (PS-PEP), onto both substrates from *n*-dodecane is examined, both indirectly using a supernatant depletion technique based on UV spectroscopy and also directly via thermogravimetric analysis (TGA). *n*-Dodecane was chosen for these studies because it is comparable to a fully saturated Group III base oil, which is widely used in modern engine oils. Finally, relative degrees of dispersion achieved for carbon black and diesel soot when utilising each copolymer dispersant are assessed using optical microscopy (OM), analytical centrifugation and SAXS.

Experimental

Materials

The two copolymers used in this Chapter were commercial products supplied by BP Formulated Products Technology and were used as received. dOCP is a statistical copolymer comprising ethylene and propylene repeat units that also contains a relatively

low level (< 1 mol %) of aromatic amine functionality. PS-PEP is a linear diblock copolymer with a polystyrene content of 28 mol%, as judged by ^{1}H NMR spectroscopy (see Chapter 2), see Table 5.1 for the corresponding molecular weight and M_w/M_n values. Chloroform and *n*-dodecane were obtained from Fisher Scientific UK Ltd and were used as received. The carbon black (Regal 250R) was kindly supplied by Cabot Corporation (Billerica, MA, USA). Diesel soot was a gift from BP Formulated Products Technology. This material was generated using a Cambustion Diesel Particulate Generator (DPG) at a loading temperature of 240ºC under the following standard 'light duty' test conditions: 1.1 kg h^{-1} fuel flow (standard Euro reference Diesel), 250 kg h^{-1} total flow, and a rate of soot generation of 10 g h^{-1}. The soot was then back-blown off the Diesel Particulate Filter (DPF) and collected for analysis. Both colloidal substrates were used as received.

Characterisation Techniques

Gel permeation chromatography. The molecular weight distribution of each copolymer was assessed by gel permeation chromatography (GPC) using THF eluent. The THF GPC set-up comprised two 5 μm 'Mixed C' 30 cm columns, a Varian 290-LC pump and a WellChrom K-2301 refractive index detector operating at 950 ± 30 nm. The THF mobile phase contained 2.0 v/v% triethylamine and 0.05 w/v% butylhydroxytoluene (BHT) and the flow rate was fixed at 1.0 mL min^{-1}. A series of ten near-monodisperse polystyrene standards (M_n = 580 to 552,500 g mol^{-1}) were used for calibration.

Dynamic light scattering. Hydrodynamic diameters were determined by DLS at 25°C using a Malvern Zetasizer NanoZS model ZEN 3600 instrument equipped with a 4 mW He−Ne solid-state laser operating at 633 nm. Back-scattered light was detected at 173° and the particle size was calculated from the quadratic fitting of the correlation function over thirty runs each of ten seconds duration. More specifically, the sphere-equivalent hydrodynamic diameter of the carbon black particles was calculated from the particle diffusion coefficient via the Stokes-Einstein equation, using a solution viscosity of 1.34 cP for *n*-dodecane at 25°C. All measurements were performed in triplicate and data were analysed by cumulants analysis of the experimental correlation function using

Dispersion Technology Software version 6.20. Copolymer concentrations of 0.01 % w/v were utilised in all DLS experiments.

Aqueous electrophoresis. Zeta potentials were determined for both carbon black and diesel soot particles dispersed in deionised H_2O using the same Malvern Zetasizer Nano ZS instrument described above. The solution pH was initially adjusted to pH 11 in the presence of 1 mM KCl, using 0.1 M NaOH. The solution pH was then manually lowered using either 0.1 M or 0.01 M HCl as required.

Transmission electron microscopy. Studies were conducted using a Phillips CM100 microscope operating at 100 kV on unstained samples prepared by drying a drop of dilute dispersion (approximately 0.01 wt%) onto a carbon-coated copper grid.

Small-angle X-ray scattering. SAXS patterns were acquired at a synchrotron source (Diamond Light Source, station I22, Didcot, UK) using monochromatic X-ray radiation (λ = 0.10 nm) and a 2D Pilatus 2M detector. A camera length of 10 m provided a q range from 0.014 nm^{-1} to 1.85 nm^{-1}, where $q = \frac{4\pi \sin\theta}{\lambda}$ is the length of the scattering vector and θ is half of the scattering angle). A liquid cell comprising two mica windows (each of 25 μm thickness) separated by a 1 mm polytetrafluoroethylene spacer was used as a sample holder. In order to avoid sedimentation of the carbon particles on the time scale of the SAXS experiments, the liquid cell was mounted on a continuously rotating stage during data collection. Dawn software developed at Diamond Light Source was used for SAXS data reduction (i.e., integrating, normalisation and background-subtraction). Irena SAS macros for Igor Pro[33] was used for SAXS data analysis.

Helium pycnometry. The solid-state densities of the Regal 250R carbon black and genuine diesel soot were determined using a Micrometrics AccuPyc 1330 helium pycnometer at 20°C.

Surface area analysis. BET surface area measurements were performed using a Quantachrome Nova 1000e instrument with dinitrogen gas (mean area per molecule = 16.2 $Å^2$) as an adsorbate at 77 K. Samples were degassed under vacuum at 100°C for at

least 15 h prior to analysis. The particle diameter, *d*, was calculated using the equation $d = 6/(\rho.A_s)$, where A_s is the BET specific surface area in $m^2\ g^{-1}$ and ρ is the carbon black density in $g\ m^{-3}$ obtained from helium pycnometry.

UV spectroscopy. UV spectra were recorded at 20°C using a Perkin Elmer Lambda 25 instrument operating between 200 and 800 nm for dOCP in *n*-dodecane directly, while dilute solutions of PS-PEP diblock copolymer micelles were diluted with an equal volume of chloroform in order to ensure micellar dissolution and hence avoid the problem of UV scattering (see Chapter 2). A calibration curve was constructed for dOCP in *n*-dodecane and also for PS-PEP in chloroform. The latter copolymer had a molar extinction coefficient of 222 ± 2 $mol^{-1}\ dm^3\ cm^{-1}$ at 262 nm, which was close to the literature value reported for polystyrene at the same wavelength.[34] The supernatant depletion assay was conducted as follows. The desired mass of copolymer (3.0 – 90.0 mg) was weighed into a glass vial. *n*-Dodecane (5.00 mL) was added to this vial and stirred at 20°C (Turrax stirrer, 1 minute), followed by heating to 110°C for 1 h. The resulting solution was added to a second glass vial containing carbon black (300.0 mg), stirred (Turrax stirrer, 1 minute), sonicated for 1 h, then placed on a roller mill for 16 h overnight to aid dispersion. The resulting carbon black dispersion was centrifuged for 4 h at 18,000 rpm in a centrifuge rotor that was pre-cooled to 15°C so as to minimise solvent evaporation. Taking care not to disturb the sedimented carbon black particles, the supernatant was decanted into an empty vial and then analysed by UV spectroscopy. For PS-PEP micelles, 0.40 mL of this decanted solution was diluted with an equal volume of chloroform to ensure molecular dissolution of the copolymer micelles prior to analysis by UV spectroscopy. The aromatic chromophore at 262 nm corresponding to the polystyrene block in the PS-PEP copolymer was used to quantify the copolymer concentration remaining in the supernatant after exposure to the carbon black, thus enabling the adsorbed amount to be determined by difference. Essentially the same protocol was used for the dOCP, but in this case the aromatic amine chromophore at 292 nm was used for quantification. No chloroform dilution was required in this latter case, since this copolymer does not form micelles in *n*-dodecane. The same analytical protocol was also used for genuine diesel soot, although in this case only 100.0 mg was used in each experiment.

Thermogravimetric analysis. Analyses were conducted on the two copolymers alone, the pristine carbon black and diesel soot, copolymer-coated carbon black particles and copolymer-coated soot particles. Each sample was heated up to 800^{o}C under a nitrogen atmosphere at a heating rate of 10^{o}C min^{-1} using a Q500 TGA instrument (TA Instruments). The mass loss observed between 300 and 550^{o}C confirmed complete pyrolysis of both copolymers under these conditions, enabling the remaining incombustible residues to be attributed to either carbon black or diesel soot, respectively.

X-ray photoelectron spectroscopy. Studies were conducted on carbon black and genuine diesel soot samples pressed onto indium foil using a Kratos Axis Ultra DLD X-ray photoelectron spectrometer equipped with a monochromatic Al X-ray source (*hν* = 1486.6 eV) operating at 6.0 mA and 15 kV at a typical base pressure of 10^{-8} torr. The step size was 1.0 eV for all survey spectra (pass energy = 160 eV). Spectra were typically acquired from at least two separate sample areas. CasaXPS software (version 2.3.15) was used to analyse the spectra, including background subtraction (using the Shirley algorithm), elemental quantification and peak deconvolution.

Analytical centrifugation. Carbon black aggregate diameters were determined using a LUMiSizer® analytical photocentrifuge (LUM GmbH, Berlin, Germany) at 20^{o}C using 2 mm path length polyamide cells. The LUMiSizer® is a microprocessor-controlled instrument that employs STEP™ Technology (Space- and Time-resolved Extinction Profiles) allowing the measurement of the intensity of transmitted light as a function of time and position over the entire cell length simultaneously. The progression of these transmission profiles contains information on the rate of sedimentation and, given knowledge of the effective particle density, enables calculation of the particle size distribution. Measurements were conducted on 1.0 % w/w carbon black or diesel soot dispersions in *n*-dodecane at 200-4000 rpm. In the present case, the effective particle density is significantly lower than that of either carbon black or diesel soot alone because of the presence of a relatively thick solvated shell of adsorbed copolymer.

Results and Discussion

Carbon black and diesel soot characterisation

The Regal 250R carbon black used in this Chapter was compared in terms of its particle size, morphology, specific surface area and surface chemistry to a particular diesel soot. BET surface area analysis yielded 43 $m^2 g^{-1}$ for the carbon black particles and 55 $m^2 g^{-1}$ for the diesel soot, while helium pycnometry gave densities of 1.89 g cm^{-3} and 1.94 g cm^{-3}, respectively. These data are in sufficiently close agreement to suggest that this particular grade of carbon black may be a useful mimic for diesel soot. Representative TEM images obtained for both carbon black and soot are shown in Figure 5.1. Analysis of these two images enables number-average diameters of 70 nm for carbon black and 50 nm for genuine soot to be estimated. In Chapter 3, SAXS has been used to identify three hierarchical structures for this particular grade of carbon black when prepared as a dispersion in *n*-dodecane. Similar structures have been observed in the current study, see later.

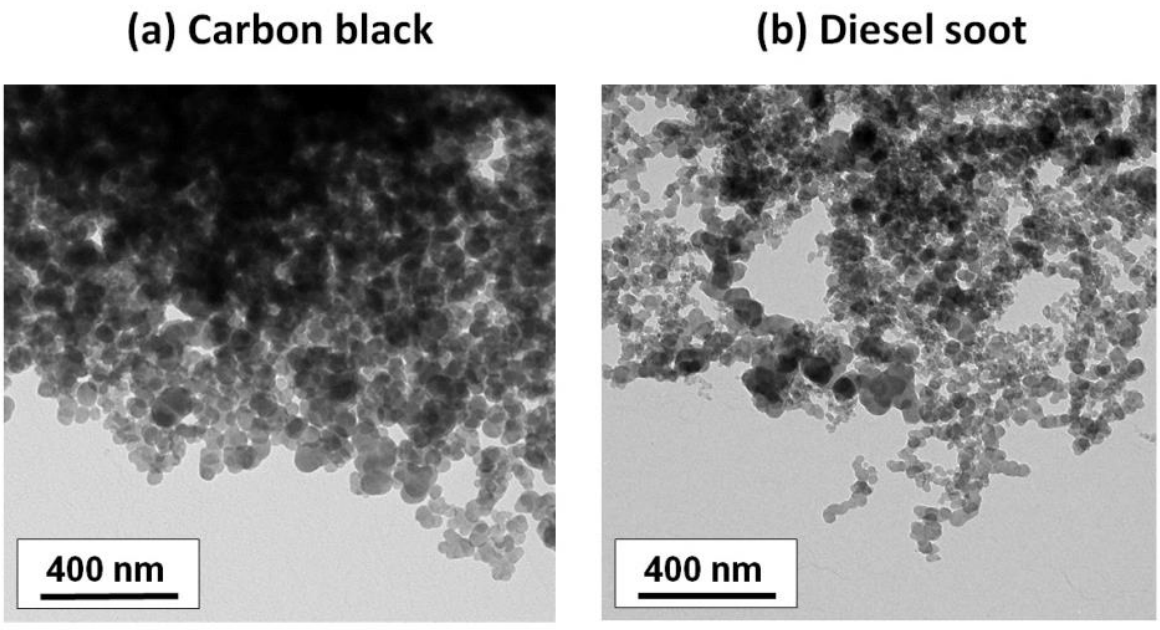

Figure 5.1. Transmission electron microscopy (TEM) images obtained for (a) carbon black and (b) diesel soot suspensions dried from *n*-heptane. The estimated number-average particle diameters are (a) 70 nm and (b) 50 nm.

The carbon black and diesel soot particles formed stable colloidal suspensions when dispersed in water. Although not necessarily representative of those formed in *n*-dodecane, such suspensions do enable aqueous electrophoresis studies to be conducted. The variation of both zeta potential and intensity-average particle diameter with solution pH for both colloidal substrates is shown in Figure 5.2. Carbon black aggregates are highly anionic (-30 to -45 mV) between pH 6 and pH 11. Below pH 6, the gradual reduction in surface charge leads to their progressive aggregation, from an initial characteristic sphere-equivalent diameter of 200 nm in alkaline media to flocs of more than 800 nm at an isoelectric point (IEP) of approximately pH 4.2 and micron-sized aggregates with appreciable cationic surface charge at pH 2-3. The diesel soot particles exhibit broadly similar behaviour, but with some subtle differences. The aggregates formed in alkaline media are somewhat larger, with sphere-equivalent diameters of 400-440 nm and zeta potentials of around -40 mV; they remain more or less stable from pH 11 to around pH 4, with an isoelectric point at approximately pH 3. Micron-sized aggregates are formed between pH 2 and pH 3.

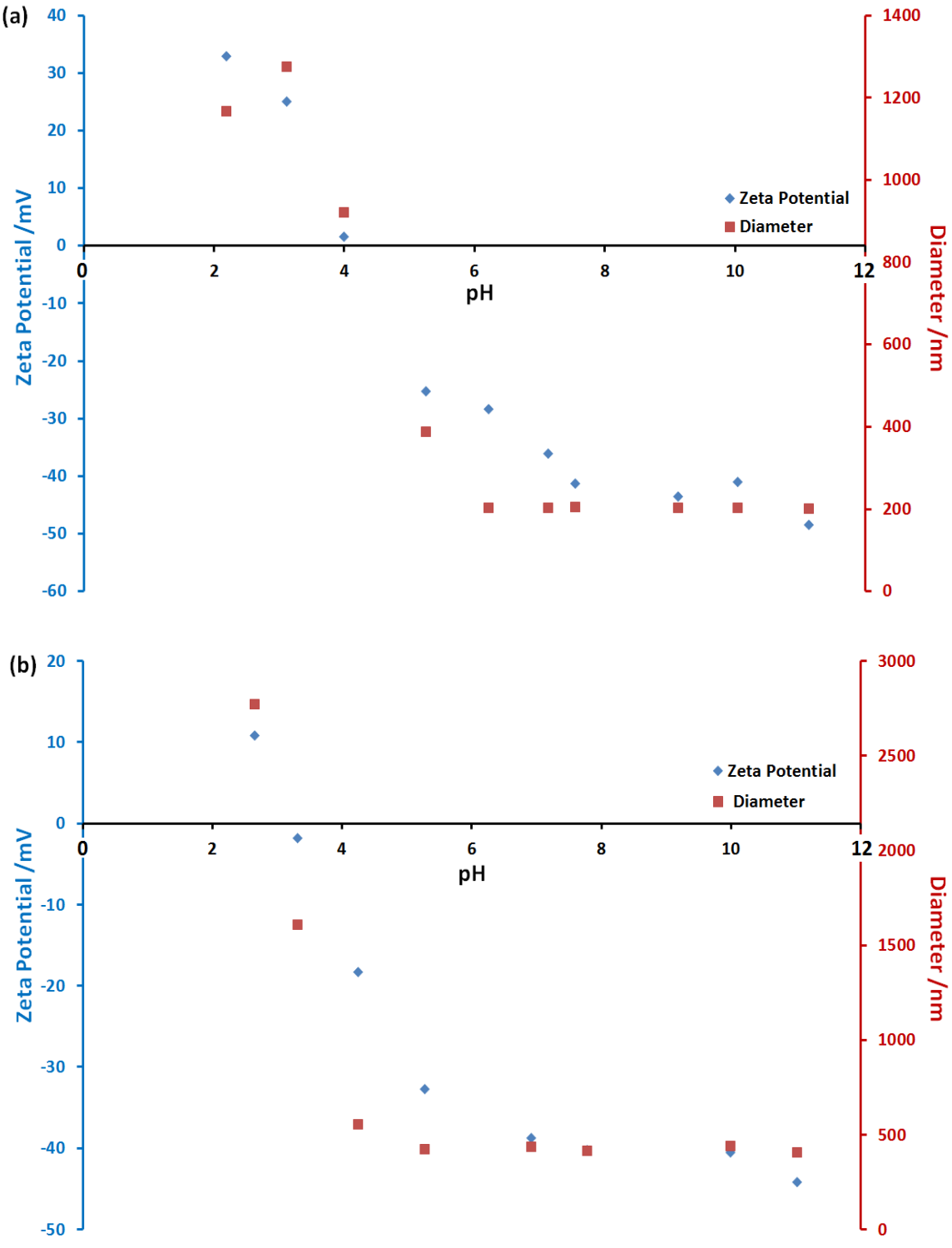

Figure 5.2. Zeta potential and intensity-average diameter versus pH for dilute (0.002 % w/w) aqueous suspensions of (a) carbon black and (b) diesel soot particles at 25°C.

X-ray photoelectron spectroscopy (XPS) is a well-established surface analysis technique with a typical sampling depth of 2-5 nm.[35, 36, 37] Figure 5.3 shows the survey spectra and core-line spectra (S 2p and O 1s) recorded for carbon black and diesel soot, respectively. The former substrate contains 98.3 atom % carbon, 1.1 atom % oxygen, and 0.6 atom % sulphur. In contrast, the latter substrate contains significantly more oxygen (6.3 atom %), but essentially zero sulphur (and 93.7 atom % carbon). As expected,[27] examination of the C 1s core-line spectra shows little difference between carbon black and diesel soot (see Figure 5.4)**.** These spectra are best fitted using an asymmetric graphitic carbon signal at 284.4 eV plus a shake-up satellite at approximately 291 eV. Unfortunately, this does not allow quantification of the degree of surface functionalisation of the carbon black and diesel soot. However, analysis of the O 1s spectra (Figures 5.3c and 5.3d) indicates the presence of at least two surface oxygen species for both carbon black and diesel soot. Following the work of Müller *et al*.,[27] the two main O 1s species are assigned as C-O-C and C-O-H plus a possible minor carbonyl signal contributing to the carbon black spectrum. The latter two species could account for the anionic surface charge observed above pH 7, as indicated by aqueous electrophoresis studies (see Figure 5.2).

DLS diameters obtained for carbon black and diesel soot particles suspended in *n*-dodecane are comparable, with a slightly higher intensity-average diameter being observed for the former substrate (see Figure 5.5). This agrees with TEM studies, which suggest a lower number-average diameter for diesel soot (50 vs. 70 nm, see Figure 5.1). SAXS analyses are also consistent with these observations, see later.

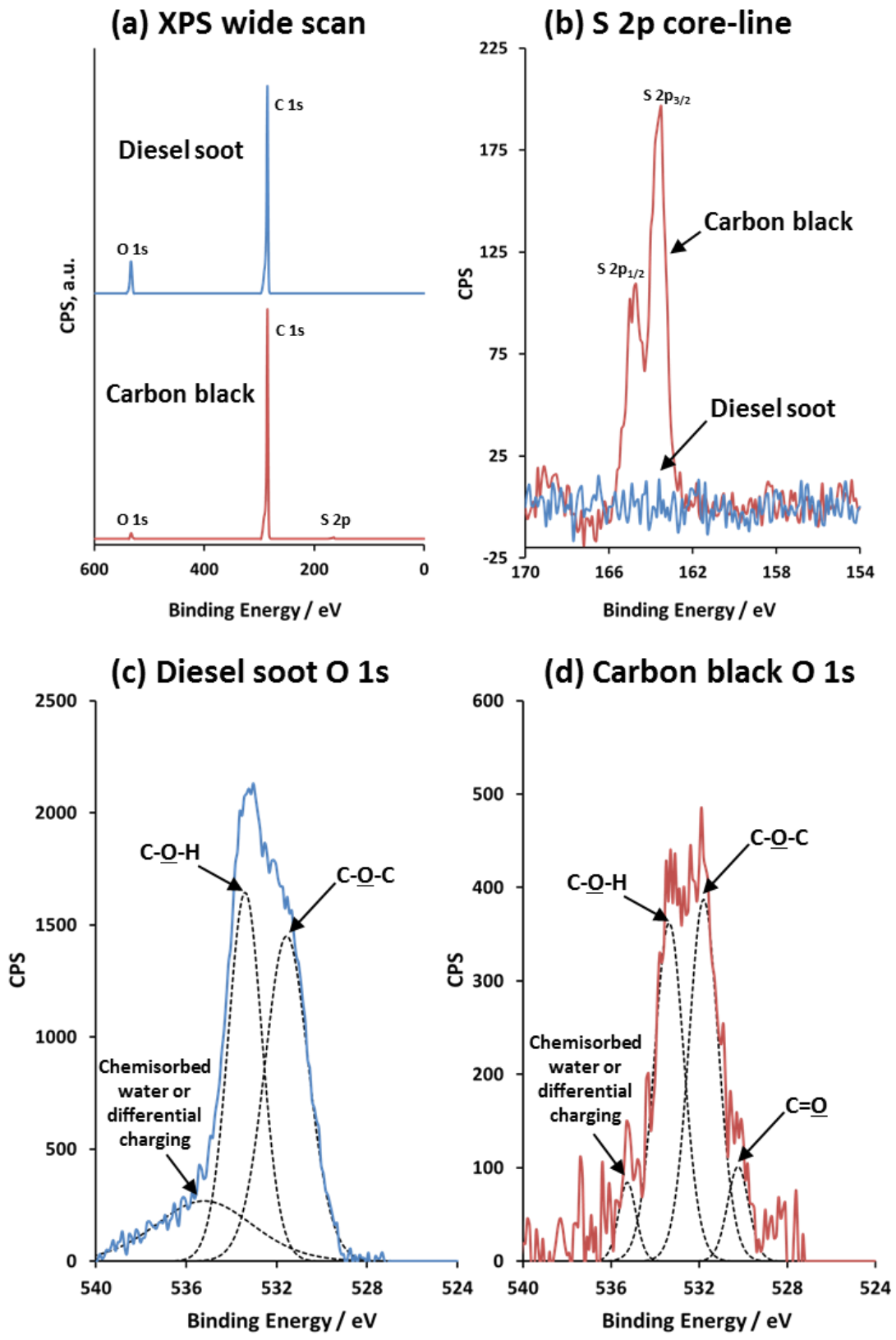

Figure 5.3. X-ray photoelectron spectra recorded for both carbon black and diesel soot particles: (a) survey spectra; (b) S 2p core-line spectra; (c) peak-fitted diesel soot O 1s core-line and (d) peak-fitted carbon black O 1s core-line spectra.

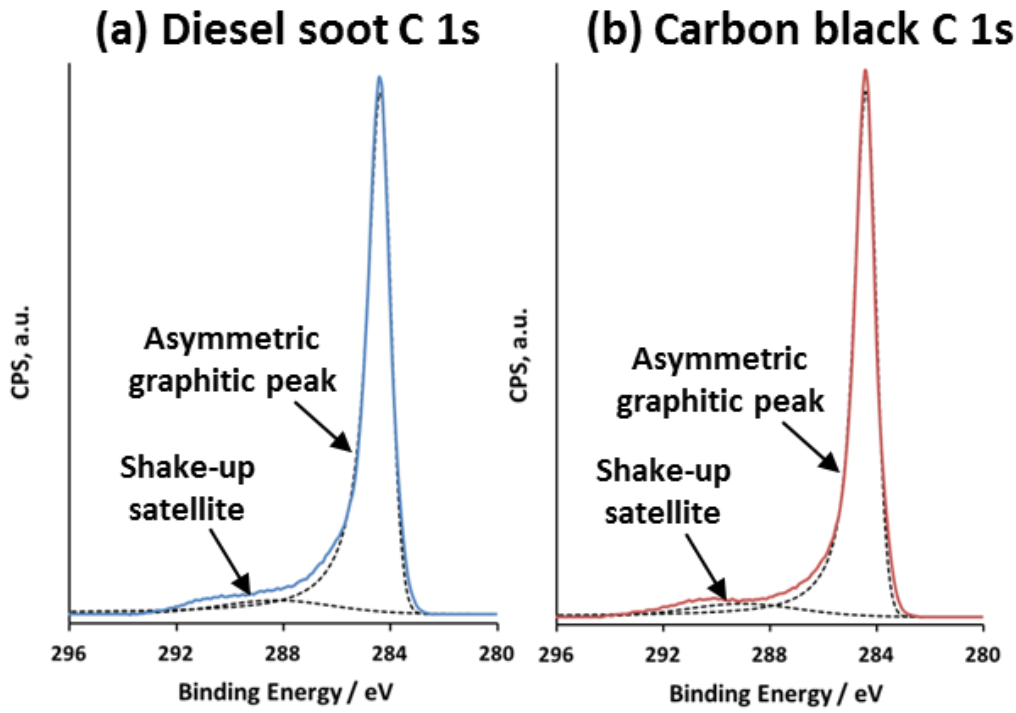

Figure 5.4. XPS C 1s core-line spectra recorded for both diesel soot and carbon black. The envelopes were fitted assuming an asymmetric graphitic carbon species at 284.4 eV and a broad shake-up satellite at approximately 291 eV.

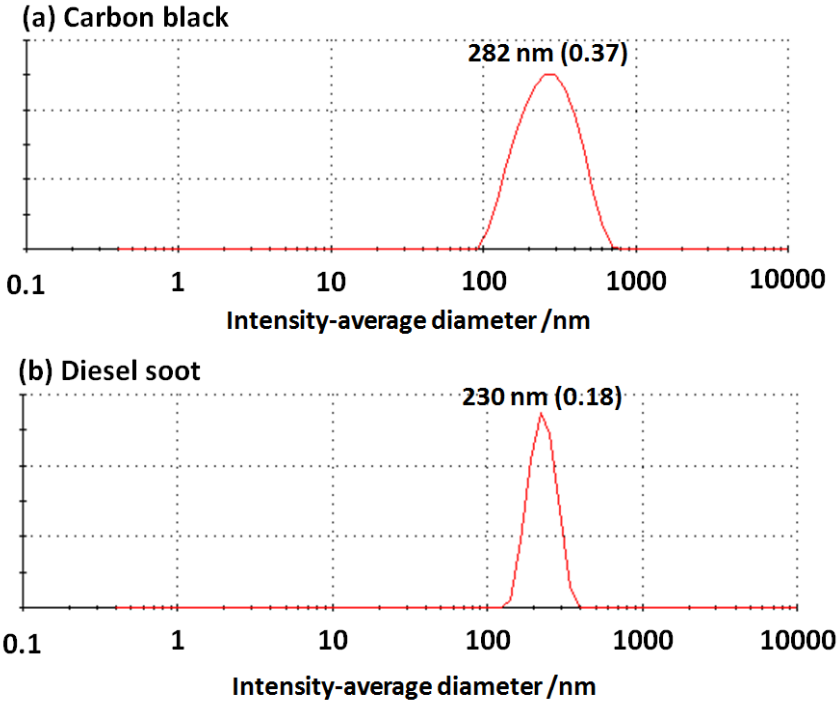

Figure 5.5. DLS particle size distributions obtained at 20°C for 0.001 % w/w suspensions of (a) Regal 250R carbon black and (b) diesel soot in *n*-dodecane. The polydispersity index (PDI) is shown in brackets.

Thermogravimetric analysis was used to assess the thermal stabilities of both carbon black and diesel soot on heating under a nitrogen atmosphere (see Figure 5.6). The former substrate exhibits a somewhat higher thermal stability than the latter, with mass losses of 0.75% and 6 % respectively being observed at 600^{o}C. Above 600^{o}C, substantial mass loss was observed for the diesel soot. However, this does not adversely affect the assessment of copolymer adsorption using this method, since complete pyrolysis of both copolymers used in this study is observed between 300 and 550^{o}C under the same conditions, see below.

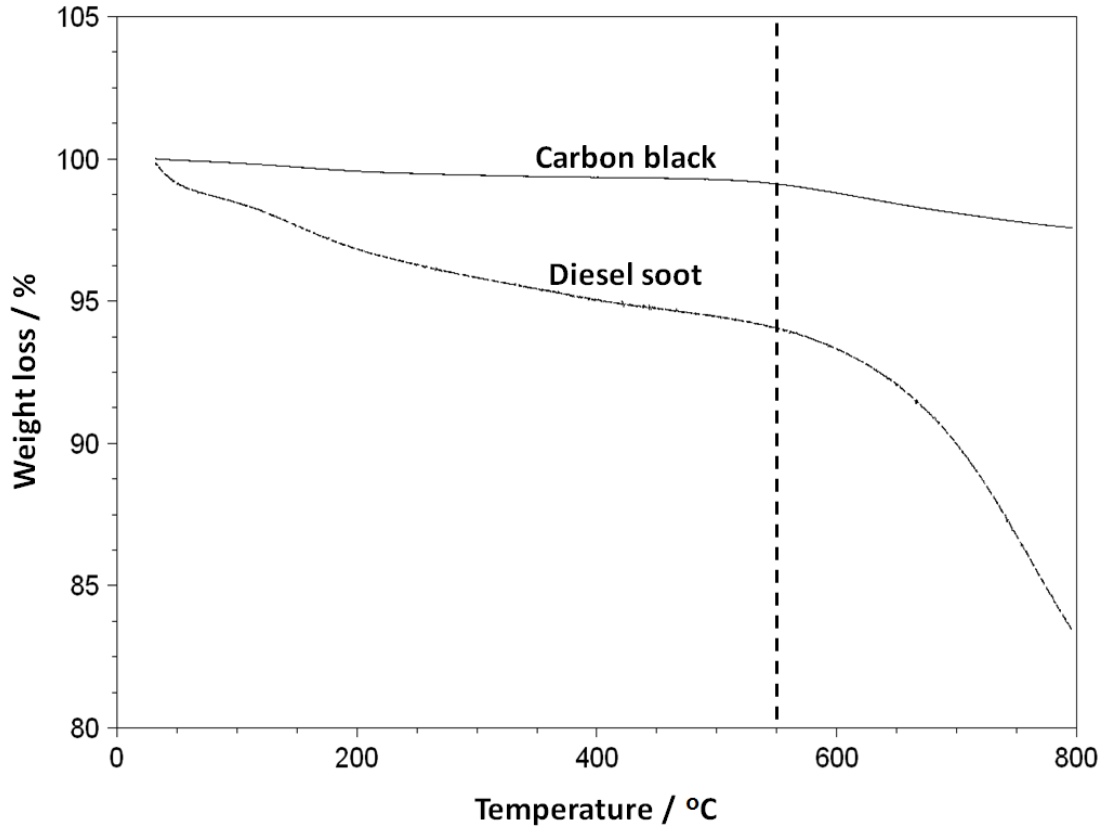

Figure 5.6. Thermogravimetric curves obtained for carbon black and diesel soot. Analyses were performed under a nitrogen atmosphere at a heating rate of 10^{o}C per min.

Copolymer characterisation

The two copolymers used in this Chapter were characterised using THF GPC and ^{1}H NMR ($CDCl_3$), see Table 5.1. These copolymers were selected because they represent two important classes of copolymer dispersant used for commercial engine oil formulations. PS-PEP is a polystyrene-block-poly(ethylene-co-propylene) diblock copolymer dispersant which forms polystyrene-core micelles in selective solvents such as *n*-alkanes (or engine oil). Such micelles adsorb intact onto carbon black particles to confer steric stabilisation at 20^{o}C, as discussed in Chapter 2. However, it is not clear whether micelle adsorption also occurs at typical engine operating temperatures of 90-100^{o}C. In contrast, dOCP is a poly(ethylene-co-propylene) statistical copolymer containing a relatively low level of aromatic amine functionality.

Copolymer ID	**Copolymer Description**	**Polystyrene content, mol% (^{1}H NMR, $CDCl_3$)**	**M_n kg mol^{-1}**	**M_w kg mol^{-1}**	**M_w/ M_n**
dOCP	Poly(ethylene-co-propylene) statistical copolymer	N/A	98	146	1.49
PS-PEP	Polystyrene-block-poly(ethylene-co-propylene) diblock copolymer	28	117	121	1.04

Table 5.1. Summary of copolymer composition, number-average molecular weight (M_n), weight-average molecular weight (M_w) and polydispersity (M_w/M_n) as determined by ^{1}H NMR spectroscopy ($CDCl_3$) and THF GPC (refractive index detector, vs. polystyrene standards) analysis of the two commercial copolymers used in this Chapter.

Copolymer adsorption isotherms on carbon black and diesel soot

Isotherms were constructed for the adsorption of each copolymer onto both carbon black and soot from *n*-dodecane using a supernatant depletion assay based on UV absorption spectroscopy, after centrifugal sedimentation of the carbon black particles (see Figure 5.7). *n*-Dodecane was selected instead of an engine base oil because the

latter solvent invariably contains UV-absorbing species, which renders UV spectroscopy analysis problematic. For PS-PEP, the polystyrene block acts as a convenient UV chromophore, since it gives rise to a strong signal at 262 nm.[38] In the case of dOCP, a strong absorbance at 292 nm resulting from its aromatic amine functionality provides a suitable UV signal. It is well known that PS-PEP forms polystyrene-core micelles in *n*-alkanes.[22, 39, 40] Hence the supernatant assay cannot be performed directly in such solvents because of light scattering at shorter wavelengths. Instead, the supernatant solution obtained after centrifugation of the carbon particles is diluted with an equal volume of chloroform. It was introduced in Chapter 2 that addition of this good solvent for the polystyrene chains causes micellar dissociation, producing molecularly-dissolved copolymer chains that are suitable for the UV assay. Addition of chloroform was not required for the dOCP, since this copolymer does not form micellar structures in *n*-dodecane. Langmuir-type adsorption is observed for both copolymers, with the plateau region indicating monolayer coverage.[41] Such behaviour is expected for adsorption of individual copolymer chains, but it is worth emphasising that PS-PEP is actually adsorbed in the form of micelles (see Chapter 2). Thus it seems rather counter-intuitive that PS-PEP actually has a *lower* maximum adsorbed amount (Γ = 2.4 mg m^{-2}) than the latter (Γ = 3.1 mg m^{-2}). One explanation for this apparent discrepancy is that the dOCP copolymer forms intermolecular aggregates in solution, rather than molecularly dissolved chains. Indeed, this is consistent with the observed sedimentation of dOCP during centrifugation (see below).

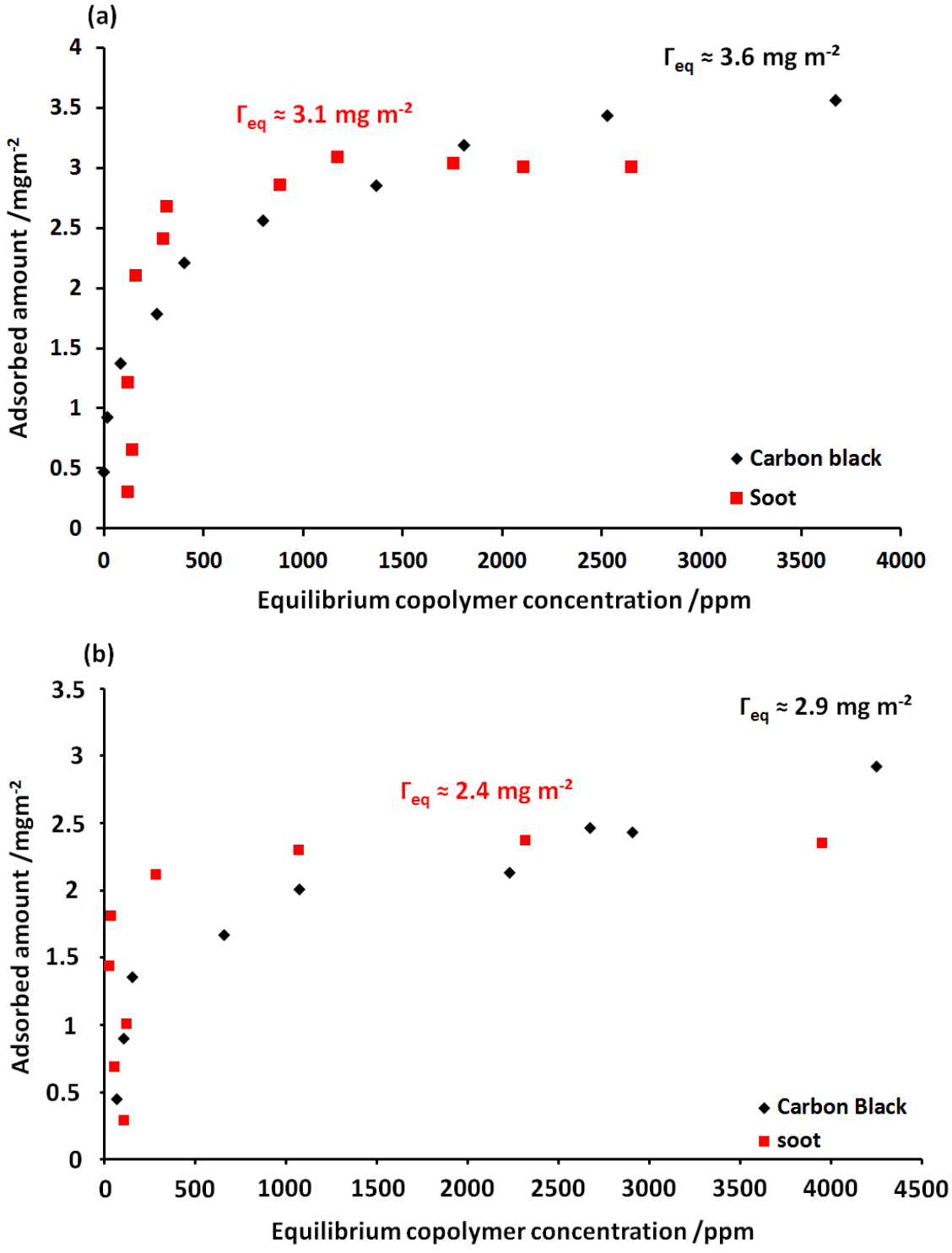

Figure 5.7. Adsorption isotherms obtained for (a) dOCP and (b) PS-PEP additives adsorbed onto carbon black (black) and diesel soot (red) from *n*-dodecane (after heating to 110°C for 1 h) at 20°C, as determined using a UV spectroscopy-based supernatant depletion assay.

Thermogravimetric analysis (TGA) was also used to quantify the extent of adsorption of each copolymer on the surface of carbon black and diesel soot particles from *n*-dodecane. Minimal mass loss occurred on heating such particles to 550^{o}C under an inert atmosphere (see Figure 5.6). In contrast, both copolymers were fully pyrolysed under these conditions (see inset thermograms in Figure 5.8). Thus pyrolysis of the copolymer-coated carbon black and soot particles (isolated as compacted sediments after centrifugation) allows the adsorbed amount of copolymer to be determined directly. A series of thermograms are shown in Figure 5.8. Higher mass losses are observed between 300 and 550^{o}C as the initial copolymer concentration is gradually increased. Initially, similar adsorption affinities are observed for each copolymer on both carbon black and diesel soot, while the maximum adsorbed amount (corresponding to monolayer coverage) was higher for the latter substrate. Adsorption isotherms constructed using each technique for both copolymers adsorbed onto soot are shown in Figure 5.9. When assessed using TGA, the apparent adsorbed amount continues to increase beyond the monolayer coverage value indicated by UV spectroscopy. However, control experiments conducted in the absence of any carbon black (or diesel soot) confirm that both copolymers are partially sedimented under the centrifugation conditions used for the adsorption studies. This observation is understandable for the PS-PEP copolymer, because TEM, DLS and SAXS studies indicate micelle formation in *n*-dodecane (see Chapter 2). It is perhaps less clear why the dOCP copolymer should form aggregates in solution, but this may be related to its low degree of diphenylamine functionality, which is likely to lead to intermolecular π-π stacking interactions.[42] In view of these observations, TGA should be reliable below (and up to) monolayer coverage, because under these conditions there is essentially no excess copolymer in the supernatant. However, the adsorbed amount tends to be *overestimated* by this technique when either copolymer is present in excess, since non-adsorbed copolymer is sedimented along with the carbon black (or diesel soot) particles. For the same reason, the UV supernatant depletion assay necessarily *underestimates* the adsorbed amount of copolymer when working above monolayer coverage. Although this technical problem is an important caveat, the TGA data nevertheless confirms a higher equilibrium adsorbed amount for dOCP compared to PS-PEP for both substrates (see Table 5.2).

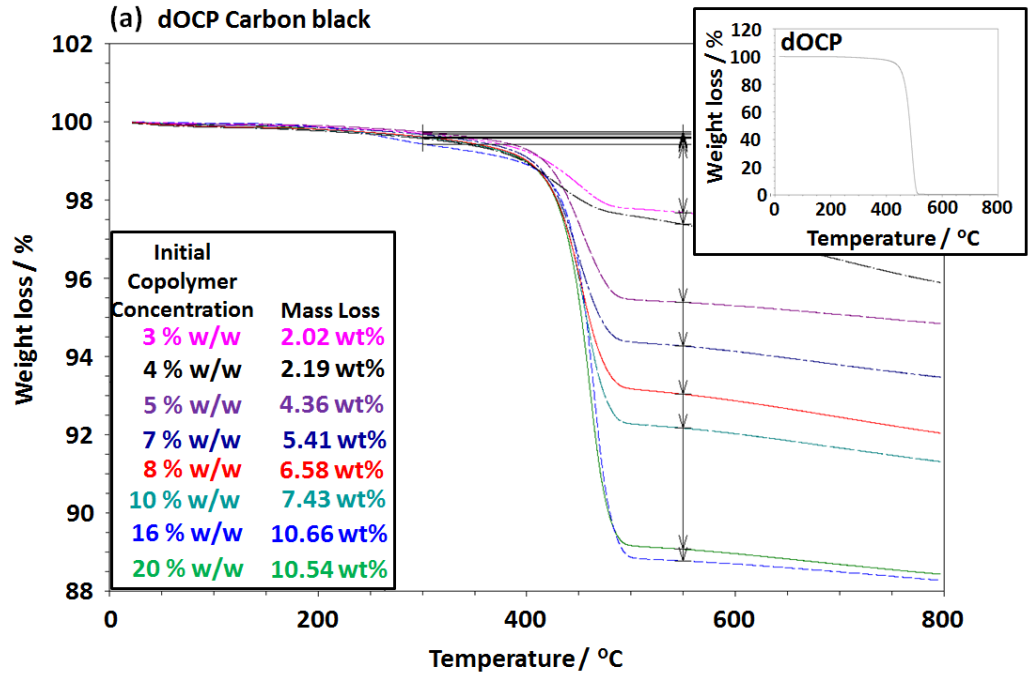
(a) dOCP Carbon black
Weight loss / %
Temperature / °C
Initial Copolymer Concentration
Mass Loss
3 % w/w 2.02 wt%
4 % w/w 2.19 wt%
5 % w/w 4.36 wt%
7 % w/w 5.41 wt%
8 % w/w 6.58 wt%
10 % w/w 7.43 wt%
16 % w/w 10.66 wt%
20 % w/w 10.54 wt%
dOCP
Weight loss / %
Temperature / °C

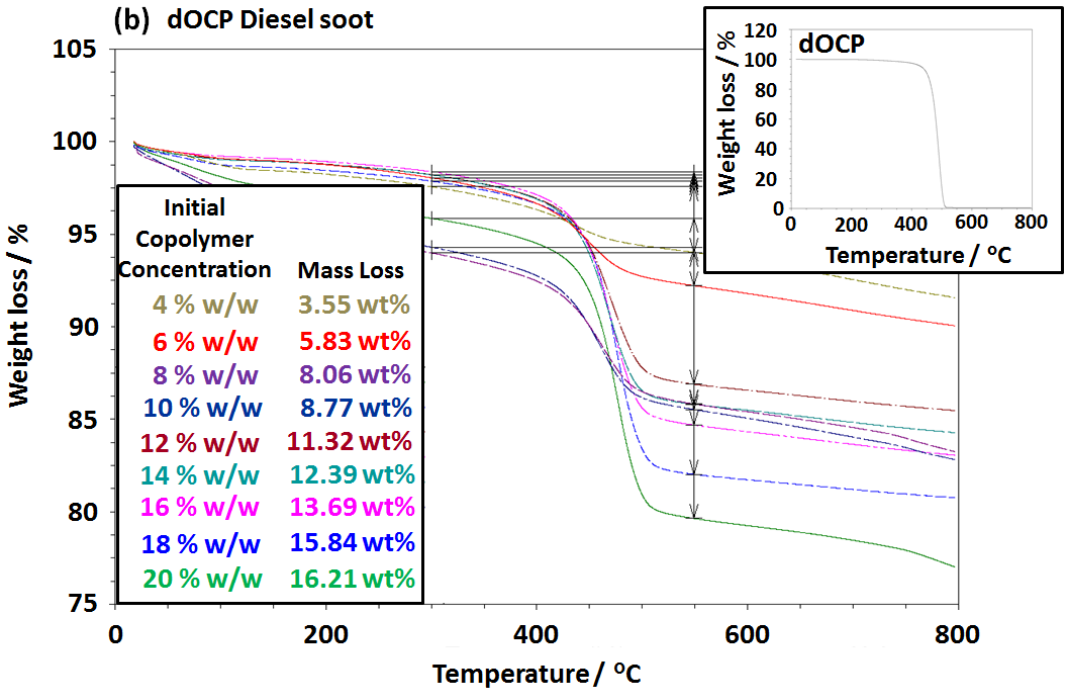
(b) dOCP Diesel soot
Weight loss / %
Temperature / °C
Initial Copolymer Concentration
Mass Loss
4 % w/w 3.55 wt%
6 % w/w 5.83 wt%
8 % w/w 8.06 wt%
10 % w/w 8.77 wt%
12 % w/w 11.32 wt%
14 % w/w 12.39 wt%
16 % w/w 13.69 wt%
18 % w/w 15.84 wt%
20 % w/w 16.21 wt%
dOCP
Weight loss / %
Temperature / °C

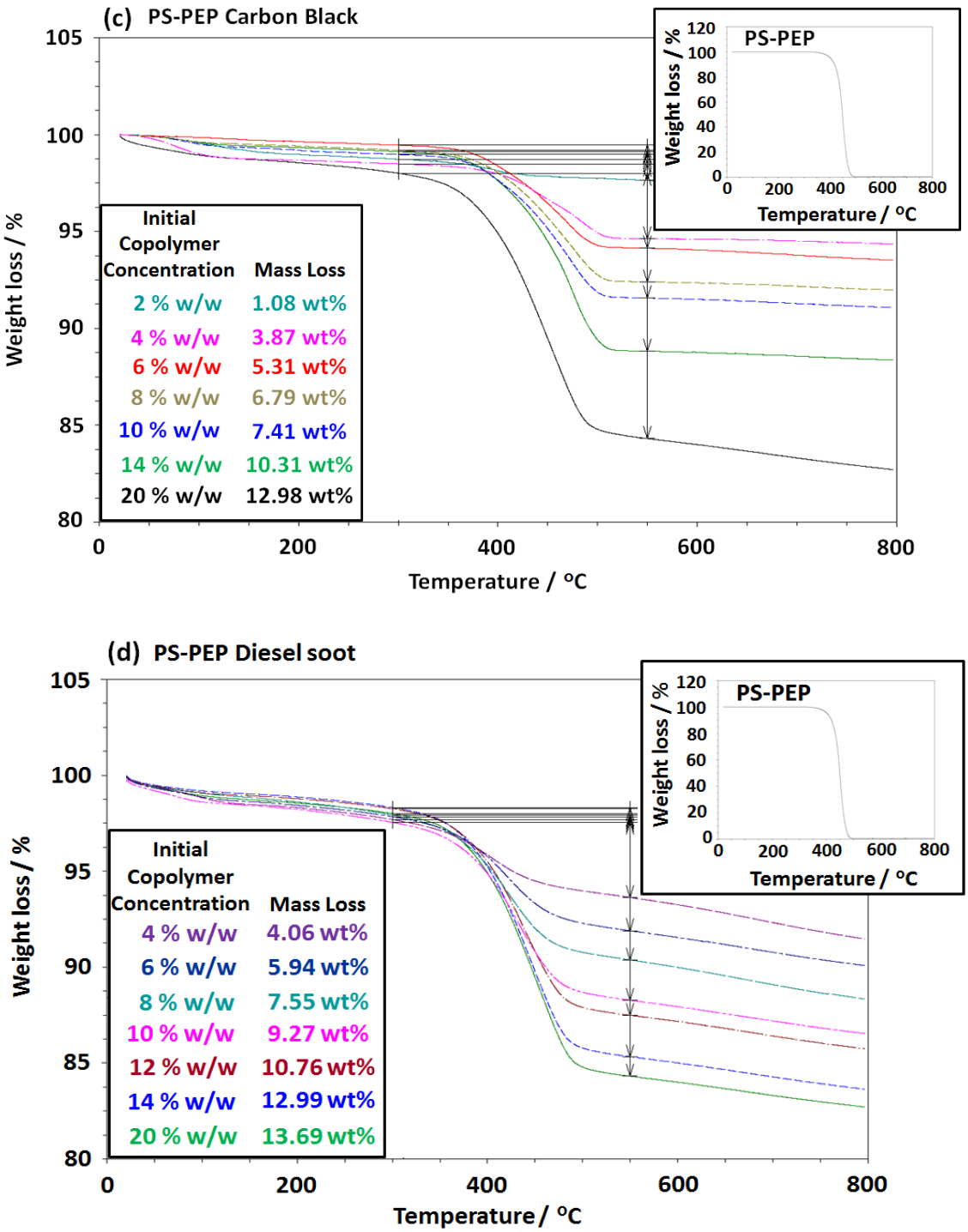

Figure 5.8. Thermogravimetric curves obtained for the adsorption of increasing amounts of dOCP onto (a) carbon black and (b) diesel soot, and PS-PEP onto (c) carbon black and (d) diesel soot from *n*-dodecane at 20°C. Analyses were performed under a nitrogen atmosphere at a heating rate of 10°C per min. Under these conditions, the copolymers are completely pyrolysed between 300 and 550°C (see insets). Thus the observed mass loss at 550°C for copolymer-coated soot particles can be attributed to the copolymer content (after correcting for the diesel soot mass loss over the same temperature range). This direct method for determining the adsorbed amount of copolymer is in reasonable agreement (at least up to monolayer coverage) with the indirect UV supernatant assay method (see adsorption isotherms shown in Figure 5.9).

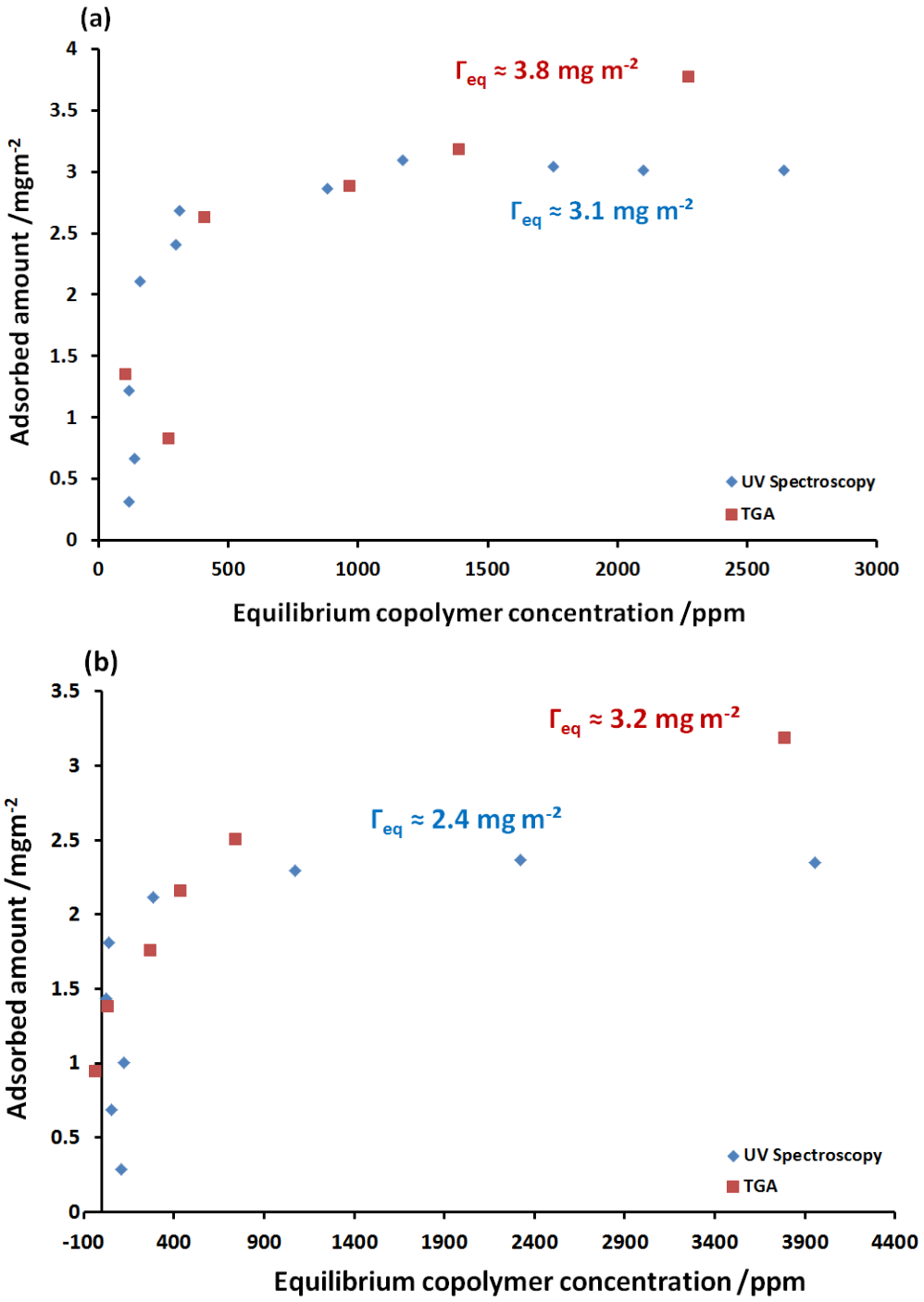

Figure 5.9. Adsorption isotherms obtained for (a) dOCP and (b) PS-PEP copolymers adsorbed onto diesel soot from *n*-dodecane at 20°C (after initial heating to 110°C for 1 h to aid dissolution), as determined using a UV spectroscopy-based supernatant depletion assay (blue data points) and directly via thermogravimetric analysis (red data points).

Copolymer ID	Γ (UV) / mg m^{-2}		Γ (TGA) / mg m^{-2}	
	Carbon Black	Diesel Soot	Carbon Black	Diesel Soot
dOCP	3.6	3.1	2.5	3.8
PS-PEP	2.9	2.4	2.4	3.2

Table 5.2. Adsorbed amounts (Γ) obtained at monolayer coverage for the dOCP and PS-PEP copolymers on carbon black and diesel soot as determined indirectly via supernatant depletion assay using UV spectroscopy and directly via thermogravimetric analysis.

Relative degrees of dispersion of carbon black and diesel soot in n-dodecane

In principle, a smaller apparent particle size indicates a higher degree of dispersion for the carbon black or diesel soot particles in *n*-dodecane. In this context, there are two particle size regimes of interest. *Micron-sized* agglomerates (or mass fractals[43]) are readily visualised by optical microscopy.[44] Figure 5.9 shows representative optical microscopy images obtained for both carbon black and diesel soot particles when using PS-PEP copolymer as a dispersant (at 10 % w/w based on the mass of particles). Clearly, similar degrees of dispersion are observed for each substrate. Moreover, TEM images recorded for the *submicron-sized* populations of carbon black and diesel soot particles are also comparable. In principle, analysis of these submicron-sized populations can be achieved for both colloidal substrates using analytical centrifugation (LUMiSizer® instrument).[45, 46, 47] In practice, this technique requires an accurate particle density. However, determining this parameter can be problematic for sterically-stabilised particles, particularly for thick stabiliser layers on relatively small particles. In Chapter 4, an effective particle density of 0.91 g cm^{-3} has been calculated for PS-PEP-coated carbon black particles in *n*-dodecane. This density is significantly lower than that of carbon black alone (1.89 g cm^{-3}), which leads to a substantial correction to the volume-average particle diameter determined by analytical centrifugation. In the absence of any other data, the above effective particle density has been used for both dOCP-coated carbon black particles and also for both types of copolymer-coated diesel soot particles.

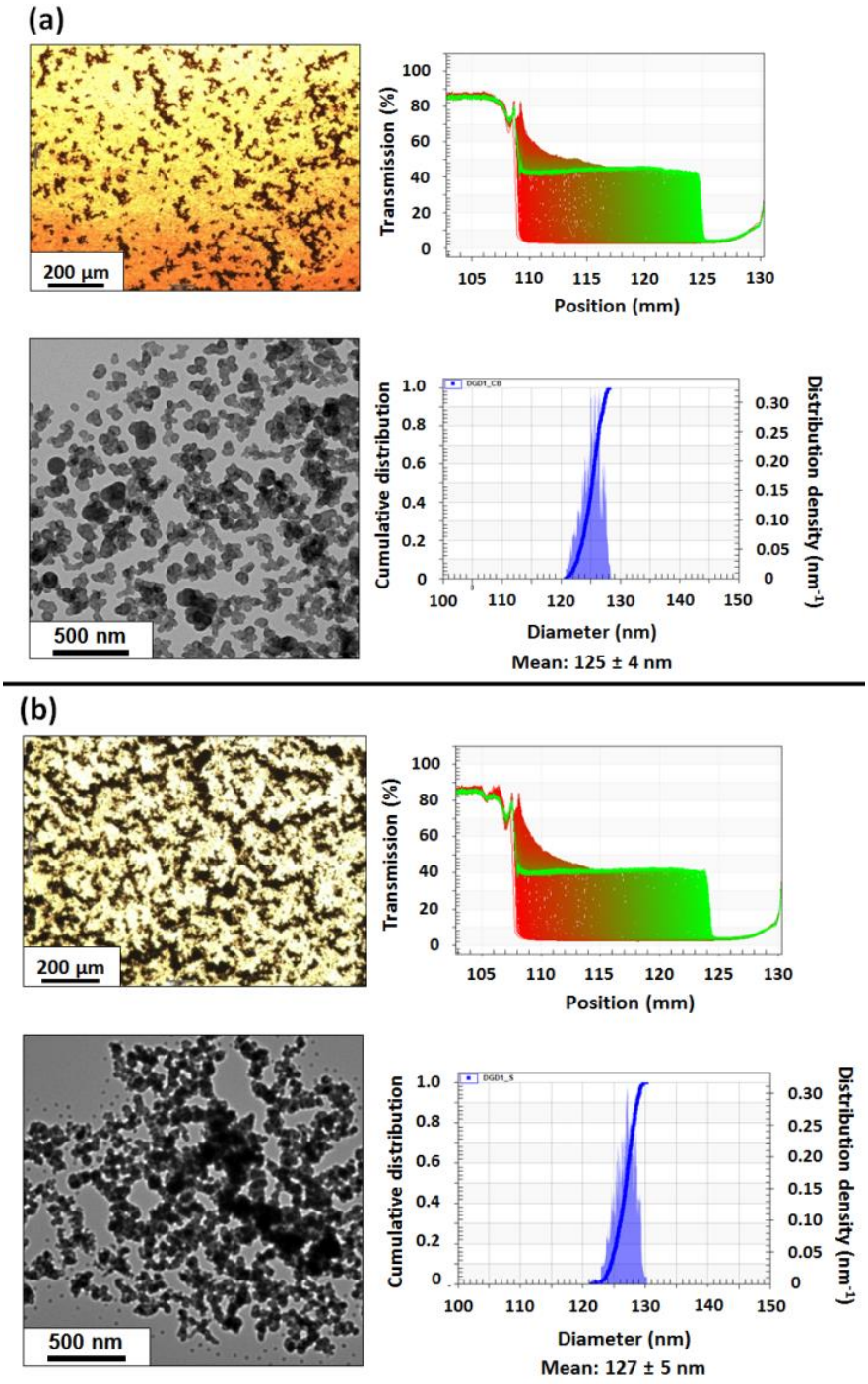

Figure 5.9. Optical microscopy, TEM and LUMiSizer® raw profile plots and volume-average particle size distributions obtained at 20°C for: (a) carbon black particles dispersed in *n*-dodecane; (b) diesel soot particles dispersed in *n*-dodecane. In each case 10 % PS-PEP copolymer by mass was utilised relative to the colloidal substrate.

The volume-average particle size distributions determined for PS-PEP-coated carbon black and diesel soot particles using this effective particle density are shown in Figure 5.9. This analysis was conducted at a concentration of 1.0 % w/w carbon black (based on solvent), since higher concentrations tend to give artificially low volume-average diameters due to hindered settling and multiple scattering,[46] see Figure 5.10. Remarkably similar volume-average particle diameters (125 nm vs. 127 nm) are calculated, which suggests that carbon black is a useful model substrate for understanding the behaviour of diesel soot, at least for this particular copolymer under these conditions.

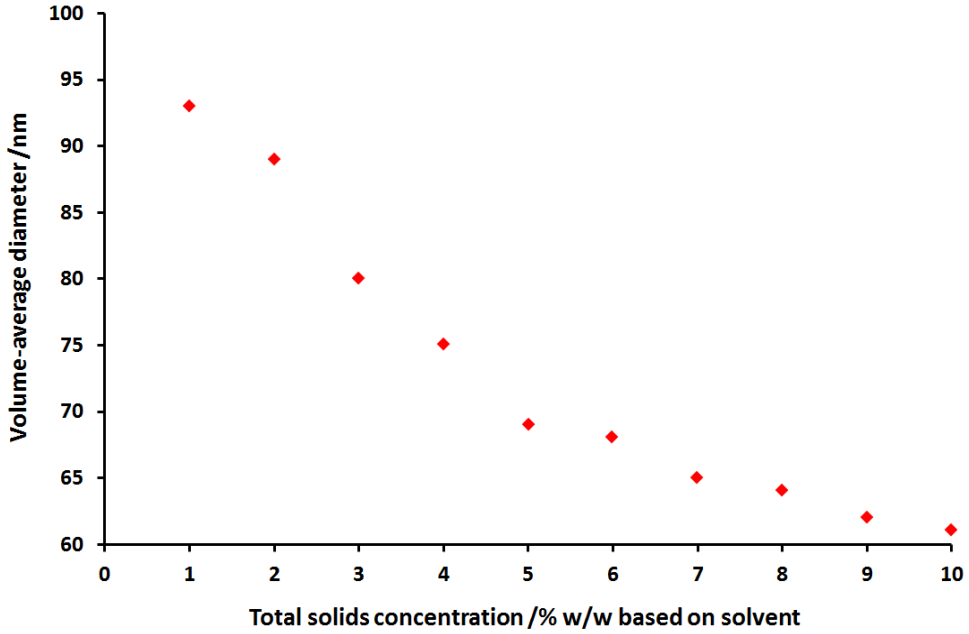

Figure 5.10. A plot of LUMiSizer® volume-average diameter versus total solids concentration obtained at 20°C for carbon black particles dispersed in *n*-dodecane with 10 % PS-PEP copolymer by mass (relative to carbon black).

In Figure 5.11, the equivalent optical microscopy and TEM images obtained for dOCP-coated carbon black (or diesel soot) particles are presented. However, in this case the diesel soot is substantially more aggregated than carbon black particles prepared under the same conditions. This conclusion is reinforced by the analytical centrifugation data, which report an apparent volume-average particle diameter of 5.2 μm for the diesel soot particles, but only 128 nm for the carbon black particles. Thus, for this particular copolymer at this specific concentration, it is clear that carbon black is a poor mimic for the behaviour of diesel soot. These differences are most likely the result of a specific acid-base interaction between the diphenylamine-functionalised dOCP copolymer and

the carboxylic acid-rich surface of the diesel soot, which leads to bridging flocculation rather than steric stabilisation.

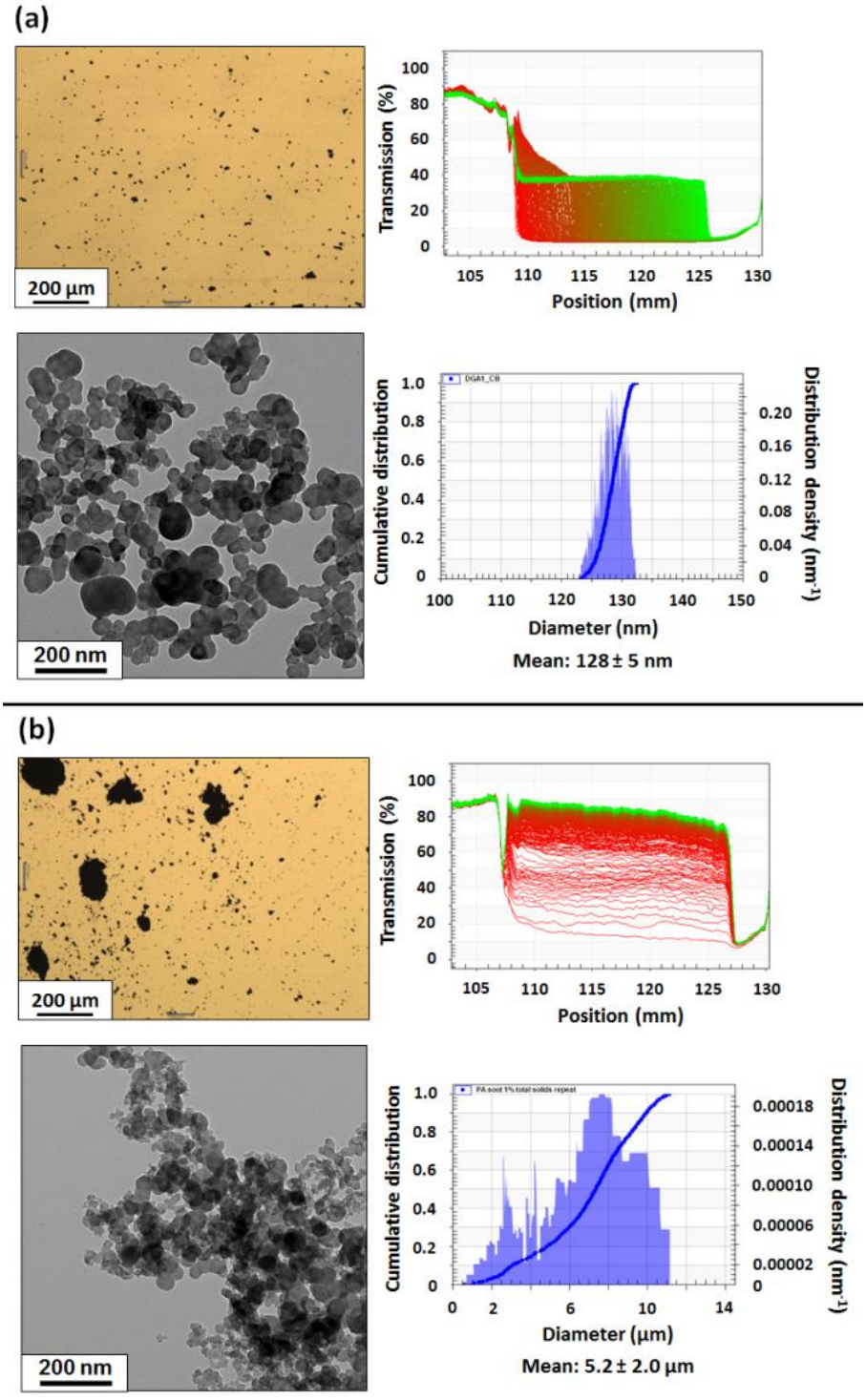

Figure 5.11. Optical microscopy, TEM and LUMiSizer® raw profile plots and volume-average particle size distributions obtained at 20°C for: (a) carbon black particles dispersed in *n*-dodecane; (b) diesel soot particles dispersed in *n*-dodecane. In each case 10 % dOCP copolymer by mass was utilised relative to the colloidal substrate.

SAXS analysis

It is well known that the morphology of carbon black (and diesel soot) can be described as a complex hierarchy composed of five structures/levels: (i) fractal agglomerates at the micron length scale, (ii) aggregates and (iii) primary particles at the nm scale, (iv) sub-units (a turbostratic structure comprising graphite-like layers arranged in non-aligned basal planes) at the sub-nm scale, and finally (v) graphite-like carbon layers at the atomic scale.[48, 49, 50, 51, 52] The first three structures can be analysed by SAXS/USAXS (ultrasmall-angle X-ray scattering) and are shown in cartoon format in Figure 5.12, while the remaining two structures can be characterised using wide-angle X-ray scattering (WAXS).

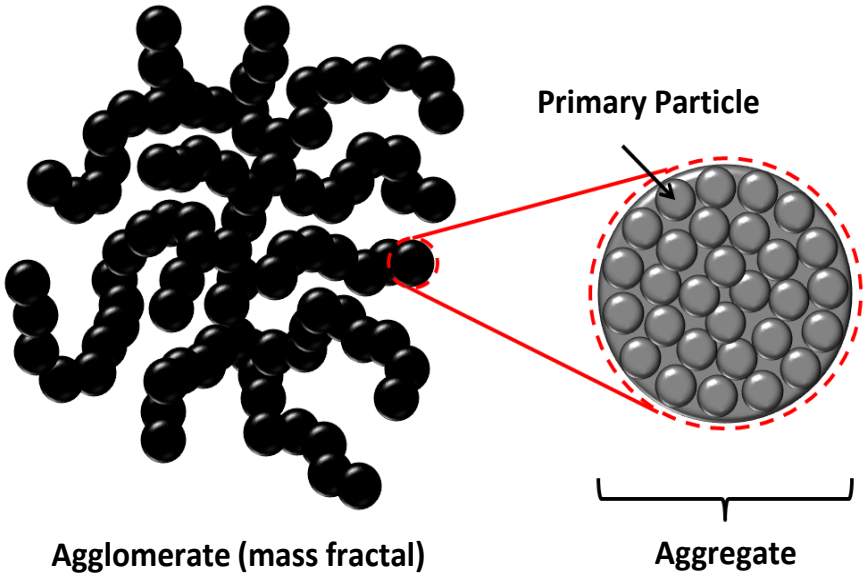

Figure 5.12. Schematic cartoon illustrating the three structural morphologies identified for carbon black and diesel soot via SAXS analysis. The rough surface fractal nature of the primary particles (and aggregates) is not shown in this cartoon.

The primary particles are fused together to form aggregates that are considered to be unbreakable via dispersion processes,[51] but the larger hierarchical structures can be affected by the processing conditions.[48, 53, 54] Thus SAXS/USAXS measurements are often employed for characterisation of carbon black/diesel soot in order to obtain structural information regarding the organisation of the aggregated particles.[51, 54, 55] In this context, the unified Guinier plus power law approach proposed by Beaucage is commonly employed,[56, 57, 58] since it enables an arbitrary number of interrelated structural features at various length scales to be described.[51, 59] The scattering profile is

decomposed into the scattering intensity, $I(q)$, arising from each structural element comprising the hierarchical structures. It can be expressed analytically as follows:

$$I(q) \cong \sum_{i=1}^{N} \left[G_i \exp\left(-\frac{q^2 R_{g,i}^2}{3} \right) + B_i \exp\left(-\frac{q^2 R_{g,i+1}^2}{3} \right) \left(\frac{[\mathrm{erf}(q k_i R_{g,i} / \sqrt{6})]^3}{q} \right)^{P_i} \right] S_i(q) \qquad (1)$$

where N is the number of structural elements, and the scattering intensity originating from each structural element (the expression enclosed by the square brackets) is represented as the sum of two components describing the Guinier and power laws respectively. G_i is the Guinier pre-exponential factor of the i^{th} structural element and B_i is a prefactor of the power-law scattering. $R_{g,i}$ and $R_{g,i+1}$ are radii of gyration of a large-scale structure and a small-scale substructure, respectively. The exponent term associated with $R_{g,i+1}$ provides a high q cut-off for the power law component, which is incorporated into equation 1 in order to describe scattering from a system with inter-related multi-scale features. This factor is commonly used to describe mass fractals.[33, 57] If it is not required, the exponent term is assumed to be unity. P_i is a scaling exponent of the power law assigned to the larger structure $R_{g,i}$. Generally, the numerical value of the exponent enables the structural morphology to be classified. For mass fractals $P_i < 3$, for surface fractals $3 < P_i < 4$, for Porod's law (smooth surface with a sharp interface) $P_i = 4$ and for diffuse interfaces $P_i > 4$ (negative deviation from Porod's law). k_i is an empirical constant that is either unity for steep power law decays ($P_i > 3$) or equal to 1.06 for mass fractals ($1.5 < P_i < 3$).[57] Weakly-correlated particles can also be considered using equation 1 by incorporating a structure factor, $S_i(q)$,[58, 60] which comprises a damped spherical correlation of colloidal particles:

$$S_i(q) = [1 + \eta_i f(qR_{c,i})]^{-1} \qquad (2)$$

where $f(qR_{c,i}) = 3[\sin(qR_{c,i}) - qR_{c,i}\cos(qR_{c,i})]/(qR_{c,i})^3$ is the form factor for spherical interactions correlated over a distance R_c and η describes the degree of correlation, which is assumed to be weak if $\eta < 3$. If no correlations are present for the i^{th} structural element/level, then $S_i(q) = 1$. The multi-level unified fit, equation 1, is implemented as a routine in the SAXS data analysis software Irena SAS macros for Igor Pro.[33]

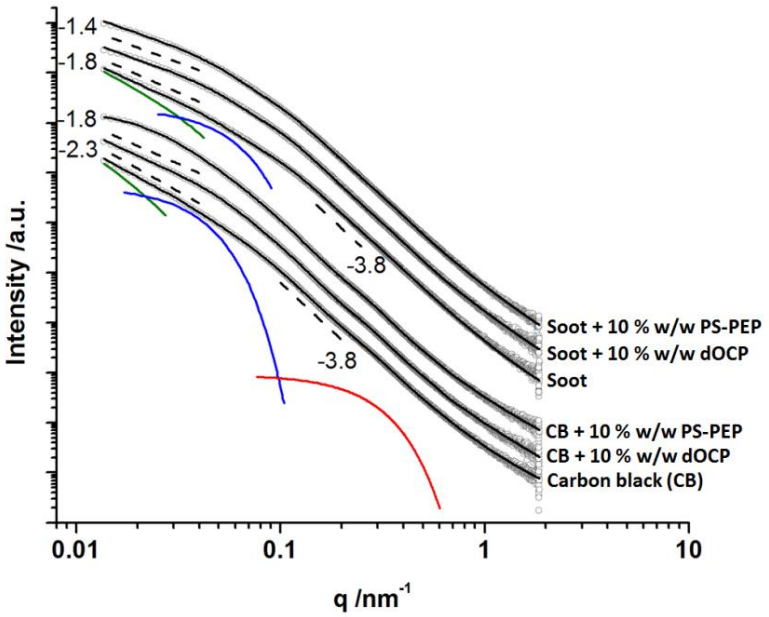

Figure 5.13. Representative SAXS patterns recorded for 1.0 % w/w carbon black or diesel soot dispersions in *n*-dodecane in the absence and presence of two commercial copolymer dispersants (dOCP and PS-PEP; 10.0 % w/w loading based on carbon black or diesel soot particles). The lower group of patterns were obtained for carbon black particles and the upper group were obtained for diesel soot. Dashed lines indicate power law gradients for the scattering intensity. Solid black lines indicate multi-level unified fits to the data. Coloured lines indicate unified fits to the mass fractals (green), and the Guinier components of the unified fits to both the agglomerates (blue) and the primary particles (red).

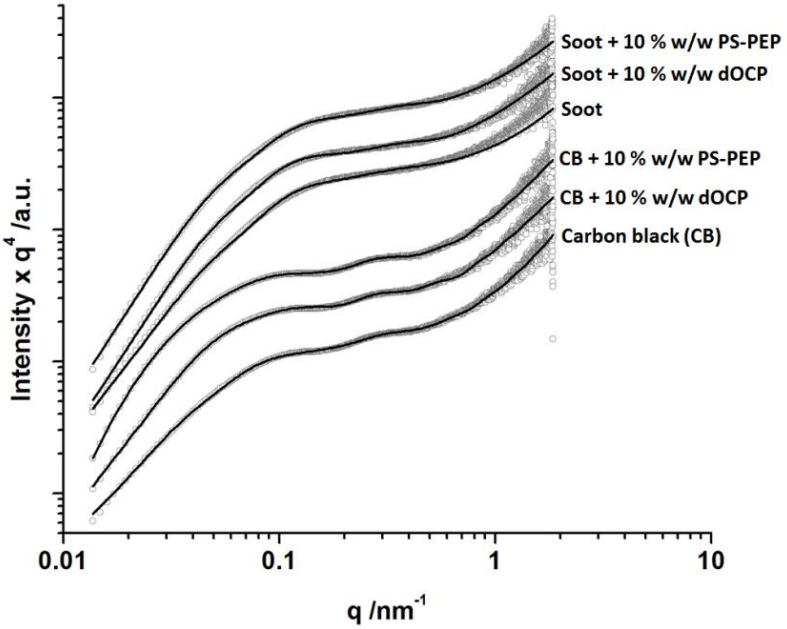

Figure 5.14. Porod plots for representative SAXS patterns recorded for 1.0 % w/w carbon black or diesel soot dispersions in *n*-dodecane in the absence and presence of two commercial copolymer dispersants (dOCP and PS-PEP; 10.0 % w/w loading based on carbon black or diesel soot particles). The lower group of patterns were obtained for carbon black particles and the upper group were obtained for diesel soot. Solid lines indicate multi-level unified fits to the experimental data.

Three hierarchical structures can be identified in the SAXS pattern recorded for the original carbon black dispersed in *n*-dodecane (Figure 5.13 and Figure 5.14, low SAXS pattern). By analogy with previous work,[55] the SAXS intensity gradient of -2.3 for $q < 0.03$ nm^{-1} is associated with mass fractals formed by carbon black aggregates and the corresponding gradient of -3.8 for 0.1 nm^{-1} < q < 0.2 nm^{-1} is assigned to surface fractals of the aggregates. Primary particles can be clearly identified as an upturn in SAXS intensity at $q \sim 0.3$ nm^{-1} via a Porod plot (Figure 5.14, low pattern). Thus SAXS patterns obtained for the original carbon black dispersion in *n*-dodecane can be interpreted as a superposition of scattering from primary particles (level 3), aggregates of these primary particles (level 2) and mass fractals of the aggregates (level 1), Table 5.3.

Sample description	Level 1 (fractals)	Level 2 (aggregates)		Level 3 (primary particles)			
	P_1	$2R_{g,2}$ /nm	P_2	$2R_{g,3}$ /nm	P_3	$R_{c,3}$	η_3
Carbon black particles	2.7	105	3.8	14.2	1.7	20	2.2
Carbon black particles plus 10 % w/w dOCP	2.0	76	4.2	13.0	2.2	22	2.3
Carbon black particles plus 10 % w/w PS-PEP	2.3*	102	4.0	13.6	2.0	22	2.2
Diesel soot particles	2.1	74	3.8	14.0**	1.8	-	-
Diesel soot particles plus 10 % w/w dOCP	1.7	70	4.1	14.0**	2.4	-	-
Diesel soot particles plus 10 % w/w PS-PEP	1.7	71	4.0	14.0**	2.2	-	-

Table 5.3. Calculated parameters for three hierarchical structures (levels) derived from multi-level unified fits to the experimental SAXS patterns recorded for 1.0 % w/w carbon black or diesel soot dispersions in the absence and presence of two commercial copolymer dispersants (dOCP and PS-PEP). P_1, P_2 or P_3 is the relevant power law exponent, $2R_{g,2}$ or $2R_{g,3}$ is the size of the structural element, $R_{c,3}$ is the correlation distance and η is the corresponding degree of correlation.

N.B. Errors in the fitted parameters shown in this Table are within a unit of the last digit of the values given.
* A radius of gyration of the agglomerate was incorporated into the fitting model, $R_{g,1}$ = 340 nm.
** This parameter was fixed during SAXS data fitting.

Structural characteristics of the carbon black can be determined by fitting the unified model to the scattering patterns, equation 1. A multi-level unified fit approach described in a previous study[51] has been employed for the SAXS analysis in this work. The SAXS pattern for the initial dispersion of carbon black in *n*-dodecane is reasonably well described by this model (see the lowest patterns in Figures 5.13 and 5.14). The mean primary particle size, $2R_{g,3}$, is 14.2 nm (Table 5.3, level 3) ,which is comparable to data reported in other studies.[48, 51, 55] The aggregate size, $2R_{g,2}$ = 105 nm (Table 5.3, level 2) corresponding to particle diameter 81 nm ($2R_{g,2}\sqrt{3/5}$) is also within the size range observed previously.[48] The power law exponent for these aggregates, P_2 is equal to 3.8 (Table 5.3). Since this value is just below 4.0, it suggests that the primary particles comprising these aggregates have a slightly rough surface. It is usually found that the power law exponent for such aggregates ranges from 3.4 to 4.0,[48, 51, 52, 54, 59] suggesting that the electron density distribution at the primary particle surface can vary according to the synthesis method and processing conditions. The power law exponent of the mass fractals formed by the aggregates (Table 5.3, level 1) corresponds to a fractal dimension D_m (or P_1) of 2.7. A similar fractal dimension was observed for diesel soot dispersed in acetone.[55] Thus the structural morphology of the carbon black particles dispersed in *n*-dodecane can be described as relatively compact mass fractals (Figure 5.1). It was also found that incorporating an appropriate structure factor into the model produced a better fit to the SAXS pattern recorded for the primary particles (level 3). More detailed analysis revealed a weak correlation between the primary particles ($\eta_3 < 3$, see Table 5.3). The power law exponent calculated for the primary particles, P_3, is also given in Table 5.3. This parameter is based on the scattering at high *q*. However, it is difficult to interpret such exponents as this region of the scattering pattern is influenced by excess scattering from a smaller hierarchical carbon structure (sub-units of ~ 1.5 - 2.0 nm) and also by internal inhomogeneities within carbon particles comprising both crystalline and amorphous phases.[49, 51, 59]

The model incorporating three hierarchical levels utilised for the carbon black particles also produced a reasonably good fit to the SAXS patterns recorded for a 1.0% w/w diesel soot dispersion in *n*-dodecane (see Figures 5.13 and 5.14). However, inspection of Figure 5.14 reveals some structural organisation differences between carbon black and diesel soot particles. For example, there were no pronounced features at q ~ 0.3 nm^{-}

[1] corresponding to primary particles (level 3). Thus $R_{g,3}$ was assumed to be similar to that of carbon black (14 nm; see Table 5.3) and this parameter was held constant during data fitting. SAXS analysis showed that the radius of gyration of the soot aggregates, $R_{g,2}$ = 37 nm (Table 5.3, Level 2), which corresponds to a mean particle diameter of 57 nm ($2R_{g,2}\sqrt{3/5}$), is significantly smaller than that calculated for the carbon black aggregates. This result is consistent with TEM observations and DLS data. The power law exponent, P_2, for these aggregates is 3.8. This value is quite similar to that of carbon black (see Table 5.3), suggesting a comparable degree of surface roughness for the diesel soot primary particles. The power law exponent for the mass fractals formed by the aggregates (Table 5.3, level 1) corresponds to a fractal dimension of 2.1. Thus, compared to the carbon black particles, the structural morphology of the soot particles dispersed in *n*-dodecane can be described as relatively loose mass fractals. This conclusion is also supported by TEM studies (see Figure 5.1).

SAXS patterns indicate that addition of either dOCP or PS-PEP has a similar effect on the hierarchical structure of both carbon black and diesel soot particles. In all cases, the characteristic mass fractal dimension, P_1, is significantly reduced (see Table 5.3), suggesting that the addition of either copolymer transforms the initially compact agglomerates into relatively loose aggregates. In the case of dOCP, the mean size of the carbon black aggregates is also reduced. There is also a discernible increase in the power law exponent for the aggregates, P_2, from 3.8 up to 4.2 (see Table 5.3). This suggests copolymer adsorption, since copolymer chains of relatively low electron density coating relatively high electron density carbon black aggregates is expected to produce a diffuse interface between the aggregates and the surrounding environment. This leads to a negative deviation from Porod's law, for which the scattering intensity gradient is normally equal to -4.0. SAXS analysis of the carbon black also confirms that the primary particle size remains approximately 14 nm, with insignificant deviations in the other parameters associated with this structural level. Thus addition of either dOCP or PS-PEP to the carbon black does not significantly affect the structure of its primary particles. It is assumed that this is also the case for diesel soot.

Conclusions

In summary, certain grades of carbon black such as the one studied herein can be useful mimics for understanding the behaviour of specific types of diesel soot. These two colloidal substrates can possess rather similar fractal morphologies, grain sizes and densities. Moreover, copolymer adsorption behaviour may be reasonably comparable, despite discernible differences in surface elemental composition.

SAXS can be used to assess the various hierarchical structures of both carbon black and diesel soot. For example, the mean radius of gyration determined for soot aggregates is significantly smaller than that calculated for carbon black aggregates. In the absence of any copolymer, soot particle suspensions in *n*-dodecane comprise relatively loose mass fractals compared to the corresponding carbon black suspensions. SAXS also provides evidence for copolymer adsorption and indicates that addition of either copolymer transforms the initially compact agglomerates into relatively loose aggregates. Based on SAXS analysis, addition of either dOCP or PS-PEP to the carbon black does not significantly affect the structure of its primary particles. It is believed that this is also the case for diesel soot.

In favourable cases, remarkably similar experimental data can be obtained for carbon black and diesel soot when using dOCP and PS-PEP as copolymer dispersants. However, it is not difficult to identify certain copolymer-particle-solvent combinations for which substantial differences can be observed. Such observations are most likely the result of dissimilar surface chemistries, which can have a profound effect on the colloidal stability.

References

1. Lloyd, A. C.; Cackette, T. A. Diesel engines: environmental impact and control. *Journal of the Air & Waste Management Association* **2001,** *51*, 809-847.
2. Nehmer, D. R., R. Measurement of the effect of injection rate and split injections on diesel engine soot and NO_x emissions. *SAE Technical Paper* **1994,** *940668*.
3. Pope, C. A.; Thun, M. J.; Namboodiri, M. M.; Dockery, D. W.; Evans, J. S.; Speizer, F. E.; Heath, C. W. Particulate air pollution as a predictor of mortality in a prospective study of U.S. adults. *American Journal of Respiratory and Critical Care Medicine* **1995,** *151*, 669-674.
4. Matti Maricq, M. Chemical characterization of particulate emissions from diesel engines: A review. *Journal of Aerosol Science* **2007,** *38*, 1079-1118.
5. Kittelson, D. B. Engines and nanoparticles: a review. *Journal of Aerosol Science* **1998,** *29*, 575-588.
6. Virtanen, A. K. K.; Ristimäki, J. M.; Vaaraslahti, K. M.; Keskinen, J. Effect of Engine Load on Diesel Soot Particles. *Environmental Science & Technology* **2004,** *38*, 2551-2556.
7. Shank, G.; Goshorn, K.; Cooper, M.; Van Dam, W.; Richards, S. *A history of mack engine lubricant tests from 1985-2005: Mack T-7 through mack T-12*; SAE Technical Paper2005-01-3713.
8. Kinker, B.; Fischer, M.; Bollinger, M.; Cybert, R.; Bielmeier, E.; Cooper, D.; Fischer, A.; Croessmann, M. Exhaust gas recirculation (EGR). US Patent 7560420 B2, 2009.
9. Maiboom, A.; Tauzia, X.; Hétet, J.-F. Experimental study of various effects of exhaust gas recirculation (EGR) on combustion and emissions of an automotive direct injection diesel engine. *Energy* **2008,** *33*, 22-34.
10. Zheng, M.; Reader, G. T.; Hawley, J. G. Diesel engine exhaust gas recirculation—a review on advanced and novel concepts. *Energy Conversion and Management* **2004,** *45*, 883-900.
11. Abd-Alla, G. H. Using exhaust gas recirculation in internal combustion engines: a review. *Energy Conversion and Management* **2002,** *43*, 1027-1042.
12. Cadman, W. J., J. The Study of the Effect of Exhaust Gas Recirculation on Engine Wear in a Heavy-Duty Diesel Engine Using Analytical Ferrography. *SAE Technical Paper* **1986,** *860378*.
13. Ladommatos, N., Balian, R., Horrocks, R., and Cooper, L. The Effect of Exhaust Gas Recirculation on Soot Formation in a High-Speed Direct-injection Diesel Engine. *SAE Technical Paper* **1996,** *960841*.
14. Selby, K. *Rheology of soot thickened diesel engine oils* 0148-7191; SAE Technical Paper1998-981369.
15. Kuo, C. C.; Passut, C. A.; Jao, T.-C.; Csontos, A. A.; Howe, J. M. *Wear mechanism in Cummins M-11 high soot diesel test engines*; SAE Technical Paper1998-981372.
16. Devlin, M. T.; Li, S.; Burgess, T.; Jao, T.-C. *Film formation properties of polymers in the presence of abrasive contaminants* 0148-7191; SAE Technical Paper2002-01-2793.
17. Li, S.; Csontos, A. A.; Gable, B. M.; Passut, C. A.; Jao, T.-C. *Wear in Cummins M-11/EGR test engines* 0148-7191; SAE Technical Paper2002-01-1672.

18. Gautam, M.; Chitoor, K.; Durbha, M.; Summers, J. C. Effect of diesel soot contaminated oil on engine wear — investigation of novel oil formulations. *Tribology International* **1999,** *32*, 687-699.
19. Green, D. A.; Lewis, R. The effects of soot-contaminated engine oil on wear and friction: A review. *Proceedings of the Institution of Mechanical Engineers, Part D: Journal of Automobile Engineering* **2008,** *222*, 1669-1689.
20. Zheng, R.; Liu, G.; Devlin, M.; Hux, K.; Jao, T. Friction Reduction of Lubricant Base Oil by Micelles and Crosslinked Micelles of Block Copolymers. *Tribology Transactions* **2009,** *53*, 97-107.
21. Diatto, P.; Anzani, M.; Tinucci, L.; Tripaldi, G.; Vettor, A. Investigation on soot dispersant properties and wear effects in the boundary lubrication regime. *Tribology Series* **1999,** *36*, 809-819.
22. Shar, J. A.; Cosgrove, T.; Obey, T. M.; Warne, M. R.; Wedlock, D. J. Adsorption studies of diblock copolymers at the cyclohexane/carbon black interface. *Langmuir* **1999,** *15*, 7688-7694.
23. Bartha, L.; Deák, Y. G.; Hancsók, J.; Baladincz, J.; Auer, J.; Kocsis, Z. Polyfunctional PIB succinimide type engine oil additives. *Lubrication Science* **2001,** *13*, 313-328.
24. Kozak, D.; Moreton, D.; Vincent, B. The adsorption of non-ionic surfactants on carbon black particles in hydrocarbon media. *Colloids and Surfaces A: Physicochemical and Engineering Aspects* **2009,** *347*, 245-250.
25. Hu, E.; Hu, X.; Liu, T.; Fang, L.; Dearn, K. D.; Xu, H. The role of soot particles in the tribological behavior of engine lubricating oils. *Wear* **2013,** *304*, 152-161.
26. Smiechowski, M. F.; Lvovich, V. F. Characterization of non-aqueous dispersions of carbon black nanoparticles by electrochemical impedance spectroscopy. *Journal of Electroanalytical Chemistry* **2005,** *577*, 67-78.
27. Clague, A. D. H.; Donnet, J. B.; Wang, T. K.; Peng, J. C. M. A comparison of diesel engine soot with carbon black. *Carbon* **1999,** *37*, 1553-1565.
28. Pahalagedara, L.; Sharma, H.; Kuo, C.-H.; Dharmarathna, S.; Joshi, A.; Suib, S. L.; Mhadeshwar, A. B. Structure and oxidation activity correlations for carbon blacks and diesel soot. *Energy & Fuels* **2012,** *26*, 6757-6764.
29. Bezot, P.; Hesse-Bezot, C.; Rousset, B.; Diraison, C. Effect of polymers on the aggregation kinetics and fractal structure of carbon black suspensions in an aliphatic solvent. A static and dynamic light scattering study. *Colloids and Surfaces A: Physicochemical and Engineering Aspects* **1995,** *97*, 53-63.
30. Bezot, P.; Hesse-Bezot, C.; Diraison, C. Aggregation kinetics of colloidal suspensions of engine soots. Influence of polymeric lubricant additives. *Carbon* **1997,** *35*, 53-60.
31. Müller, J. O.; Su, D. S.; Jentoft, R. E.; Wild, U.; Schlögl, R. Diesel Engine Exhaust Emission: Oxidative Behavior and Microstructure of Black Smoke Soot Particulate. *Environmental Science & Technology* **2006,** *40*, 1231-1236.
32. Müller, J.-O.; Su, D. S.; Wild, U.; Schlögl, R. Bulk and surface structural investigations of diesel engine soot and carbon black. *Physical Chemistry Chemical Physics* **2007,** *9*, 4018-4025.
33. Ilavsky, J.; Jemian, P. R. Irena: tool suite for modeling and analysis of small-angle scattering. *Journal of Applied Crystallography* **2009,** *42*, 347-353.
34. Scares, B. G.; de Souza Gomes, A. Spectrophotometric determination of the styrene content of alpha-methylstyrene—styrene copolymers. *Polymer Bulletin* **1988,** *20*, 543-548.

35. Watts, J. F. X-ray photoelectron spectroscopy. *Vacuum* **1994,** *45,* 653-671.
36. Kirchner, U.; Vogt, R.; Natzeck, C.; Goschnick, J. Single particle MS, SNMS, SIMS, XPS, and FTIR spectroscopic analysis of soot particles during the AIDA campaign. *Journal of Aerosol Science* **2003,** *34,* 1323-1346.
37. Swartz, W. E. X-ray photoelectron spectroscopy. *Analytical Chemistry* **1973,** *45,* 788A-800a.
38. Scares, B.; de Souza Gomes, A. Spectrophotometric determination of the styrene content of alpha-methylstyrene — styrene copolymers. *Polymer Bulletin* **1988,** *20,* 543-548.
39. Choi, S.-H.; Bates, F. S.; Lodge, T. P. Structure of Poly(styrene-b-ethylene-alt-propylene) Diblock Copolymer Micelles in Squalane. *The Journal of Physical Chemistry B* **2009,** *113,* 13840-13848.
40. Quintana, J. R.; Villacampa, M.; Katime, I. A. Micellization of a polystyrene-b-poly(ethylene/propylene) block copolymer in n-dodecane/1,4-dioxane mixtures. 2. Structure and dimensions of micelles. *Macromolecules* **1993,** *26,* 606-611.
41. Cohen Stuart, M. A.; Cosgrove, T.; Vincent, B. Experimental aspects of polymer adsorption at solid/solution interfaces. *Advances in Colloid and Interface Science* **1985,** *24,* 143-239.
42. Pirouz, S. D. J. J., S.; Duggal, A.;. Quantifying the Level of Intermacromolecular Interactions in Ethylene–Propylene Copolymers by Using Pyrene Excimer Formation. **DOI 10.1021/acs.macromol.5b00806, 2015**.
43. Rieker, T. P.; Misono, S.; Ehrburger-Dolle, F. Small-angle X-ray scattering from carbon blacks: crossover between the fractal and porod regimes. *Langmuir* **1999,** *15,* 914-917.
44. Won, Y.-Y.; Meeker, S. P.; Trappe, V.; Weitz, D. A.; Diggs, N. Z.; Emert, J. I. Effect of temperature on carbon-black agglomeration in hydrocarbon liquid with adsorbed dispersant. *Langmuir* **2004,** *21,* 924-932.
45. Lerche, D.; Sobisch, T. Consolidation of concentrated dispersions of nano- and microparticles determined by analytical centrifugation. *Powder Technology* **2007,** *174,* 46-49.
46. Detloff, T.; Sobisch, T.; Lerche, D. Particle size distribution by space or time dependent extinction profiles obtained by analytical centrifugation (concentrated systems). *Powder Technology* **2007,** *174,* 50-55.
47. Detloff, T.; Sobisch, T.; Lerche, D. Particle size distribution by space or time dependent extinction profiles obtained by analytical centrifugation. *Particle & Particle Systems Characterization* **2006,** *23,* 184-187.
48. Braun, A.; Huggins, F. E.; Seifert, S.; Ilavsky, J.; Shah, N.; Kelly, K. E.; Sarofim, A.; Huffman, G. P. Size-range analysis of diesel soot with ultra-small angle X-ray scattering. *Combustion and Flame* **2004,** *137,* 63-72.
49. di Stasio, S.; Mitchell, J. B. A.; LeGarrec, J. L.; Biennier, L.; Wulff, M. Synchrotron SAXS (in situ) identification of three different size modes for soot nanoparticles in a diffusion flame. *Carbon* **2006,** *44,* 1267-1279.
50. Hessler, J. P.; Seifert, S.; Winans, R. E.; Fletcher, T. H. Small-angle X-ray studies of soot inception and growth. *Faraday Discussions* **2001,** *119,* 395-407.
51. Koga, T.; Hashimoto, T.; Takenaka, M.; Aizawa, K.; Amino, N.; Nakamura, M.; Yamaguchi, D.; Koizumi, S. New insight into hierarchical structures of carbon black dispersed in polymer matrices: A combined small-angle scattering study. *Macromolecules* **2008,** *41,* 453-464.

52. Sorensen, C. M.; Oh, C.; Schmidt, P. W.; Rieker, T. P. Scaling description of the structure factor of fractal soot composites. *Physical Review E* **1998,** *58,* 4666-4672.
53. Koga, T.; Takenaka, M.; Aizawa, K.; Nakamura, M.; Hashimoto, T. Structure factors of dispersible units of carbon black filler in rubbers. *Langmuir* **2005,** *21,* 11409-11413.
54. Rieker, T. P.; Hindermann-Bischoff, M.; Ehrburger-Dolle, F. Small-angle X-ray scattering study of the morphology of carbon black mass fractal aggregates in polymeric composites. *Langmuir* **2000,** *16,* 5588-5592.
55. Braun, A.; Ilavsky, J.; Seifert, S.; Jemian, P. R. Deformation of diesel soot aggregates as a function of pellet pressure: A study with ultra-small-angle x-ray scattering. *Journal of Applied Physics* **2005,** *98,* 073513-1-073513-5.
56. Beaucage, G. Approximations leading to a unified exponential power-law approach to small-angle scattering. *Journal of Applied Crystallography* **1995,** *28,* 717-728.
57. Beaucage, G. Small-angle scattering from polymeric mass fractals of arbitrary mass-fractal dimension. *Journal of Applied Crystallography* **1996,** *29,* 134-146.
58. Beaucage, G.; Schaefer, D. W. Structural studies of complex-systems using small-angle scattering - A unified guinier power-law approach. *Journal of Non-Crystalline Solids* **1994,** *172,* 797-805.
59. Braun, A.; Shah, N.; Huggins, F. E.; Kelly, K. E.; Sarofim, A.; Jacobsen, C.; Wirick, S.; Francis, H.; Ilavsky, J.; Thomas, G. E.; Huffman, G. P. X-ray scattering and spectroscopy studies on diesel soot from oxygenated fuel under various engine load conditions. *Carbon* **2005,** *43,* 2588-2599.
60. Beaucage, G.; Ulibarri, T. A.; Black, E. P.; Schaefer, D. W. Multiple size scale structures in silica-siloxane composites studied by small-angle scattering. In *Hybrid Organic-Inorganic Composites*, 1995; Vol. 585, pp 97-111.

Chapter 6

Conclusions and Future Work

Conclusions

In this thesis, the adsorption of five commercial copolymer engine oil additives onto both genuine diesel soot and carbon black (a model colloidal substrate) has been investigated. Characterising copolymer-stabilised carbon black particles is not trivial. For example, sizing such particles via analytical centrifugation first requires accurate knowledge of copolymer-adsorbed particle densities. This has been successfully calculated for four commercial copolymers using Stokes' law. One of the fundamental questions at the start of this project was whether a poly(styrene-*b*-hydrogenated isoprene) diblock copolymer adsorbs onto carbon black/soot particles as micelles or as individual copolymer chains. It has been shown that such copolymers adsorb as *micelles* at 20^{o}C, and an understanding of such adsorption behaviour can be used to identify how such a dispersant additive can be modified to improve diesel soot dispersibility. For example, cross-linking of the polystyrene core should achieve more robust micelles that are no longer capable of dissociation into molecularly dissolved copolymer chains. Furthermore, an increase in polystyrene content should lead to larger micelle cores with a greater surface affinity and capable of forming a thicker layer.

The construction of adsorption isotherms for each copolymer onto carbon black and diesel soot allows the opportunity to develop more efficient formulations by preventing the use of excess additive. Indeed, analytical centrifugation has shown that the volume-average aggregate diameter of both carbon black and diesel soot remain relatively constant above the knee of each adsorption isotherm (see Chapters 3, 4 and 5). Furthermore, understanding how a copolymer designed for a specific purpose can in fact affect other properties of an engine oil formulation may explain why seemingly good oil formulations sometimes fail engine tests. For example, a poly(styrene-*b*-hydrogenated isoprene) star copolymer used commercially as a viscosity index improver has been assessed for its efficacy as a carbon black dispersant in Chapter 3. Surprisingly, it was found that this copolymer actually acts as a flocculant at low concentrations, which could prove catastrophic in engine oil formulations, where such flocculation could lead to substantial abrasion and long-term engine wear.

It has become clear that changes in temperature affect various physical properties of an engine oil formulation. Additive solvency plus oil density and viscosity are altered. Since a typical automotive diesel engine typically operates over a range of ~ -10^{o}C to 110^{o}C, a detailed understanding of the effect of temperature on carbon black/diesel soot dispersion stability is paramount. In Chapter 4, it was found that carbon black dispersion stability is reduced at elevated temperatures, and this is dependent on the type of copolymer used to stabilise such dispersions. An increase in copolymer solvency plus a change in stabiliser chain conformation are two factors that are expected to influence the dispersion stability. Thus, the importance of designing dispersant copolymer additives that are effective over a wide range of operating temperatures is highlighted.

In Chapter 5, a specific grade of carbon black (Regal 250R) has been proven to be a good mimic for genuine diesel engine soot under certain conditions, despite obvious differences in surface elemental composition highlighted by X-ray photoelectron spectroscopy. Subtle differences in dispersion stabilities and aggregate diameters have been demonstrated, although such differences do not appear to have much of an effect on dispersant copolymer adsorption or substrate dispersion stabilities. However, it is not difficult to identify conditions under which substantial differences between carbon black and diesel soot can be observed, at least for certain commercial copolymers.

A number of analytical techniques have been used to better understand the efficacy of various commercial copolymers as soot dispersants in engine oil. Of these techniques, small-angle X-ray scattering (SAXS) and analytical centrifugation have proven to be the most powerful. SAXS has enabled detailed characterisation of the self-assembled micelles formed by three diblock copolymers in *n*-alkane solvents. Furthermore, it has enabled a better understanding of the multi-levelled hierarchical structures of both carbon black and genuine diesel soot, and confirmed the presence of copolymer chains adsorbed on the substrate surface. Analytical centrifugation using a LUMiSizer® instrument has been invaluable in assessing how carbon black and soot dispersion stabilities depend on both copolymer concentration and temperature. Although a disc centrifuge photosedimentometer was also available, the LUMiSizer® instrument was preferred since it allowed analysis between 4^{o}C and 60^{o}C, the use of *n*-alkane solvents,

a small sample volume (~1.0 ml) when using expensive solvents such as d_{26}-dodecane, and the simultaneous analysis of multiple samples in disposable cells, removing the necessity of cleaning between runs.

Further techniques were utilised, albeit with associated caveats. For example, UV spectroscopy and thermogravimetric analysis (TGA) were used to quantify the adsorbed amount of each copolymer onto the surface of carbon black and soot. While comparable up to monolayer coverage, these techniques subsequently diverged, hence giving different isotherms for the same copolymer in this region. Sedimentation of excess non-adsorbed copolymer was shown to be the reason for this unexpected problem. This highlights the care which must be taken when drawing conclusions from a single set of experimental results.

Overall, an improved understanding of both the performance of commercial copolymer dispersants as engine oil additives and the fundamental interactions between such additives and the surface of carbon black and genuine diesel engine soot has been achieved. Effective densities of copolymer-stabilised carbon black particles have been calculated, and their importance demonstrated in the context of meaningful analytical centrifugation. Furthermore, a critical examination of the optimum concentration of each copolymer has been undertaken, hence providing a valuable insight into the optimisation of diesel engine oil formulation at a given soot loading.

Future Work

This thesis has shown that poly(styrene-*b*-hydrogenated isoprene) and poly(styrene-*b*-hydrogenated butadiene) diblock copolymers adsorb onto the surface of carbon black and genuine diesel soot from an *n*-alkane solvent as micelles rather than individual copolymer chains at 20^{o}C. To extend this work, a similar investigation focusing on the effect of temperature on the equilibrium adsorbed amount could be conducted. Ideally, temperatures of up to 90-110^{o}C should be examined, because this range corresponds to the operating temperature of an automotive diesel engine. However, this would require

access to a high temperature centrifuge in order to separate the copolymer-coated carbon black particles from the excess non-adsorbed copolymer chains.

In Chapter 4, the adsorption of three diblock copolymers onto carbon black has been examined, and the resulting dispersion stabilities assessed. These copolymers differed in polystyrene content, solvophilic stabiliser block and molecular weight. Ideally, each of these parameters should be altered independently and systematically, hence allowing their effect on copolymer adsorption and carbon black dispersion stability to be determined. For example, a higher polystyrene content is likely to lead to a higher copolymer adsorbed amount and a thicker stabiliser layer. This should in turn lead to more colloidally stable dispersions.

The effective density of copolymer-stabilised carbon black particles has been determined using four diblock copolymers. Such effective densities should also be calculated for these copolymers adsorbed onto genuine diesel soot. It can be expected that these densities will be slightly higher to those calculated for carbon black, since diesel soot has a higher density than carbon black (1.94 g cm^{-3} versus 1.89 g cm^{-3}) and the equilibrium adsorbed amount of copolymer is substrate-dependent.

In Chapter 4, the effect of temperature on carbon black dispersion stability is briefly discussed. Although this was assessed at the micron length scale by optical microscopy (OM), a quantitative study of such dispersions at the submicron length scale using analytical centrifugation was not possible. This is because effective densities have not been calculated for such sterically-stabilised particles at elevated temperatures. In principle, this could be achieved by measuring sedimentation velocities at 60^{o}C using the LUMiSizer instrument. This would then enable accurate particle size analysis of dispersions at this temperature. This would provide a better understanding of how this important parameter affects carbon black dispersion stability. Further high temperature OM studies could provide better insight into the effect of temperature on the colloidal stability of carbon black and diesel soot dispersions, at least at the micron length scale. Quantification would require digital image processing to obtain statistically significant data. However, unlike analytical centrifugation, OM does not require any knowledge of the effective particle density and is hence readily extended from model solvents such as

n-dodecane to genuine engine base oils. Moreover, in principle this approach could be used to assess the degree of dispersion of diesel soot particles in aged fully-formulated engine oils.

In an engine oil formulation, a collection of polymer additives must perform their functions harmoniously. In this thesis, five copolymer additives have been assessed *individually* in order to gain a better understanding of their carbon black and engine soot dispersion efficiency. While this is beneficial in optimising a specific copolymer additive, it does not reflect the more complex environment in which such additives operate. Thus, an investigation into binary (and ternary) mixtures of copolymer dispersants, plus the addition of further copolymer additives present in a formulation (an 'ad pack') would most likely prove highly beneficial from an industrial perspective. The competitive adsorption of binary (or ternary) mixtures, plus the adsorption of one copolymer followed by its attempted displacement by a second copolymer should prove useful in helping to understand how best to optimise engine oil formulations.

SAXS has proven invaluable in helping to develop an understanding of copolymer interactions with carbon black and diesel soot dispersions in *n*-alkanes. An extension of this work could look at the effect of temperature on dispersion stability. The adsorbed copolymer layer thickness on carbon black or diesel soot may well change due to either desorption or stabiliser collapse at elevated temperatures. Furthermore, SAXS can be used to calculate particle densities; hence the *effective* particle densities of copolymer-stabilised carbon black and diesel soot particles could be calculated using this technique. This would help to verify the accuracy of effective particle densities determined via analytical centrifugation.